

PEPTIDE-BASED DRUG SYSTEMS

A THESIS SUBMITTED TO  
THE GRADUATE SCHOOL OF NATURAL AND APPLIED SCIENCES  
OF  
MIDDLE EAST TECHNICAL UNIVERSITY

BY  
MELEK PARLAK

IN PARTIAL FULFILLMENT OF THE REQUIREMENTS  
FOR  
THE DEGREE OF DOCTOR OF PHILOSOPHY  
IN  
CHEMISTRY

SEPTEMBER 2017



Approval of the thesis:

**PEPTIDE-BASED DRUG SYSTEMS**

submitted by **MELEK PARLAK** in partial fulfillment of the requirements for the degree of **Doctor of Philosophy in Chemistry Department, Middle East Technical University** by

Prof. Dr. Gülbin Dural Ünver  
Dean, Graduate School of **Natural and Applied Sciences** \_\_\_\_\_

Prof. Dr. Cihangir Tanyeli  
Head of Department, **Chemistry** \_\_\_\_\_

Assist. Prof. Dr. Salih Özçubukçu  
Supervisor, **Dept. of Chemistry, METU** \_\_\_\_\_

**Examining Committee Members:**

Prof. Dr. Cihangir Tanyeli  
Dept. of Chemistry., METU \_\_\_\_\_

Assist. Prof. Dr. Salih Özçubukçu  
Dept. of Chemistry, METU \_\_\_\_\_

Assoc. Prof. Dr. Can Özen  
Dept. of Biochemistry, METU \_\_\_\_\_

Assist. Prof. Dr. Yunus Emre Türkmen  
Dept. of Chemistry, BILKENT UNIVERSITY \_\_\_\_\_

Assist. Prof. Dr. Rukan Genç  
Chemical Engineering Dept. MERSIN UNIVERSITY \_\_\_\_\_

**Date: 07.09.2017**

**I hereby declare that all information in this document has been obtained and presented in accordance with academic rules and ethical conduct. I also declare that, as required by these rules and conduct, I have fully cited and referenced all material and results that are not original to this work.**

Name, Last name:

Signature:

## **ABSTRACT**

### **PEPTIDE-BASED DRUG SYSTEMS**

Melek Parlak

PhD in Chemistry Department, METU

Supervisor: Salih Özçubukçu

September 2017, 173 pages

The increasing appeal of safe, cheap and effective treatments against various type of diseases has paved the way for the discovery and development of innovative peptide-based drug and drug delivery systems. The relative ease with which peptide based-materials can be synthesized and the wide range of synthetic techniques available have ensured that these materials can be tuned to adopt specific conformation or modified to contain specific functional groups.

Our major focus in this thesis is developing peptides with different scaffolds. In one study, we synthesized small peptides that mimic the correctly folded state of the fusion protein of the Respiratory syncytial virus (RSV) that causes respiratory tract infections. As small peptides generally do not retain their native conformation, they were stabilized through construction of intramolecular bridges that hold the peptides in the right conformation. A various type and size of intramolecular bridges were established in different part of the peptide sequences. Constrained peptides that both showing binding against specific antibodies and having helical structures as in their native structures were covalently linked to carrier protein for further immunological studies.

In another study, poor therapeutic properties of pro-apoptotic Smac peptide (AVPIAQK) were improved. Apoptotic peptide was fused to a well-known octaarginine cell-penetrating peptide for promoting its access to a cell's interior. Smac and octaarginine containing linear, monocyclic and bicyclic peptides were successfully synthesized. The biological properties of designed peptides in terms of cell-permeability, cytotoxicity and apoptotic efficiency were studied.

As a final study, anthracene containing peptide nanofibers and peptide vesicles were designed, synthesized and changes in their self-assembled structure upon light exposure at 365 nm were investigated. It was proved that such systems have a potential as light-driven drug delivery.

Keywords: Respiratory syncytial virus, Smac peptide, Octaarginine, Apoptotic peptide, self-assembled structures.

## ÖZ

### PEPTİT BAZLI İLAÇ SİSTEMLERİ

Melek Parlak

Doktora, Kimya Bölümü, ODTÜ

Danışman: Salih Özçubukçu

Eylül 2017, 173 sayfa

Çeşitli hastalık türlerine karşı güvenli, ucuz ve etkili tedavilere olan giderek artan ilgi, yenilikçi peptit bazlı ilaç ve ilaç dağıtım sistemlerinin keşfedilmesi ve geliştirilmesinin yolunu açmıştır. Peptit bazlı materyallerin sentezlenmesinin göreceli kolaylığı ve mevcut geniş sentetik teknik çeşitliliği, bu materyallerin spesifik konformasyonu benimsemek üzere ayarlanmasını veya spesifik fonksiyonel grupları ihtiva edecek şekilde modifiye edilmesini sağlamıştır.

Bu tezdeki ana odak noktamız, farklı iskelet özelliklerine sahip peptitlerin geliştirilmesidir. Bir çalışmada, solunum yolu enfeksiyonlarına neden olan Respiratuar sinsityal virüse (RSV) ait füzyon proteininin katlanmış halini taklit eden küçük peptitleri sentezledik. Küçük peptitler genellikle doğal konformasyonlarını muhafaza etmediğinden, peptitler, onları doğru konformasyonda tutabilen intramoleküler köprüler kurularak sağlamlaştırılmıştır. Çeşitli tip ve boyutlarda intramoleküler köprüler, peptit dizilerinin farklı bölümlerinde kurulmuştur. Hem spesifik antikora karşı bağlanma gösteren hem de doğal yapılarında olduğu gibi sarmal yapıya sahip olan sınırlandırılmış peptitler, daha ileri immünolojik çalışmalar için taşıyıcı proteine kovalent olarak bağlanmıştır.

Bir başka çalışmada, pro-apoptotik Smac peptidinin (AVPIAQK) zayıf terapötik özellikleri geliştirildi. Apoptotik peptit, hücrenin iç kısmına erişimi sağlamak için, iyi bilinen bir hücre penetrasyon peptiti olan oktaarjinine eklendi. Smac ve oktaarjinin içeren lineer, monosiklik ve bisiklik peptitler başarıyla sentezlendi. Tasarlanan peptitlerin hücre geçirgenliği, sitotoksikite ve apoptotik etkinlik açısından biyolojik özellikleri araştırıldı.

Son çalışmada, antrasen içeren peptit nanofiberleri ve peptit vezikülleri tasarlandı, sentezlendi ve 365 nm'de ışığa maruz bırakıldıklarında kendi kendine düzenlenen yapılarıdaki değişiklikler araştırıldı. Bu tür sistemlerin ışığa dayalı ilaç dağıtım potansiyeline sahip olduğu kanıtlandı.

Anahtar Kelimeler: Respiratuvar sinsityal virüs, Smac peptit, Oktaarjinin, Apoptotik peptit, Kendi kendine düzenlenen yapılar.



To My Parents  
Mehmet and Keziban Parlak  
For their love, and endless patience

## ACKNOWLEDGEMENT

Foremost, I would like to thank to my supervisor Assist. Prof. Dr. Salih Özçubukçu, He made enormous contribution to my intellectual knowledge with his inspiring comments and suggestions. Without his guidance and persistent help that much work would not have been possible. I was very lucky to be a part of his research groups. I have acquired precious experiences which will help me a lot in my new life as an independent researcher.

I would also express my appreciation to Prof. Dr. Jan Van Hest, for accepting me in his group for 15 months in Radboud University, The Netherlands. I owe a very important debt to Dr. Dennis Lowik, Radboud University. He has been actively interested in my work and has always been available to advise me. I am very grateful for his patience, motivation, enthusiasm.

Advice and comments given by research assistant Hans Adams from Radboud University has been a great help in peptide synthesis.

I am deeply grateful to Prof. Dr. Ayhan Sıtkı Demir. I was lucky enough to work with him for two years. The most important thing that I learned from him is self-discipline and working hard.

Special thanks to Assoc. Prof Dr. Can Özen, from Biotechnology department of METU. Biological studies in Chapter 3 were done in his research group.

For instrumental usage, I also would like to thank Prof. Dr. Ahmet Önal (Fluorescence Spectrometry), Doç. Dr. Irem Erel Göktepe (DLS), Yrd. Doç. Dr. Yunus Emre Türkmen (Photoreactor) and Prof. Dr. Cihangir Tanyeli (Ultra-Sensitive Balance).

I would like to acknowledge TÜBİTAK (The Scientific and Research Council of Turkey) BİDEB 2211/A scholarship.

I would like to thank my friends Ceren Kazancı, Seda Okumus Karahan, Erolcan Vatansever, Eylem Canbolat, Shakhawoat Hossain, and Gökçil Bilir from Ayhan Sıtkı Demir Research group. I have bunch of unforgettable memories with them.

I would like to thank my friends Gözde Esan, Güzide Aykent, Aytül Saylam, Burcu Okyar, Tuğçe Yılmaz, Mehmet Seçkin Kesici, Volkan Dolgun, Muzaffer Gökçe from Özçubukçu Research group for providing a very nice and warm friendship environment which made my research joyful and easy going.

And finally, my deepest appreciation goes to Aref Khalily, for being my best friend and beloved husband.

## TABLE OF CONTENTS

ABSTRACT.....	v
ÖZ.....	vii
ACKNOWLEDGEMENT.....	x
TABLE OF CONTENTS.....	xii
LIST OF FIGURES.....	xv
LIST OF TABLES.....	xx
LIST OF SCHEMES.....	xxiii
LIST OF ABBREVIATIONS.....	xxiv
CHAPTERS	
1. PEPTIDE-BASED THERAPEUTICS.....	1
1.1 Introduction.....	1
1.2 Chemical Approaches for Effective Development of Peptide Therapeutics.....	3
1.2.1 Solid Phase Peptide Synthesis (SPPS).....	3
1.2.2 Chemical modification.....	14
1.3 References.....	21
2. CONFORMATIONALLY-CONSTRAINED PEPTIDE MIMICS OF A KEY RSV NEUTRALIZING EPITOPE.....	31
2.1 Introduction.....	31
2.2 Results and Discussion.....	34
2.2.1 Characterization of wild type (WT) peptide.....	34
2.2.2 Alanine Scan.....	36
2.2.3 Synthesis, secondary structure and binding activity of peptides.....	37

2.2.4	Conjugation of potent peptides to KLH via SPAAC reaction .....	50
2.3	Experimental .....	54
2.3.1	General Peptide Synthesis and Purification Procedures .....	54
2.3.2	Lactamization.....	55
2.3.3	On Resin Side-Chain Cyclization Using CuAAC .....	56
2.3.4	Disulfide bridge formation.....	56
2.3.5	Peptide Conjugation to KLH via SPAAC reaction.....	57
2.3.6	Circular Dichroism Spectroscopy .....	57
2.3.7	Fluorescence Spectroscopy .....	58
2.3.8	Enzyme-linked Immunosorbent Assay (ELISA) Analysis of Peptide.....	58
2.4	References .....	58
3.	STRUCTURE-BASED DESIGN AND SYNTHESIS OF KILLER CYCLIC PEPTIDES FOR MULTIPLE MYELOMA TUMOR CELLS .....	63
3.1	Introduction .....	63
3.2	Results and Discussion.....	66
3.3	Experimental .....	77
3.3.1	Chemicals.....	77
3.3.2	General Method for Solid-Phase Peptide Synthesis .....	77
3.3.3	Reverse Phase High Performance Liquid Chromatography (RP-HPLC) analysis.....	78
3.3.4	Mass analysis of peptides.....	79
3.3.5	Preparation of Pd (PPh <sub>3</sub> ) <sub>4</sub> <sup>25</sup> .....	79
3.3.6	Attachment of FITC .....	79
3.3.7	Cell Culture .....	80
3.3.8	Flow cytometry .....	80
3.3.9	Cellular Uptake .....	80
3.3.10	Cell viability assays .....	80

3.3.11	Cell cycle analysis.....	80
3.3.12	Apoptosis assays .....	81
3.3.13	Statistical analysis.....	81
3.4	References .....	81
4.	DESIGN AND SYNTHESIS OF A PHOTOCONTROLLED DRUG CARRIER .....	85
4.1	Introduction .....	85
4.2	Results and Discussion.....	88
4.3	Experimental .....	98
4.3.1	Synthesis of anthraquinone-2-carboxylic acid (2) <sup>18</sup> .....	98
4.3.2	Synthesis of anthracene-2-carboxylic acid (3) <sup>18</sup> .....	98
4.3.3	Synthesis of Ant-PK peptide.....	99
4.3.4	Synthesis of Ant-VY peptide .....	99
4.3.5	NMR analysis.....	100
4.3.6	Transmission electron microscopy (TEM) .....	101
4.3.7	Dynamic light scattering (DLS) measurements .....	101
4.3.8	Photodimerization reaction .....	101
4.3.9	Fluorescence Spectroscopy .....	101
4.4	References .....	102
	APPENDICES .....	105
	A: AMINO ACID CODE TABLE.....	105
	B: DATA RELATED TO CHAPTER 2 .....	107
	C: DATA RELATED TO CHAPTER 3 .....	151
	D: DATA RELATED TO CHAPTER 4.....	165
	CURRICULUM VITAE.....	171

## LIST OF FIGURES

### FIGURES

Figure 1. 1 Attachment of the peptide sequence to a solid support via a linker .....	8
Figure 1. 2 Structure of coupling reagents A. Phosphonium salts, B. uronium/aminium salts, C. immonium salts, D. Carbodiimides reagents, E. Additives used with carbodiimides. ....	13
Figure 1. 3 The four possible ways a peptide can be constrained in a macrocycle. N represent the N-terminus (head) of peptides, C represents the C-terminus (tail) of peptides.....	15
Figure 2. 1 Prefusion and postfusion conformation of RSV F.....	33
Figure 2. 2 Analysis of WT and deletion mutant peptides. Interaction of WT and deletion mutant peptides with limiting dilutions of A) D25, B) AM22, C) CD spectrum of the WT peptide and deletion mutant peptides.....	35
Figure 2. 3 Interaction of WT and peptides containing different Ala substitutions with limiting amounts of A) D25 and B) AM22. ....	37
Figure 2. 4 Single bridged Lys-Glu (KE) peptides. A) Binding affinity of peptides against D25, B) Binding affinity of peptides against AM22, C) Normalized CD spectra.....	40
Figure 2. 5 Double bridged Lys-Glu (KE) peptides. A) Binding affinity of peptides against D25, B) Binding affinity of peptides against AM22, C) Normalized CD spectra.....	41
Figure 2. 6 Single bridged Lys-Asp (KD) peptides. A) Binding affinity of peptides against D25, B) Binding affinity of peptides against AM22, C) Normalized CD spectra.....	43
Figure 2. 7 Single bridged peptides varying in bridge length and type. A) Binding affinity of peptides against D25, B) Binding affinity of peptides against AM22, C) Normalized CD spectra of peptides. (C denotes a homocysteine).....	46

Figure 2. 8 Double and a triple bridged peptides. A) Binding affinity of peptides against D25, B) Binding affinity of peptides against AM22, C) Normalized CD spectra of peptides.....	48
Figure 2. 9 Alpha helical wheel representation of triple bridged peptide K190D194-K193D197-K211D215 (This image was drawn in web-based program created by Don Armstrong and Raphael Zidovetzki).....	49
Figure 2. 10 Modified azido peptides	50
Figure 2. 11 The intensity of clicked azido coumarin fluorescence (a. u.) against wavelength (nm) as a result of SPAAC reaction.....	52
Figure 2. 12 Reactivity of pooled human control sera A) 50% Virus neutralization titer B) Binding of human control sera to stabilized peptides .....	53
Figure 3. 1 Sequences of P1-7. Lactam bridges are shown as thin lines. The thick line joining the N and C termini of P6 indicates backbone cyclization.....	66
Figure 3. 2 Cellular uptake assessment of linear and cyclic SMAC peptides. Asterisks (**and ***) denote statistical significance at $p < 0.01$ and $p < 0.001$ , respectively (n=2).....	73
Figure 3. 3 Viability assessment and cell cycle analysis of U266 cells after 48 h treatment.....	75
Figure 3. 4 Induction of apoptosis upon treatment with 25 $\mu\text{M}$ peptides; Mitochondrial Membrane Depolarization State (MMD state), Caspase-3 Activity Change, Cell Membrane Asymmetry Change.....	76
Figure 4. 1 [4+4] cycloaddition reaction of anthracene molecules and its reverse reaction.....	88
Figure 4. 2 Structure of Ant-PK and Ant-VY peptides .....	89
Figure 4. 3 Positively stained TEM image of Ant-PK peptide at pH 4 .....	90
Figure 4. 4 Dynamic light scattering size distribution graph of Ant-PK peptide before irradiation .....	91
Figure 4. 5 Fluorescence emission intensity of Ant-PK at 125 $\mu\text{M}$ (0.5 wt. %) with $\lambda_{\text{ex}}$ 365nm.....	92
Figure 4. 6 A) TEM images of micellar peptides after irradiation B) Dynamic light scattering size distribution graph of peptide after irradiation .....	93
Figure 4. 7 TEM image of Ant-VY peptide at pH 4.....	94



Figure 4. 8 Fluorescence emission spectra of Ant-VY peptide at 122 $\mu$ M with $\lambda_{ex}$ 365nm.....	95
Figure 4. 9 UV-Vis absorption spectra of Ant-VY at pH 10, pH 4 and after irradiation at pH 4. ....	96
Figure 4. 10 UV-Vis absorption spectra of Fmoc-VY at pH 10, pH 4 and after irradiation at pH 4. ....	97
Figure A. 1 Amino Acids with Electrically Charged Residues.....	105
Figure A. 2 Amino Acids with Polar Uncharged Residues .....	105
Figure A. 3 Unique Amino Acids .....	106
Figure A. 4 Amino Acids with Hydrophobic residues.....	106
Figure B. 1 Mass and RP-HPLC chromatogram of WT.....	107
Figure B. 2 Mass and RP-HPLC chromatogram of $\Delta$ 12.....	109
Figure B. 3 Mass and RP-HPLC chromatogram of $\Delta$ 6.....	110
Figure B. 4 Mass and RP-HPLC chromatogram of N197A. ....	111
Figure B. 5 Mass and RP-HPLC chromatogram of Y198A. ....	112
Figure B. 6 Mass and RP-HPLC chromatogram of I199A.....	113
Figure B. 7 Mass and RP-HPLC chromatogram of Q210A. ....	114
Figure B. 8 Mass and RP-HPLC chromatogram of I214A.....	115
Figure B. 9 Mass and RP-HPLC chromatogram of C212A.....	116
Figure B. 10 Mass and RP-HPLC chromatogram of K193E197.....	117
Figure B. 11 Mass and RP-HPLC chromatogram of K199E203.....	118
Figure B. 12 Mass and RP-HPLC chromatogram of K203E207.....	119
Figure B. 13 Mass and RP-HPLC chromatogram of K207E211.....	120
Figure B. 14 Mass and RP-HPLC chromatogram of K212E216.....	121
Figure B. 15 Mass and RP-HPLC chromatogram of K193E197-K199E203.....	122
Figure B. 16 Mass and RP-HPLC chromatogram of K193E197-K203E207.....	123
Figure B. 17 Mass and RP-HPLC chromatogram of K193E197-K207E211.....	124
Figure B. 18 Mass and RP-HPLC chromatogram of K193E197-K212E216.....	125
Figure B. 19 Mass and RP-HPLC chromatogram of K207E211-K212E216.....	126
Figure B. 20 Mass and RP-HPLC chromatogram of K190E194-K193E197.....	127
Figure B. 21 Mass and RP-HPLC chromatogram of K193D197. ....	128
Figure B. 22 Mass and RP-HPLC chromatogram of K199D203. ....	129
Figure B. 23 Mass and RP-HPLC chromatogram of K203D207. ....	130

Figure B. 24 Mass and RP-HPLC chromatogram of K207D211. ....	131
Figure B. 25 Mass and RP-HPLC chromatogram of K212D216. ....	132
Figure B. 26 Mass and RP-HPLC chromatogram of K193D197-K199D203. ....	133
Figure B. 27 Mass and RP-HPLC chromatogram of K193D197-K203D207. ....	134
Figure B. 28 Mass and RP-HPLC chromatogram of K193D197-K207D211. ....	135
Figure B. 29 Mass and RP-HPLC chromatogram of K193D197-K211D215. ....	136
Figure B. 30 Mass and RP-HPLC chromatogram of K193D197-K212D216. ....	137
Figure B. 31 Mass and RP-HPLC chromatogram of K190D194-K193D197. ....	138
Figure B. 32 Mass and RP-HPLC chromatogram of K190D194-K193D197- K211D215. ....	139
Figure B. 33 Mass and RP-HPLC chromatogram of O193D197. ....	140
Figure B. 34 Mass and RP-HPLC chromatogram of C193C197. ....	141
Figure B. 35 Mass and RP-HPLC chromatogram of C193C197. ....	142
Figure B. 36 Mass and RP-HPLC chromatogram of C193C197. ....	143
Figure B. 37 Mass and RP-HPLC chromatogram of X193Z197. ....	144
Figure B. 38 Mass and RP-HPLC chromatogram of N <sub>3</sub> -PEG <sub>4</sub> -WT. ....	145
Figure B. 39 Mass and RP-HPLC chromatogram of N <sub>3</sub> -PEG <sub>4</sub> -K193D197. ....	146
Figure B. 40 Mass and RP-HPLC chromatogram of N <sub>3</sub> -PEG <sub>4</sub> -K190D194- K193D197. ....	147
Figure B. 41 Mass and RP-HPLC chromatogram of Biotin-PEG <sub>4</sub> -WT. ....	148
Figure B. 42 Mass and RP-HPLC chromatogram of Biotin-PEG <sub>4</sub> -K193D197. ....	149
Figure B. 43 Mass and RP-HPLC chromatogram of Biotin-PEG <sub>4</sub> -K190D194- K193D197. ....	150
Figure C. 1 Structure of P1. ....	151
Figure C. 2 Mass and RP-HPLC chromatogram of P1. ....	152
Figure C. 3 Structure of P2. ....	153
Figure C. 4 Mass and RP-HPLC chromatogram of P2. ....	154
Figure C. 5 Structure of P3. ....	155
Figure C. 6 Mass and RP-HPLC chromatogram of P3. ....	156
Figure C. 7 Structure of P4. ....	157
Figure C. 8 Mass and RP-HPLC chromatogram of P4. ....	158
Figure C. 9 Structure of P5. ....	159
Figure C. 10 Mass and RP-HPLC chromatogram of P5. ....	160

Figure C. 11 Structure of P6 .....	161
Figure C. 12 Mass and RP-HPLC chromatogram of P6.....	162
Figure C. 13 Structure of P7 .....	163
Figure C. 14 Mass and RP-HPLC chromatogram of P7.....	164
Figure D. 1 <sup>1</sup> H NMR spectrum of anthraquinone-2-carboxylic acid (2).....	165
Figure D. 2 <sup>13</sup> C NMR spectrum of anthraquinone-2-carboxylic acid (2).....	166
Figure D. 3 <sup>1</sup> H NMR spectrum of anthracene-2-carboxylic acid (3).....	166
Figure D. 4 <sup>13</sup> C NMR spectrum of anthracene-2-carboxylic acid (3) .....	167
Figure D. 5 Mass and RP-HPLC chromatogram of Ant-PK.....	168
Figure D. 6 Mass and RP-HPLC chromatogram of Ant-VY.....	169
Figure D. 7 Mass and RP-HPLC chromatogram of Fmoc-VY.....	170

## LIST OF TABLES

### TABLES

Table 1 1 Commonly used protecting groups compatible with Fmoc/tBu SPPS <sup>a</sup> .....	9
Table 2. 1 The list of peptides for alanine scan and deletion mutant peptides.....	36
Table 2. 2 Sequences of Lys-Glu (KE) single and double bridged peptides and a linear WT peptide (residues that are used for linkage are highlighted in red) .....	39
Table 2. 3 The list of WT and KD mono-bridged peptides in this study (residues that are used for linkage are highlighted in red) .....	42
Table 2. 4 The list of monocyclic peptides with different type and length of bridges. (O = ornithine, C = homo-Cysteine, X = azido-Lysine and Z = propargyl-Glycine, yellow colored A represents the cysteine substituted with alanine) .....	44
Table 2. 5 The list of double bridged KD peptides and the WT peptide .....	47
Table B. 1 Sequence, accurate mass and retention time of WT.....	107
Table B. 2 Sequence, accurate mass and retention time of Δ12. ....	109
Table B. 3 Sequence, accurate mass and retention time of Δ6. ....	110
Table B. 4 Sequence, accurate mass and retention time of N197A. ....	111
Table B. 5 Sequence, accurate mass and retention time of Y198A. ....	112
Table B. 6 Sequence, accurate mass and retention time of I199A. ....	113
Table B. 7 Sequence, accurate mass and retention time of Q210A. ....	114
Table B. 8 Sequence, accurate mass and retention time of I214A. ....	115
Table B. 9 Sequence, accurate mass and retention time of C212A. ....	116
Table B. 10 Sequence, accurate mass and retention time of K193E197. ....	117
Table B. 11 Sequence, accurate mass and retention time of K199E203. ....	118
Table B. 12 Sequence, accurate mass and retention time of K203E207. ....	119
Table B. 13 Sequence, accurate mass and retention time of K207E211. ....	120
Table B. 14 Sequence, accurate mass and retention time of K212E216. ....	121
Table B. 15 Sequence, accurate mass and retention time of K193E197-K199E203. .....	122

Table B. 16 Sequence, accurate mass and retention time of K193E197-K203E207. .....	123
Table B. 17 Sequence, accurate mass and retention time of K193E197-K207E211. .....	124
Table B. 18 Sequence, accurate mass and retention time of K193E197-K212E216. .....	125
Table B. 19 Sequence, accurate mass and retention time of K207E211-K212E216. .....	126
Table B. 20 Sequence, accurate mass and retention time of K190E194-K193E197. .....	127
Table B. 21 Sequence, accurate mass and retention time of K193D197. ....	128
Table B. 22 Sequence, accurate mass and retention time of K199D203. ....	129
Table B. 23 Sequence, accurate mass and retention time of K203D207. ....	130
Table B. 24 Sequence, accurate mass and retention time of K207D211. ....	131
Table B. 25 Sequence, accurate mass and retention time of K212D216. ....	132
Table B. 26 Sequence, accurate mass and retention time of K193D197-K199D203. .....	133
Table B. 27 Sequence, accurate mass and retention time of K193D197-K203D207. .....	134
Table B. 28 Sequence, accurate mass and retention time of K193D197-K207D211. .....	135
Table B. 29 Sequence, accurate mass and retention time of K193D197-K211D215. .....	136
Table B. 30 Sequence, accurate mass and retention time of K193D197-K212D216. .....	137
Table B. 31 Sequence, accurate mass and retention time of K190D194 K193D197. .....	138
Table B. 32 Sequence, accurate mass and retention time of K190D194-K193D197- K211D215. ....	139
Table B. 33 Sequence, accurate mass and retention time of O193D197. ....	140
Table B. 34 Sequence, accurate mass and retention time of C193C197. ....	141
Table B. 35 Sequence, accurate mass and retention time of C193C197. ....	142
Table B. 36 Sequence, accurate mass and retention time C193C197. ....	143

Table B. 37 Sequence, accurate mass and retention time of X193Z197. X = azido-Lysine and Z = propargyl glycine. ....	144
Table B. 38 Sequence, accurate mass and retention time of N <sub>3</sub> -PEG <sub>4</sub> -WT.....	145
Table B. 39 Sequence, accurate mass and retention time of N <sub>3</sub> -PEG <sub>4</sub> -K193D197.	146
Table B. 40 Sequence, accurate mass and retention time of N <sub>3</sub> -PEG <sub>4</sub> -K190D194-K193D197.....	147
Table B. 41 Sequence, accurate mass and retention time of Biotin-PEG <sub>4</sub> -WT. In order to proceed octet analysis, N-termini of linear peptide was biotinylated....	148
Table B. 42 Sequence, accurate mass and retention time of Biotin-PEG <sub>4</sub> -K193D197. In order to proceed octet analysis, N-termini of monocyclic peptide was biotinylated.....	149
Table B. 43 Sequence, accurate mass and retention time of Biotin-PEG <sub>4</sub> -K190D194-K193D197. In order to proceed octet analysis, N-termini of bicyclic peptide was biotinylated.....	150
Table C. 1 Accurate mass, retention time and percentage purity of P1 .....	151
Table C. 2 Accurate mass, retention time and percentage purity of P2 .....	153
Table C. 3 Accurate mass, retention time and percentage purity of P3 .....	155
Table C. 4 Accurate mass, retention time and percentage purity of P4.....	157
Table C. 5 Accurate mass, retention time and percentage purity of P5 .....	159
Table C. 6 Accurate mass, retention time and percentage purity of P6.....	161
Table C. 7 Accurate mass, retention time and percentage purity of P7.....	163

## LIST OF SCHEMES

### SCHEMES

Scheme 1. 1 SPPS principles .....	5
Scheme 1. 2 Fmoc removal mechanism. ....	7
Scheme 1. 3. Resin cleavage mechanism, A) Rink resin, B) 2-Chlorotrityl chloride resin (R represents amino acid sequence). ....	14
Scheme 2. 1 Synthesis of monocyclic K193E197 peptide with Alloc/OAll Strategy.....	38
Scheme 2. 2 Strategy used for the synthesis of Lys-Asp (KD) mono bridge using acid labile methyltrityl (Mtt) and phenylisopropyl (Pip) groups. ....	42
Scheme 2. 3 Azide–alkyne cycloaddition in the synthesis of bridged peptide .....	45
Scheme 2. 4 Strategy used for the synthesis of Lys-Asp (KD) double bridges using both acid labile Mtt/Pip groups and catalytically cleavable of Alloc/Allyl groups. ....	47
Scheme 2. 5 KLH Conjugation of Peptides via SPAAC reaction. Before and after the conjugation the decrease of BCN concentration was followed by fluorescence intensity of clicked 3-Azido-7-hydroxycoumarin .....	51
<b>Scheme 3. 1</b> Synthetic pathway of bicyclic <b>P7</b> peptide.....	68
Scheme 4. 1 Synthesis pathway of Anthracene-2-carboxylic acid.....	88

## LIST OF ABBREVIATIONS

<b>ACN</b>	: Acetonitrile
<b>CD</b>	: Circular dichroism
<b>CuAAC</b>	: Copper-Catalyzed Azide-Alkyne Cycloaddition
<b>DCM</b>	: Dichloromethane
<b>DIEA</b>	: N, N-Diisopropylethylamine
<b>DMF</b>	: N, N-Dimethylformamide
<b>DLS</b>	: Dynamic Light Scattering
<b>EtOH</b>	: Ethanol
<b>Fmoc</b>	: Fluorenylmethyloxycarbonyl
<b>HATU</b>	: 1-[Bis(dimethylamino)methylene]-1H-1,2,3-triazolo[4,5b]pyridinium 3-oxid hexafluorophosphate
<b>HBTU</b>	: <i>N,N,N',N'</i> -Tetramethyl-O-(1H-benzotriazol-1-yl)uronium Hexafluorophosphate
<b>HCTU</b>	: O-(1H-6-Chlorobenzotriazole-1-yl)-1,1,3,3-tetramethyluronium hexafluorophosphate
<b>HPLC</b>	: High performance liquid chromatography
<b>KLH</b>	: Keyhole limpet hemocyanin
<b>LC-MS</b>	: Liquid chromatography-mass spectrometry
<b>MW</b>	: Microwave
<b>NMR</b>	: Nuclear magnetic resonance spectroscopy
<b>PA</b>	: Peptide amphiphiles
<b>PyBroP</b>	: Bromotripyrrolidinophosphonium hexafluorophosphate
<b>Q-TOF</b>	: Quadrupole time of flight
<b>RT</b>	: Room Temperature



<b>SPAAC</b>	: Strain-Promoted Alkyne-Azide Cycloaddition
<b>SPPS</b>	: Solid Phase Peptide Chemistry
<b>TIS</b>	: Triisopropylsilane
<b>TEM</b>	: Transmission electron microscopy
<b>TFA</b>	: Trifluoroacetic acid
<b>tR</b>	: Retention time
<b>TEM</b>	: Transmission electron microscopy
<b>UV-Vis</b>	: UltraViolet-Visible Spectroscopy



## CHAPTER 1

### PEPTIDE-BASED THERAPEUTICS

#### 1.1 Introduction

Peptides are biologically active molecules, consisted of short chains of amino acid monomers linked together via amide bonds ( $-\text{CONH}-$ ) or disulfide bond ( $-\text{S}-\text{S}-$ ). These molecules are attractive building blocks in bioorganic and supra-molecular chemistry due to available diversity of amino acid sequences and their predictable conformational properties.

Emil Fischer, along with Ernest Fourneau, synthesized the first synthetic peptide, ‘dipeptide’—glycylglycine, in 1901.<sup>1</sup> This is considered as beginning of peptide chemistry. Progress however was slow for the next 50 years. Therefore medicinal use of synthetic peptides started after the Second World War. In 1953, the chemical synthesis of the first polypeptide—‘oxytocin’ by du Vigneaud was a milestone in peptide history.<sup>2</sup> However, amount of time and effort that peptide synthesis took was enormous by conventional methods. In 1963, Bruce Merrifield accelerated and automated this long process using the method he named Solid Phase Peptide Synthesis (SPPS). SPPS method paved the way for simple, rapid and effective preparation of peptides and small proteins. This technological leap has remarkably sparked progress in biochemistry, molecular biology, pharmacology and medicine. With their excellent specificity which is transferred into remarkable safety, tolerability and efficacy, peptides became an excellent starting point for the design of novel therapeutics.

The study of peptide-based biomaterials is an alluring target because it scrutinizes and advances basic understanding of how natural biomaterials are constructed and used in

biological systems. They often have essential roles in human physiology, including actions as hormones, neurotransmitters, growth factors or ion channel ligands.<sup>3</sup> They are very specific in activity. This feature of peptides might also be the primary differentiating factor of peptides compared with traditional small molecules when used as a drug candidate.<sup>4</sup> Another peculiar attribute of peptides is structural similarity between the constructed peptide and the physiologically active parent molecules from which they are derived, which helps depicting the risk of unforeseen side-reactions.<sup>5</sup> Furthermore, peptide therapeutics have lower production complexity with recent technological enhancements in peptide synthesis compared to protein-based biopharmaceuticals, therefore the production costs are also lower, generally approaching those of small molecules. In spite of all given attractive features, they also have some limitations. One of the most difficult challenges for peptides is the need for effective and patient-friendly delivery technologies. They have to be injected or special formulations have to be designed to accommodate them. The proteolytic stability of natural peptides is one of the primary limitation of their use as drug candidates. Despite such negations, therapeutic peptides has shown wide applications in medicine and biotechnology as diagnostics as well as therapeutics and came into prominence as potential drug of future.

The therapeutic peptides market has appeared in the 1970s, when Novartis launched Lypressin, a Vasopressin analogue. In 2000 the total ethical pharmaceutical market was accounted as \$265 billion, with peptides and proteins, excluding vaccines, reporting for more than 10 % of the market.<sup>6</sup> Approximately 30 peptides had reached the market in the period between 1970 and 2003.

The number of new chemical drugs had been almost stable for about 10 years, with around 35–40 each year, but the number of peptide and protein based drugs had been constantly increasing during these years. The most remarkable peptide drug in approved in 2003 was Enfuvirtide, which blocks HIV entry into cellular CD4 and can be considered the turning point of investor attitude to biotech in general and to peptide drugs in particular.<sup>7</sup> In 2010, there were a total of 60 peptide had been approved in the USA by the Food and Drug Administration (FDA) and their total sales are approximately 13 billion USD. Among these, the multiple sclerosis therapy Copaxone and the hormone-related products Leuprolide, Octreotide, and Goserelin have annual sales of more than \$1 billion each.<sup>8</sup> The year 2012 is considered as prominent year for

the peptide therapeutics sector. Six peptide therapeutics was granted marketing approvals in a single year. It had been estimated that the peptide market sales reached \$ 12 billion in 2013.<sup>9</sup> As of now there are over 100 approved peptide-based therapeutics on the market for the prosperity of patients. For all these reasons, the commercial value of peptide therapeutics are undeniable, and their market share could substantially increase as recently approved products and those seen on the horizon.

## **1.2 Chemical Approaches for Effective Development of Peptide Therapeutics**

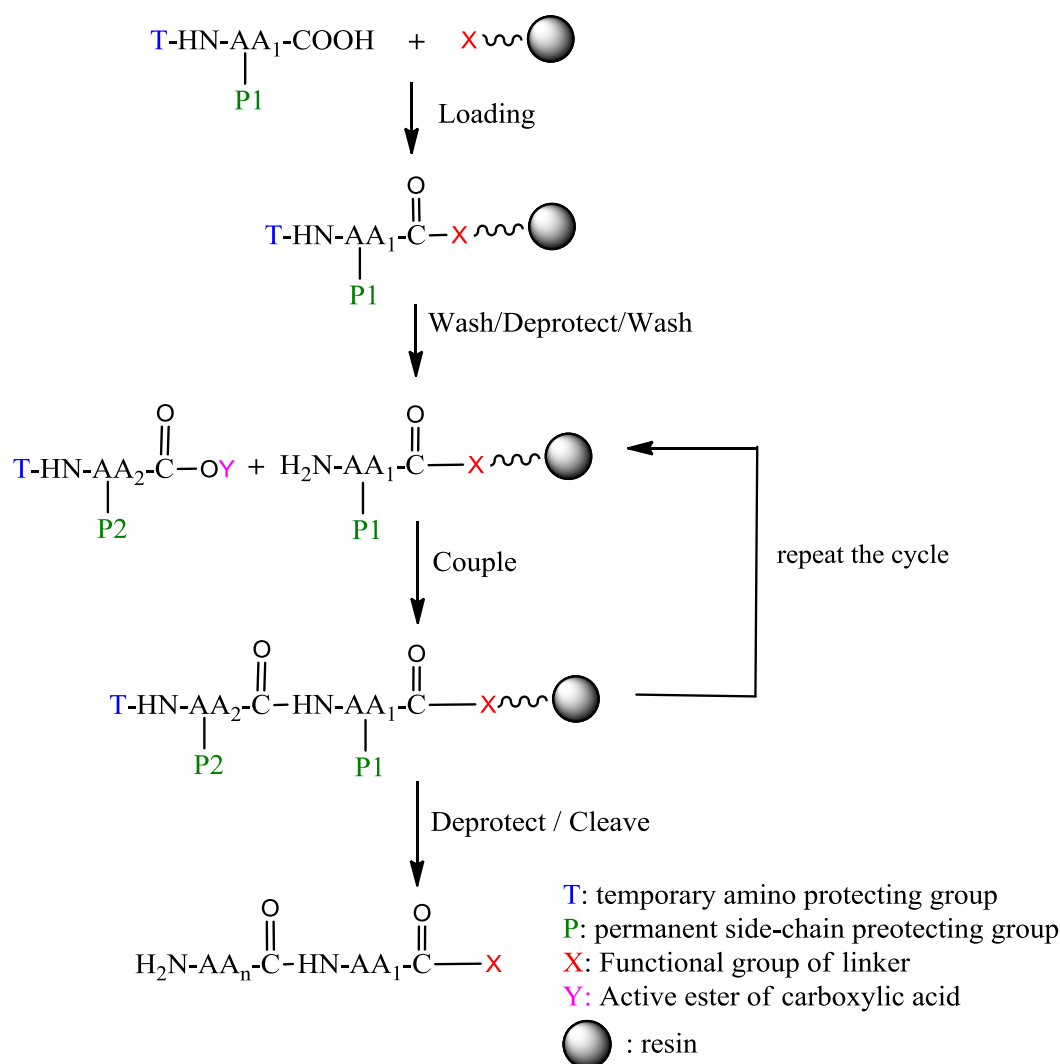
The phenomenal progress in synthetic methodologies and peptidomimetics lead the beginning of a new era in peptide therapeutics with the vision that chemists are now able to prepare without restraint, essentially any desired peptide sequence. At this juncture, the role of chemical biology is indispensable. The disadvantages in peptide design such as long sequences, short half-life, rapid proteolytic cleavage, and low oral bioavailability have been overcome by utilizing some biochemical strategies and approaches. Since the biggest obstacles in peptide chemistry was circumvented with the discovery of Solid Phase Peptide Synthesis, it will be explained in detail. Then, other developed techniques used for enhancing druggability of peptides will be briefly discussed.

### **1.2.1 Solid Phase Peptide Synthesis (SPPS)**

Introduced by Merrifield in 1963, solid phase peptide synthesis (SPPS) has immediately become one of the most powerful and versatile molecular tool for the construction of peptides.<sup>10</sup> Importance of this technique was fully appreciated and brought Nobel Prize to Robert Bruce Merrifield "for his development of methodology for chemical synthesis on a solid matrix". This technique based on the fact that the peptide chain is covalently attached to an insoluble polymeric resin. Growing peptides on an insoluble solid support has some distinct advantages. Firstly, separation of peptide from soluble reagents and solvents simply carried out with filtration and washing, which requires less time and labor compared to tedious work-up procedure. Moreover, many operations are amenable to mechanization and extensive range of robotic instrumentation are available now. After programming the amino acid sequence of peptides and describing synthesis parameter, machines can automatically perform

all the synthesis steps required to prepare peptide samples. Additionally, excess reagents can be used to help to drive reactions to completion and physical losses of peptides stay in minimum level due to robust covalent attachment of peptide resin in reaction condition. The major problem with this approach is the absence of feasible analytical techniques employed for following the course of the reactions. Progress of the reactions are depend on qualitative color tests.

The principles of SPPS are illustrated in Scheme 1.1.<sup>11</sup> The first amino acid residue is tethered to insoluble polymeric resin via a linker (between the solid support and the synthesized peptide) functionality. Any functional group in amino acid side chains must be protected with ‘permanent’ masking groups that must stay intact in reaction conditions during peptide chain assembly. After loading the first amino acid, the ‘temporary’ masking groups on  $\alpha$ -amino group is removed, then second amino acid is introduced. The carboxy group of the second amino acid being activated for amide bond formation through the generation of an active ester or by reaction with coupling reagent. Following with the coupling, excess reagents are washed away throughout the resin. The protecting group is removed from the N-terminus of the resulted dipeptide, prior to addition of third amino acid, then third amino acid was coupled by activation of its  $\alpha$ -carboxylic group. This deprotection/coupling cycle is repeated until the target sequence is obtained. At the end of the synthesis the peptide is released from the resin and the side chain protecting groups simultaneously removed.



**Scheme 1. 1** SPPS principles

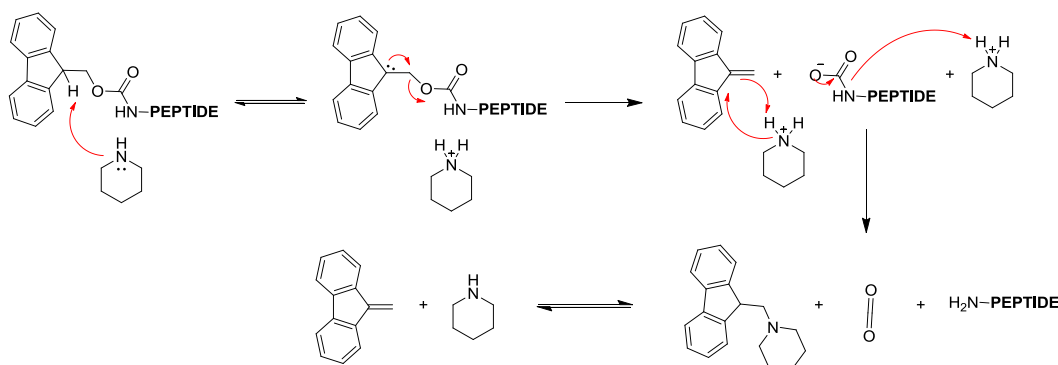
There are two categories of SPPS known as Boc/Benzyl and Fmoc/t-Bu SPPS, where the names refer to temporary N-terminal protecting group of the amino acid/permanent side chain protecting groups.

Initially, Boc-SPPS, which is also called Merrifield SPPS, was the main form of SPPS.<sup>12</sup> The *tert*-butoxycarbonyl (Boc) group is used for temporary protection of  $\alpha$ -amino group and removal of this group is effected with neat trifluoroacetic acid (TFA) or TFA in dichloromethane (DCM). The resulting trifluoroacetate is neutralized before the coupling with diisopropylethylamine (DIPEA) or neutralized in situ during the coupling reaction. Couplings were originally carried out by activation of subsequent

amino acid with dicyclohexylcarbodiimide (DCC) in DCM, but today the use of various type of potent coupling reagents in *N,N*-dimethylformamide (DMF) or *N*-methylpyrrolidone (NMP) are preferred for efficient synthesis. Permanent side-chain protecting groups (a range of benzyl based protecting groups) and peptide-resin bonds are cleaved at the end of the synthesis by usually treating the resin anhydrous hydrofluoric acid (HF). Even if this method is extremely powerful tool for efficient synthesis of large peptides and small proteins, the need to use highly toxic HF and special teflon-lined apparatus seriously hinder the usability of this approach. In addition to this, the harsh acidic conditions can cause detrimental and irreversible changes in the structure of peptides with sensitive sequences. Although Boc-SPPS is still used today, these reasons cause dwindling of Boc-SPPS method.

9-fluorenylmethoxycarbonyl (Fmoc) group was introduced in 1970 by Carpino and Han.<sup>13</sup> In the late 1970s, the Fmoc group was adopted for solid-phase applications. Fmoc based SPPS strategy employs the base-labile Fmoc group for protection of the  $\alpha$ -amino functional group, acid-labile side-chain protecting groups and acid-labile peptide-resin linkers. The temporary Fmoc protecting group is removed with 20-50% v/v piperidine in DMF as depicted in Scheme 1. 2. Couplings are typically carried out in DMF or NMP with pre-formed active esters or using activation reagents that generate in situ benzotriazolyl esters. Cleavage of the peptide from resin and the overall side-chain deprotection is achieved with maximum 95% TFA. One of the potential advantage of this strategy is that temporary and permanent orthogonal protecting groups are eliminated by completely different mechanisms, thus facilitating the use of milder acidic conditions for final deprotection and release of peptide from the resin. Moreover, elimination of repetitive acidolysis steps enables the synthesis of peptides that are susceptible to acid-catalyzed side reactions. All in all, these are the most obvious reasons for the popularity of Fmoc-SPPS approach that is actively utilized in laboratories worldwide.





**Scheme 1. 2** Fmoc removal mechanism.

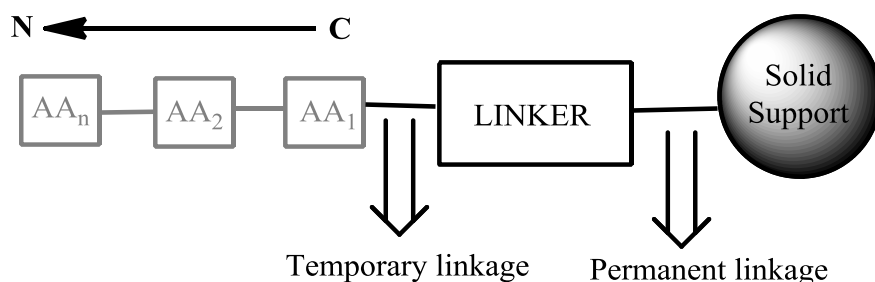
Successful SPPS is governed by several parameters: the choice of the solid support, linker, appropriately protected amino acids, coupling reagent, and protocol for cleaving the peptide from the solid support.<sup>14</sup>

The preference of the right solid support is often critical for successful, non-problematic synthesis of the desired peptide. Resin must be swelled in DCM, DMF and NMP, which are commonly used solvents. It has to be noted that effective solvation of the peptide/resin is perhaps the most crucial condition for efficient synthesis. Swollen resin beads should be reacted and washed batch-wise with agitation, then filtered either with suction or under positive nitrogen pressure. Resin must be robust and have less tendency to degrade over the course of long peptide array.

Furthermore, resins prepared as irregular shaped beads cannot always be packed properly, causing problems with channeling and irregular distribution of reagents through the resin bed. Extensive number of resins are now commercially available in the market for complex peptide synthesis.

The function of the linker is to provide temporary immobilization of the first synthetic component, an amino acid in the case of peptide synthesis to a solid support (Figure 1.1). It remains after cleavage at the support. Besides, linker protects the C-terminal of  $\alpha$ -carboxyl group during the process of peptide assembly. Functionality of the C-terminal of a final peptide depends on the choice of linker. Most of the linkers are designed to release peptide acids or amides upon the treatment with TFA. Linkers are

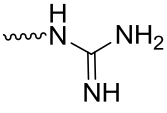
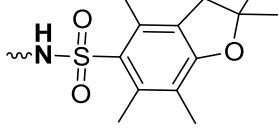
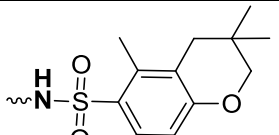
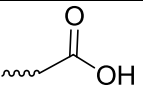
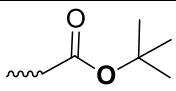
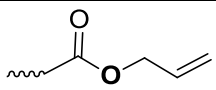
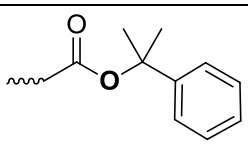
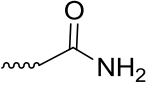
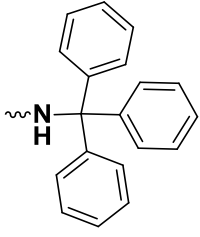
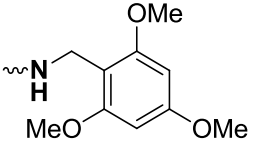
also available in which the peptide-resin linkage is cleaved with nucleophiles, enzymes or light. The primary criteria for linker selection are the structure of the target peptide and the protection strategy.



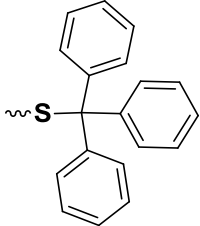
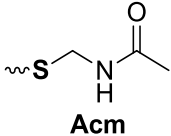
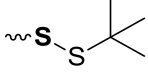
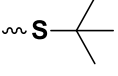
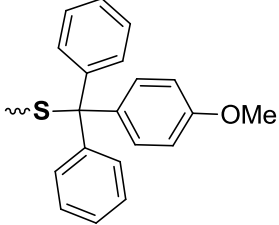
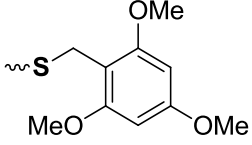
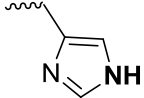
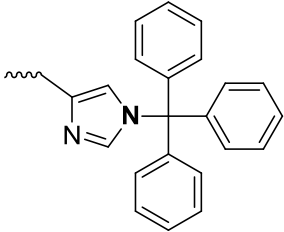
**Figure 1. 1** Attachment of the peptide sequence to a solid support via a linker

Another aspect for the successful SPPS is usage of properly protected amino acids. Most of the amino acids contain reactive functional groups. Therefore, it is usual for all these potentially reactive groups to be masked in order to avoid unwanted reactions during iterative deprotection, coupling steps and final cleavage process. For routine synthesis, protecting groups that are removed with TFA are usually employed, because unmasking of the side chain protections is occurred at the same time as peptide releases from the resin. Furthermore a wide range of groups is also available which selectively removed on solid phase, thus facilitate the selective modification of the side-chains of individual residues without chemically interacting the other amino acids. These find application in the synthesis of cyclic peptides, phosphopeptides, biotinylated and fluorescence-labeled peptides. Table 1.1 lists the frequently used side-chain protecting groups and the conditions required for removal.

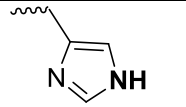
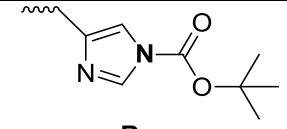
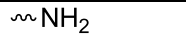
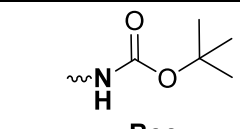
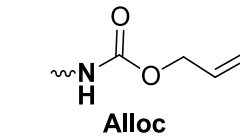
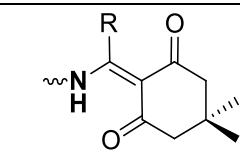

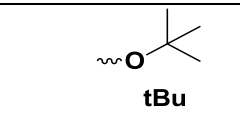

**Table 1. 1** Commonly used protecting groups compatible with Fmoc/tBu SPPS<sup>a</sup>

Functionality of side chain	Protecting groups	Cleavage conditions	References
 <b>Arg</b>	 <b>Pbf</b>	95% v/v TFA, 30min	15
	 <b>Pmc</b>	<ul style="list-style-type: none"> <li>• 50% v/v TFA in DCM, 1h</li> <li>• TFA-anisole (9:1), 30min</li> <li>• TFA-anisole-EDT-EMS, (95:3:1:1), 1,5h</li> </ul>	16, 17 17
 <b>Asp/Glu</b>	 <b>OtBu</b>	90% v/v TFA, 30min	18
	 <b>OAll</b>	Pd(Ph <sub>3</sub> P) <sub>4</sub> (0.1equiv), PhSiH <sub>3</sub> (24 equiv.) in DCM, 10-30min,	19
	 <b>OPip</b>	4% TFA in DCM, 15 min	20
 <b>Asn/Gln</b>	 <b>Trt</b>	90% v/v TFA, 30-60min	21
	 <b>Tmob</b>	90% v/v TFA, 1h	22

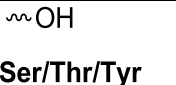
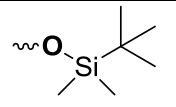
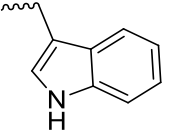
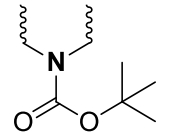
**Table 1. 1 (Continued)**

<p>~SH <b>Cys</b></p>	 <p><b>Trt</b></p>	<p>90% v/v TFA, 30min</p>	<p>23</p>
	 <p><b>Acm</b></p>	<ul style="list-style-type: none"> <li>• I<sub>2</sub></li> <li>• Tl(tfa)<sub>3</sub></li> <li>• Ag(TFMSO)</li> <li>• Hg(OAc)<sub>2</sub></li> </ul>	<p>24 25 26 27</p>
	 <p><b>StBu</b></p>	<p>PBu<sub>3</sub> or PPh<sub>3</sub> in TFE</p>	<p>28</p>
	 <p><b>tBu</b></p>	<p>HF, 20°C</p>	<p>29</p>
	 <p><b>Mmt</b></p>	<ul style="list-style-type: none"> <li>• 0.5-1 % v/v TFA in DCM-TES (95:5), 30min</li> <li>• 3 % v/v TFA, 5-10min</li> </ul>	<p>30</p>
	 <p><b>Tmob</b></p>	<p>5% v/v TFA-3% TES in DCM</p>	<p>31</p>
 <p><b>His</b></p>	 <p><b>Trt</b></p>	<p>50% v/v TFA in DCM, 30 min</p>	<p>32</p>

**Table 1. 1 (Continued)**

 <b>His</b>	 <b>Boc</b>	90% v/v TFA, 30 min	33
 <b>Lys/Orn</b>	 <b>Boc</b>	90% v/v TFA, 30 min	34
	 <b>Alloc</b>	Pd(Ph <sub>3</sub> P) <sub>4</sub> (0.1equiv), PhSiH <sub>3</sub> (24 equiv.) in DCM, 10-30min,	19
	 R: Me → <b>Dde</b> R: i-Bu → <b>Ddiv</b>	2% NH <sub>2</sub> NH <sub>2</sub> .H <sub>2</sub> O in DMF, 5-10 min	35,36
 <b>Mtt</b>		1.8% TFA in DCM, 3minx 15	37
	 <b>tBu</b>	90% v/v TFA, 30 min	38,39
 R: H → <b>Trt</b> R: Cl → <b>CIt</b> for Tyr		1-5% TFA in DCM, 2-5 min	40,41

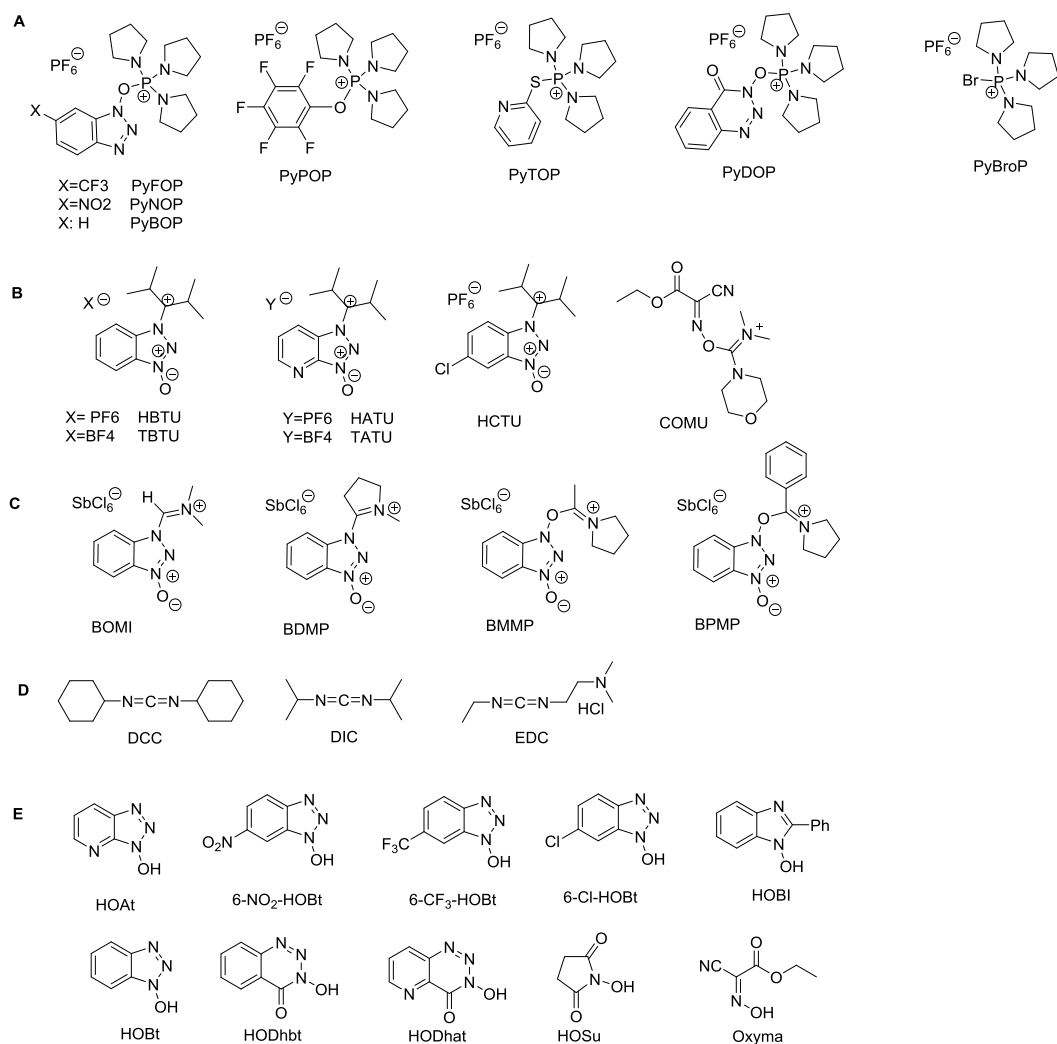
**Table 1. 1** (Continued)

 <b>Ser/Thr/Tyr</b>	 <b>Tbdms</b>	<ul style="list-style-type: none"> <li>• 0.1M TBAF-DMF, 15min (Tyr)</li> <li>• TFA, 15min (Ser/Thr)</li> </ul>	42
 <b>Trp</b>	 <b>Boc</b>	(i) 90% v/v TFA, 1h; followed by (ii) 1% aq. TFA, 1-2h	43

<sup>a</sup> The protecting groups are drawn to include masked atom of the aminoacids, shown in **bold**.

The success of the peptide synthesis relies on an efficient combination of protecting groups and coupling reagents. The term coupling refers to formation of an amide bond between two amino acids and that mainly consists of two steps. As a first and foremost step is the activation of carboxy component of the incoming amino acid. Although methods involving activation of carboxy groups commonly employed in organic synthesis, these are too extreme to be used in peptide synthesis as their tendency to side-reactions. Peptide chemists have therefore used milder activation methods, generally based on formation of active esters, pre-formed active esters or in-situ activation of carboxy group. The second step is the nucleophilic attack of the amino group of the other amino acid derivative at the active carboxylic group.

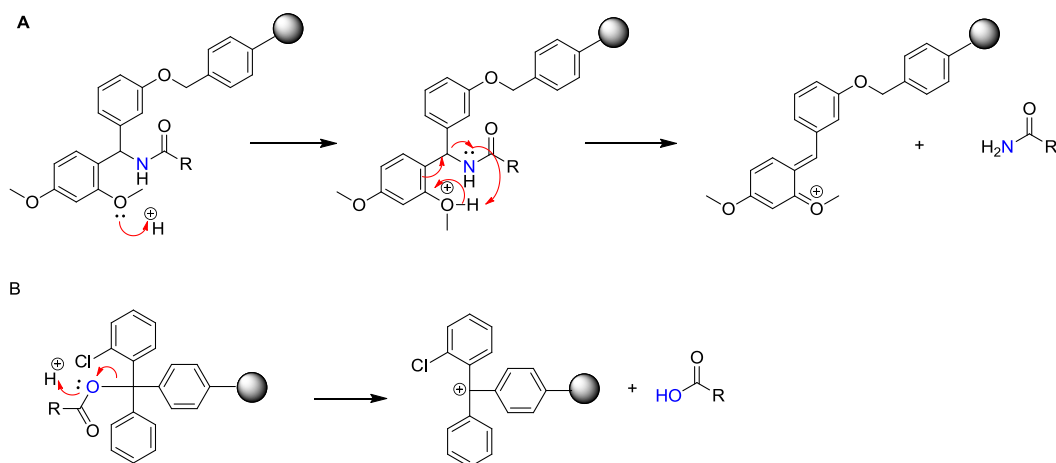
Among the vast number of coupling methods, those that require in situ activation of the carboxylic acid are most in use. The most-widely used coupling reagents are categorized as carbodiimides, uronium/aminium salts, phosphonium and immonium salts, which have structure as shown in Figure 1.2.<sup>44</sup> HBTU, HCTU, HATU, HOBT/DIC and PyBroP are highly reactive, affordable in price and they resolve racemization issue. Therefore they are utilized in peptide synthesis part of the thesis.



**Figure 1. 2** Structure of coupling reagents **A.** Phosphonium salts, **B.** uronium/aminium salts, **C.** immonium salts, **D.** Carbodiimides reagents, **E.** Additives used with carbodiimides.

When peptide construction is completed, it is released from the resin by a concentrated TFA (95%) for 1-3h. Peptide cleavage mechanisms of Rink<sup>45</sup> and 2-chlorotriyl chloride resin<sup>46</sup> are described in Scheme 1.3. Side-chain protecting groups are also removed under these highly acidic conditions, resulting peptide with fully deprotected side chains. Acidic side-chain group deprotection may yield highly reactive cationic species that are generated from the protecting groups and resin linkers. Since these species can react and result unwanted modifications, they are generally suppressed by introduction of various nucleophilic reagents called as “scavengers” into cleavage

mixture. The most frequently used scavengers are triisopropylsilane (TIS), water (H<sub>2</sub>O) and 1, 2-ethanedithiol (EDT) molecules.



**Scheme 1. 3.** Resin cleavage mechanism, **A)** Rink resin, **B)** 2-Chlorotrityl chloride resin (R represents amino acid sequence).

## 1.2.2 Chemical modification

In order to fulfill the biological requirements, peptides of interest often have to have structural elements beyond the 20 genetically encoded amino acids. Particular emphasis has been placed on peptides containing cyclic scaffolds, polyethylene glycol (PEG), D-amino acids, and lipophilic moieties and phosphorylated or glycosylated residues.

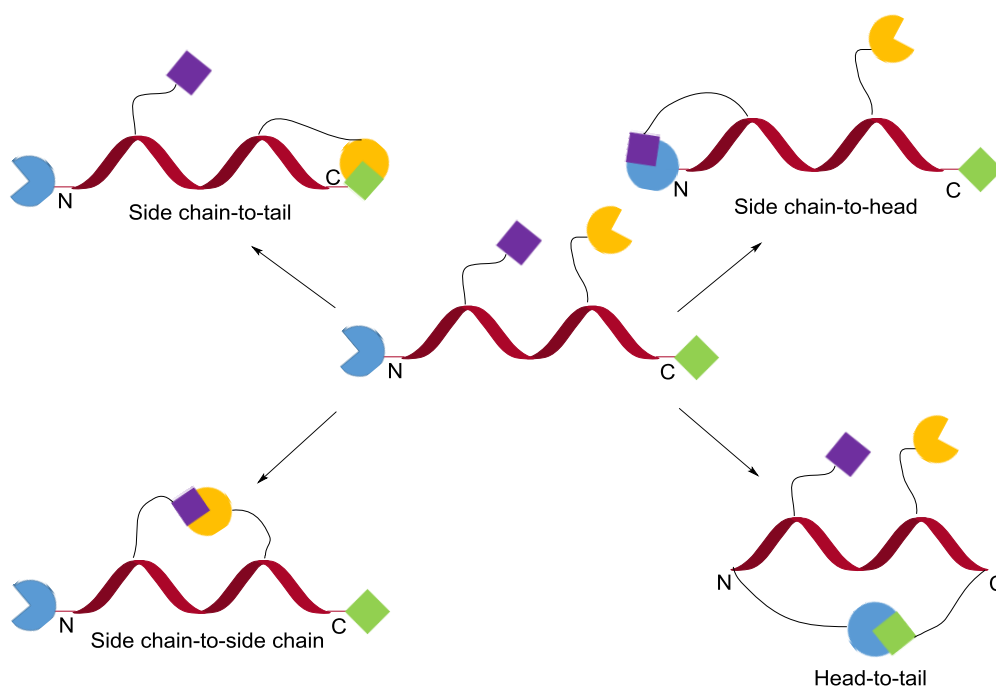
### 1.2.2.1 Macrocyclisation

Peptide macrocycles are conformationally rigidify synthetic peptides that are generally designed with the goal of increasing biological potency and/or specificity. As a characteristic feature, cyclic peptides are more resistant to enzymatic degradation than their linear variants,<sup>47</sup> which is a significant proof of therapeutic potential of this class of molecules. Cyclic peptides have proven to be useful for two main applications. One is the mimicry of secondary structures such as helicity and the other is the



optimization of peptides in terms of increased binding potency/selectivity and protease stability. There are many cyclic peptides with diverse biological activities. Octreotide, calcitonin, cyclosporine A, nisin, polymixin and colistin are the well-known peptide macrocycles that being used as therapeutic agents.<sup>48</sup>

Depending on its functional groups, there are four general methods for cyclization: head-to-tail (N-to-C), head-to-side chain, side chain-to-tail or side-chain-to-side-chain (figure 1.3). Among these four different ways for cyclization, head-to-tail and side chain-to-side chain cyclization are the most frequently utilized. While head-to-tail cycles are usually formed by amide bond formation, side-chain-to-side-chain cycles are most often synthesized via disulfide bond formation, lactamization, alkyne-azide cycloadditions and ring-closing metathesis (RCM).



**Figure 1. 3** Four possible ways a peptide can be constrained in a macrocycle. N represent the N-terminus (head) of peptides, C represents the C-terminus (tail) of peptides.

Disulphide bridging was one of the first cyclization techniques to be reported. Disulphide bridges between pairs of cysteine residues play an important structural role

in many proteins. Simultaneous deprotection of cysteines and oxidation give the disulphide bridged peptide. Their limited stability in reducing environments restrict their applicability in peptide chemistry.

Lactam refers to cyclic amide bond which is used for the preparation of head-to-tail cyclic peptides and side-chain-to-side-chain cyclic peptides. The use of amide bond has two primary advantages over disulfide bridges. First amide bond is inert to most of the conditions to which peptides are subjected, while disulfide-bridged peptides can be reduced to their acyclic thiol form in an intracellular environment.

Second, the availability of a wide variety of protecting groups for amines and carboxylic acids that are orthogonally cleavable enables the preparation of complex multicyclic peptides in more controllable and easier manner than disulfide bridge containing peptides. The construction of a monocyclic lactam-bridged peptide by SPPS will generally require a pair of selectively cleavable protecting groups for protection of the amine and carboxylic acid. After concomitant removal of the protection of amine and acid groups on resin while other aminoacids stay as protected, free amine and acid are coupled with potent coupling reagent, resulting a lactam formation. Incorporation of allyl-protecting groups (OAll/Alloc) which can be removed using the Pd<sup>0</sup> catalyst, base-labile protecting groups (Fmoc/OFm) and the protecting groups that can be cleaved under mild acidic conditions (Mtt/OPip) are largely used strategies. There has been extensive optimization and application of these strategies for development of lactam bridged peptides.

The utility of azide-alkyne cycloaddition reactions as a macrocyclisation tool is quite clear. This type of reaction encompasses an effective, highly reliable, and selective way to generate substances by joining azide and alkyne units together through triazole ring. Cu (I)-catalyzed alkyne-azide cycloaddition (CuAAC) and strain-promoted alkyne-azide cycloaddition (SPAAC) are successfully integrated to peptide chemistry, showing a great promise. The amino acids required for triazole stapling are readily accessible,<sup>49</sup> and the reaction conditions are now well-characterized.

The discovery of the olefin metathesis reaction in forming carbon-carbon bonds has led to a wide range of applications in the area of macrocyclization. Grubbs and co-workers were the first to apply the strategy of ring-closing metathesis (RCM) to conformationally restrain amino acids and peptides.<sup>50</sup> From a synthetic perspective,

the route for preparing hydrocarbon stapled peptides is investigated and optimized, however allyl containing aminoacids such as allylglycine, *O*-allyl serine and the ruthenium-based catalysts are still expensive for SPPS applications.

### **1.2.2.2 PEGylation**

Covalent attachment of non-toxic, non-immunogenic polyethylene glycol (PEG) polymer to peptides, so-called PEGylation, confers new physicochemical properties and can modify both stability and solubility. Furthermore, PEGylated peptide and protein therapeutics exhibit prolonged half-life, lower immunogenicity and antigenicity.<sup>51</sup> These consequences are attributed to increased molecular size<sup>52,53</sup> which reduces glomerular filtration and masking of the protein surface, which decreases immunorecognition response and proteolytic degradation.<sup>52, 54</sup> Due to these favorable properties, PEGylation plays a critical role in oral drug delivery, enhancing the efficacy of peptides and proteins as parenteral therapeutic agents. Another remarkable application of PEG-peptides is seen in the field of self-assembled systems. Interesting self-assembly properties arising from the amphiphilicity of PEG-peptide conjugates offers advantages for biomedical applications such as drug delivery or the development of enzyme-responsive self-assembling biomaterials.<sup>55</sup>

### **1.2.2.3 Substitution of L-amino acid with D-amino acids**

Functionality of peptides and proteins was dictated by their structure which is constituted by composition, configuration and chirality of aminoacids. Natural amino acids (except glycine) exhibit two different enantiomers (L- and D-). Although the L-form is clearly the predominant enantiomer found in nature, some peptides and proteins containing D-amino acids are also known. Their incorporation in designed peptide and proteins often make the designed therapeutics advantageous. One advantages of them is that compounds containing D-residues are much more resistant to proteolytic degradation than natural peptides, which is due to the stereospecificity of most exo- or endoproteases.<sup>56, 57</sup> For drug candidates, this feature is quite considerable. Another superiority of D-residue containing peptides and proteins is that their characteristic regions of allowed Ramachandran space make D-residues particularly suitable for stabilizing turns.<sup>58,59</sup> Therefore they can be used for structural stabilization of the secondary structures.

#### **1.2.2.4 Increasing the hydrophobicity of a peptide using lipophilic moieties**

The covalent binding of a lipid group to a peptide chain is called lipidation. It is the most common way to increase the hydrophobicity of the peptides for multiple purposes. Since the lipidation dramatically changes the physiochemical characteristic of the peptides, it is useful tool in designing peptide drugs. The number fatty acids, chain length and lipid anchor positions of fatty acids plays an important role in modulating their function.<sup>60</sup> Modification with lipids affects the absorption, distribution, metabolism and excretion (ADME) and bioavailability of drugs, and thus make this strategy attractive.<sup>60</sup>

Lipidated peptides are more stable than their unlipidated analogs, attached fatty acid moieties protects them against enzymatic degradation.<sup>61</sup> Moreover these lipophilic units improves their permeation of biological membranes to a certain extent and therefore increases their bioavailability and activity<sup>62</sup> Lipidic moieties can gain selectivity to peptides and target peptides to particular cells, such as dendritic<sup>63</sup> or cancer cells,<sup>64</sup> thus increasing peptide immunogenicity or antitumor efficacy, respectively.

Importantly, lipidation can change the secondary structures of peptides through the hydrophobic interactions of the fatty acid chain with the peptide backbone or side chains. Lipidated peptides can form stable self-assembling structures (such as micelles, tubules, vesicles, mono- or bilayers, nanofibers) which are currently committed to produce materials for biotechnology and biomedical applications.<sup>65</sup>

#### **1.2.2.5 Incorporation of phosphorylated or glycosylated residues**

Modifications of peptides and proteins by means of phosphorylation, or glycosylation endow the affected biomolecules with distinctive physiological and biochemical functions and/or reinforcement of certain significant structural conformation.

In recent years, a variety of reagents have been developed for protein phosphorylation research. Among these phosphopeptides have been proven to be critical components in designing assays for protein phosphorylation. Phosphorylation may affect protein function in different ways. Phosphates add both charge and hydrophilicity to a protein's surface. These changes may either construct or destroy sites for interaction

with other proteins or they induce changes in the conformation. These effects control its activity, subcellular localization, binding properties.

Phosphorylated peptides mainly contain phosphorylated hydroxyl-bearing amino acid residues serine and threonine and to a lesser extent, on the phenolic side chain of tyrosine. Principally, methodology of the chemical synthesis of phosphopeptides can be divided into two strategies: (1) preparation of the corresponding phosphorylated building blocks of amino acids and incorporation of them into the stepwise mode of solid phase synthesis by Fmoc or Boc chemistry; (2) the peptide can be phosphorylated after solid phase synthesis from hydroxyl substituents on the unprotected Ser/Thr/ Tyr residues.<sup>66</sup> This latter approach is referred to as global phosphorylation.

The introduction of carbohydrate moieties is another chemical strategy to improve therapeutic efficacy of peptide. First advantage of this strategy is the selective targeting to specific organs and enhancing biodistribution in tissues, which is fundamental for drug delivery. Carbohydrates are useful candidates for receptor-targeted peptide delivery. Therefore, the therapeutic agents conjugated with carbohydrate units can be recognized by lectin receptors, are expressed in the membrane of different cells, such as liver, tumor, and kidney cells.<sup>67</sup> As a second utility, carbohydrate incorporation enhances the permeability<sup>68</sup> of drugs across the cell membrane both by targeting glucose transporters on the surface of biological membranes 24 and increasing the hydrophobic character of peptides. Importantly, glycosylation can improve the metabolic stability and lowers the clearance rate.<sup>69</sup>

### **1.2.2.6 Introduction of peptidomimetics elements**

Self-assembly is a spontaneous process of organization of irregularly distributed molecular units into well-ordered structures as a result of intramolecular/intermolecular interactions.<sup>70</sup> It is a powerful tool in the synthesis of functional nanostructures such as nanofibers, nanotubes, nanovesicles, nanoribbons and etc. Many self-assembling systems have been developed from polymers, carbohydrates, nucleic acids and peptides. Among them peptide self-assembled nanostructures are extensively preferred for biomedical applications such as tissue engineering, biosensors, antimicrobial agents and carrier-mediated drug delivery. The features of biocompatibility, biodegradability, and versatility of peptides make them more valuable than the other conventional structures.

By manipulating the number, type, and sequence of amino acids, different type self-assembled structures can be designed. Depending upon these elements, it is possible to establish a relative control over morphology of a target nanostructure and thus achieve controlled assembly.<sup>71,72</sup> Different types and structures of peptides including aromatic dipeptides, cyclic peptides, dendritic peptides, amphiphilic peptides,  $\alpha$ -helical peptides, and  $\beta$ -sheet peptides have been utilized to self-assemble into nanostructures.<sup>73</sup>

Noncovalent interactions such as electrostatic interaction, hydrophobic interaction, hydrogen bonding, and  $\pi$ - $\pi$  stacking mediate the peptide self-assembly. Electrostatic interactions involve both attractive and repulsive forces between charged residues from amino acids in the peptide self-assembly. There are many studies that utilize the electrostatic interactions to direct the assembly process and fold the peptide into certain morphology. For example, nanotape structures were observed when C16-KTTKS was mixed with C16-ETTES.<sup>74</sup> Electrostatic interactions between anionic residue E (glutamic acid) and cationic residue K (lysine) led to the formation of fibrillar self-assembled structures. The hydrophobic interaction is one of the most important effects among various noncovalent interactions in the peptide self-assembly process. For instance, amphiphilic peptides that can be self-assembled into nanostructures were developed based on the magnitude of hydrophobic interactions. Hydrogen bonding is another significant input in the formation and stabilization of the peptide secondary structure and protein folding. Hydrogen bonding pattern interactions through the amide and carbonyl groups in the backbone direct the construction of peptide assembly. For aromatic moiety containing peptides,  $\pi$ - $\pi$  stacking from the aromatic groups can be the major driving force for stabilizing the self-assembled nanostructures as seen in the diphenylalanine (FF) peptide.<sup>75</sup> All these noncovalent interactions are easily affected by the external stimuli including pH, temperature, and solvent polarity, enabling the stimulation and manipulation of the self-assembly process.

For successful fabrication of self-assembled peptide nanostructures in drug delivery applications, tunable management of the physical and biological properties of peptide self-assembled nanostructures is highly desired.

When designing peptide self-assembled nanostructures for drug delivery, all of the noncovalent interactions should be taken into consideration and be rationally applied in the strategies.

### 1.3 References

1. Fischer, E., & Fourneau, E. (1901). Ueber einige Derivate des Glykocolls. *Berichte der deutschen chemischen Gesellschaft*, 34(2), 2868-2877. doi:10.1002/cber.190103402249
2. Babu, V. V. (2001). One hundred years of peptide chemistry. *Resonance*, 6(10), 68-75. doi:10.1007/bf02836969
3. Fosgerau, K., & Hoffmann, T. (2015). Peptide therapeutics: current status and future directions. *Drug Discovery Today*, 20(1), 122-128. doi:10.1016/j.drudis.2014.10.003
4. Vlieghe, P., Lisowski, V., Martinez, J., & Khrestchatisky, M. (2010). Synthetic therapeutic peptides: science and market. *Drug Discovery Today*, 15(1-2), 40-56. doi:10.1016/j.drudis.2009.10.009
5. Ali R, Rani R, Kumar S (2013). New peptide based therapeutic approaches. In: Ghulam Md A, Ishfaq Ahmed S (ed). *Advances in Protein Chemistry*. Retrieved from <https://www.esciencecentral.org/ebooks/ebookchapter/new-peptide-based-therapeutic-approaches-191/9>
6. Sachdeva, S. (2016). Peptides as ‘Drugs’: The Journey so Far. *International Journal of Peptide Research and Therapeutics*, 23(1), 49-60. doi:10.1007/s10989-016-9534-8
7. Otvos L (2008) Peptide-based drug design: here and now. In: Otvos LJr (ed) *Methods in molecular biology peptide-based drug design*, vol 494. Humana Press, New York
8. Thayer AM (2011) Improving peptides. *Chem Eng News Arch* 89(22):13–20
9. Research, T. M. (2016, September 12). Peptide Therapeutics Market - Increasing Demand for Peptide Therapeutics in Cancer and Diabetes Treatment to Boost Sales; Global Industry Analysis, Size, Share, Growth, Trends and Forecast 2020: TMR. Retrieved August 24, 2017, from <https://globenewswire.com/news-release/2016/09/12/871199/0/en/Peptide-Therapeutics-Market-Increasing->

[Demand-for-Peptide-Therapeutics-in-Cancer-and-Diabetes-Treatment-to-Boost-Sales-Global-Industry-Analysis-Size-Share-Growth-Trends-and-Forecas.html](#)

10. Merrifield, R. B. (1963). Solid Phase Peptide Synthesis. I. The Synthesis of a Tetrapeptide. *Journal of the American Chemical Society*, 85(14), 2149-2154. doi:10.1021/ja00897a025
11. White, P. D., & Chan, W. C. (2004). *Fmoc solid phase peptide synthesis: a practical approach*. New York: Oxford University Press.
12. Stewart, J. M., & Young, J. D. (1969). *Solid phase peptide synthesis*. San Francisco: W.H. Freeman.
13. Carpino, L. A., & Han, G. Y. (1970). 9-Fluorenylmethoxycarbonyl function, a new base-sensitive amino-protecting group. *Journal of the American Chemical Society*, 92(19), 5748-5749. doi:10.1021/ja00722a04
14. Angeletti, R. H., Bonewald, L. F., & Fields, G. B. (1997). [32] Six-year study of peptide synthesis. *Solid-Phase Peptide Synthesis Methods in Enzymology*, 697-717. doi:10.1016/s0076-6879(97)89071-4
15. Carpino, L. A., Shroff, H., Triolo, S. A., Mansour, E. M., Wenschuh, H., & Albericio, F. (1993). The 2,2,4,6,7-pentamethyldihydrobenzofuran-5-sulfonyl group (Pbf) as arginine side chain protectant. *Tetrahedron Letters*, 34(49), 7829-7832. doi:10.1016/s0040-4039(00)61487
16. Ramage, R., & Green, J. (1987). NG-2,2,5,7,8-pentamethylchroman-6-sulphonyl-L-arginine: A new acid labile derivative for peptide synthesis. *Tetrahedron Letters*, 28(20), 2287-2290. doi:10.1016/s0040-4039(00)96103-3
17. Ramage, R., Macleod, A. M., & Rose, G. W. (1991). Dioxalanones as synthetic intermediates. Part 6. Synthesis of 3-deoxy-D-manno-2-octulosonic acid (KDO), 3-deoxy-D-arabino-2-heptulosonic acid (DAH) and 2-keto-3-deoxy-D-gluconic acid (KDG). *Tetrahedron*, 47(29), 5625-5636. doi:10.1016/s0040-4020(01)80993-5
18. Schwyzer, R., & Dietrich, H. (1961). L-Asparaginsäure- $\beta$ -t-butylester und Derivate. *Helvetica Chimica Acta*, 44(7), 2003-2006. doi:10.1002/hlca.19610440724



19. Grieco, P., Gitu, P., & Hruby, V. (2001). Preparation of side-chain-to-side-chain cyclic peptides by Allyl and Alloc strategy: potential for library synthesis. *Journal of Peptide Research*, 57(3), 250-256. doi:10.1111/j.1399-3011.2001.00816.x
20. Yue, C., Thierry, J., & Potier, P. (1993). 2-phenyl isopropyl esters as carboxyl terminus protecting groups in the fast synthesis of peptide fragments. *Tetrahedron Letters*, 34(2), 323-326. doi:10.1016/s0040-4039(00)60578-6
21. Sieber, P., & Riniker, B. (1991). Protection of carboxamide functions by the trityl residue. Application to peptide synthesis. *Tetrahedron Letters*, 32(6), 739-742. doi:10.1016/s0040-4039(00)74872-6
22. Weygand, F., Steglich, W., & Bjarnason, J. (1968). Leicht abspaltbare Schutzgruppen für die Säureamidfunktion, 3. Derivate des Asparagins und Glutamins mit 2.4-dimethoxy-benzyl-und 2.4.6-trimethoxy-benzyl-geschützten Amidgruppen. *Chemische Berichte*, 101(10), 3642-3648. doi:10.1002/cber.19681011038
23. Hiskey, R. G., Mizoguchi, T., & Igeta, H. (1966). Sulfur-Containing Polypeptides. II. Selective Removal of S-Protective Groups from Some L-Cysteinyl-L-cysteine Derivatives<sup>1,2</sup>. *The Journal of Organic Chemistry*, 31(4), 1188-1192. doi:10.1021/jo01342a048
24. Kamber, B., Hartmann, A., Eisler, K., Riniker, B., Rink, H., Sieber, P., & Rittel, W. (1980). The Synthesis of Cystine Peptides by Iodine Oxidation of S-Trityl-cysteine and S-Acetamidomethyl-cysteine Peptides. *Helvetica Chimica Acta*, 63(4), 899-915. doi:10.1002/hlca.19800630418
25. Fujii, N., Otaka, A., Funakoshi, S., Bessho, K., & Yajima, H. (1987). ChemInform Abstract: New Procedure for the Synthesis of Cystine-Peptides by Oxidation of S-Substituted Cysteine-Peptides with Thallium (III) Trifluoroacetate. *ChemInform*, 18(32). doi:10.1002/chin.198732312
26. Fujii, N., Otaka, A., Watanabe, T., Okamachi, A., Tamamura, H., Yajima, H., Asano, K. (1989). Silver trifluoromethanesulphonate as an S-deprotecting reagent for the synthesis of cystine peptides. *Journal of the Chemical Society, Chemical Communications*, (5), 283. doi:10.1039/c39890000283

27. Veber, D., Milkowski, J., Varga, S., Denkwalter, R., & Hirschmann, R. (1972). Acetamidomethyl. A Novel Thiol Protecting Group for Cysteine. *Journal of the American Chemical Society*, 94(15), 5456-5461. doi:10.1021/ja00770a600
28. L. Moroder, M. Gemeiner, W. Göhring, E. Jaeger, E. Wunsch, In K. Brundfeldt (ed.): *Peptides 1980*, Scriptor, Copenhagen, Denmark, 1981 p.
29. McCurdy SN. (1989). The investigation of Fmoc-cysteine derivatives in solid phase peptide synthesis. *Pept Res.*, 2(1), 147-52
30. Barlos K, Gatos D, Hatzi O, Koch N, Koutsogianni S. (1996). Synthesis of the very acid-sensitive Fmoc-Cys(Mmt)-OH and its application in solid-phase peptide synthesis. *Int. J Pept Protein Res.*, 47(3), 148-53. doi: 10.1111/j.1399-3011.1996.tb01338.x
31. Munson, M. C., Garcia-Echeverria, C., Albericio, F., & Barany, G. (1992). S-2,4,6-trimethoxybenzyl (Tmob): a novel cysteine protecting group for the N.alpha.-(9-fluorenylmethoxycarbonyl) (Fmoc) strategy of peptide synthesis. *The Journal of Organic Chemistry*, 57(11), 3013-3018. doi:10.1021/jo00037a013
32. Sieber, P., & Riniker, B. (1987). Protection of histidine in peptide synthesis: A Reassessment of the trityl group. *Tetrahedron Letters*, 28(48), 6031-6034. doi:10.1016/s0040-4039(00)96856-4
33. Yamashiro, D., Blake, J., & Li, C. H. (1972). Use of N.alpha.,Nim-bis(tert-butylloxycarbonyl)histidine and N.alpha.-2-(p-biphenyl)isopropylloxycarbonyl-Nim-tert-butylloxycarbonylhistidine in the solid-phase synthesis of histidine-containing peptides. *Journal of the American Chemical Society*, 94(8), 2855-2859. doi:10.1021/ja00763a053
34. Chang, C., Waki, M., Ahmad, M., Meienhofer, J., Lundell, E. O., & Haug, J. D. (1980). ChemInform Abstract: preparation and properties of  $\alpha$ -9-fluorenylmethyloxycarbonylamino acids bearing tert-butyl side chain protection. *Chemischer Informationsdienst*, 11(17). doi:10.1002/chin.198017294
35. Bycroft, B. W., Chan, W. C., Chhabra, S. R., & Hone, N. D. (1993). A novel lysine-protecting procedure for continuous flow solid phase synthesis of branched peptides. *Journal of the Chemical Society, Chemical Communications*, (9), 778. doi:10.1039/c39930000778

36. Chhabra, S. R., Hothi, B., Evans, D. J., White, P. D., Bycroft, B. W., & Chan, W. C. (1998). An appraisal of new variants of Dde amine protecting group for solid phase peptide synthesis. *Tetrahedron Letters*, 39(12), 1603-1606. doi:10.1016/s0040-4039(97)10828-0
37. Li, D., & Elbert, D. L. (2002). The kinetics of the removal of the N-methyltrityl (Mtt) group during the synthesis of branched peptides. *Journal of Peptide Research*, 60(5), 300-303. doi:10.1034/j.1399-3011.2002.21018.x
38. Beyerman, H. C., & Bontekoe, J. S. (2010). The t-butoxy group, a novel hydroxyl-protecting group for use in peptide synthesis with hydroxy-amino acids. *Recueil des Travaux Chimiques des Pays-Bas*, 81(8), 691-698. doi:10.1002/recl.19620810808
39. Callahan, F. M., Anderson, G. W., Paul, R., & Zimmerman, J. E. (1963). The Tertiary Butyl Group as a Blocking Agent for Hydroxyl, Sulfhydryl and Amido Functions in Peptide Synthesis. *Journal of the American Chemical Society*, 85(2), 201-207. doi:10.1021/ja00885a020
40. Barlos, K., Gatos, D., Koutsogianni, S., Schäfer, W., Stavropoulos, G., & Wenging, Y. (1991). Darstellung und einatz von N-Fmoc-O-Trt-hydroxyaminosäuren zur "solid phase" synthese von peptiden. *Tetrahedron Letters*, 32(4), 471-474. doi:10.1016/s0040-4039(00)79471-8
41. Barlos, K., Gatos, D., & Koutsogianni, S. (2009). Fmoc/Trt-amino acids: comparison to Fmoc/tBu-amino acids in peptide synthesis. *The Journal of Peptide Research*, 51(3), 194-200. doi:10.1111/j.1399-3011.1998.tb01216.x
42. Fischer, P. M. (1992). Application of t-Butyldimethylsilyl Ethers of Serine, Threonine and Tyrosine in Peptide Synthesis. *Tetrahedron Letters*, 33, 7605-7608
43. White, P. (1992). Peptides: chemistry and biology (ed. J.A. Smith and J. E. Rivier), p.537. ESCOM, Leiden
44. Han, S., & Kim, Y. (2004). Recent development of peptide coupling reagents in organic synthesis. *Tetrahedron*, 60(11), 2447-2467. doi:10.1016/j.tet.2004.01.020

45. Rink, H. (1987). Solid-phase synthesis of protected peptide fragments using a trialkoxy-diphenyl-methylester resin. *Tetrahedron Letters*, 28(33), 3787-3790. doi:10.1016/S0040-4039(00)96384-6
46. Barlos, K., Chatzi, O., Gatos, D., Stavropoulos, G. (1991). 2-Chlorotrityl chloride resin Studies on anchoring of Fmoc-amino acids and peptide cleavage, *International Journal of Peptide Research and Therapeutics*, 37(6), 513-520.
47. Tyndall, J. D., Nall, T., & Fairlie, D. P. (2005). Proteases Universally Recognize  $\beta$  Strands in Their Active Sites. *ChemInform*, 36(21). doi:10.1002/chin.200521283
48. Sewald, N., & Jakubke, H. (2009). *Peptides: chemistry and biology*. Weinheim: Wiley-VCH.
49. Spring, D., & Lau, Y. (2011). Efficient Synthesis of Fmoc-Protected Azido Amino Acids. *Synlett*, 2011(13), 1917-1919. doi:10.1055/s-0030-1260950
50. Miller, S. J., Blackwell, H. E., & Grubbs, R. H. (1996). Application of Ring-Closing Metathesis to the Synthesis of Rigidified Amino Acids and Peptides. *Journal of the American Chemical Society*, 118(40), 9606-9614. doi:10.1021/ja961626l
51. Ryan, S. M., Mantovani, G., Wang, X., Haddleton, D. M., & Brayden, D. J. (2008). Advances in PEGylation of important biotech molecules: delivery aspects. *Expert Opinion on Drug Delivery*, 5(4), 371-383. doi:10.1517/17425247.5.4.371
52. Fee, C. J. (2007). Size comparison between proteins PEGylated with branched and linear poly (ethylene glycol) molecules. *Biotechnology and Bioengineering*, 98(4), 725-731. doi:10.1002/bit.21482
53. Bailon, P., & Berthold, W. (1998). Polyethylene glycol-conjugated pharmaceutical proteins. *Pharmaceutical Science & Technology Today*, 1(8), 352-356. doi:10.1016/s1461-5347(98)00086-8
54. Youn, Y. S., Jung, J. Y., Oh, S. H., Yoo, S. D., & Lee, K. C. (2006). Improved intestinal delivery of salmon calcitonin by Lys18-amine specific PEGylation: Stability, permeability, pharmacokinetic behavior and in vivo hypocalcemic

- efficacy. *Journal of Controlled Release*, 114(3), 334-342.  
doi:10.1016/j.jconrel.2006.06.007
55. Hamley, I. W. (2014). PEG–Peptide Conjugates. *Biomacromolecules*, 15(5), 1543-1559. doi:10.1021/bm500246w
56. Pohl, E., Sheldrick, G. M., Fischer, S., & Lackner, H. (1994). Structure of cyclo-(L-threonyl-D-valyl-L-prolyl-sarcosyl-N-methyl-L-valyl-OThr) at 153 K. *Acta Crystallographica Section C Crystal Structure Communications*, 50(1), 100-103. doi:10.1107/s0108270193007334
57. Mitchell, J. B., & Smith, J. (2003). D-amino acid residues in peptides and proteins. *Proteins: Structure, Function, and Bioinformatics*, 50(4), 563-571. doi:10.1002/prot.10320
58. Struthers, M. D., Cheng, R. P., & Imperiali, B. (1996). Economy in Protein Design: Evolution of a Metal-Independent  $\beta\beta\alpha$  Motif based on the Zinc Finger Domains. *Journal of the American Chemical Society*, 118(13), 3073-3081. doi:10.1021/ja954014u
59. Imperiali, B., Moats, R. A., Fisher, S. L., & Prins, T. J. (1992). A conformational study of peptides with the general structure Ac-L-Xaa-Pro-D-Xaa-L-Xaa-NH<sub>2</sub>: spectroscopic evidence for a peptide with significant  $\beta$ -turn character in water and in dimethyl sulfoxide. *Journal of the American Chemical Society*, 114(9), 3182-3188. doi:10.1021/ja00035a002
60. Zhang, L., & Bulaj, G. (2012). Converting Peptides into Drug Leads by Lipidation. *Current Medicinal Chemistry*, 19(11), 1602-1618. doi:10.2174/092986712799945003
61. Simerska P, Moyle PM, Toth I (2011) Modern lipid-, carbohydrate-, and peptide-based delivery systems for peptide, vaccine, and gene products. *Med Res. Rev.*, 31, 520–547
62. Yamamoto, A. (1998) Improvement of intestinal absorption of peptide and protein drugs by chemical modification with fatty acids. *Nippon Rinsho*, 56(3), 601-607.

63. Hennessy, E. J., Parker, A. E., & Oneill, L. A. (2010). Targeting Toll-like receptors: emerging therapeutics. *Nature Reviews Drug Discovery*, 9(4), 293-307. doi:10.1038/nrd3203
64. Skwarczynski, M., Hayashi, Y., & Kiso, Y. (2006). Paclitaxel Prodrugs: Toward Smarter Delivery of Anticancer Agents. *Journal of Medicinal Chemistry*, 49(25), 7253-7269. doi:10.1021/jm0602155
65. Cavalli, S., & Kros, A. (2008). Scope and Applications of Amphiphilic Alkyl- and Lipopeptides. *Advanced Materials*, 20(3), 627-631. doi:10.1002/adma.200701914.
66. McMurray, J. S., Coleman, D. R., Wang, W., & Campbell, M. L. (2001). The synthesis of phosphopeptides. *Biopolymers*, 60(1), 3-31. doi:10.1002/1097-0282(2001)60:1<3::aid-bip1001>3.0.co;2-1
67. Jain, K., Kesharwani, P., Gupta, U., & Jain, N. K. (2012). A review of glycosylated carriers for drug delivery. *Biomaterials*, 33(16), 4166-4186. doi:10.1016/j.biomaterials.2012.02.033
68. Varamini, P., Mansfeld, F. M., Blanchfield, J. T., Wyse, B. D., Smith, M. T., & Toth, I. (2012). Synthesis and Biological Evaluation of an Orally Active Glycosylated Endomorphin-1. *Journal of Medicinal Chemistry*, 55(12), 5859-5867. doi:10.1021/jm300418d
69. Costa, A. R., Rodrigues, M. E., Henriques, M., Oliveira, R., & Azeredo, J. (2013). Glycosylation: impact, control and improvement during therapeutic protein production. *Critical Reviews in Biotechnology*, 34(4), 281-299. doi:10.3109/07388551.2013.793649
70. Lehn, J. M. (2002). Toward complex matter: Supramolecular chemistry and self-organization. *Proceedings of the National Academy of Sciences USA*, 99, 4763-4768. doi: 10.1073/pnas.072065599
71. Palmer, L. C., Velichko, Y. S., Cruz, M. O., & Stupp, S. I. (2007). Supramolecular self-assembly refercodes for functional structures. *Philosophical Transactions of the Royal Society A: Mathematical, Physical and Engineering Sciences*, 365(1855), 1417-1433. doi:10.1098/rsta.2007.2024

72. Mandal, D., Shirazi, A. N., & Parang, K. (2014). Self-assembly of peptides to nanostructures. *Org. Biomol. Chem.*, 12(22), 3544-3561. doi:10.1039/c4ob00447g
73. Panda, J. J., & Chauhan, V. S. (2014). Short peptide based self-assembled nanostructures: implications in drug delivery and tissue engineering. *Polym. Chem.*, 5(15), 4431-4449. doi:10.1039/c4py00173g
74. Hamley, I. W., Dehsorkhi, A., & Castelletto, V. (2013). Coassembly in Binary Mixtures of Peptide Amphiphiles Containing Oppositely Charged Residues. *Langmuir*, 29(16), 5050-5059. doi:10.1021/la400163qI.
75. Silva, R. F., Araújo, D. R., Silva, E. R., Ando, R. A., & Alves, W. A. (2013). L-Diphenylalanine Microtubes As a Potential Drug-Delivery System: Characterization, Release Kinetics, and Cytotoxicity. *Langmuir*, 29(32), 10205-10212. doi:10.1021/la4019162.





## CHAPTER 2

### CONFORMATIONALLY-CONSTRAINED PEPTIDE MIMICS OF A KEY RSV NEUTRALIZING EPITOPE

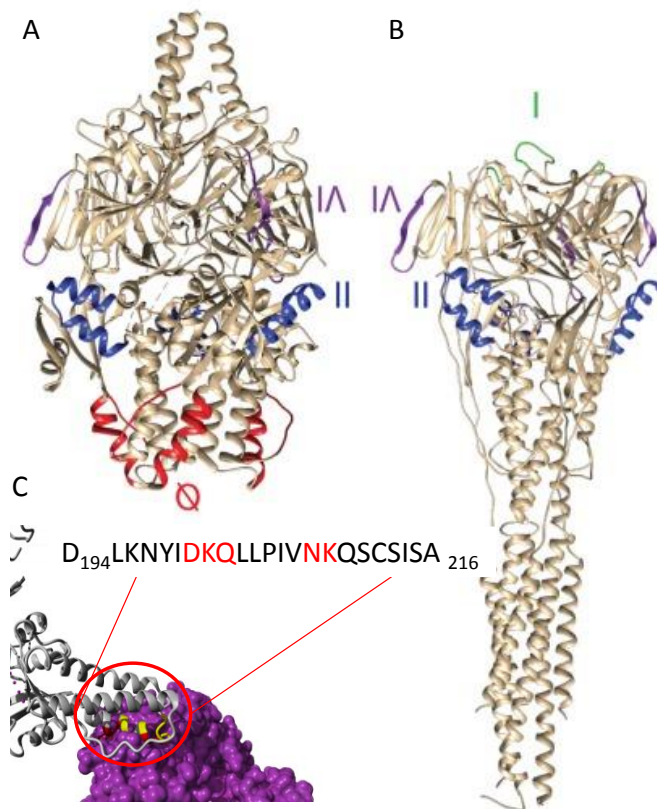
Respiratory syncytial virus (RSV) is a major pathogen that causes severe respiratory diseases in newborns and immune-compromised people. In spite of several attempts, vaccine against RSV has not yet been developed. The viral fusion glycoprotein (RSV F) plays a major role in the entry process and is the main target of neutralizing antibodies. In this study, 23 and 27-residue peptide sequences present most potent RSV antigenic site called Ø (zero) from a prefusion state of the RSV fusion protein were constrained in a helical conformation. Constraining the peptides with a single i, K (i) - D (i+4) lactam bridges was not sufficient to keep the structure helical as in its native form. However, the insertion of double staples side by side or interlocked led to formation of helical structure as proven with Circular Dichroism (CD) spectroscopy. Systematic work that we have proceeded in this study proved that designed helical peptides have potential as vaccine antigens and can be also used for the detection of antigenic site Ø specific antibodies in human sera.

#### 2.1 Introduction

Essentially all children become infected with respiratory syncytial virus (RSV) during an early stage of life. While most children show only mild respiratory disease, some may develop severe bronchiolitis and pneumonia, making RSV a major cause for hospitalization of infants.<sup>1-3</sup> In addition, RSV is a significant problem in adults and the elderly, causing morbidity and mortality similar to those seen with influenza virus.<sup>4</sup> Currently, the only available option to prevent RSV-mediated disease is the passive administration of the commercially available RSV-neutralizing monoclonal antibody (MAb) Palivizumab.<sup>5</sup> However, passive immunization provided by this antibody doesn't last season to season and its use is restricted to infants considered at high risk

of developing severe respiratory disease due to its high costs. A vaccine against RSV is not yet available.

The RSV envelope contains two glycoproteins that are the main target of the immune system: the attachment protein G and the fusion protein F (reviewed by<sup>6, 7</sup>). The F protein is considered an attractive target for the development of an effective vaccine in view of its limited antigenic variability between different RSV strains and the effectiveness of Palivizumab, which targets the F protein.<sup>5</sup> Several current RSV vaccine approaches therefore particularly focus on the induction of anti-F neutralizing antibodies.<sup>8</sup> The RSV F protein is present on infected cells and on virus particles in two conformations: the metastable prefusion and the very stable post-fusion conformation.<sup>9,10</sup> The structures of these two F protein conformations (Figure 2.1 A and figure 2.1 B) have been solved.<sup>11-13</sup> The conversion of the prefusion into the post-fusion conformation drives the fusion between the virus and host cell membranes and is essential for virus entry.



**Figure 2. 1** Prefusion and postfusion conformation of RSV F. **A)** Prefusion<sup>12</sup> and **B)** postfusion<sup>11</sup> structures of RSV F. Antigenic sites are indicated (according to reference<sup>12</sup>) as follows: prefusion-specific site  $\emptyset$  (recognized by MAbs D25 and AM22), postfusion-specific site I, site II (recognized by MAb palivizumab), and site IV, **C)** Structural analysis of D25 (shown in purple) binding to to prefusion F (1 protomer is shown in grey). D25 interacts with several residues in a helix (D200, K201, Q202 and N208 and K209, colored red) and a single residue (N63) in a loop. The sequence of the wild type (WT) peptide is indicated.

MAbs binding to different epitopes on prefusion and/or post-fusion F differ in their neutralizing capacity. Palivizumab binds to antigenic site II, which is present on both prefusion and post-fusion F. Post-fusion specific antibodies targeting antigenic site I have a much lower neutralizing capacity, while antibodies targeting the prefusion-specific antigenic site  $\emptyset$  (AM22 and D25) neutralize RSV much more effectively than Palivizumab.<sup>14</sup> In agreement herewith, vaccination with F proteins stabilized in the prefusion conformation was more effective than vaccination with post-fusion F. Moreover, analysis of RSV-specific antibody responses revealed that levels of

antibodies recognizing the prefusion-specific antigenic site correlate better with virus neutralization than levels of other antibodies.

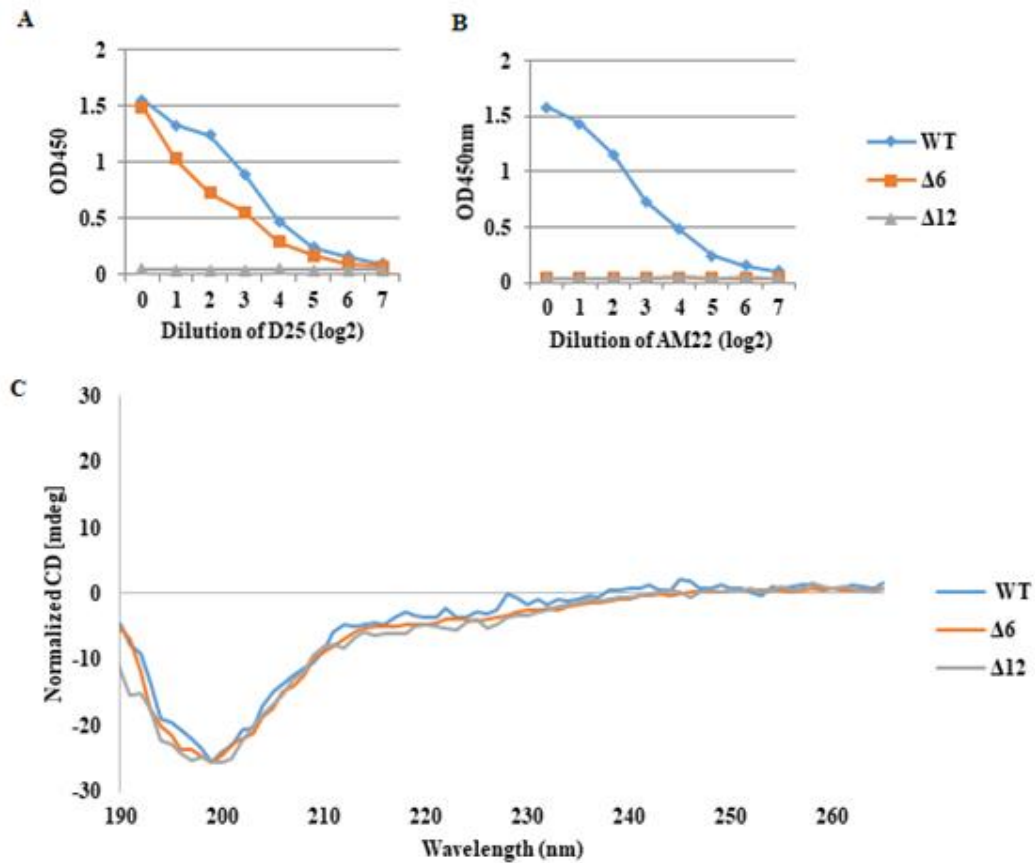
The much greater contribution of antibodies recognizing antigenic site Ø to neutralization compared to other antibodies binding to F suggests that an RSV vaccine that solely induces antigenic site Ø-specific antibodies is preferred over a vaccine that also induces antibodies against other parts of F. In addition, the absence of antibodies binding poorly or non-neutralizing antibodies is preferred as these antibodies may contribute to vaccination-induced enhancement of disease,<sup>15,16</sup> as opsonization of RSV with non-neutralizing antibodies may facilitate infection of macrophage-like cells.<sup>17</sup> In this study, we generated synthetic peptides that were recognized by different MAbs (D25 and AM22) that recognize antigenic site Ø. Subsequently, we stabilized these peptides in a helical conformation, in order to induce the conformation, found in the crystal structure of prefusion F with MAb D25, by incorporating side chain cross-links in the peptides. Peptides were selected which displayed increased binding of both D25 and AM22 and a helical conformation. Finally, we studied whether vaccination with these peptides resulted in the induction of neutralizing antibodies and whether these peptides are suitable for the detection of antigenic site Ø-specific antibody levels in human sera.

## **2.2 Results and Discussion**

### **2.2.1 Characterization of wild type (WT) peptide**

Analysis of the crystal structure of prefusion F bound with D25 shows that several residues in RSV F interact with D25, which are D200, K201, Q202 and N208 and K209 located in a helix and N63 present in a loop of the prefusion F protein<sup>12</sup> (Figure 2.1 C). As most antibody contacts were observed for this helix, we analyzed whether synthetic peptides of different lengths corresponding to this part of F (D<sub>200</sub>LKNYIDKQLLPVINKQSCSISA<sub>222</sub>, D<sub>200</sub>LKNYIDKQLLPVINKQ<sub>216</sub>, and D<sub>206</sub>KQLLPVINKQ<sub>216</sub>, referred to as WT, Δ6 and Δ12, respectively) were recognized by antibodies D25 and AM22. These antibodies were previously shown to both bind antigenic Ø, but at different angles as determined by negative stain electron microscopy<sup>12</sup> suggesting them to recognize different residues in RSV F. Binding of the antibodies was analyzed in an ELISA set up, in which the different peptides were

coated. As shown in Figure 2.2 A and B, both D25 and AM22 efficiently bound to the WT peptide. C-terminal deletion of 6 amino acids completely abrogated binding of AM22, while binding of D25 was hardly affected. No binding was observed for both antibodies with the shortest peptide. These results indicate that the WT peptide contains the minimal requirements for binding of both prefusion-specific antibodies. Furthermore, AM22 binding is more sensitive for deletion of C-terminal residues than binding of D25 is. Analysis of the conformations of these three peptide by circular dichroism showed them to be structurally disordered (Figure 2.2 C).



**Figure 2. 2** Analysis of WT and deletion mutant peptides. Interaction of WT and deletion mutant peptides with limiting dilutions of **A)** D25, **B)** AM22, **C)** CD spectrum of the WT peptide and deletion mutant peptides.

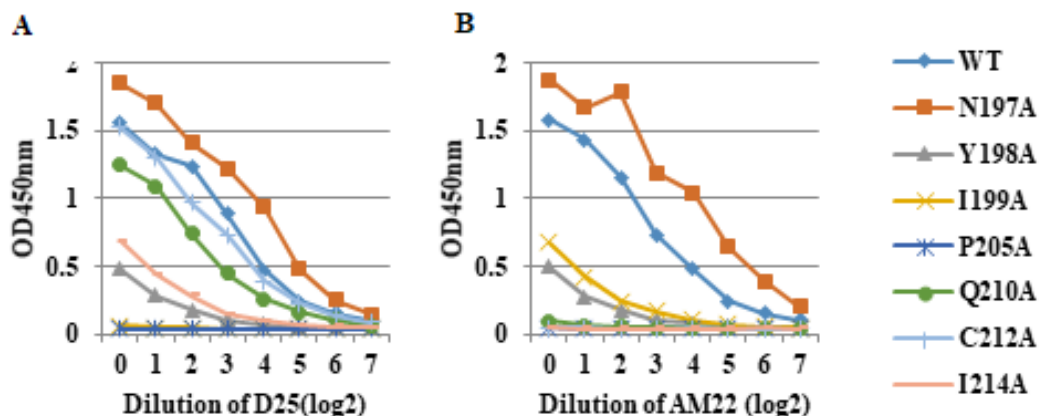
### 2.2.2 Alanine Scan

As we aim to stabilize the RSV F peptide in a (prefusion-like) helix conformation, we first investigated which side chain residues of the amino acids contribute to the binding affinity of the prefusion-specific antibodies and which residues can be modified to induce a helical conformation onto the peptide. To this end a limited alanine scan was performed on residues other than those that were already apparent to be contributing to binding to antibodies D25<sup>12, 18</sup> (Table 2.1).

**Table 2. 1** The list of peptides for alanine scan and deletion mutant peptides

Entry		
1	WT	H-DLKNYIDKQLLPIV NKQSCSISA-NH <sub>2</sub>
2	Δ12	H-DKQLLPIV NKQ-NH <sub>2</sub>
3	Δ6	H-DLKNYIDKQLLPIV NKQ-NH <sub>2</sub>
4	N197A	H-DLKAYIDKQLLPIV NKQSCSISA-NH <sub>2</sub>
5	Y198A	H-DLKNAYIDKQLLPIV NKQSCSISA-NH <sub>2</sub>
6	I199A	H-DLKNYADKQLLPIV NKQSCSISA-NH <sub>2</sub>
7	P205A	H-DLKNYIDKQLLAIV NKQSCSISA-NH <sub>2</sub>
8	Q210A	H-DLKNYIDKQLLPIV NKASCSISA-NH <sub>2</sub>
9	C212A	H-DLKNYIDKQLLPIV NKQASISA-NH <sub>2</sub>
9	I214A	H-DLKNYIDKQLLPIV NKQSCSASA-NH <sub>2</sub>

Our observations reveal that several mutations including Y198A, I199A, P205A and I214A significantly decreased binding affinity towards both antibodies (Figure 2.3 A and 2.3 B). Mutations Q210A and C212A abolished binding of AM22, but not of D25, in agreement with these antibodies displaying different binding to the deletion mutant peptides. The N197A mutation did not negatively affect binding of D25 and AM22. Hence, bridge positions were selected to avoid substitution of residues critical for the binding of both antibodies.

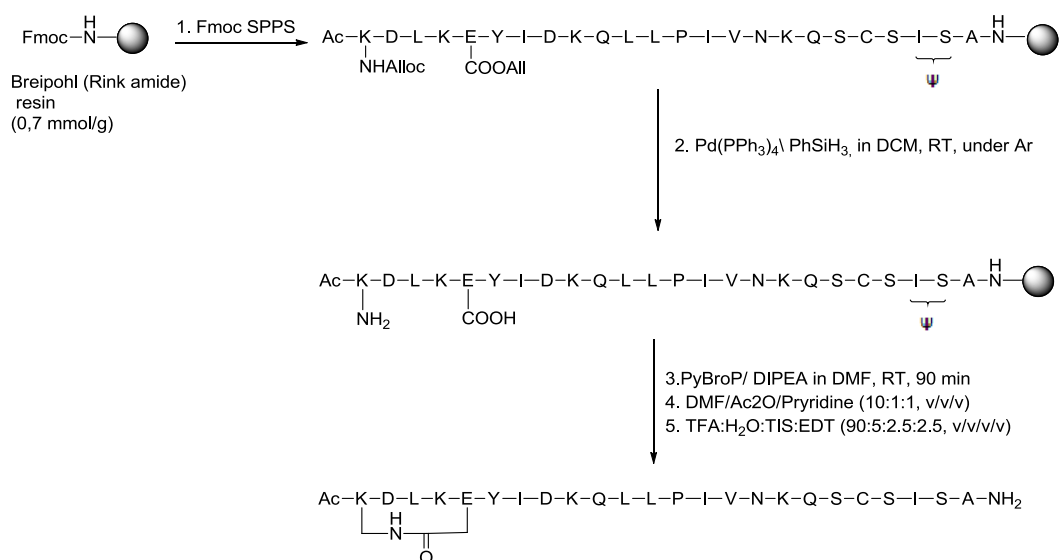


**Figure 2. 3** Interaction of WT and peptides containing different Ala substitutions with limiting amounts of **A)** D25 and **B)** AM22.

### 2.2.3 Synthesis, secondary structure and binding activity of peptides

Cyclic peptides were synthesized by cyclizing linear precursors on resin. The principle of on-resin cyclization is relied on removal of orthogonal protecting groups from the side chain of the amino acids and then ring closure while peptide is still on resin. In these work, we have used three different well-characterized methods towards the synthesis of cyclic peptides.

Our initial attempt to synthesize conformationally-constrained peptides, was based on side-chain-to-side-chain lactam bridge formation, which is one of the most applied methodology.<sup>19</sup> Amide bond was constructed between glutamic acid and lysine residues after orthogonally and selectively removal of Alloc and Allyl groups on resin Scheme 2.1.



**Scheme 2. 1** Synthesis of monocyclic K193E197 peptide with Alloc/OAll Strategy

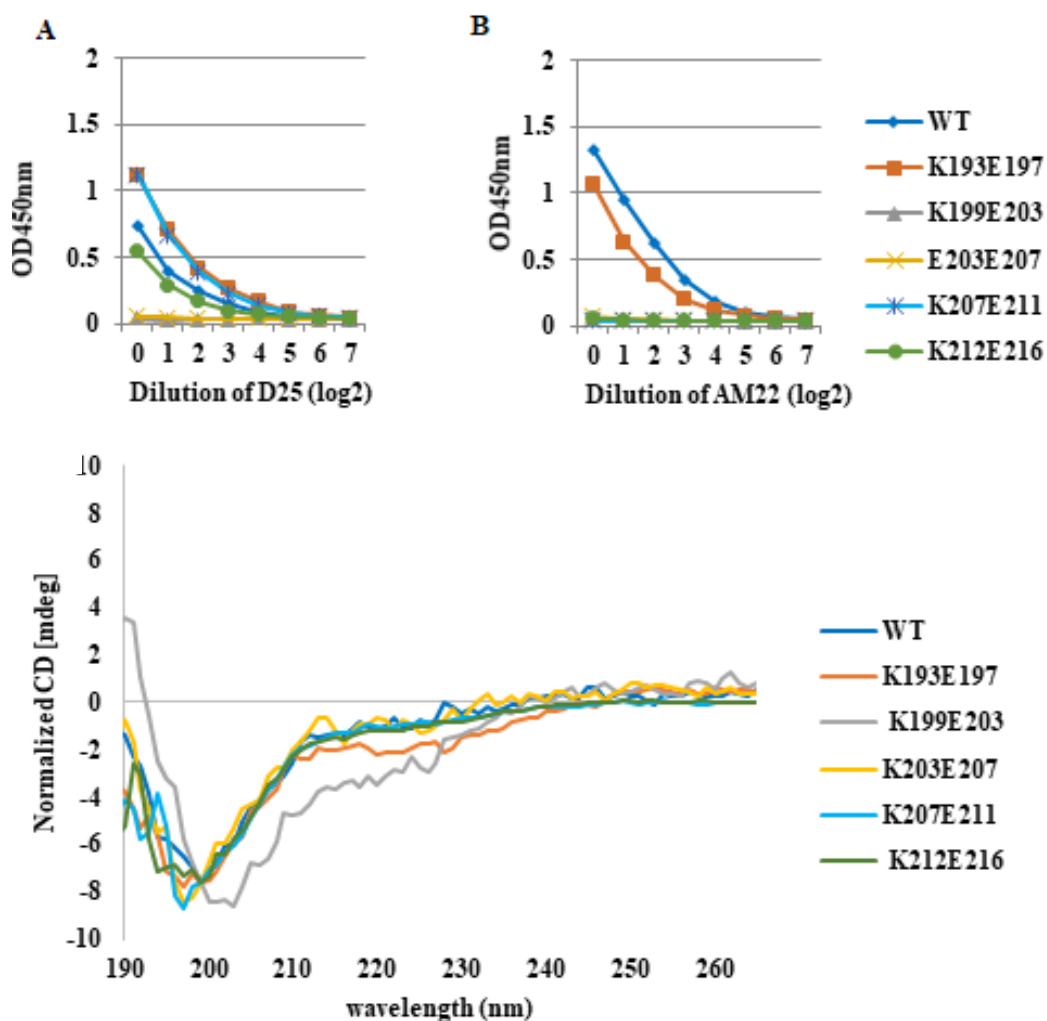
We found that the synthesis of the peptide using standard Fmoc protected amino acids was rather cumbersome because of a very difficult coupling after Ser210, but when we included a pseudo-proline<sup>20</sup> for residues Ile-214 and Ser-215 the synthesis went smoothly. Using this strategy, firstly, monocyclic Lys-Glu (KE) bridged-peptides were successfully synthesized by moving the position of the bridge from N-terminus to C-terminus (Table 2.2 entries 2-6). We positioned the bridges such that residues shown to be important for antibody binding either by the Ala scan or by the structural analysis were avoided as much as possible. In order to be able to make a bridge with the N-terminal residue 197, we extended the peptide sequence with an additional lysine (K193).



**Table 2. 2** Sequences of Lys-Glu (KE) single and double bridged peptides and a linear WT peptide (residues that are used for linkage are highlighted in red).

Entry		
1	WT	---DLK <b>N</b> YIDKQLLP <b>I</b> VNKQSCSISA
<b>KE single bridged peptides</b>		
2	K193E197	---KDL <b>K</b> EYIDKQLLP <b>I</b> VNKQSCSISA
3	K199E203	---DLK <b>N</b> Y <b>K</b> DKQ <b>E</b> LPIV <b>N</b> KQSCSISA
4	K203E207	---DLK <b>N</b> YIDKQ <b>K</b> LPI <b>E</b> NKQSCSISA
5	K207E211	---DLK <b>N</b> YIDKQLLP <b>I</b> K <b>N</b> KQ <b>E</b> CSISA
6	K212E216	---DLK <b>N</b> YIDKQLLP <b>I</b> V <b>N</b> KQ <b>S</b> K <b>S</b> I <b>S</b> E
<b>KE double bridged peptides</b>		
7	K193E197-K199E203	---KDL <b>K</b> EY <b>K</b> DKQ <b>E</b> LPIV <b>N</b> KQSCSISA
8	K193E197-K203E207	---KDL <b>K</b> EYIDKQ <b>K</b> LPI <b>E</b> NKQSCSISA
9	K193E197-K207E211	---KDL <b>K</b> EYIDKQLLP <b>I</b> K <b>N</b> KQ <b>E</b> CSISA
10	K193E197-K212E216	---KDL <b>K</b> EYIDKQLLP <b>I</b> V <b>N</b> KQ <b>S</b> K <b>S</b> I <b>S</b> E
11	K207E211-K212E216	---DLK <b>N</b> YIDKQLLP <b>I</b> K <b>N</b> KQ <b>E</b> K <b>S</b> I <b>S</b> E
12	K190E194-K193E197	<b>K</b> KV <b>K</b> E <b>L</b> K <b>E</b> YIDKQLLP <b>I</b> V <b>N</b> KQSCSISA

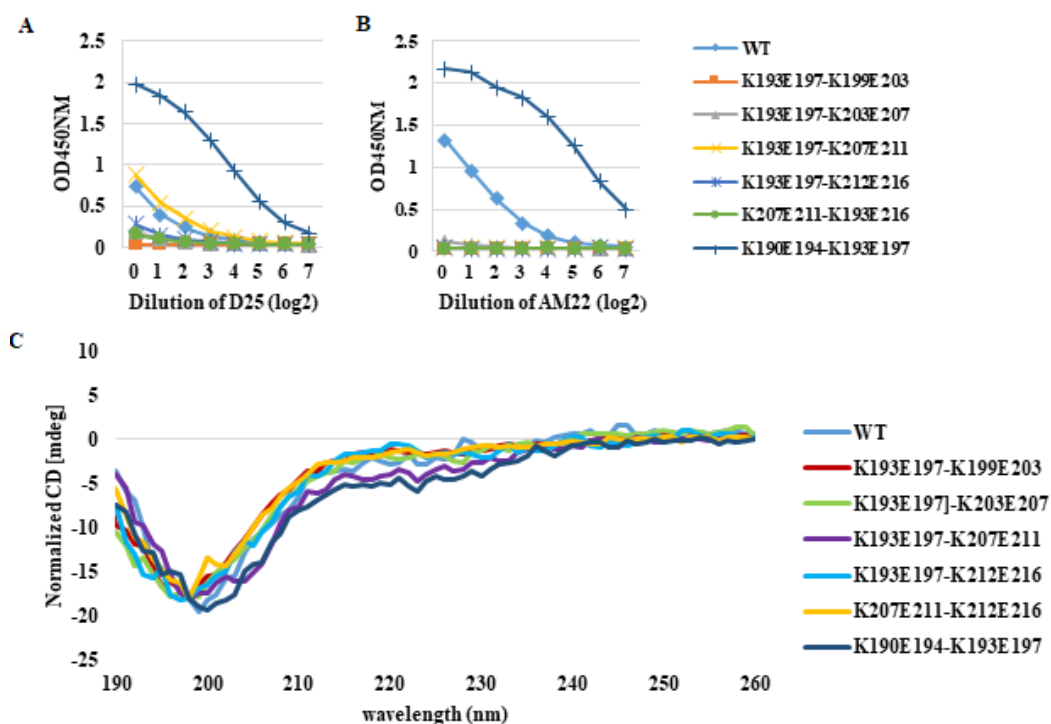
Typically, circular dichroism (CD) spectroscopy revealed that these constrained peptides still adopted a random coil with no defined – random coil - secondary structure. In addition to this, antibody binding to the bridged analogs was either similar or much reduced compared with the native sequence (WT). In addition, besides WT only the K193E197 peptide was efficiently bound by both antibodies (Figure 2.4).



**Figure 2. 4** Single bridged Lys-Glu (KE) peptides. **A)** Binding affinity of peptides against D25, **B)** Binding affinity of peptides against AM22, **C)** Normalized CD spectra.

Since these constrained peptides did not show any trace of helicity and poor binding, we decided to incorporate an additional bridge in the sequence and prepared double-bridged KE peptides (Table 2.2 entries 7-12). Since some minor improvement was observed when bridge formation was carried out in position 193 and 197, second bridges were constructed in addition to K193E197 bridge. Peptide sequence was extended for the synthesis of entry 12, with four more aminoacids from N-terminus of WT peptide (Table 2.2). To our surprise, again no specific secondary structure was observed by CD spectroscopy and binding to the antibodies was completely suppressed (Figure 2.5 C).

Apparently, the doubly bridged peptides were constrained to conformations that are not compatible with the binding sites of the site  $\emptyset$  specific antibodies (Figure 2.5 A, 2.5 B).



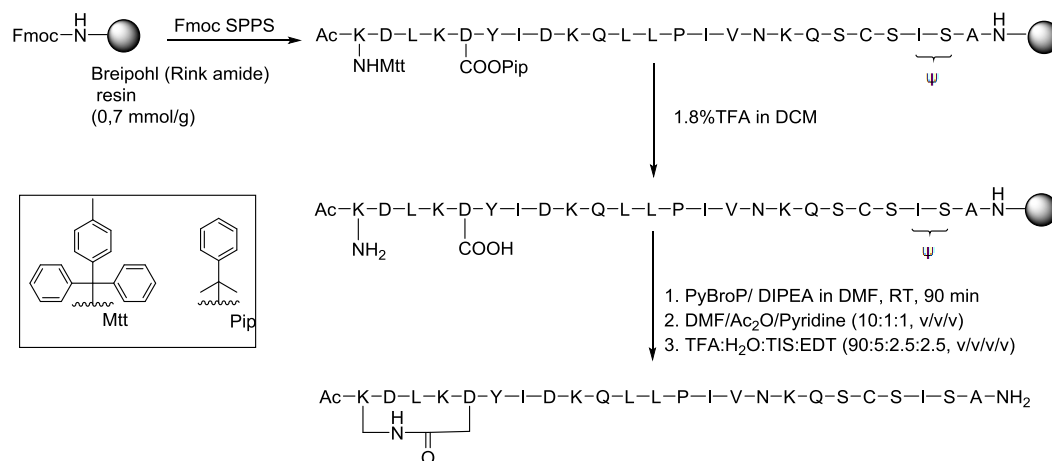
**Figure 2. 5** Double bridged Lys-Glu (KE) peptides. **A)** Binding affinity of peptides against D25, **B)** Binding affinity of peptides against AM22, **C)** Normalized CD spectra

Next, we embarked on the synthesis of an analogous series monocyclic Lys-Asp (KD) bridged peptides (table 1, entries 7-11) to examine the effect of bridge size on both secondary structure formation and binding affinity.

**Table 2. 3** The list of WT and KD mono-bridged peptides in this study (residues that are used for linkage are highlighted in red).

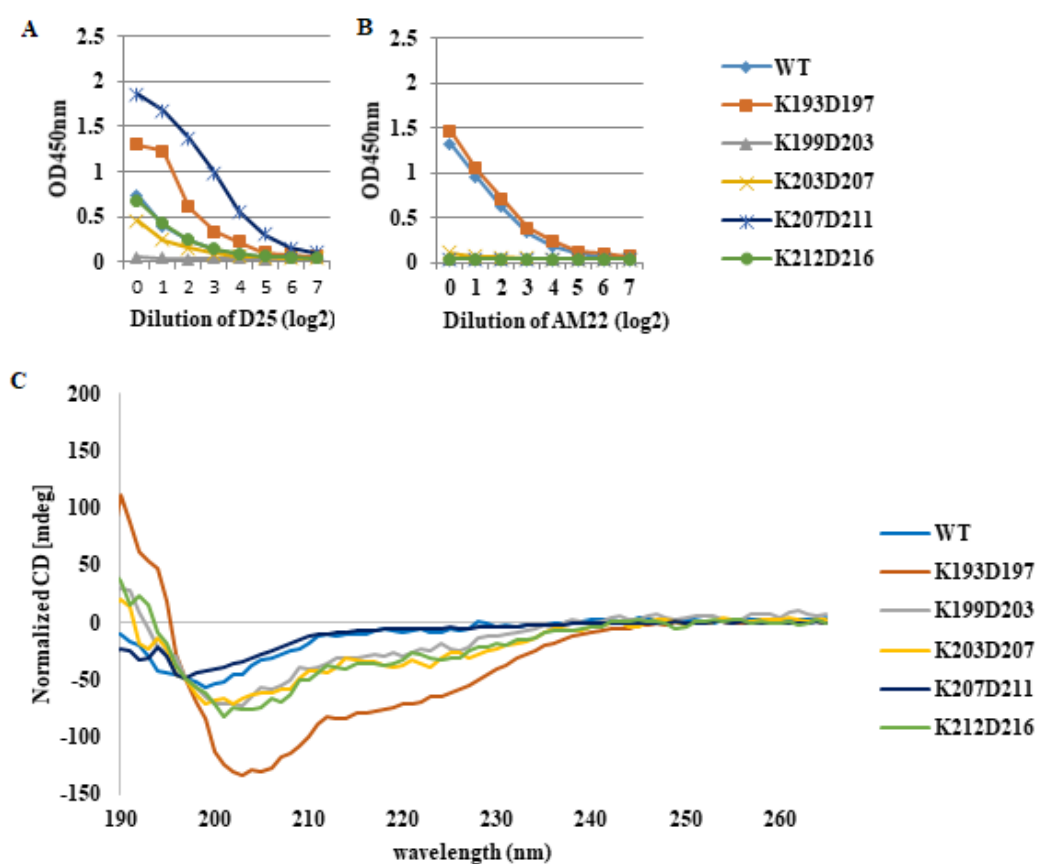
Entry		
1	WT	----DLK <sup>N</sup> YIDKQLLP <sup>I</sup> IVNKQSCSISA
<b>Single bridged peptides</b>		
2	K193D197	<b>KDLKD</b> YIDKQLLP <sup>I</sup> IVNKQSCSISA
3	K199D203	-DLK <sup>N</sup> Y <b>KDKQD</b> LPIV <sup>N</sup> NKQSCSISA
4	K203D207	-DLK <sup>N</sup> YIDKQ <b>KLPID</b> NKQSCSISA
5	K207D211	-DLK <sup>N</sup> YIDKQLLP <b>IKNKQD</b> CSISA
6	K212D216	-DLK <sup>N</sup> YIDKQLLP <sup>I</sup> IVNKQ <b>KSISD</b>

Again, an Alloc/Allyl strategy<sup>21</sup> was applied, but this was found to fail for some sequences due to the propensity of allyl ester protected aspartates to undergo base-induced aspartimide formation.<sup>22</sup> To circumvent this problem we decided to resort to the mild acid-labile protecting groups N-methyltrityl (Mtt) and phenylisopropyl (Pip) for the lysine and aspartic acid residues<sup>23</sup> respectively (Scheme 2.2 ).



**Scheme 2. 2** Strategy used for the synthesis of Lys-Asp (KD) mono bridge using acid labile methyltrityl (Mtt) and phenylisopropyl (Pip) groups.

Circular dichroism spectra of four out of five Asp-Lys bridged peptides revealed secondary structure formation, having negative bands at 205 and 222 nm, indicative of some helical structure (Figure 2.6 C). Of these peptides again the peptide bridged between residue 193 and 197 (K193D197) was the only one that displayed increased (D25) or comparable (AM22) binding compared to the linear WT peptide (Figure 2.6 A and 2.6 B). This time also some helicity could be observed as determined by CD spectroscopy (Figure 2.6 C).



**Figure 2. 6** Single bridged Lys-Asp (KD) peptides. **A)** Binding affinity of peptides against D25, **B)** Binding affinity of peptides against AM22, **C)** Normalized CD spectra

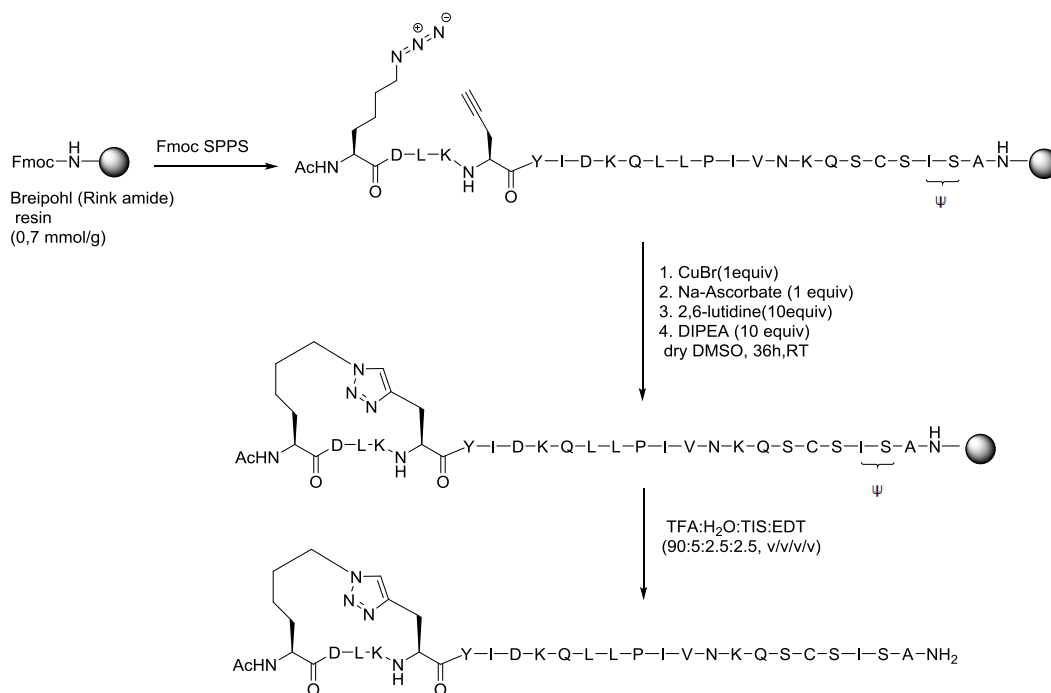
With this knowledge, we decided to focus on the 193-197 position for bridge formation (Table 2.4). Firstly, we decreased the bridge length by substituting lysine to

ornithine (O) and synthesized O193D197 macrocycle. However, the introduction of this shorter lactam bridge into that position caused reduction of binding and loss of helicity (Figure 2.7).

**Table 2. 4** The list of monocyclic peptides with different type and length of bridges. (O = ornithine, C = homo-Cysteine, X = azido-Lysine and Z = propargyl-Glycine, yellow colored A represents the cysteine substituted with alanine)

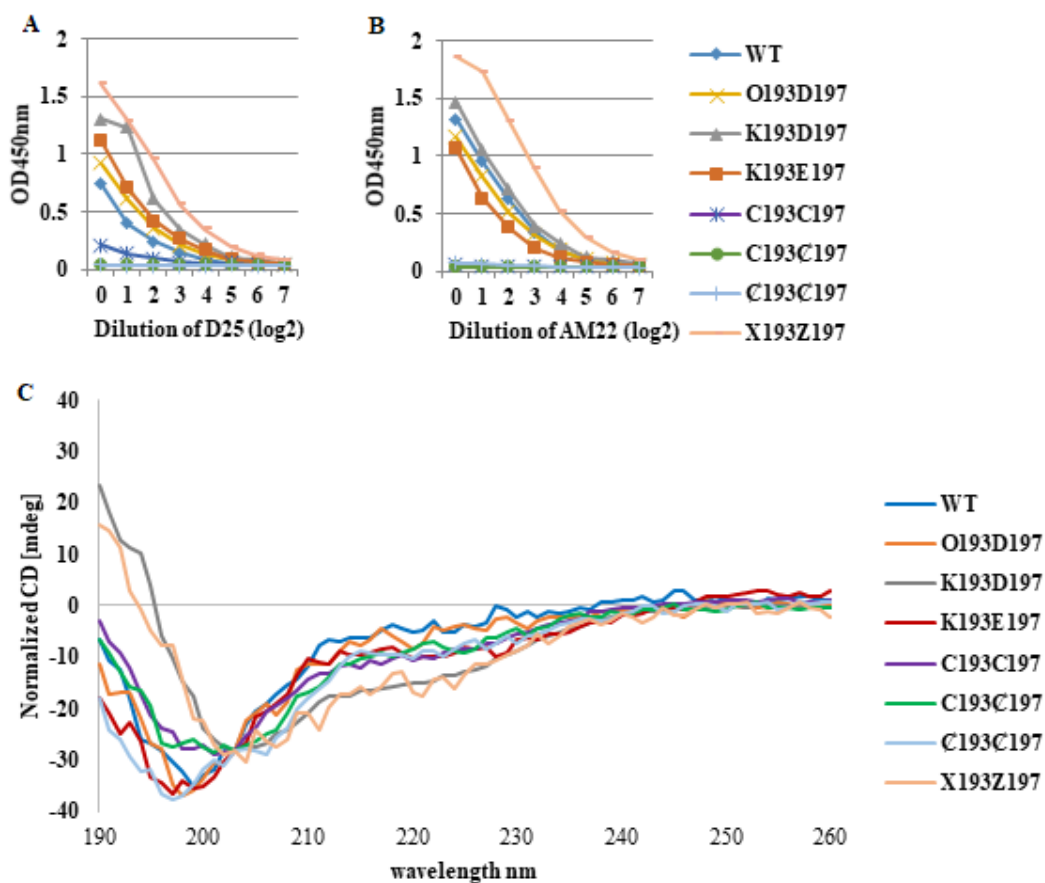
Entry		
1	WT	----DLK <b>N</b> YIDKQLLP <b>I</b> VNKQSCSISA
2	O193D197	<b>O</b> DLK <b>D</b> YIDKQLLP <b>I</b> VNKQSCSISA
3	X1193Z197	<b>X</b> DLK <b>Z</b> YIDKQLLP <b>I</b> VNKQSCSISA
4	C193C197	<b>C</b> DLK <b>C</b> YIDKQLLP <b>I</b> VNKQ <b>S</b> A <b>S</b> ISA
5	C193C197	<b>C</b> DLK <b>C</b> YIDKQLLP <b>I</b> VNKQ <b>S</b> A <b>S</b> ISA
6	C193 C197	<b>C</b> DLK <b>C</b> YIDKQLLP <b>I</b> VNKQ <b>S</b> A <b>S</b> ISA

The bridge type is another factor that was examined. For this purpose, X193Z197 (X = azido-Lysine and Z = propargyl glycine) triazole bridged peptide was synthesized using CuAAC on resin <sup>24</sup> (Scheme 2.3). Although this mimetic showed a slightly increased binding affinity, no significant increase on helicity compared to K193D197 was found (Figure 2.7).



**Scheme 2. 3** Azide–alkyne cycloaddition in the synthesis of bridged peptide

Another convenient and straightforward method for constraining a peptide into a macrocycle is the bridging of two internal thiol groups forming a disulfide bridge after a simultaneous oxidation.<sup>25</sup> With the synthesis of, C193C197, C193C197, C193C197 (C: Cysteine, C: Homocysteine) sulfur bridge peptides with decreasing bridge size, the effect of both bridge type and size was evaluated. None of these cysteine bridged peptides displayed any helicity nor significant binding against the antibodies (Figure 2.7). We inferred that ring size is the most important factor that governs helicity and for this peptide an ideal ring size is obtained when it is bridged between a lysine and aspartic acid residue.



**Figure 2. 7** Single bridged peptides varying in bridge length and type. **A)** Binding affinity of peptides against D25, **B)** Binding affinity of peptides against AM22, **C)** Normalized CD spectra of peptides. (C denotes a homocysteine).

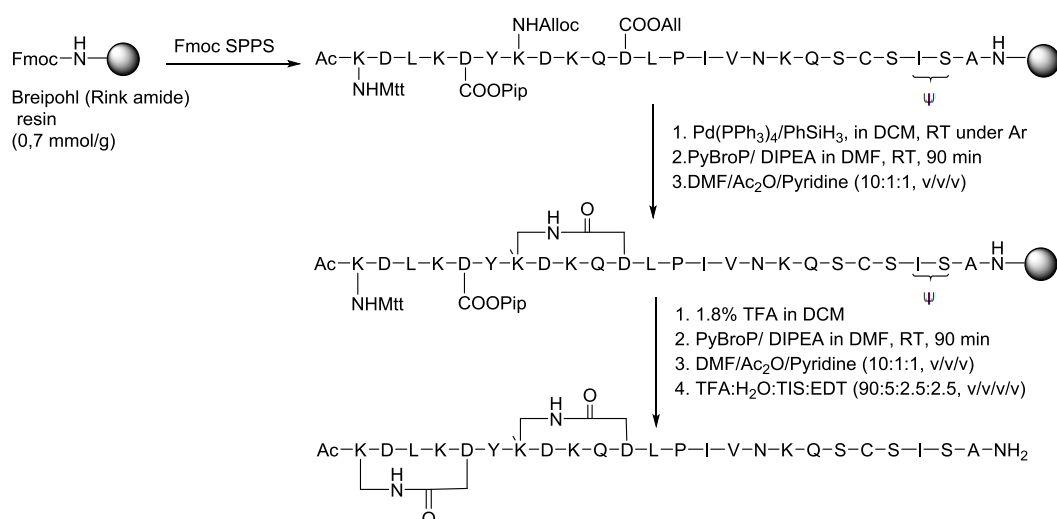
Encouraged by both the presence of helicity and affinity for the two of K193D197 bridged peptide we decided to synthesize bicyclic KD-bridged peptides (Table 2.5).



**Table 2. 5** The list of double bridged KD peptides and the WT peptide

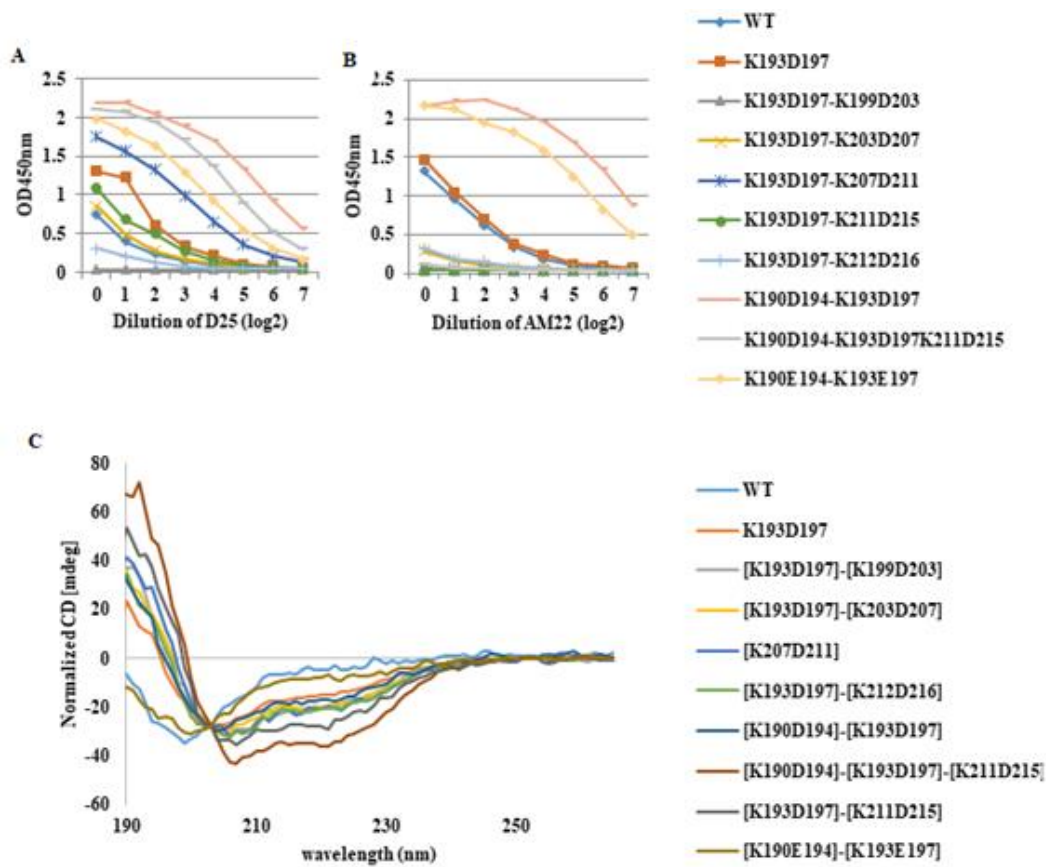
Entry		
1	WT	---DLKNYIDKQLLPVINKQSCSISA
2	K193D197-K199D203	---KDLKDYKDKQDLPIVINKQSCSISA
3	K193D197-K203D207	---KDLKDYIDKQKLPIDNKQSCSISA
4	K193D197-K207D211	---KDLKDYIDKQLLPINKKQDCSISA
5	K193D197-K211D215	---KDLKDYIDKQLLPVINKQKCSIDA
6	K193D197-K212D216	---KDLKDYIDKQLLPVINKQKSISD
7	K190D194-K193D197	KKVKDLKDYIDKQLLPVINKQSCSISA
8	K190D194-K193D197-K211D215	KKVKDLKDYIDKQLLPVINKQKCSIDA

KD double-bridged peptides were synthesized using both Alloc/Mtt protected lysines and Allyl/Pip protected aspartic acids were used in same sequence. The two bridges were constructed, by first removing the Alloc group from the lysine and the Allyl group from aspartic acid and closing of the first bridge after which unreacted lysine residues were capped. Subsequently, Mtt and Pip protections were removed using mild acidic cleavage conditions followed by a second cyclization (Scheme 2.4).



**Scheme 2. 4** Strategy used for the synthesis of Lys-Asp (KD) double bridges using both acid labile Mtt/Pip groups and catalytically cleavable of Alloc/Allyl groups.

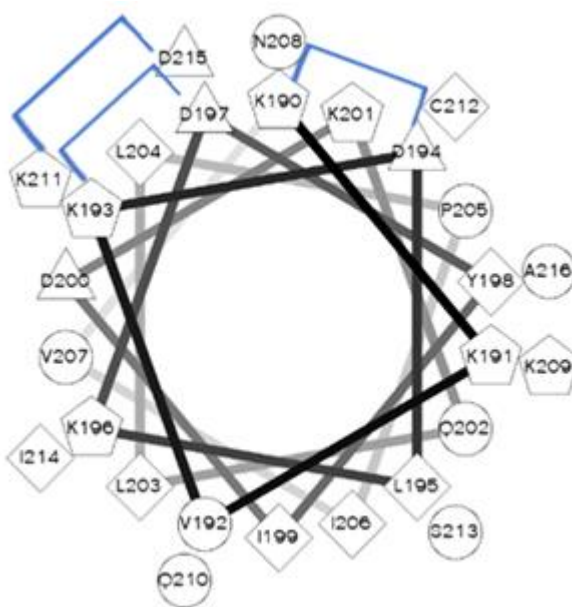
Reversing the order of both orthogonal cleavage-cyclization methods did not have any influence on the synthesis. In order to be able to introduce two bridges N-terminally without having to replace any critical residues we included a peptide that was extended N-terminally with three residues. Of these bicyclic peptides, K190E194-K193E197 and K190D194-K193D197 of which only the latter showed helicity and increased binding compared to linear WT (Figure 2.8).



**Figure 2. 8** Double and a triple bridged peptides. **A)** Binding affinity of peptides against D25, **B)** Binding affinity of peptides against AM22, **C)** Normalized CD spectra of peptides

As seen in the alpha-helical diagram (Figure 2.9), when an additional bridge at the position K211D215 is introduced, it will be on the same side of a potential helix as the K193D197 bridge which may help to constrain the peptide even further. To test this

hypothesis, we introduced a third bridge by synthesizing tricyclic peptide, K190D194-K193D197-K211D215. As envisioned, addition of this third bridge induced more helicity than the double bridged peptide. However, binding affinity of this peptide was lost this time (Figure 2.8 A and 2.8 B). This indicates that introduction of further helicity does not necessarily increase binding affinity for the two antibodies. In specific we found that introduction of a bridge in the 211-215 position resulted in reduced affinity for the AM22 antibody. A possible explanation for this could be that in a bound state, this part of the peptide only has 58% helicity and thus constraining this part too much will also result in loss of binding.<sup>12</sup> Moreover, the C-terminal is apparently important in binding to AM22 as it was also found for the truncated and single bridged peptides (*vide infra*).

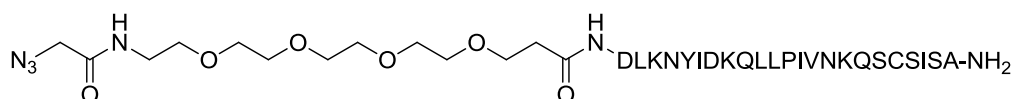


**Figure 2. 9** Alpha helical wheel representation of triple bridged peptide K190D194-K193D197-K211D215 (This image was drawn in web-based program created by Don Armstrong and Raphael Zidovetzki).

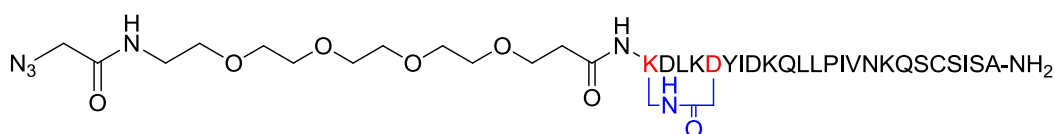
## 2.2.4 Conjugation of potent peptides to KLH via SPAAC reaction

Two of the conformationally constrained peptides (K193D197 and K190D194-K193D197), showing a markedly enhanced helicity and binding to D25 and AM22 antibodies (Figure 2.7), were selected for the further immunization assays. Since the substitution of Cys212 with another amino acid resulted in losing binding affinity, we avoided using thiol-maleimide chemistry for conjugation of the peptides. Instead, biorthogonal Strain-Promoted Azide Alkyne Click (SPAAC) reaction was employed.<sup>26-29</sup>

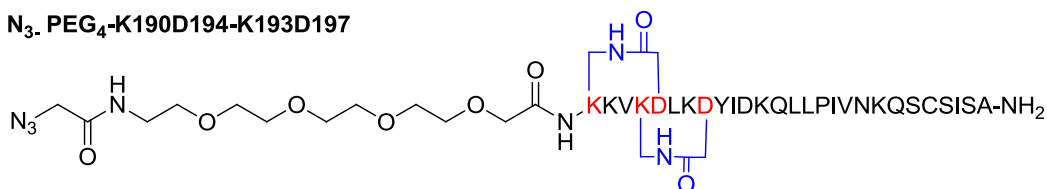
### N<sub>3</sub>-PEG<sub>4</sub>-WT



### N<sub>3</sub>-PEG<sub>4</sub>-K193D197



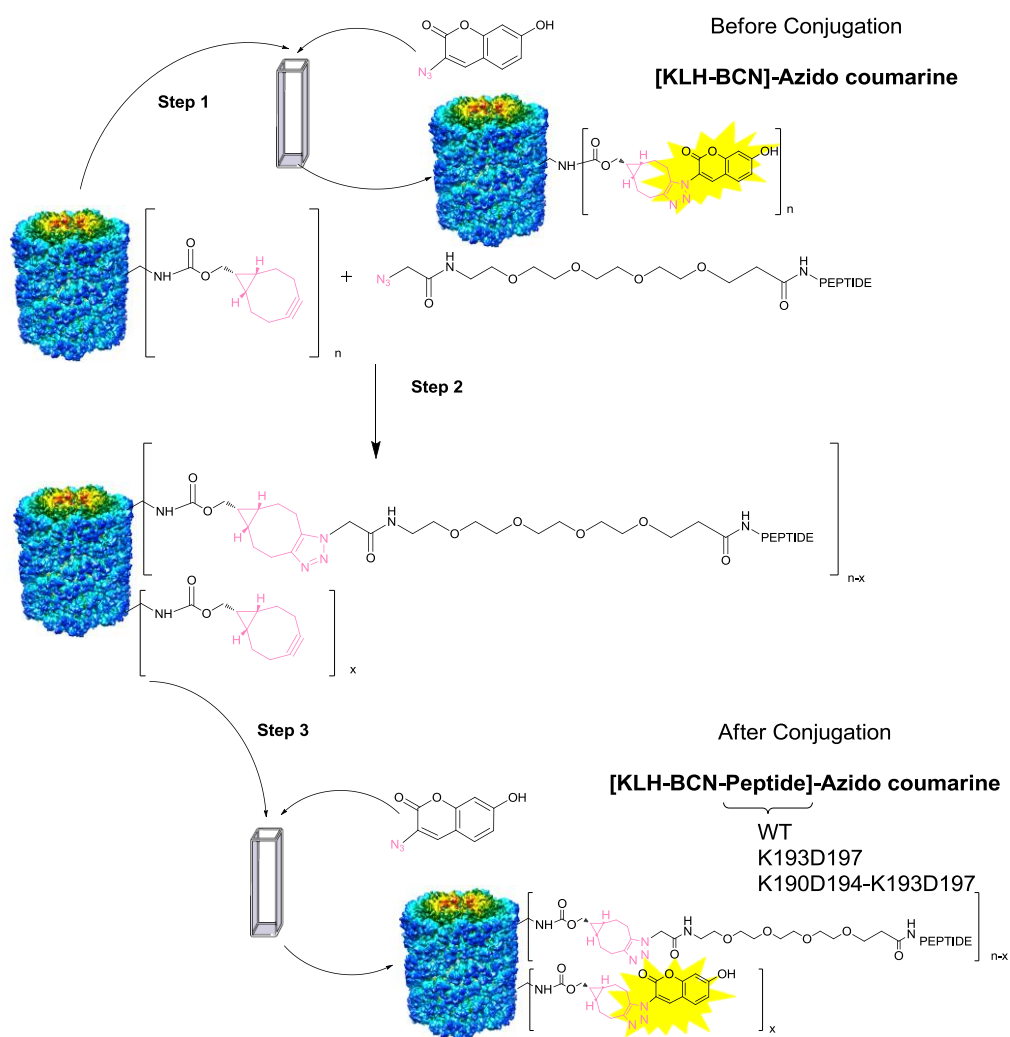
### N<sub>3</sub>-PEG<sub>4</sub>-K190D194-K193D197



**Figure 2. 10** Modified azido peptides

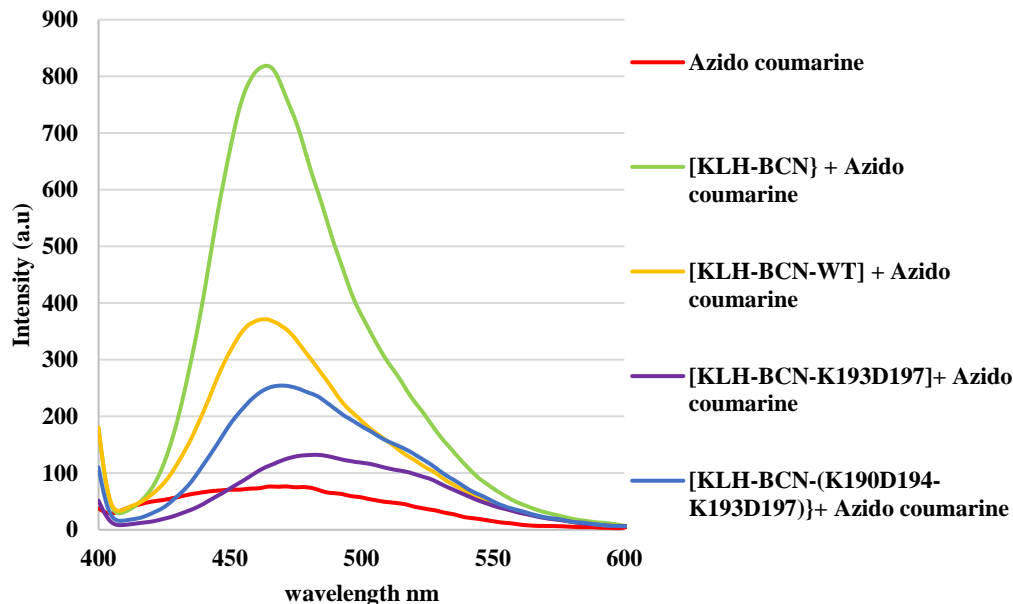
KLH (Keyhole Limpet Hemocyanin) protein was derivatized with a BCN (bicyclo [6.1.0] nonyne) group from the lysines, such that the strained alkyne group can be reacted with an azide group on our peptides. In order to monitor the BCN modification, 3-Azido-7-hydroxycoumarin (N<sub>3</sub>-Coumarin) fluorophore was added to aliquots of protein solutions and emission of clicked coumarin was measured at 460 nm.

The N-terminus of the selected conformationally constrained peptides and the linear control peptide were extended with a small PEG<sub>4</sub> spacer and subsequently coupled to 2-azido acetic acid (Figure 2.8). It was proved with both ELISA and octet analysis assays that linker is essential for efficient binding. Synthesized azido peptides were conjugated to KLH via a SPAAC reaction, obtaining peptide-carrier protein conjugates (Scheme 2.5).



**Scheme 2. 5** KLH Conjugation of Peptides via SPAAC reaction. Before and after the conjugation the decrease of BCN concentration was followed by fluorescence intensity of clicked 3-Azido-7-hydroxycoumarin.

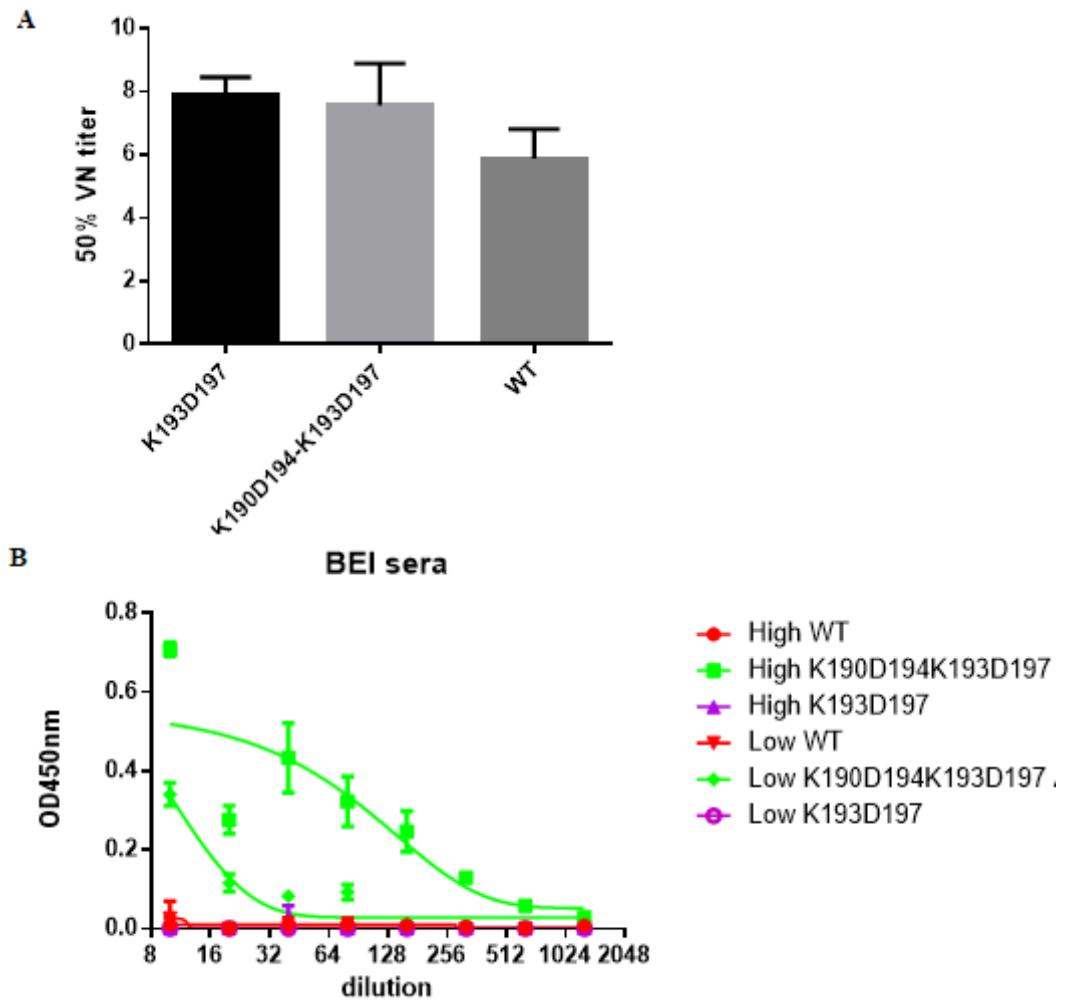
Peptide conjugation was also visualized with the help of N<sub>3</sub>-coumarin, since the amount of free BCN was decreased after the peptide conjugations, the signal of clicked coumarin at 460nm also decreased (Figure 2.11).



**Figure 2. 11** The intensity of clicked azido coumarin fluorescence (a. u.) against wavelength (nm) as a result of SPAAC reaction.

Mice were immunized with the peptides conjugated to KLH. VN titers were determined using a luciferase expressing RSV. VN50% titers were determined (Figure 2.12 A). Titers of the mice that received the stabilized peptides were significantly higher than the titers of the mice that received the WT peptide, which were similar to the titers observed in non-immunized mice. Titers were however relatively low indicating that there is room for improvement. The different ELISAs (using helical peptides and a WT peptide) were validated using pooled human control sera that were obtained from beiRESOURCES (Figure 2.12 B) and that have either a low or high RSV-neutralizing titer (beiRESOURCES NR-4023 and NR-4021, respectively). These sera have been shown by us<sup>30</sup> and others to differ in VN and F-ELISA titers. Only the double-bridged peptide result in detectable binding of antibodies present in

pooled human control sera. These control sera were previously shown to significantly differ in the amount of antigenic site Ø specific antibodies by competition ELISA. Our results indicate that also the double-bridged peptide can be used to analyze antigenic Ø specific antibody levels in sera. (Much easier assay than competition Elisa).



**Figure 2.12** Reactivity of pooled human control sera **A)** 50% Virus neutralization titer **B)** Binding of human control sera to stabilized peptides

## 2.3 Experimental

### 2.3.1 General Peptide Synthesis and Purification Procedures

All chemical reagents and solvents were of ACS grade or higher and purchased from commercial sources unless otherwise stated. Breipohl (Rink amide) resin was obtained from Bachem, coupling reagents and protected amino acids were obtained from Novabiochem, Bachem or Iris Biotech GmbH. MilliQ was double deionized using a Labconca Water Pro PS purification system (18.1 MW).

Peptides were prepared using Fmoc solid-phase peptide chemistry on Breipohl resin (Rink amide resin) with a loading capacity of 1 mmol/g. The dry resin was swelled with DMF before use. Fmoc deprotections were achieved with 3x6 min treatment of resin with 20% piperidine in DMF. Couplings were carried out with 3.0 equivalents of the required amino acid, 3.3 equivalents of DIPCDI and 3.6 equivalents of HOBT in DMF. After each coupling unreacted N-terminal of peptides were capped with solution of DMF/Ac<sub>2</sub>O/Pyridine (10:1:1). After each coupling and deprotection Kaiser Test was used to ensure the reaction had gone to completion<sup>1</sup>. Double couplings were performed if necessary. As a result of difficulty encountered during the coupling of Fmoc-Ile-OH at position 214 Fmoc-Ile-Ser (psiMe, Mepro)-OH dipeptide was used. When the synthesis finished, resin was washed with DMF, DCM, MeOH, DCM and ether respectively and air-dried for at least 1h. The peptide was cleaved from the resin and fully deprotected by treatment of the resin with a mixture of TFA/TIS/H<sub>2</sub>O/EDT (90: 2.5: 2.5: 2.5, v/v/v/v) for 3 hours. Free peptides were separated from the resin by filtration and the resin was further washed with TFA. Collected filtrate was precipitated in diethyl ether and centrifuged. The supernatant was removed and diethyl ether was further added to repeat the washing step up to three times. The precipitate was dried, lyophilized in water and purified using preparative RP-HPLC. Purity was evaluated by analytical RP-HPLC and identity confirmed by mass spectrometry.

Preparative HPLC was performed on a Shimadzu LC-20AT Prominence system, employing a Phenomenex C18 column (21.2 × 150 mm, 10 μm) at flow rate of was 6ml/min. Acetonitrile/water gradient containing 0.1% trifluoroacetic acid (5-100%, 1-



70 min) was utilized as eluent. Purity of each fraction was assessed with analytical RP-HPLC, before combining pure fractions.

Analytic HPLC was performed on a Shimadzu LC-20AT Prominence system equipped with a ReproSil C18 column (150 x 3 mm, 3  $\mu$ m). After purity of collected fractions confirmed by analytical HPLC, lyophilization was achieved using an ilShin Freeze Dryer. Elution of the peptides was achieved using an acetonitrile/water gradient containing 0.1% trifluoroacetic acid (5-100%, 1-50 min, flow 0.4 mL/min).

LC-MS was performed on a Thermo Finnigan LCQ-Fleet ESI-ion trap equipped with a ReproSil-Pur C18-AQ column (2x200 mm, 3 $\mu$ m), 0,2 ml\min flow and using the same gradient as used for HPLC (5-100%, 1-50 min) , only trifluoroacetic acid was replaced with formic acid

### **2.3.2 Lactamization**

#### *Alloc/OAll Strategy*

When the elongation of peptide sequence was complete, resin was washed with dry DCM (3x2 min) and suspended in DCM. In the presence of argon was added of PhSiH<sub>3</sub> (24 equiv.) and the resin was stirred for 2 min. Subsequently, a solution of Pd(PPh<sub>3</sub>)<sub>4</sub> (0.25 equiv.) in DCM was added while argon passing continuously through the resin and left to stirring for 30 minute, after which ninhydrin test gave an intense blue color. The reaction was also monitored with LC-MS after cleavage of peptides from a resin aliquot, additional treatments were done if Alloc or/and Allyl still on resin. Freshly prepared catalyst was used to obtain complete removal of the protections. After finishing the deprotection, the peptidyl resin was washed with DCM, DMF, and again with DCM and the process was repeated if necessary. The peptide resin was re-suspended in DMF, followed by on-resin cyclization of the peptide via the free carboxylic acid side-chain of glutamic acid and the free amino group side-chain of lysine by addition of PyBroP (3 equiv.), DIPEA (6 equiv.) for 90 min. This process was repeated until a negative Kaiser test obtained. Acetylation of unreacted amines was accomplished using typical capping solution. Finally, the cyclic peptides were removed from the resin, purified and characterized as previously described methods.

### ***Mtt/OPip Strategy***

Breipohl resin carrying Mtt/Pip protected peptide was swollen in DCM prior to use and then treated with 1.8% TFA (v/v) in DCM for 3 min at room temperature, repeated 10 times, using 10ml solution per 1 g of resin<sup>4</sup>. Methyltrityl cation produces yellow color in DCM/TFA solution, and Varian Cary® 50 UV-Vis spectrophotometer was used to measure absorbance of collected samples at 460 nm. When the removal of Mtt protection was finished, resin was washed with DCM, then DMF and free amine and acid were coupled with PyBroP (3 equiv.), DIPEA (8 equiv.) for 90 min. Excess DIPEA was used as a precaution for the presence of TFA, trapped into the resin beads.

### **2.3.3 On Resin Side-Chain Cyclization Using CuAAC**

200mg of resin (0.016mmol) was placed in 10ml reaction vessel and allowed to swell in DCM under flow of argon for 30min. After removal of DCM, CuBr (0.016mmol) completely dissolved in dry DMSO (1 mL) sodium ascorbate (3.17 mg, 0.016 mmol) dissolved in water (200  $\mu$ L), 2, 6-lutidine (18.0  $\mu$ L, 0.16 mmol), and DIEA (28  $\mu$ L, 0.16 mmol) were added to the resin. Argon was purged through the reaction vessel for 10 min, and reaction vessel was sealed and gently shaken on roller band at room temperature for 36h (Scheme 4.1). Resin was then successively washed with Isopropanol: DMSO (5:3, 3 mL x3), followed by DMF (3 mL x3) and DCM (3 mL x 3). The resin was then dried under vacuum before cleavage

### **2.3.4 Disulfide bridge formation**

Simultaneous iodine oxidation of S-Trityl-cysteine and S-Acetamidomethyl-cysteine residues was used give cystine peptides<sup>5</sup>. 0.1g of both S-trityl and S-acetamidomethyl cysteine containing peptidyl resin was exposed to 10ml solution of  $4 \cdot 10^{-2}$ M iodine in DMF with air bubbling. After a reaction time of 5 min. excess iodine was reduced with ascorbic acid. Resin was washed with DMF, DCM, MeOH and ether respectively and dried with suction in an open air. 5mg of resin was transferred into the eppendorf and 2 ml of a solution of Ellman's reagent ( $2.5 \times 10^{-3}$  M, in methanol), is added followed by 5  $\mu$ L DIPEA, then left on a shaker for 30min. Solution was diluted with methanol, then absorbance at 412 nm measured against a methanol reference<sup>6</sup>.

### 2.3.5 Peptide Conjugation to KLH via SPAAC reaction

BCN-NHS was purchased from SynAffix. Hemocyanin from *Megathura crenulata* (keyhole limpet) PBS solution 3.0-7.0 mg/mL protein ( $A_{280}$ ) was supplied from Sigma. Amicon Ultra-0.5 mL Centrifugal Filters were bought from Merck Millipore. 3-azido-7-coumarin ( $N_3$ -coumarin) was kindly donated by research assistant Jan Dommerholt from Radboud University.

KLH (Keyhole Limpet Hemocyanin) protein was derivatized with a BCN (bicyclo [6.1.0] nonyne) group from the lysines, such that alkyne group can be reacted with azide group on peptide mimetics, in a biorthogonal click chemistry reaction.

50  $\mu$ l of 3-7 mg/ml KLH solutions in PBS was transferred into a vial and 400 equiv. of BCN-NHS dissolved in DMSO was added on it. Reaction mixture was left stirring on roller band for 4h and then spin-filtered with Amicon Ultra-0.5 mL Centrifugal Filters. Solution left in the filtered (20  $\mu$ l) were washed with PBS (0.9M NaCl containing, pH 7.2). Total volume completed to 200  $\mu$ l and analyzed with by SEC using a Superose 6 increase 10/300 column in order to confirm absence of unreacted BCN-NHS. Spin filtration was repeated if necessary. Concentration of BCN modified KLH protein was measured using absorption of the protein at 280 nm. In order to monitor BCN modification,  $N_3$ -coumarin fluorophore was added to aliquot of protein solution and emission of clicked coumarin was measured at 480nm.

Azido peptides were dissolved in PBS and transferred into the vials that contain BCN modified KLH solution separately and left stirring for 24h. Peptide conjugation was also visualized with the help of  $N_3$ -coumarin, since the amount of free BCN was decreased after the peptide conjugations, signal of clicked coumarin at 480nm decreased as well.

### 2.3.6 Circular Dichroism Spectroscopy

CD measurements were performed using a Jasco model J-815 spectropolarimeter. Peptides were dissolved in 10 mM phosphate buffer (peptide concentration 100-180 $\mu$ M) at pH 7.2. Spectra were recorded at room temperature (298 K), with a 0.1 cm quartz cell over the wavelength range 265-185 nm at 50nm/min with a bandwidth of 1.0 nm, response time of 2 s, resolution step width of 0.1 nm, and standard sensitivity.

### **2.3.7 Fluorescence Spectroscopy**

Fluorescence measurements were performed on an LS 55 fluorescence spectrophotometer (Perkin-Elmer Ltd., Beaconsfield, UK) using  $\lambda_{exc}$  and  $\lambda_{em}$  of 380nm and 480nm, respectively. An emission scan was performed between 400 and 600 nm. Excitation slit was fixed at 15 nm, emission slit was fixed at 10nm. Hellma 105.253-QS 100  $\mu$ l Ultra-Micro Fluorescence Cell was used for each measurement. To determine the background fluorescence, N3-coumarin dissolved in 5% DMSO containing PBS buffer.

### **2.3.8 Enzyme-linked Immunosorbent Assay (ELISA) Analysis of Peptides**

96-well Nunc maxisorp plates were coated with peptides (50 ng/well) o/n at 4°C. After blocking (phosphate buffered saline [PBS] with 0.1% Tween-20 v/v and 3% bovine serum albumin w/v) and extensive washing (PBS with 0.05% Tween-20 v/v), the plates were incubated with limiting dilutions of AM22 (starting with a 200-fold dilution of a 0.7 mg/ml stock) or D25 (starting with a 60-fold dilution of a 1 mg/ml stock). After extensive washing, the plates were incubated with HRP conjugated goat-anti-human IgG antibodies (ITK Southern Biotech) at a 1:1000 dilution for one hour at room temperature. Detection of HRP reactivity was performed using tetramethylbenzidine substrate (BioFX) and a ELISA plate reader (EL-808 from Biotek). All experiments were repeated 2–3 times.

## **2.4 References**

1. Glezen, W. P. (1986). Risk of Primary Infection and Reinfection with Respiratory Syncytial Virus. *Archives of Pediatrics & Adolescent Medicine*, 140(6), 543. doi:10.1001/archpedi.1986.02140200053026
2. Welliver, R. C. (2003). Review of epidemiology and clinical risk factors for severe respiratory syncytial virus (RSV) infection. *The Journal of Pediatrics*, 143(5), 112-117. doi:10.1067/s0022-3476(03)00508-0
3. Leader, S. and Kohlhase, K. (2003) Recent trends in severe respiratory syncytial virus (RSV) among US infants 1997 to 2000. *Journal of Pediatrics*, 143, S127-S132. doi:10.1067/S0022-3476(03)00510-9

4. Falsey, A. R., & Walsh, E. E. (2005). Respiratory Syncytial Virus Infection in Elderly Adults. *Drugs & Aging*, 22(7), 577-587. doi:10.2165/00002512-200522070-00004
5. Colman, P. M., & Lawrence, M. C. (2003). The structural biology of type I viral membrane fusion. *Nature Reviews Molecular Cell Biology*, 4(4), 309-319. doi:10.1038/nrm1076
6. McLellan, J. S., Ray, W. C., & Peeples, M. E. (2013). Structure and Function of Respiratory Syncytial Virus Surface Glycoproteins. *Current Topics in Microbiology and Immunology Challenges and Opportunities for Respiratory Syncytial Virus Vaccines*, 83-104. doi:10.1007/978-3-642-38919-1\_4
7. Collins, P. L., & Graham, B. S. (2007). Viral and Host Factors in Human Respiratory Syncytial Virus Pathogenesis. *Journal of Virology*, 82(5), 2040-2055. doi:10.1128/jvi.01625-07
8. Melero, J. A., & Mas, V. (2015). The Pneumovirinae fusion (F) protein: A common target for vaccines and antivirals. *Virus Research*, 209, 128-135. doi:10.1016/j.virusres.2015.02.024
9. McLellan, J. S. (2015). Neutralizing epitopes on the respiratory syncytial virus fusion glycoprotein. *Current Opinion in Virology*, 11, 70-75. doi:10.1016/j.coviro.2015.03.002
10. Liljeroos, L., Krzyzaniak, M. A., Helenius, A., & Butcher, S. J. (2013). Architecture of respiratory syncytial virus revealed by electron cryotomography. *Proceedings of the National Academy of Sciences*, 110(27), 11133-11138. doi:10.1073/pnas.1309070110
11. McLellan, J. S., Yang, Y., Graham, B. S., & Kwong, P. D. (2011). Structure of Respiratory Syncytial Virus Fusion Glycoprotein in the Postfusion Conformation Reveals Preservation of Neutralizing Epitopes. *Journal of Virology*, 85(15), 7788-7796. doi:10.1128/jvi.00555-11
12. McLellan, J. S., Chen, M., Leung, S., Graepel, K. W., Du, X., Yang, Y., Graham, B. S. (2013). Structure of RSV Fusion Glycoprotein Trimer Bound to a Prefusion-

- Specific Neutralizing Antibody. *Science*, 340(6136), 1113-1117.  
doi:10.1126/science.1234914
13. Swanson, K. A., Settembre, E. C., Shaw, C. A., Dey, A. K., Rappuoli, R., Mandl, C. W., Carfi, A. (2011). Structural basis for immunization with postfusion respiratory syncytial virus fusion F glycoprotein (RSV F) to elicit high neutralizing antibody titers. *Proceedings of the National Academy of Sciences*, 108(23), 9619-9624. doi:10.1073/pnas.1106536108
  14. Kwakkenbos, M. J., Diehl, S. A., Yasuda, E., Bakker, A. Q., Geelen, C. M., Lukens, M. V., . . . Beaumont, T. (2009). Generation of stable monoclonal antibody-producing B cell receptor-positive human memory B cells by genetic programming. *Nature Medicine*, 16(1), 123-128. doi:10.1038/nm.2071
  15. Graham, B. S. (1995). Pathogenesis of Respiratory Syncytial Virus Vaccine-augmented Pathology. *American Journal of Respiratory and Critical Care Medicine*, 152(4\_pt\_2). doi:10.1164/ajrccm/152.4\_pt\_2.s63
  16. Osioy, C., Horne, D., Anderson, R. (1994). Antibody-dependent enhancement of respiratory syncytial virus infection by sera from young infants. *Clinical and Diagnostic Laboratory Immunology*, 1(6), 670-677
  17. Krilov, L. R., Anderson, L. J., Marcoux, L., Bonagura, V. R., & Wedgwood, J. F. (1989). Antibody-Mediated Enhancement of Respiratory Syncytial Virus Infection in Two Monocyte/Macrophage Cell Lines. *Journal of Infectious Diseases*, 160(5), 777-782. doi:10.1093/infdis/160.5.777
  18. McLellan, J. S., Chen, M., Joyce, M. G., Sastry, M., Stewart-Jones, G. B., Yang, Y., Kwong, P. D. (2013). Structure-Based Design of a Fusion Glycoprotein Vaccine for Respiratory Syncytial Virus. *Science*, 342(6158), 592-598. doi:10.1126/science.1243283
  19. Taylor, J. W. (2002). The synthesis and study of side-chain lactam-bridged peptides. *Biopolymers*, 66(1), 49-75. doi:10.1002/bip.10203
  20. Wöhr, T., Wahl, F., Nefzi, A., Rohwedder, B., Sato, T., Sun, X., & Mutter, M. (1996). Pseudo-Prolines as a Solubilizing, Structure-Disrupting Protection

- Technique in Peptide Synthesis. *Journal of the American Chemical Society*, 118(39), 9218-9227. doi:10.1021/ja961509q
21. Grieco, P., Gitu, P., & Hruby, V. (2001). Preparation of side-chain-to-side-chain cyclic peptides by Allyl and Alloc strategy: potential for library synthesis. *Journal of Peptide Research*, 57(3), 250-256. doi:10.1111/j.1399-3011.2001.00816.x
  22. Offer, J., Quibell, M., & Johnson, T. (1996). On-resin solid-phase synthesis of asparagine N-linked glycopeptides: use of N-(2-acetoxy-4-methoxybenzyl)(AcHmb) aspartyl amide-bond protection to prevent unwanted aspartimide formation. *Journal of the Chemical Society, Perkin Transactions 1*, (2), 175. doi:10.1039/p19960000175
  23. Li, D., & Elbert, D. L. (2002). The kinetics of the removal of the N-methyltrityl (Mtt) group during the synthesis of branched peptides. *Journal of Peptide Research*, 60(5), 300-303. doi:10.1034/j.1399-3011.2002.21018.x
  24. Ingale, S., & Dawson, P. E. (2011). On Resin Side-Chain Cyclization of Complex Peptides Using CuAAC. *Organic Letters*, 13(11), 2822-2825. doi:10.1021/ol200775h
  25. Kamber, B., Hartmann, A., Eisler, K., Riniker, B., Rink, H., Sieber, P., & Rittel, W. (1980). The Synthesis of Cystine Peptides by Iodine Oxidation of S-Trityl-cysteine and S-Acetamidomethyl-cysteine Peptides. *Helvetica Chimica Acta*, 63(4), 899-915. doi:10.1002/hlca.19800630418
  26. Baskin, J. M., Prescher, J. A., Laughlin, S. T., Agard, N. J., Chang, P. V., Miller, I. A., Bertozzi, C. R. (2007). Copper-free click chemistry for dynamic in vivo imaging. *Proceedings of the National Academy of Sciences*, 104(43), 16793-16797. doi:10.1073/pnas.0707090104
  27. Codelli, J. A., Baskin, J. M., Agard, N. J., & Bertozzi, C. R. (2008). Second-Generation Difluorinated Cyclooctynes for Copper-Free Click Chemistry. *Journal of the American Chemical Society*, 130(34), 11486-11493. doi:10.1021/ja803086r
  28. Sletten, E. M., & Bertozzi, C. R. (2011). From Mechanism to Mouse: A Tale of Two Bioorthogonal Reactions. *Accounts of Chemical Research*, 44(9), 666-676. doi:10.1021/ar200148z

29. Patterson, D. M., Nazarova, L. A., & Prescher, J. A. (2014). Finding the Right (Bioorthogonal) Chemistry. *ACS Chemical Biology*, 9(3), 592-605. doi:10.1021/cb400828a
30. Widjaja, I., Wicht, O., Luytjes, W., Leenhouts, K., Rottier, P. J., Kuppeveld, F. J., Haan, C. A. (2016). Characterization of Epitope-Specific Anti-Respiratory Syncytial Virus (Anti-RSV) Antibody Responses after Natural Infection and after Vaccination with Formalin-Inactivated RSV. *Journal of Virology*, 90(13), 5965-5977. doi:10.1128/jvi.00235-16



## CHAPTER 3

### STRUCTURE-BASED DESIGN AND SYNTHESIS OF KILLER CYCLIC PEPTIDES FOR MULTIPLE MYELOMA TUMOR CELLS

The second mitochondria-derived activator of caspase (Smac/DIABLO) is a recently identified, novel pro-apoptotic protein, released from mitochondria into the cytosol in response to apoptotic stimuli. Smac promotes apoptosis in cell by eliminating the caspase-inhibitory properties of the inhibitors of apoptosis proteins (IAP), particularly XIAP. In this study, heptamer Smac peptide (AVPIAQK) fused to a well-known octaarginine (Arg8) cell-penetrating peptide and either one part of the peptide or both part constrained in a cyclic structure. The biological properties of designed peptides in terms of cell-permeability, cytotoxicity and apoptotic efficiency have been studied. Significant contribution of cyclization on cytotoxicity and apoptosis have been demonstrated in multiple myeloma (MM) cells.

#### 3.1 Introduction

Apoptosis is a very tightly programmed cell death which contributes to the elimination of unnecessary and unwanted cells to maintain the convenient balance between cell division and cell death. The loss of this balance is associated with wide variety of illnesses, including cancer. If the rate of cell division is greater than the rate of cell death, cells accumulate (cancer expands); conversely, if the rate of cell death is greater than the rate of cell division, the cancer regress. This means that anything that shifts the balance toward cell division over cell death will result in the expansion of a cancer.<sup>1</sup> Tumor suppressors, whether they act by inhibiting cell cycle or promoting apoptosis, push the balance the other way, and in general, causes the intervention of cancer. Therefore, there are therapies

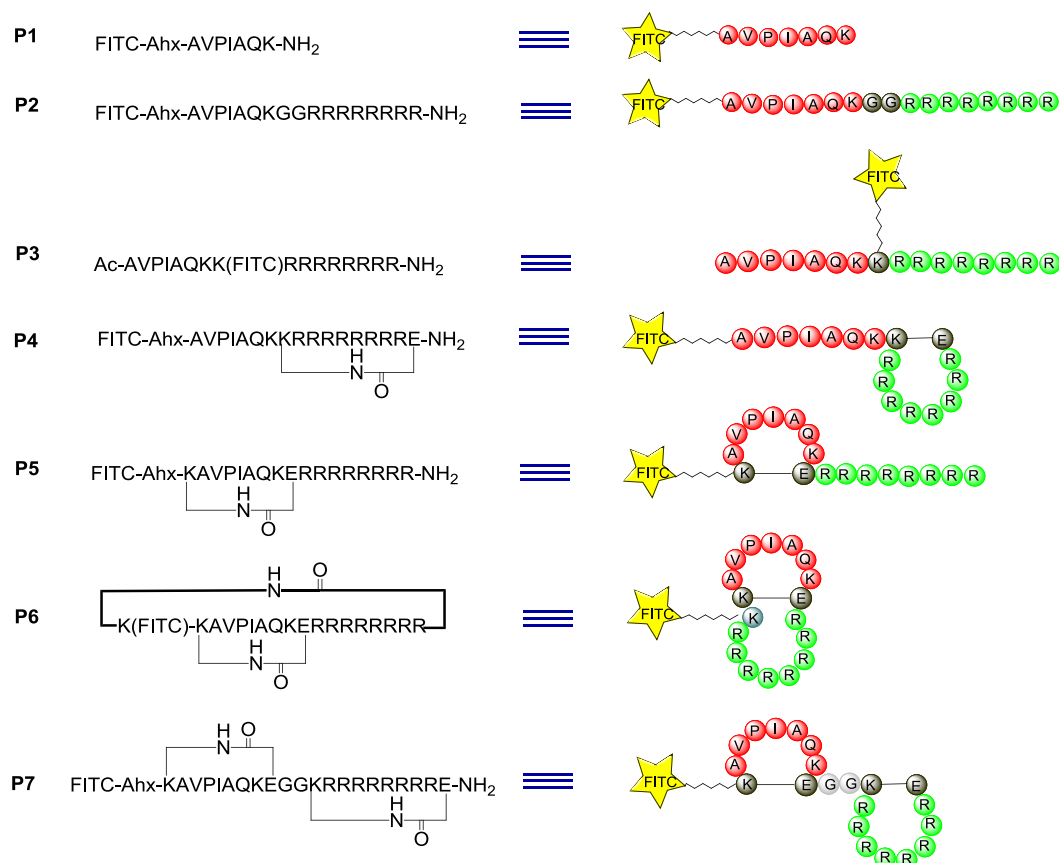
that aim for such an out-come.<sup>2,3</sup> The induction of apoptosis is one of the key strategies for preventing the emerge of cancer<sup>4</sup> and there is a variety of pathways for activation of apoptosis in tumor cells use.<sup>5</sup>

Mitochondria-dependent apoptosis is the major pathway for apoptosis induction. In this pathway, conditions that promote cell death engage a set of related proteins, called BCL-2 family. The proteins in question control the integrity of the outer membranes of mitochondria in the cell. When mitochondrial outer membrane permeabilization (MOMP) occurs, soluble proteins of the intermembrane space diffuse into cytosol. Among these Smac/DIABLO is a recently identified pro-apoptotic protein released from mitochondria upon apoptotic stimulation.<sup>6,7</sup> Caspases, a family of intracellular cysteine proteases, are the effectors of apoptosis. When the mitochondrial pathway of apoptosis is engaged, activated executioner caspases gain access to inner membrane of mitochondria and they cleave hundreds or thousands of substrates in the cell to orchestra apoptosis. Some caspases are inhibited by members of the inhibitor of apoptosis proteins (IAP) family. The role of Smac in here is promoting apoptosis in cells, by eliminating the caspase-inhibitory properties of the inhibitors of apoptosis proteins (IAP), particularly XIAP. It forms an elongated dimer and targets both the BIR2 and BIR3 domains in XIAP. It removes the XIAP inhibition of caspase-9 by binding to the BIR3 domain in XIAP through its AVPI tetrapeptide binding motif.<sup>8,9</sup> The ability of the Smac (AVPI tetrapeptide) to neutralize XIAP and induce apoptosis has initiated multiple drug discovery efforts aimed at producing peptidyl and non-peptidyl small molecules with drug-like properties as candidate therapeutics for cancer.<sup>10</sup>

Smac mimetics have several limitations (e.g., poor cell permeability and poor in vivo stability and bioavailability) as potentially useful therapeutic agents. Therefore, our laboratory, like the others, has focused on developing a number of Smac mimetics<sup>10</sup> and conjugates<sup>17, 18, 19</sup> with the aim of improved binding affinities, cell-permeability, and in vivo stability and biocompatibility. A heptapeptide AVPIAQK (SmacN7) that contain binding sequence was targeted. SmacN7 peptide was fused with a well-established cell-penetrating peptide octaarginine (Arg8) to achieve cellular uptake. In order to increase therapeutic efficacy of the bifunctional sequence, the peptide conformation was locked via cyclization, which leads to reduction of polarity, increase in proteolytic stability.<sup>11-15</sup> Structural variants of the linear peptide backbone have

always played an important role on specific characteristics of a peptide. One possible consequence of linear nature is rapid degradation by proteases. Furthermore, to provide a therapeutic effect, a peptide must bind to its target. The flexible nature of linear peptides can limit their affinity making it difficult to bind to some challenging cellular targets, such as protein surfaces involved in protein–protein interactions. In contrast, the reduced flexibility of cyclic peptides decreases the entropic penalty associated with binding, making them much more suitable for inhibiting some difficult targets.<sup>16</sup> Overall, constraining a peptide into a cyclic structure may significantly increase its efficacy in different ways.

In this study, we examined the effects of cyclization of SmacN7-Arg8 fused peptides on both cellular uptake and cytotoxicity. Different variants SmacN7-Arg8 peptides were designed, synthesized, and tested for U266 multiple myeloma cell line (Figure 3.1).



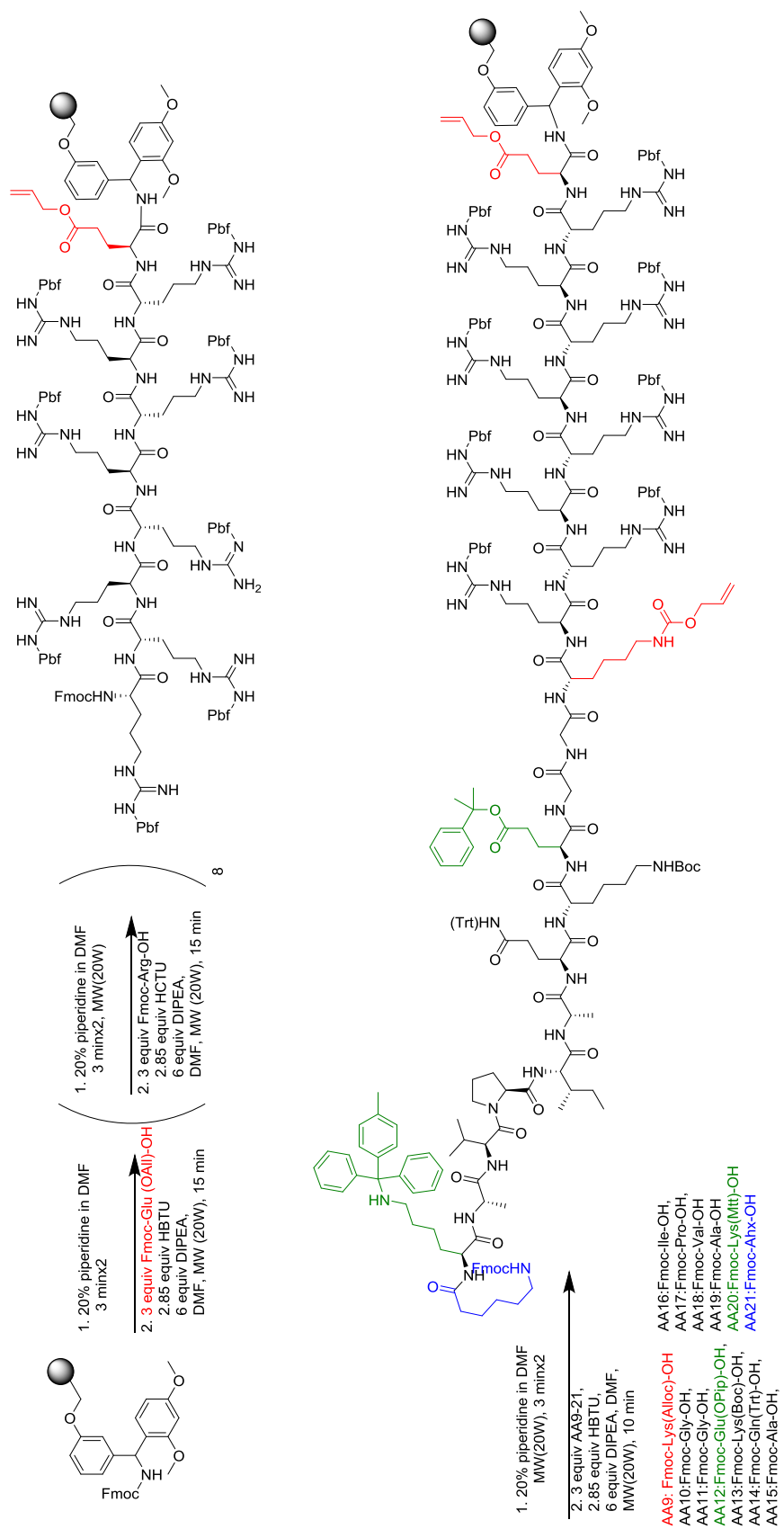
**Figure 3. 1** Sequences of **P1-7**. Lactam bridges are shown as thin lines. The thick line joining the N and C termini of **P6** indicates backbone cyclization. For better visualization, schematic representation of each peptide is shown from the right-hand side.

### 3.2 Results and Discussion

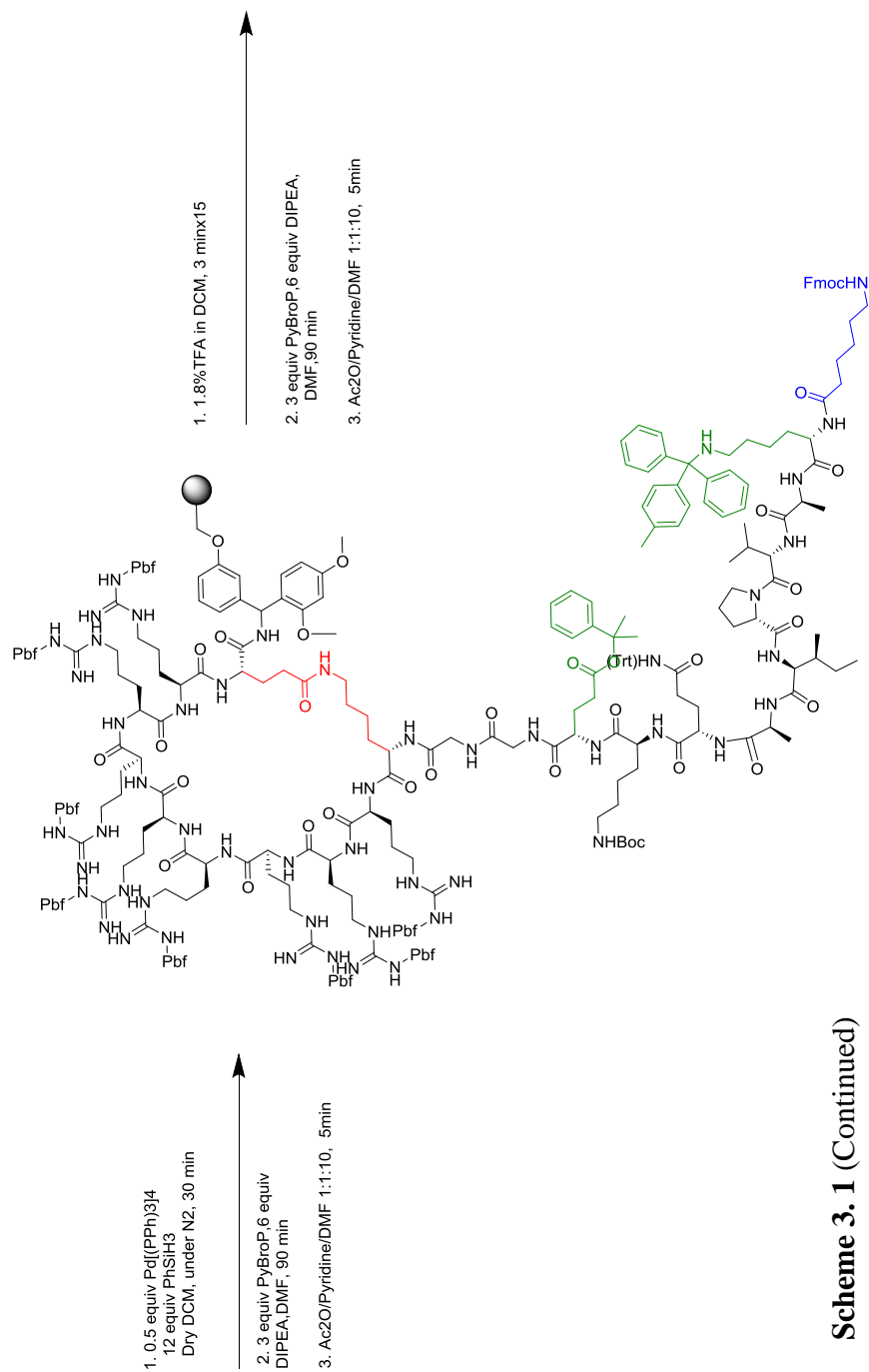
Macrocyclisation strategy that we typically utilized is a side-chain-to-side-chain lactamization (**P4-P7**), but head to tail lactam formation was also used to obtain **P6**. Fluorescein isothiocyanate (FITC) was also coupled to these fusion peptides at different positions (**P2 and P3**) to measure cellular uptake by flow cytometry. For the comparison of the cellular uptake between SmacN7 with or without octarginine, **P1** also synthesized.

In order to proceed cyclization via lactam formation on resin, amine and acid functionality of lysine and glutamic acid must be free while other aminoacids are fully protected. For this purpose, we utilized two different strategy for different peptides.

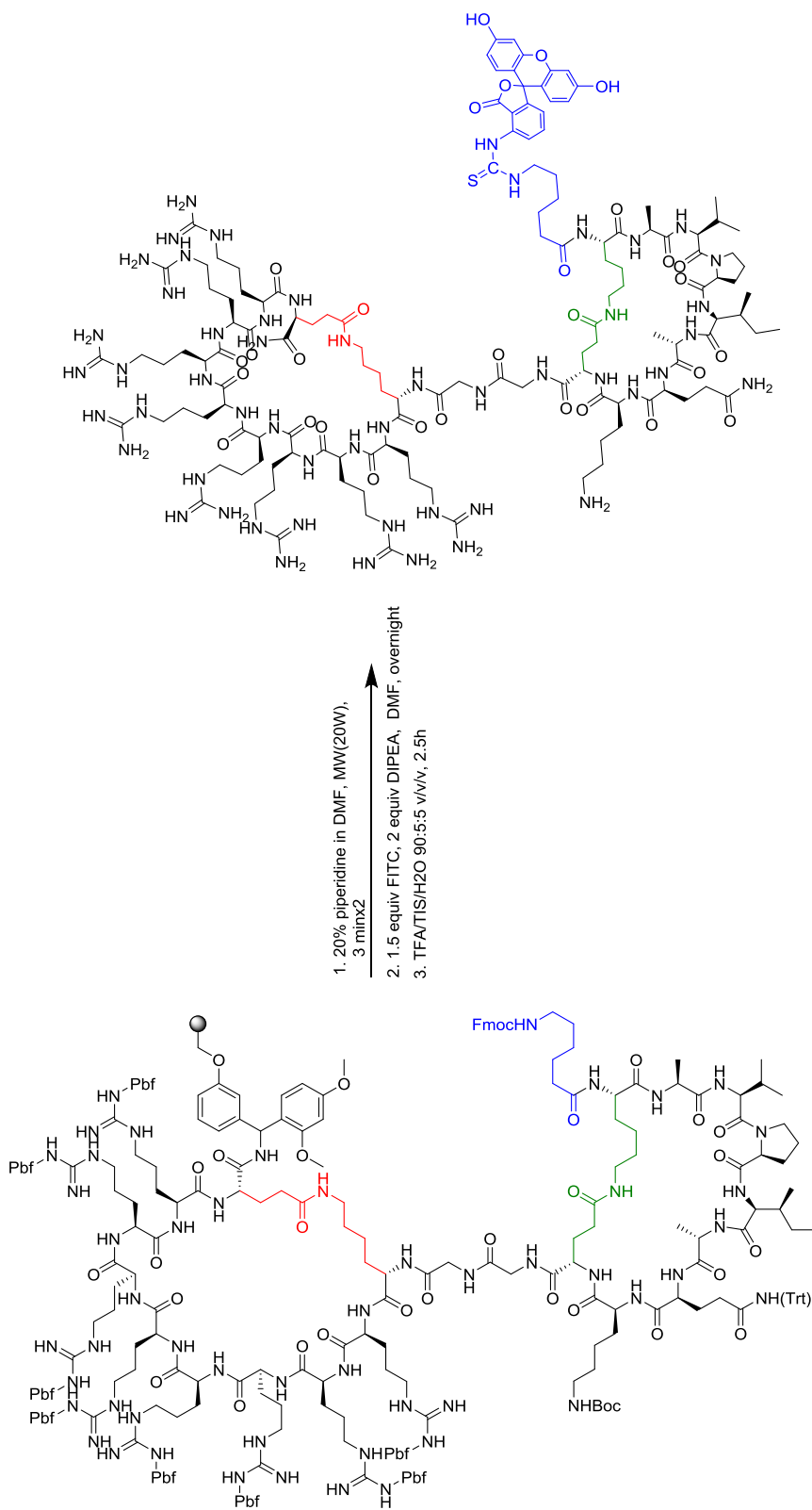
Initially, we used orthogonal Alloc/OAll deprotection strategy.<sup>20</sup> Alloc/OAll deprotection was done with freshly-prepared Pd (PPh<sub>3</sub>)<sub>4</sub> (0.5 equiv.) as a catalyst and PhSiH<sub>3</sub> (12 equiv.) as an allyl scavenger. Lactam formation between free amine and acid functional groups were carried out with 3.0 equivalents of phosphonium based coupling reagent, bromo-tris(pyrrolidino)- phosphonium hexafluorophosphate (PyBroP) and 6.0 equiv of DIPEA for 90 min to 2h, at room temperature in DMF. The other convenient and straightforward strategy that we used is removal of acid-labile Mtt/OPip groups.<sup>21</sup> After completion of synthesis, resin amide resin carrying Mtt/OPip protected peptide was swollen in dichloromethane (DCM) prior to use and then treated with 1.8% trifluoroacetic acid (TFA) (v/v) in DCM for 3 min at room temperature, repeated 10 times, using 1 ml solution per 100 mg of resin. The peptide resin was then re-suspended in DMF, followed by on-resin cyclization of the peptide via the free carboxylic acid side-chain of glutamic acid and the free amino group side-chain of lysine by addition of PyBroP (3 equiv.), DIPEA (6 equiv.) for 1.5 to 2 h. Excess DIPEA was used as a precaution for the presence of TFA, trapped into the resin beads. Coupling time was extended until a negative Kaiser test obtained (Scheme 3.1)



**Scheme 3. 1** Synthetic pathway of bicyclic **P7** peptide



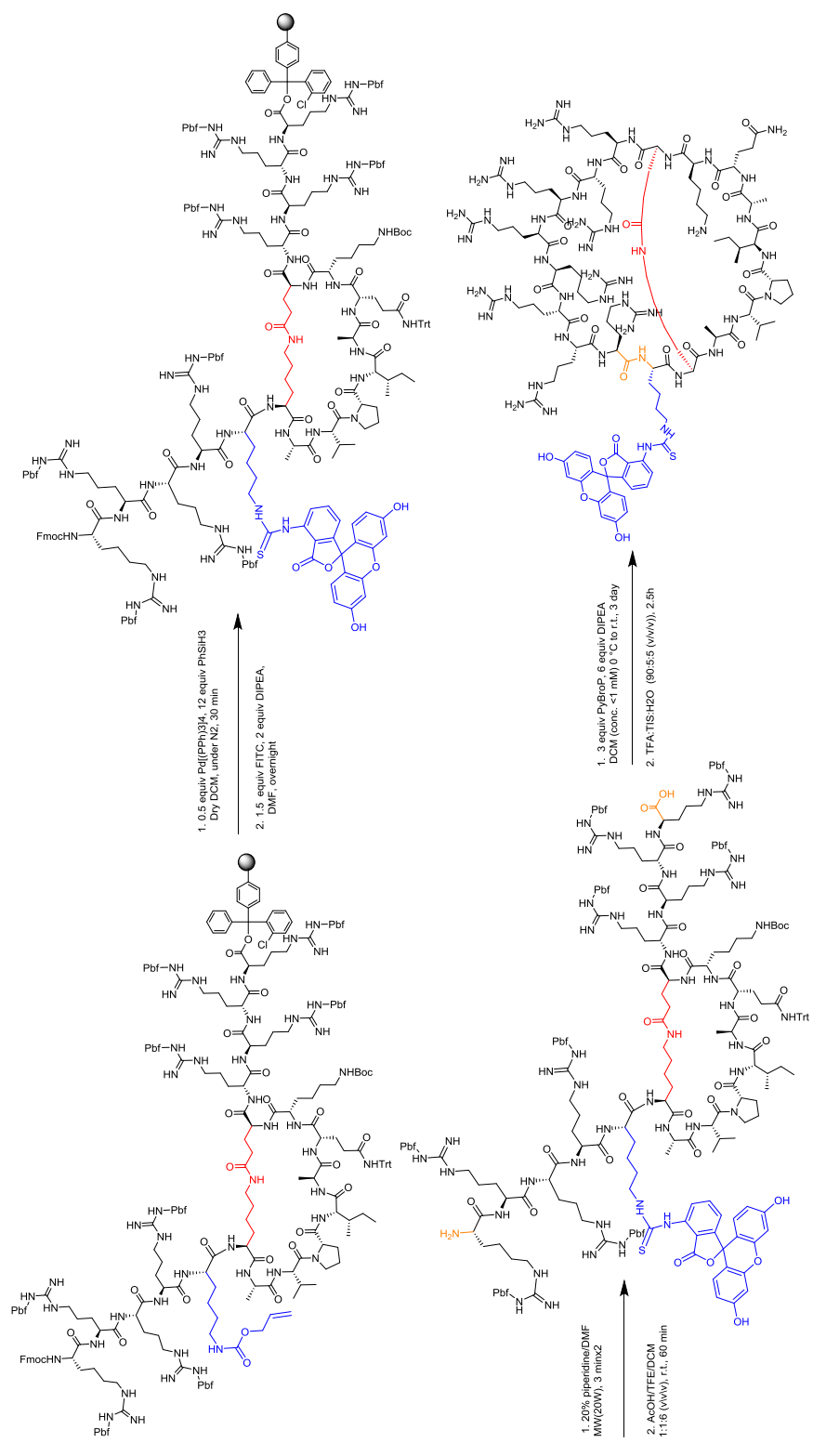
**Scheme 3. 1 (Continued)**



**Scheme 3. 1 (Continued)**

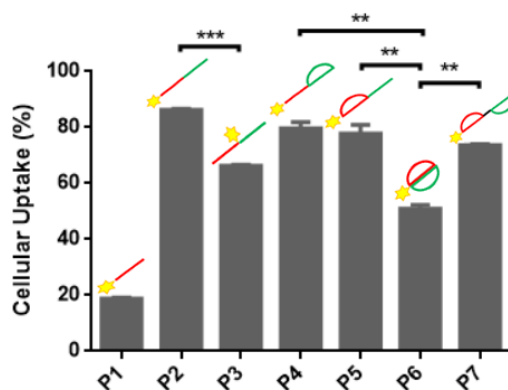


As another strategy, head-to tail cyclization was also employed for the synthesis of **P6**. When the synthesis is complete, the first monocyclic peptide was constructed on resin, then labeled with FITC after selective removal of Alloc group from the lysine. After Fmoc removal from the N-terminus of peptide (head), peptide was cleaved from the resin by the treatment with Acetic acid/ trifluoroethanol (TFE)/DCM = 1:1:6 (v/v/v) for 60 min at room temperature. The solution was filtered and concentrated in vacuo and precipitated with ether. The monocyclic peptide that all side chains are still protected was subjected to head-to-tail cyclization in solution for 3 days. The reaction using PyBrOP under the conditions high dilution in DCM (<1 mM) was afforded the desired fully-protected cyclic peptide. Finally, deprotection of side chains were done with TFA/TIS/H<sub>2</sub>O=90:5:5 (v/v/v) for 2.5 h, ended up with bicyclic **P6** (Scheme 3.2).



**Scheme 3. 2 Synthetic pathway of bicyclic P6 peptide**

Cellular uptake studies showed that **P1** has the lowest cellular entry, as expected, due to lack of transmembrane transport polyarginine peptide.<sup>17,19</sup> We found strong cellular uptake (>65%) for most of the Smac conjugates other than **P6** (Figure 3.2).

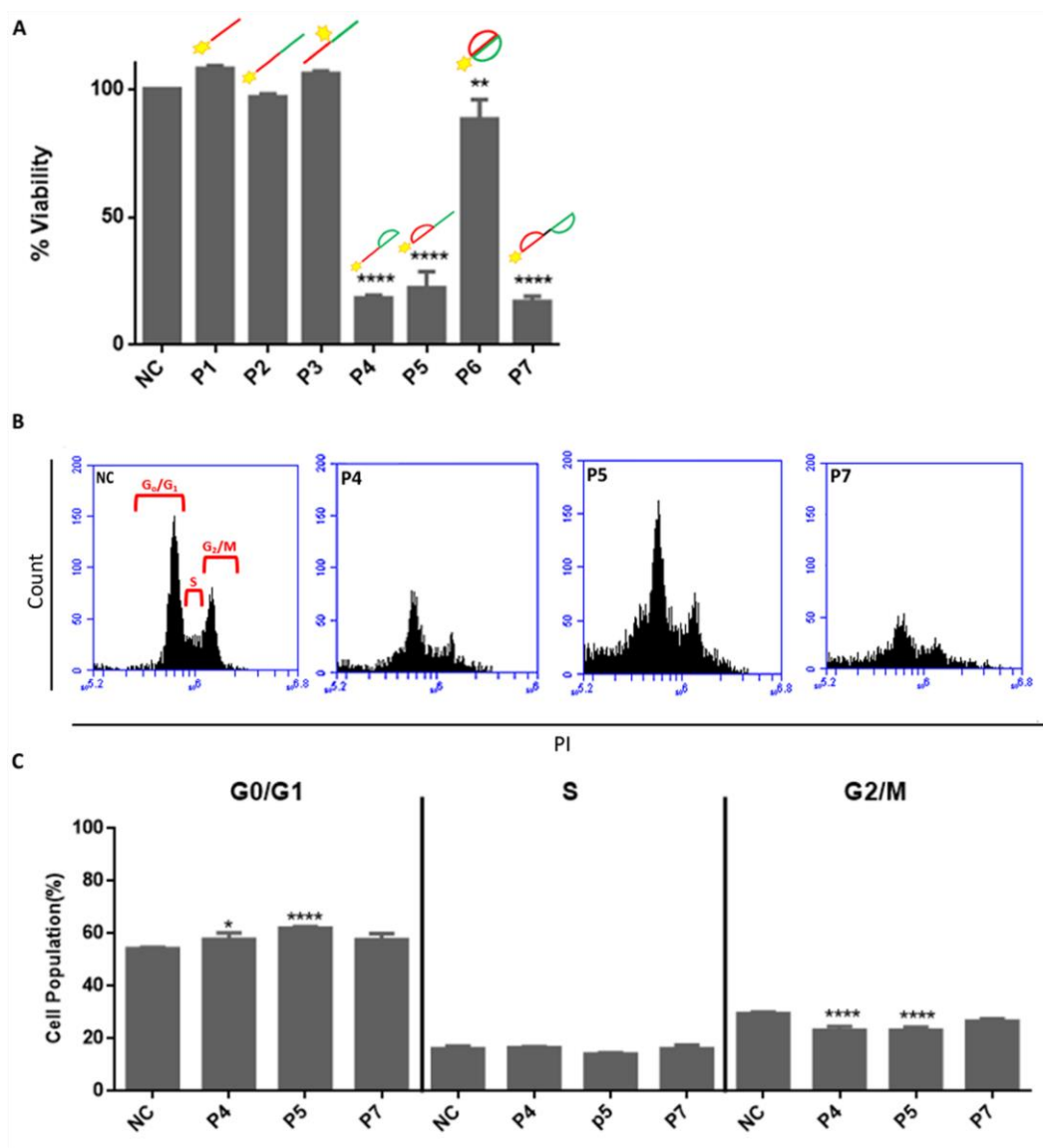


**Figure 3. 2** Cellular uptake assessment of linear and cyclic SMAC peptides. Asterisks (\*\*and \*\*\*) denote statistical significance at  $p < 0.01$  and  $p < 0.001$ , respectively (n = 2).

Position of FITC had an effect on cellular uptake. When FITC-labelled lysine was flanked between Smac and Arg8, peptide (**P3**) resulted less internalization than other linear variant (**P2**) which shows that slight alterations of structure may result unpredictable outcomes. On the contrary to the previous report<sup>22</sup> when octaarginine part of the peptide was constrained in a cycle, while keeping the Smac part linear (**P4**), there wasn't any enhancement of uptake. Similarly, when Smac part is cyclized, while octaarginine part is linear (**P5**), there was no improvement either. When two part of the peptide cyclized as two adjacent cycle (**P6**), cellular uptake went even worse. One explanation for this can be that second backbone cyclization causes distortion of the geometry which blocks cell-permeable function of polyarginine.

To assess our claim, we synthesized another bicyclic peptide (**P7**) with double side-chain-side-chain cyclization with additional –GlyGly– as a spacer. It is observed that cellular uptake of bicyclic **P7** is higher than the other compact bicyclic **P6**. This result showed that too much constrained in the cyclic structure of peptide might have adverse effect to its function.

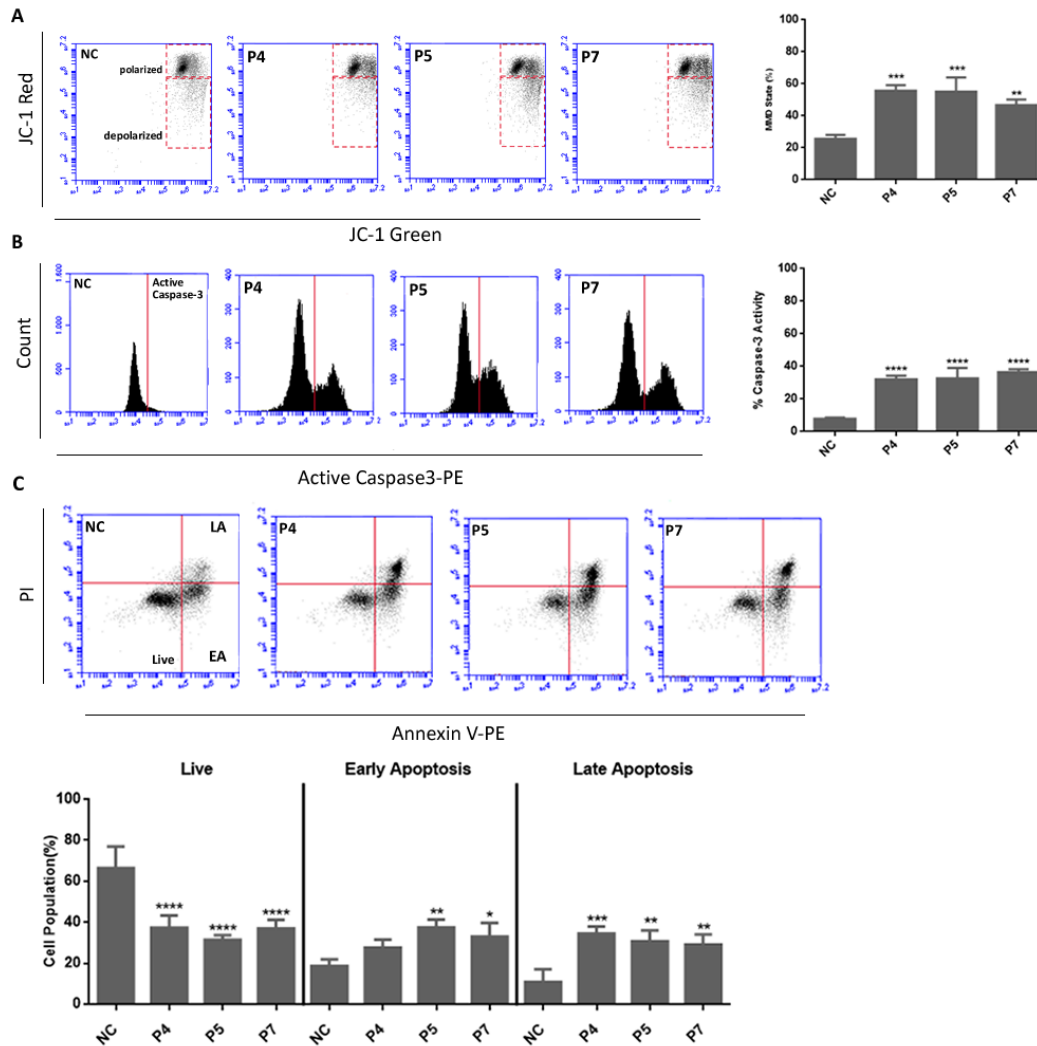
Cellular cytotoxicity experiments were also conducted to show the therapeutic potential of designed peptides. As shown in Figure 3.3, cyclization led increase in cytotoxicity. **P6** showed the lowest toxicity among all designed cyclic peptides due to both lower cellular uptake and reduction of Smac activity caused by structural distortion. Another interesting observation here is that linear **P2** and **P3** peptides are not cytotoxic, although their cellular uptake were very high. This supports our claim that cyclization increases stability of peptides in cellular environment and thus biological functions.



**Figure 3.3** Viability assessment and cell cycle analysis of U266 cells after 48 h treatment. **A)** Effect of 50  $\mu$ M peptide treatment on the viability of U266 MM cell line. **B)** Flow cytometry fluorescence intensity histograms of cells stained with PI. Intensity ranges for the corresponding cell cycle phases (G<sub>0</sub>/G<sub>1</sub>, S, and G<sub>2</sub>/M) are shown on the untreated sample. **C)** Bar plots of normalized count values of each phase for untreated and treated cells with 25  $\mu$ M peptides. Asterisks (\*\*and \*\*\*\*) denote statistical significance at  $p < 0.01$  and  $p < 0.001$ , respectively ( $n = 3$ ).

Cytotoxicity mechanism of potent cyclic peptides (**P4**, **P5**, **P7**) was also investigated with cell cycle arrest and apoptosis assays. As consistent with the literature<sup>23</sup>, three cyclic peptides have effect on G<sub>0</sub>/G<sub>1</sub> stage of cell proliferation (Figure 3.4 B). All

three apoptosis assays, which shows identical results, also indicate that **P4, P5** and **P7** induces apoptosis on U266 MM cells (Figure 3.4).



**Figure 3.4** Induction of apoptosis upon treatment with 25  $\mu$ M peptides; Mitochondrial Membrane Depolarization State (MMD state), Caspase-3 Activity Change, Cell Membrane Asymmetry Change. **A)** Flow cytometry fluorescence intensity dot plots of cells stained with JC-1. Gated fluorescence intensity values for polarized and depolarized states are labeled. Bar plots of normalized mitochondrial membrane polarization state values. **B)** Flow cytometry fluorescence intensity histograms and corresponding bar plots. **C)** Dot plots of Annexin V-PE vs 7-AAD signals gated as live, early apoptotic and late apoptotic events, and cell population bar graphs. Asterisks (\*\*and \*\*\*, \*\*\*\*) denote statistical significance at  $p < 0.01$  and  $p < 0.001$ , respectively ( $n = 3$ ).

In conclusion, we have reported the design, synthesis, and characterization of a peptidic, cell-permeable, easily accessible bifunctional Smac conjugates and demonstrated that alterations in the structure of Smac-Arg8 peptide via cyclization shows different cytotoxicity and uptake results. These designed three apoptotic cyclic peptides have also tested for the first time on U266 MM cell line. Although the exact mechanism of cell death and cellular uptake remains further investigated, this study proves that developed cyclic peptides are good candidates as therapeutics.

### **3.3 Experimental**

#### **3.3.1 Chemicals**

All chemical reagents and solvents were ACS grade or higher and purchased from commercial sources other than tetrakis(triphenylphosphine) palladium (0) (Pd(PPh<sub>3</sub>)<sub>4</sub>). All Fmoc-protected-L-aminoacids, coupling reagents, Rink amide MBHA resin (200-400 mesh, 0.52 meq/g loading capacity) and 2-chlorotrityl chloride resin (100-200 mesh, 1.0-2.0 meq/g loading capacity) were obtained from Chem-impex (USA). Dichloromethane (DCM) distilled over calcium hydride. Dimethylsulfoxide was pre-dried over calcium sulfate for approximately 2 days, and then dried with vacuum distillation. MilliQ water was double deionized using a Milli-Q® Advantage A10® Water Purification Systems (18.2 MΩ.cm at 25 °C, TOC: 7 ppb). 5 mM stock peptide solutions in MilliQ were prepared for cell assays and stored at -20 °C.

#### **3.3.2 General Method for Solid-Phase Peptide Synthesis**

All peptides were synthesized with CEM Discover Bio - Manual Microwave Peptide Synthesizer by using Fmoc-based solid-phase peptide synthesis (SPPS) strategy either on a Rink amide resin or a Trt (2-Cl) resin at different scales between 0.1 mmol and 0.25 mmol. N-terminus of peptides except P6 and P3 were extended with an aminohexanoic acid (Ahx) spacer to attach the fluorescein moiety needed to follow cellular uptake by flow cytometry. Attachment of fluorescein for P6 and P3 was done from the lysine after selectively removal of allyloxycarbonyl (Alloc) or methyltrityl (Mtt) protections on resin. All arginines were coupled with potent coupling reagent HCTU (2-(6-chloro-1-H-benzotriazole-1-yl)-1, 1, 3, 3-tetramethylammonium hexafluorophosphate). Other aminoacids were coupled with HBTU (N, N, N', N'-

tetramethyl-O-(1H-benzotriazol-1-yl) uronium hexafluorophosphate). Couplings were carried out with 3.0 equivalents of Fmoc-L-amino acids, 2.85 equiv of coupling reagent, 6 equivalents of N, N-diisopropylethylamine (DIPEA) in dimethylformamide (DMF) with assistance of MW heating (20 W, 10-15 min). All deprotections were achieved with 5 ml solution of 20% piperidine in DMF with MW heating (20 W, 3x2 min). Completion of each coupling and deprotection was monitored by Kaiser test<sup>24</sup> except Fmoc-Pro-OH.

After peptide elongation was complete, peptide was cleaved from the resin and fully deprotected by treatment of the resin with a mixture of trifluoroacetic acid (TFA) /triisopropylsilane (TIS)/H<sub>2</sub>O (95: 2.5: 2.5 v/v/v) for 3-4 hours at room temperature. Free peptides were separated from the resin by filtration and the resin was further washed with TFA. Collected filtrate was precipitated in diethyl ether and centrifuged. The supernatant was removed and diethyl ether was further added to repeat the washing step up to three times. The precipitate was dried, lyophilized in water and purified using preparative reverse phase high performance chromatography (RP-HPLC). Purity was evaluated by analytical RP-HPLC and identity confirmed by mass spectrometry.

### **3.3.3 Reverse Phase High Performance Liquid Chromatography (RP-HPLC) analysis**

Reverse phase preparative HPLC was performed on a Dionex UltiMate 3000 Hplc system, employing a Thermo Scientific Hypersil Gold C18 column (250× 10 mm, 5 μm) at flow rate of 2ml/min at 40 °C. Acetonitrile/water gradient containing 0.1% trifluoroacetic acid (5-100%, 1-70 min) was utilized as eluent. All polyarginine containing peptides were dissolved in 10% Acetic acid containing MilliQ. The concentration of the peptides was adjusted as 20 mg/ml. 1.5 ml of this peptide solution was purified for one batch by using 2ml injection loop and purification repeated consecutively. Purity of each fraction was assessed with analytical RP-HPLC, before combining pure fractions.

Analytical HPLC was performed on a Dionex UltiMate 3000 Hplc system equipped with a Thermo Scientific Acclaim™ 120 C18 column (46 x 150 mm, 3 μm). Elution of the peptides was achieved using an acetonitrile/water gradient containing 0.1% trifluoroacetic acid (5-100%, 1-30 min, flow 0.4 mL/min). After purity of collected



fractions confirmed by analytical HPLC, lyophilization was achieved using a Telstar Cryodos Freeze Dryer and peptides were stored at -20 °C.

### 3.3.4 Mass analysis of peptides

The concentration synthesized peptides was adjusted as 1 mg/ml with water and characterized by mass spectrometry on an Agilent 6530 Q-TOF mass spectrometer equipped with ESI (Electrospray Ionization) source.

### 3.3.5 Preparation of Pd (PPh<sub>3</sub>)<sub>4</sub><sup>25</sup>

40 ml dry DMSO was deoxygenated by vigorously flushing nitrogen gas for 30 minutes in a two-neck round bottom flask equipped with a magnetic stirring bar and a reflux condenser. PdCl<sub>2</sub> (0.5 g, 2.8 mmol, 1.0 equiv.) and PPh<sub>3</sub> (3.7 g, 14.1 mmol, 5 equiv.) were added under nitrogen atmosphere. The orange mixture is heated to ~150 °C by means of an oil bath with stirring until complete solution occurs (~ 1 h). The bath is then taken away, and the solution is stirred for approximately 15 min, then hydrazine monohydrate (0.55 ml, 11.3 mmol, and 4 equiv.) was added dropwise over approximately 1 min. to form a yellow precipitate. A vigorous reaction takes place with evolution of nitrogen. The yellow solution is cooled to 0 °C with an ice bath and solid was collected by filtration and washed successively with three 50 ml portions of ethanol and three 50 ml portions of diethyl ether. The bright yellow solid was dried by passing a slow stream of nitrogen through the funnel for 1 hour, then with vacuum pump for overnight. The resulting yellow crystalline product weights 3.2 g (96-98% yield). The compound is sensitive to air, light and moisture. It was stored cold under nitrogen.

### 3.3.6 Attachment of FITC

After obtaining a free amine either deprotection of Fmoc group from N-termini of peptide or orthogonally removal of protecting groups (Mtt or Alloc) from lysine, resin was treated with solution of 1.5 equiv of FITC and 2 equiv of DIEA in DMF and, the left gentle stirring overnight. The completion of the reaction was tested using Kaiser test.<sup>24</sup>

### **3.3.7 Cell Culture**

U266 MM cells were cultured in RPMI-1640 growth medium containing 10% FBS, 1% penicillin–streptomycin and 1% non-essential amino acids at 37 °C in a 5% CO<sub>2</sub> incubator.

### **3.3.8 Flow cytometry**

Cellular uptake assessment, cell cycle analysis and apoptosis assays were performed on Accuri C6 flow cytometer (BD Biosciences). Gating was performed so that cell debris, cell clumps and doublets were excluded. Ten thousand events were recorded for each measurement.

### **3.3.9 Cellular Uptake**

Cells were treated with 10 μM of designed peptides for 48 h. Cellular uptake assessment was carried out using flow cytometer.

### **3.3.10 Cell viability assays**

Toxicity assays was done using the Cell Titer Blue Cell Viability Assay (Promega). Cells were treated with 50 μM of corresponding peptides for 48 h at a cell density of 100,000 cells/ml. For each sample, five technical replicates were used. At the end of the treatment duration, assay reagent was added and plates were incubated for an additional 4 h.

Fluorescence was measured with excitation wavelength at 555 nm and emission wavelength at 595 nm using SpectraMax® Paradigm ®Multi-Mode Microplate Reader (Molecular Devices).

### **3.3.11 Cell cycle analysis**

Cells were treated with 25 μM peptides for 48 h and harvested. After cold PBS wash, samples were fixed with 70% ethanol and kept on ice for 2 h. Following centrifugation at 800g for 5 min, cells were washed with PBS and then incubated with 25 μg/ml propidiumiodide (PI) and 3 mg/ml RNase, at 37 °C for 30 min. Stained cells were then analyzed with flow cytometry.

### **3.3.12 Apoptosis assays**

Cells were treated with 25  $\mu$ M P4, P5 and P7 peptides and analyzed at 48 h with flow cytometry. To study the effect of peptide treatment on mitochondrial membrane polarization MitoScreen Flow Cytometry Mitochondrial Membrane Potential Detection Kit (BD Biosciences) was used and samples were prepared as described by the manufacturer. Active caspase-3 was detected with PE Rabbit Anti- Active Caspase-3 Kit (BD Biosciences). Annexin V PE-7AAD Apoptosis Detection Kit from the same manufacturer was used to detect early- and late-stage apoptosis.

### **3.3.13 Statistical analysis**

Statistical significance of results was determined using one-way ANOVA with the Bonferroni post-test module or an unpaired t-test with two tails using GraphPad Prism software. P value of less than 0.05 was accepted as significant.

## **3.4 References**

1. Green, D. R. (2011). Means to an end: apoptosis and other cell death mechanisms. Cold Spring Harbor, NY: Cold Spring Harbor Laboratory Press.
2. Sherr, C. J. (2004). Principles of Tumor Suppression. *Cell*, 116(2), 235-246. doi:10.1016/s0092-8674(03)01075-4
3. Sun, W., & Yang, J. (2010). Functional Mechanisms for Human Tumor Suppressors. *Journal of Cancer*, 136-140. doi:10.7150/jca.1.136
4. Thompson, C. (1995). Apoptosis in the pathogenesis and treatment of disease. *Science*, 267(5203), 1456-1462. doi:10.1126/science.7878464
5. Fulda, S., & Debatin, K. (2006). Extrinsic versus intrinsic apoptosis pathways in anticancer chemotherapy. *Oncogene*, 25(34), 4798-4811. doi:10.1038/sj.onc.1209608
6. Du, C., Fang, M., Li, Y., Li, L., & Wang, X. (2000). Smac, a Mitochondrial Protein that Promotes Cytochrome c-Dependent Caspase Activation by Eliminating IAP Inhibition. *Cell*, 102(1), 33-42. doi:10.1016/s0092-8674(00)00008-8

7. Verhagen, A. M., Ekert, P. G., Pakusch, M., Silke, J., Connolly, L. M., Reid, G. E., Vaux, D. L. (2000). Identification of DIABLO, a Mammalian Protein that Promotes Apoptosis by Binding to and Antagonizing IAP Proteins. *Cell*, 102(1), 43-53. doi:10.1016/s0092-8674(00)00009-x
8. Chai, J., Du, C., Wu, J. W., Kyin, S., Wang, X., Shi, Y. (2000). Structural and biochemical basis of apoptotic activation by Smac/DIABLO. *Nature*, 406, 855-62. doi: 10.1038/35022514
9. Shiozaki, E. N., & Shi, Y. (2004). Caspases, IAPs and Smac/DIABLO: mechanisms from structural biology. *Trends in Biochemical Sciences*, 29(9), 486-494. doi:10.1016/j.tibs.2004.07.003
10. Fulda, S., & Vucic, D. (2012). Targeting IAP proteins for therapeutic intervention in cancer. *Nature Reviews Drug Discovery*, 11(4), 331-331. doi:10.1038/nrd3698
11. Adessi, C., & Soto, C. (2002). Converting a Peptide into a Drug: Strategies to Improve Stability and Bioavailability. *Current Medicinal Chemistry*, 9(9), 963-978. doi:10.2174/0929867024606731.
12. Gilon, C., Halle, D., Chorev, M., Selincer, Z., & Byk, G. (1991). Backbone cyclization: A new method for conferring conformational constraint on peptides. *Biopolymers*, 31(6), 745-750. doi:10.1002/bip.360310619.
13. Pauletti, G. (1997). Improvement of oral peptide bioavailability: Peptidomimetics and prodrug strategies. *Advanced Drug Delivery Reviews*, 27(2-3), 235-256. doi:10.1016/s0169-409x(97)00045-8
14. Burton, P. S., Conradi, R. A., Ho, N. F., Hilgers, A. R., & Borchardt, R. T. (1996). How Structural Features Influence the Biomembrane Permeability of Peptides. *Journal of Pharmaceutical Sciences*, 85(12), 1336-1340. doi:10.1021/js960067d
15. McGearry, R. P., Fairlie, D. P. (1998). Macrocyclic peptidomimetics: potential for drug development. *Current Opinion in Drug Discovery & Development*, 1(2), 208-217.
16. Liskamp, R. M. (2014). Peptides: Bicycling into cells. *Nature Chemistry*, 6(10), 855-857. doi:10.1038/nchem.2073

17. Yang, L., Mashima, T., Sato, S., Mochizuki, M., Sakamoto, H., Yamori, T., Oh-hara, T., Tsuruo, T. (2003). Predominant suppression of apoptosome by inhibitor of apoptosis protein in non-small cell lung cancer H460 cells: therapeutic effect of a novel polyarginine-conjugated Smac peptide. *Cancer Research*, 63(4), 831-837.
18. Fulda, S., Wick, W., Weller, M., & Debatin, K. (2002). Smac agonists sensitize for Apo2L/TRAIL- or anticancer drug-induced apoptosis and induce regression of malignant glioma in vivo. *Nature Medicine*. doi:10.1038/nm735.
19. Heckl, S., Sturzu, A., Regenbogen, M., Beck, A., Feil, G., Gharabaghi, A., & Echner, H. (2008). A Novel Polyarginine Containing Smac Peptide Conjugate that Mediates Cell Death in Tumor and Healthy Cells. *Medicinal Chemistry*, 4(4), 348-354. doi:10.2174/157340608784872217.
20. Grieco, P., Gitu, P., & Hruby, V. (2001). Preparation of side-chain-to-side-chain cyclic peptides by Allyl and Alloc strategy: potential for library synthesis. *Journal of Peptide Research*, 57(3), 250-256. doi:10.1111/j.1399-3011.2001.00816.x.
21. Li, D., & Elbert, D. L. (2002). The kinetics of the removal of the N-methyltrityl (Mtt) group during the synthesis of branched peptides. *Journal of Peptide Research*, 60(5), 300-303. doi:10.1034/j.1399-3011.2002.21018.x.
22. Lättig-Tünnemann, G., Prinz, M., Hoffmann, D., Behlke, J., Palm-Apergi, C., Morano, I., Cardoso, M. C. (2011). Backbone rigidity and static presentation of guanidinium groups increases cellular uptake of arginine-rich cell-penetrating peptides. *Nature Communications*, 2, 453. doi:10.1038/ncomms1459.
23. Jia, L., Patwari, Y., Kelsey, S. M., Srinivasula, S. M., Agrawal, S. G., Alnemri, E. S., & Newland, A. C. (2003). Role of Smac in human leukaemic cell apoptosis and proliferation. *Oncogene*, 22(11), 1589-1599. doi:10.1038/sj.onc.1206322.
24. Kaiser, E., Colecott, R., Bossinger, C., & Cook, P. (1970). Color test for detection of free terminal amino groups in the solid-phase synthesis of peptides. *Analytical Biochemistry*, 34(2), 595-598. doi:10.1016/0003-2697(70)90146-6.
25. Coulson, D. R., Satek, L. C., Grim, S. O. (1972). Tetrakis(triphenylphosphine)palladium(0). *Inorg. Synth*, 13, 121. doi:10.1002/9780470132449.ch23



## CHAPTER 4

### DESIGN AND SYNTHESIS OF A PHOTOCONTROLLED DRUG CARRIER

Light induced drug delivery has gained much attention due to the noninvasive and localized nature of this stimulus. The ultimate goal of this study is to design and synthesize a novel light sensitive peptide based nanocarriers. The designed nanocarriers are composed of peptide amphiphiles that assemble into micelles and fibers in an aqueous environment and the anthracene fluorophore that can undergo photodimerization upon irradiation at 365nm resulting partially dissociation of the assembled structures. After a drug is encapsulated within the hydrophobic core of a peptidic carrier systems, its release can be induced by exposure of anthracene moiety to UV light, which disrupts the nanostructures formed by self-assembly of small peptides and facilitates the drug release in a controlled manner.

#### 4.1 Introduction

The recent advances on stimuli responsive systems make the on-demand drug delivery feasible, in particular from the field of nanomedicine. Since the delivery of a drug in spatial-, temporal- and dosage-controlled fashions is clinically important, nanocarriers with structures that are transformable in response to an external stimuli have gained increasing attention. The serious need arises for more efficient drug carriers that have a crucial role on drug efficacy. A broad range of nanocarriers with diverse sizes, architectures and physiochemical properties have been designed. These include self-assembled peptide nanostructures, liposomes, polymer nanoparticles, dendrimers, and

inorganic nanoparticles made of iron oxide, quantum dots, and gold or metal oxide frameworks.

Material scientist have designed or modified the existing nanocarriers to fulfill the requirements of ideal drug delivery systems. Biocompatibility, large drug payload and controlled release function are the major properties of ideal drug carriers. The carrier material must be chemically and biologically inert so that it would not react with both the drug that it loaded and the human organs that it might interact. As a primary element, the dosing amount should be controlled precisely with the payload capacity. Materials with large drug storage volume are preferred. On-demand release (also termed ‘switch on/off’) enables the excellent spatial, temporal and dosage control. By answering the signals either existing inside the environment or externally created, drug carrier discharges the drug to serve its purpose. The accurate design of controlled release based on the fully understanding of relevant stimuli signals and releasing mechanism.

On-demand drug delivery systems take the advantage of stimuli signals that are basically categorized into two main types: internal stimuli and external stimuli. Intracellular environment of normal tissue and diseased tissue may differ in pH value, redox state, types and amounts of biomolecules.<sup>1</sup> These natural gradients make internal stimuli an ideal trigger for controlled release and enhanced specificity of carrier.

On the other hand, external stimuli plays an equally important role. External stimuli doesn't exist inside the human body and extra applied to the disease location by providing more accurate control over the drug carriers. The exposure of temperature changes, magnetic fields, ultrasounds, light and electric fields are generally used external stimulus that have been used.<sup>1, 2</sup>

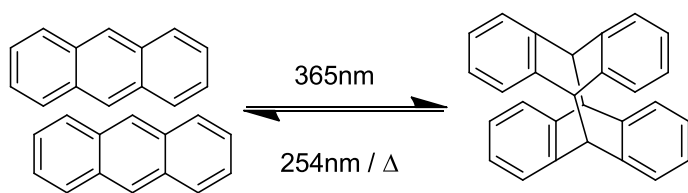
Light induced drug delivery remain among the most popular stimuli-responsive strategy owing to their non-invasive nature and the possibility of remote spatiotemporal control. The drug releasing behavior of the light triggered systems can be precisely controlled by applying specific light irradiation at a specific position. Light takes advantage of (i) photodimerizations, cis–trans photoconversions; (ii) photocleavage of chemical bonds



directly or assisted by photosensitizers; or (iii) photo-induced heating of gold nanoparticles (AuNPs) to control mass transport from pore voids to a solution.<sup>3</sup> Among all these light induced mechanism, photodimerization is one of the oldest and well-established mechanism for various type of light sensitive molecules.

Photodimerization is a bimolecular photochemical process in which an electronically excited unsaturated molecule reacts with an unexcited molecule of the same species to give addition products. This simple reaction, which allows a rapid change in the size of molecules, has been used to design stimuli responsive systems. The first example of a photo responsive delivery systems was based on photodimerization reaction of coumarin, which was developed by Fujiwara and co-workers in 2003.<sup>4,5</sup> Coumarin undergoes a [2 + 2] photodimerization in which there is a cycloaddition reaction that involves carbon-carbon double bonds of two neighboring molecules to result in a cyclobutane dimer. Photodimerization is performed in the presence of light and it is a reversible process that can be controlled by selecting the irradiation wavelength.

Apart from coumarin, anthracene and its derivatives have been used in many light responsive systems. The photophysical and photochemical properties photodimerization reaction of anthracene, which occurs favorably in UV light irradiations (250–400 nm) have been widely investigated for the application of photoresponsive materials.<sup>6-14</sup> Furthermore, the dimerization has been recently accomplished with visible light (400–700 nm) or multiphoton light in order to weaken some side effects during irradiation.<sup>15-17</sup> However typical dimerization reaction takes place upon irradiation at 365 nm, at the 9 and 10 carbons (Figure 4.1) . This photochemical transformation can be easily monitored by fluorescence spectroscopy as the anthracene core responsible for the molecule's emission at 470 nm is disrupted upon dimerization, thus providing a probe for following the progress of the reaction. The photodimer is found to be thermally stable, with no indication for dissociation at room temperature. However the dimerization may be reversed either by irradiation at 254 nm or heating over 100°C.

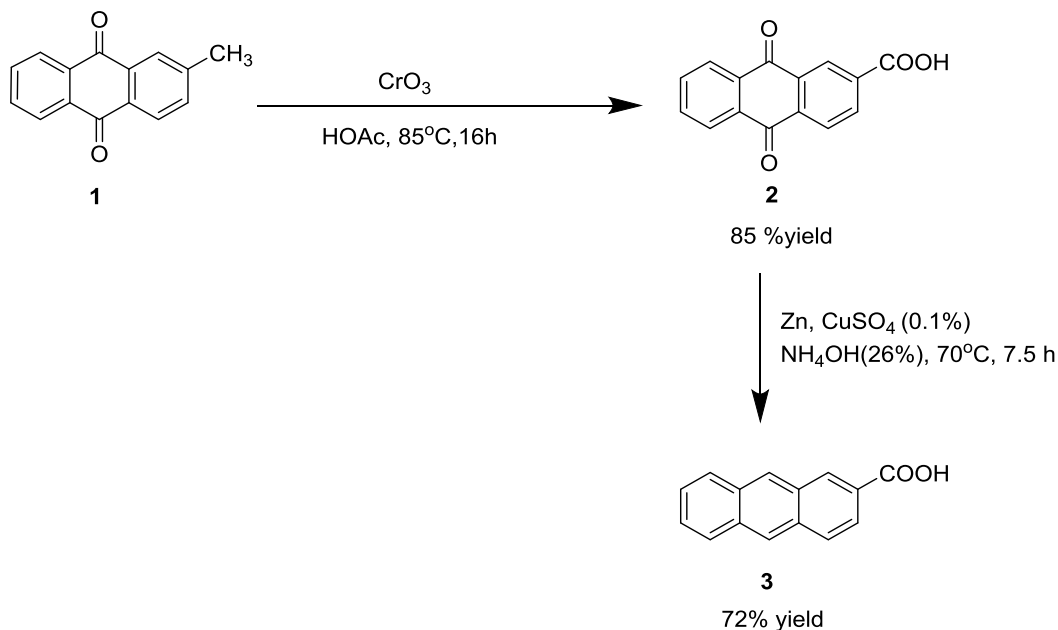


**Figure 4. 1** [4+4] cycloaddition reaction of anthracene molecules and its reverse reaction

In this study our major goal is take the advantages of photoactive anthracene moiety for light induced drug delivery systems. We have designed and synthesized a novel anthracene-containing micelle and fiber forming peptides and investigated structural disruption of peptide architecture with light.

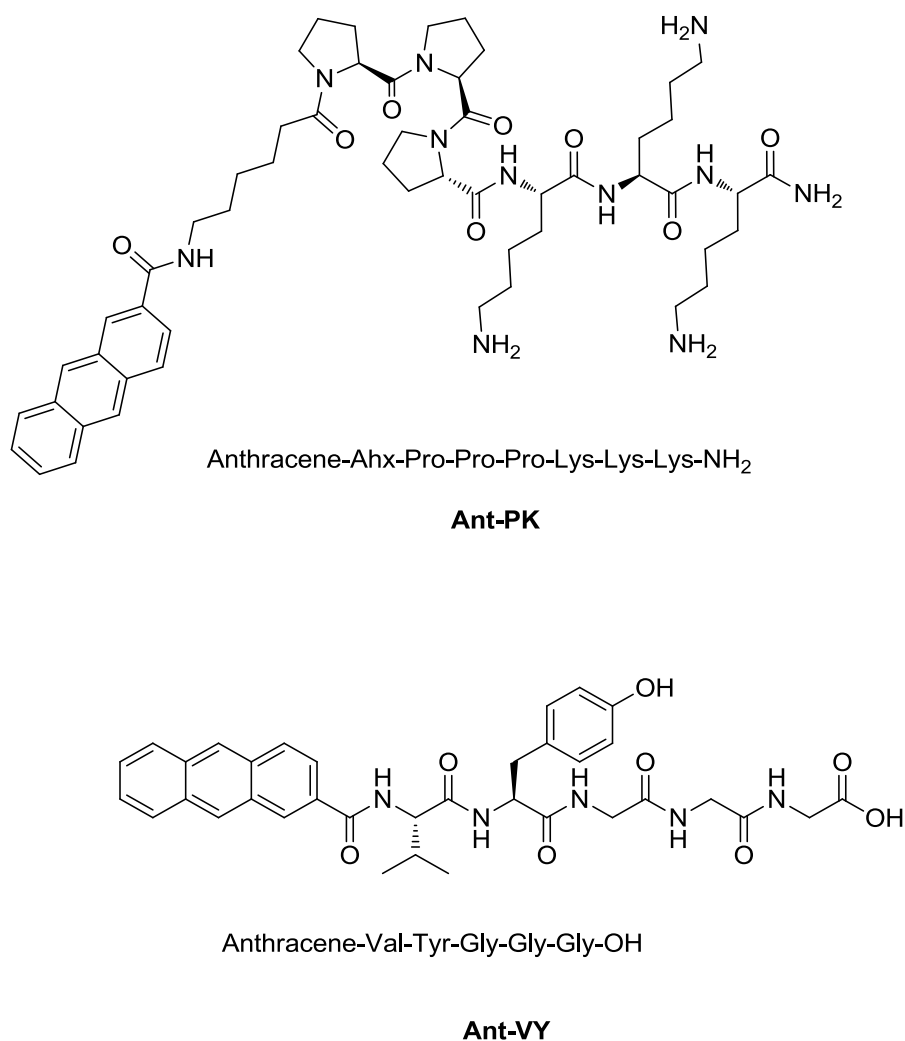
#### 4.2 Results and Discussion

In order to use in SPPS, anthracene-2 carboxylic acid was synthesized according to described procedures in literature and isolated in 72% yield (Scheme 4.1).<sup>18</sup>



**Scheme 4. 1** Synthesis pathway of Anthracene-2-carboxylic acid

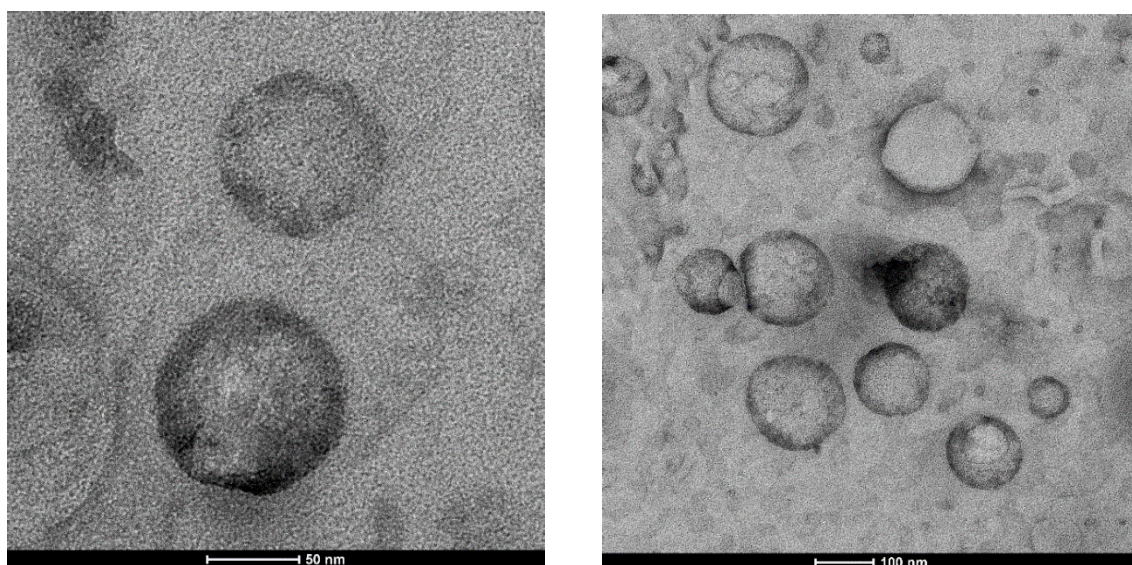
Anthracene carboxylic acid was coupled to micelle forming small AhxPPPKKK<sup>19</sup> peptide and fiber forming VYGGG peptide<sup>20</sup> while peptides were still on resin, resulting small peptide molecules which can self-assemble in aqueous media (Figure 4.2).



**Figure 4. 2** Structure of Ant-PK and Ant-VY peptides

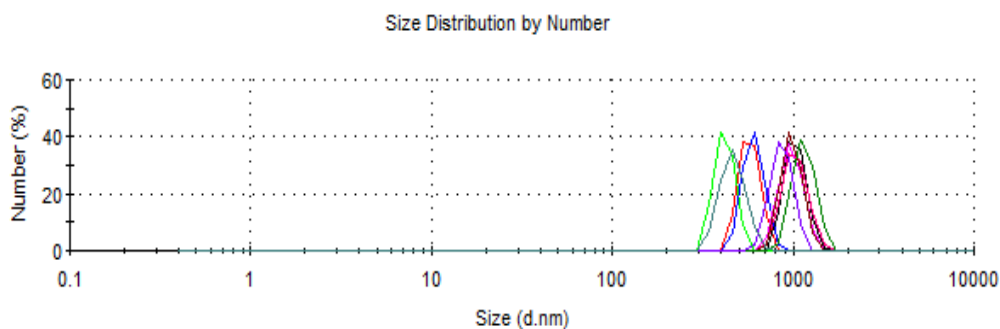
Our initial attempt was disruption of micellar structure, thereby photoresponsive micelle forming Ant-PK peptide was dissolved in water. In order to neutralize positive charges on lysine residues, basicity of the peptide solution was arranged to pH 11

using 1N NaOH solution. However, contrary to the expectations, both Transmission electron microscopy (TEM) images and Dynamic light scattering (DLS) analysis indicated no evidence of micellar structure prior to irradiation. In the light of this finding, 0.5 wt. % Ant-PK peptide solution was prepared in water and pH of the solution was fixed to pH 4 using 1N HCl solution. TEM images proved that peptides were self-assembled into micelles size ranging 100-200nm when lysines are positively charged under acidic conditions (Figure 4.3).



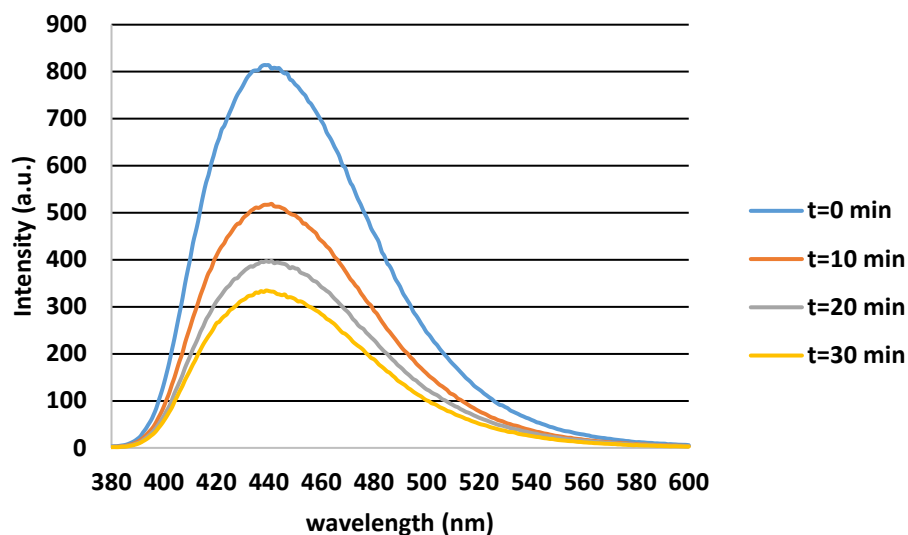
**Figure 4. 3** Positively stained TEM image of Ant-PK peptide at pH 4

Hydrodynamic size of peptidic micelles were also analyzed with DLS measurement and the mean of ten measurements was taken. Average hydrodynamic size was determined as 467.8 nm as shown in (Figure 4.4) and size distributions were around 74.42 nm.



**Figure 4. 4** Dynamic light scattering size distribution graph of Ant-PK peptide before irradiation

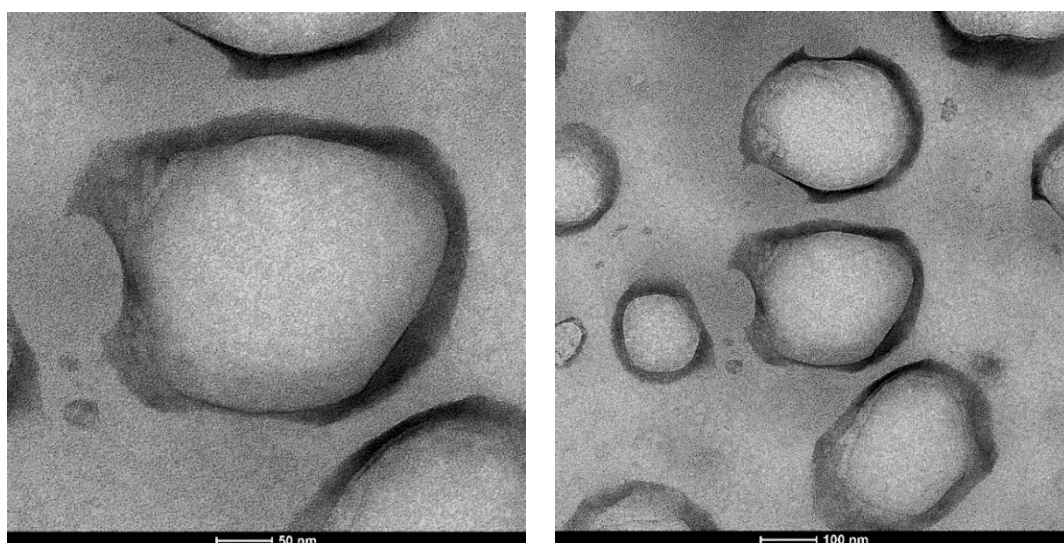
Irradiation experiments were performed with aliquots taken from the peptide solution over the course of 10 minute irradiation, total irradiation time proceeded 30 minute. Since the extended  $\Pi$ -systems in anthracene broken into dimers, cycloaddition reaction resulted in a decrement of aromaticity, which also caused decrement of fluorescence emission that drives from fully conjugated aromatic system. Therefore, dimerization reaction was followed with anthracene emission spectra in aqueous solution covering 380–600 nm intervals. The maximum emission peak around 440 nm was weaken upon irradiation. On the basis of the signal intensity decrement, overall conversion of photodimerization reaction was calculated at around 59.01% (Figure 4.5).



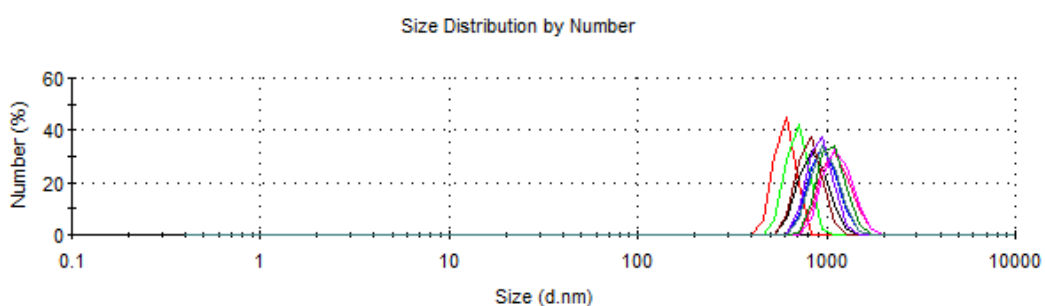
**Figure 4. 5** Fluorescence emission intensity of Ant-PK at 125  $\mu\text{M}$  (0.5 wt. %) with  $\lambda_{\text{ex}}$  365nm.

TEM image of peptide after 30 minute irradiation indicated that, drastic conformational changes in anthracene structure with light, leads partial disruption of micellar structure (Figure 4.6 A). Furthermore, DLS measurements supports this structural changes. Average hydrodynamic size determined as 993.0 nm as shown in (Figure 4.6 B) and size distributions were around 164.7 nm. In consideration of these findings, designed peptidic photoresponsive micellar system can be used a potential drug carrier.

**A**

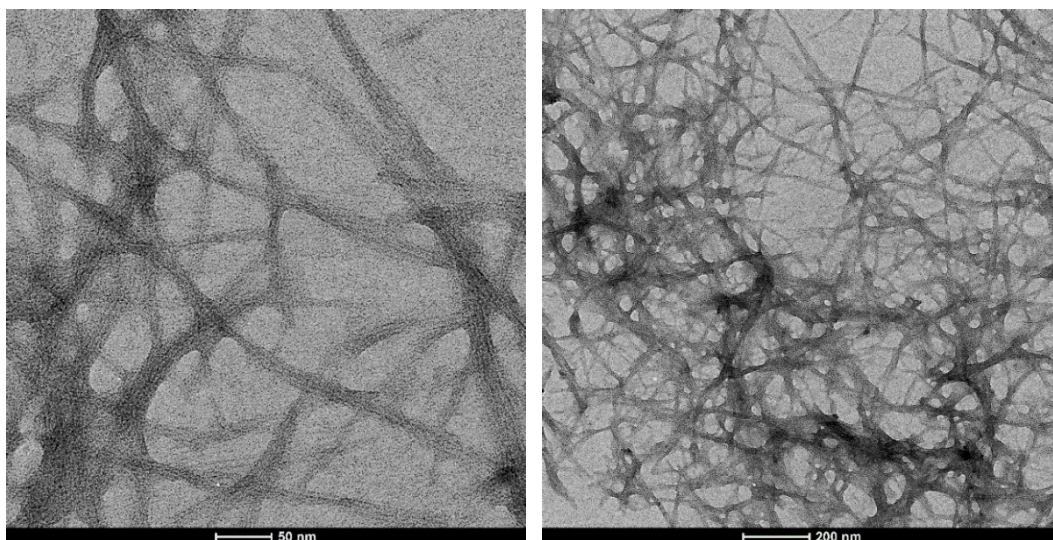


**B**



**Figure 4. 6 A)** TEM images of micellar peptides after irradiation **B)** Dynamic light scattering size distribution graph of peptide after irradiation

Ant-VY peptide that self-assembles into fibrillar structure at pH 4 (Figure 4.7) was also investigated as photocontrolled drug carrier systems. Pentapeptide VYGGG needs aromatic-aromatic interaction for stimulating self-assembly in water. Native form of this peptide doesn't form nanofibers, without the attachment of any aromatic groups.<sup>20</sup> Therefore anthracene carboxylic acid was coupled to N-termini of peptide both promoting self-assembly and disrupting it with photo irradiation.

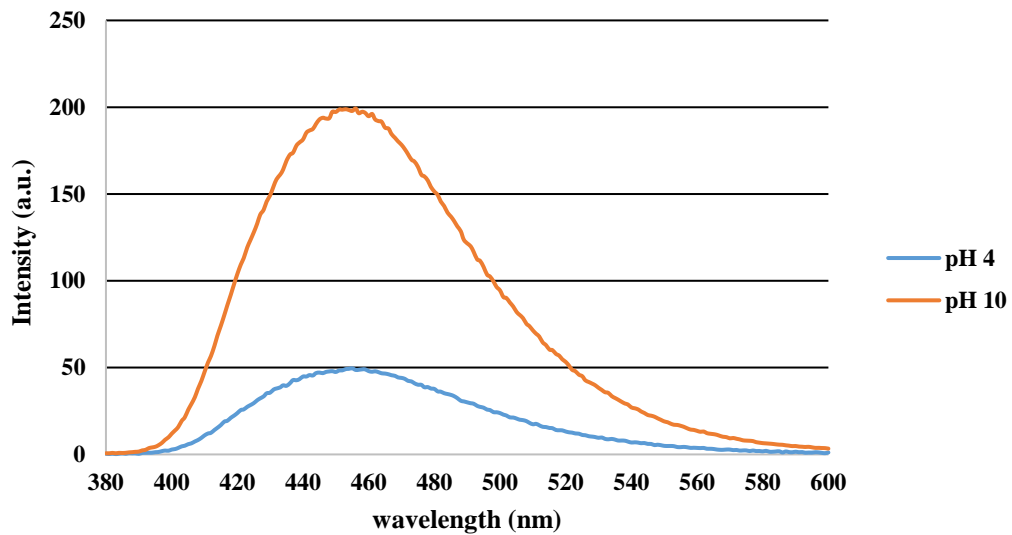


**Figure 4. 7** TEM image of Ant-VY peptide at pH 4.

Self-assembly of Ant-VY peptide was studied by TEM, UV and fluorescence spectroscopy. Although TEM images proved that peptide is forming fibrillar structure, it didn't offer clear data about whether photoirradiation works or not. The emission spectra of the peptide at pH 10 (solution formation) and pH 4 (gel formation) offer useful and relevant information regarding the interaction of the aromatic rings. The decrease of fluorescence emission peak at around 450 nm indicate quenching due to aromatic-aromatic interaction between the anthracene groups. The self-quenching effect of anthracene decreases upon light induced dimerization of anthracene moieties which causes increase in fluorescence emission (Figure 4.8). On the other hand, photodimerization causes decrease in concentration of anthracene.

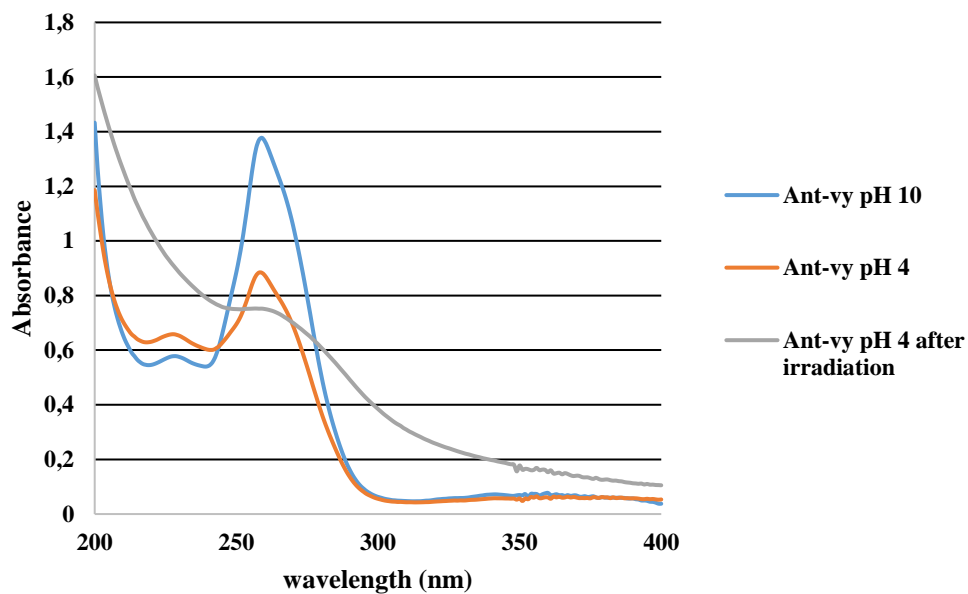
These two effect neutralized each other and resulted no change in emission spectra after irradiation. Therefore, following the photodimerization reaction with emission spectra was failed.





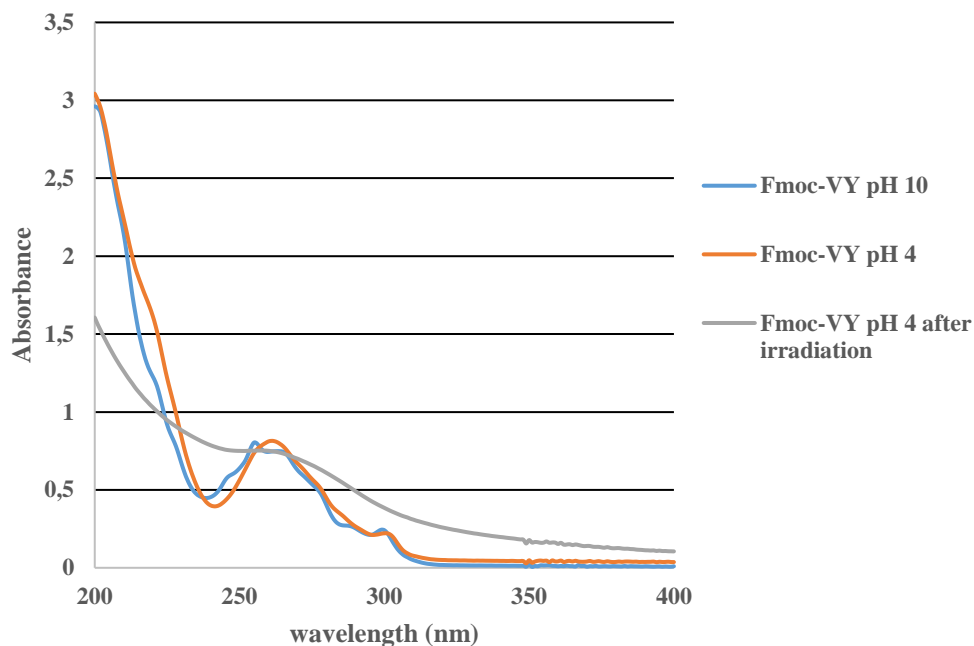
**Figure 4. 8** Fluorescence emission spectra of Ant-VY peptide at 122  $\mu$ M with  $\lambda_{ex}$  365nm.

The UV-Vis spectra of Ant-VY peptide self-assembled peptides (pH 4) showed a decrease in absorption peaks and a small shift (1 nm) in the wavelength of maximum absorption (compared with those of randomly distributed Ant-VY peptide at pH10). When peptide irradiated for 30 minute with 10 minute intervals, absorption of the self-assembled peptide decreased (Figure 4.9)



**Figure 4. 9** UV-Vis absorption spectra of Ant-VY at pH 10, pH 4 and after irradiation at pH 4.

In order to prove that photodimerization reaction causes decrease in absorbance intensity. Fmoc-VY peptide (control peptide) was irradiated with 30 minute with 10 minute intervals. Although self-assembly of peptide at pH 4 causes shift in the wavelength, photoirradiation causes nothing significant in the absorbance intensity, because Fmoc is inert against light (Figure 4.10).

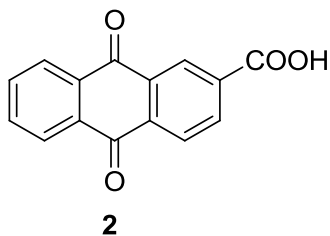


**Figure 4. 10** UV-Vis absorption spectra of Fmoc-VY at pH 10, pH 4 and after irradiation at pH 4.

To summarize, we have synthesized two different peptide based nanocarriers with photoactive anthracene moiety. Aqueous solution of Ant-PK peptide forms micellar structure and aqueous solution of Ant-VY peptide forms fibrillar structure at pH 4. Irradiation of these peptide systems with 365 nm light source partially disrupted their structure, thus providing control over their structural integrity. Despite the fact that some hurdles remain to be taken, the results presented in this chapter demonstrate that these systems are very promising for controlled drug release with non-invasive light exposure.

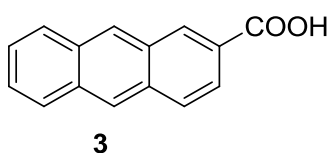
## 4.3 Experimental

### 4.3.1 Synthesis of anthraquinone-2-carboxylic acid (2)<sup>18</sup>



2-methylantraquinone (1) (1 g, 4.5 mmol) and acetic acid (50 mL) were added into two necked flask fitted with a condenser. A mechanical stirrer and a thermocouple were also placed into flask. The reaction mixture was warmed gently with stirring to dissolve 2-methylantraquinone. Then anhydrous CrO<sub>3</sub> (5.4 g, 54 mmol) was added slowly with vigorous stirring. The solution mixture was heated to 85 °C and kept at that temperature overnight (16 hours). Then, the completed reaction mixture was cooled at room temperature and diluted with 150 mL distilled water. The resulting precipitate was filtered and washed with water until the blue color of chromium salts disappeared. The obtained solid was recrystallized with acetic acid. The reaction was completed with 85% yield. <sup>1</sup>H NMR (400 MHz, DMSO) δ 13.73 (s, 1H), 8.64 (d, J = 1.7 Hz, 1H), 8.38 (dd, J = 8.0, 1.6 Hz, 1H), 8.28 (dd, J = 8.0, 1.9 Hz, 1H), 8.21 (dd, J = 5.1, 2.2 Hz, 2H), 8.01 – 7.90 (m, 2H). <sup>13</sup>C NMR (100 MHz, DMSO) δ 181.99, 181.84, 165.90, 135.60, 135.54, 134.69, 134.67, 134.35, 133.13, 132.97, 127.30, 126.81.

### 4.3.2 Synthesis of anthracene-2-carboxylic acid (3)<sup>18</sup>



Anthraquinone-2-carboxylic acid (2) (0.5 g, 2 mmol), zinc dust (2.6 g, 40 mmol), CuSO<sub>4</sub>·5H<sub>2</sub>O (0.1 g, 0.4 mmol) and aqueous ammonia (35 mL, 26%) were added into a 100 mL flask. The reaction mixture was stirred with magnetic stirrer under reflux at 70 °C for 5.5 hours. Then, the reaction temperature was increased to 85 °C and kept for 2 hours at that temperature. The completed hot reaction mixture was filtered to remove insoluble residues and the filtrate was cooled. After that, the filtrate was acidified with dilute HCl (1:1), until pH between 4-5. The precipitated yellow solid was filtered and dried in freeze dryer. Then, the yellow solid was recrystallized with acetic acid. The reaction was completed with 72% yield. <sup>1</sup>H NMR (400 MHz, DMSO) δ 8.76 (s, 2H), 8.62 (s, 1H), 8.30 – 7.92 (m, 4H), 7.55 (s, 2H).

### 4.3.3 Synthesis of Ant-PK peptide

Ant-PK peptide was synthesized using standard solid-phase peptide synthesis (SPPS) methods on rink amide MBHA resin (0.25 mM scale, 1.0 mmol/g loading) using a CEM Discover Bio - Manual Microwave Peptide Synthesizer. Each amino acid (3 equiv) was coupled by HBTU (2.85 equiv) and DIEA (6 equiv) in DMF. A standard coupling program (20 W, 75 °C, 10 min) was used for all amino acids except for the coupling of Fmoc-Pro-OH, which were double coupled (20W, 75 °C, 15 min). Deprotections were performed in 20% piperidine in DMF (20 W, 75°C, and 3 min.) and repeated two times. Each coupling and deprotection was monitored by Kaiser test except Fmoc-Pro-OH. The N-terminus of the peptides was extended with 6-aminohexanoic acid. After removal of final Fmoc group from N-terminal Fmoc-peptide-resin, 2-anthracene carboxylic acid (**3**) was coupled to the peptidyl resin with 3.0 equivalents of phosphonium- based powerful coupling reagent, bromo-tris(pyrrolidino)-phosphonium hexafluorophosphate( PyBroP) and 6.0 equiv of DIEA for 90 min to 2h, at room temperature in DMF. Anthracene was coupled as a fluorescent and photoactive part of the peptide and 6-aminohexanoic acid was used as a spacer to increase the conformational freedom of the anthracene moiety. Following with the anthracene coupling, deprotection of the side chains and cleavage of the peptide from resin were done with TFA/TIS/H<sub>2</sub>O=90:5:5 (v/v/v) for 90min, acidic peptide solution was precipitated in cold ether and collected with centrifugation. Resulting peptide was lyophilized in MilliQ and purified using preparative RP-HPLC. Purity was checked with analytical RP-HPLC and identity verified by mass spectrometry. Sample preparation and analytical and preparative RP-HPLC conditions were same as mentioned in Chapter 3. Ant-PK peptide was obtained with 99.82% purity according to absorption peak at 214 nm. Mass of purified peptide was confirmed with HRMS in positive ion mode.  $[M+H]^+$  <sub>cal</sub>: 1010.6191 and  $[M+H]^+$  <sub>obs</sub>: 1010.6215.

### 4.3.4 Synthesis of Ant-VY peptide

Ant-VY peptide was synthesized on Fmoc-Gly-Wang resin in the CEM Discover Bio - Manual Microwave Peptide Synthesizer. Addition of first amino acid to the Wang Resin was done according to literature.<sup>21</sup> 2 equiv of Fmoc-Gly-OH, 4 equiv. of HOBT, and 2 equiv. of DIC in DMF solution was transferred into pre-swelled resin and 2 equiv. of DMAP was added into this solution, then left overnight stirring. Coupling

solution was drained and the modified resin was capped with benzoyl chloride/pyridine/DMF (10:8:82, v/v/v) solution for 30 minute and wash with DMF, DCM, ether respectively. Loading capacity of prepared resin was calculated as 0.65mmol/g, by using: Loading=  $A_{290}/(\text{mg of resin} \times 1.65)$  formula ( $A_{290}$  stands for UV absorbance of Fmoc group at 290nm).

For the synthesis Fmoc chemistry was used again with a solution of 20 % piperidine in DMF as the deprotection agent, HBTU as coupling reagent and DIPEA as base. Standard coupling and deprotection programs were applied as in Ant-PK peptide synthesis. 2-anthracene carboxylic acid (**3**) was coupled to the peptidyl resin as a final residue with 3.0 equivalents of PyBroP and 6.0 equiv of DIEA for 90 min to 2h, at room temperature in DMF. Deprotection of the side chains and cleavage of the peptide from resin were done with TFA/TIS/H<sub>2</sub>O=90:5:5 (v/v/v) for 60min, basic peptide solution was precipitated in cold ether and collected with centrifugation. Resulting peptide was lyophilized in MilliQ and purified using preparative RP-HPLC. Purity was checked with analytical RP-HPLC and identity verified by mass spectrometry. Since resulting peptide was acidic (the overall charge of a peptide is negative), 0.1% NH<sub>4</sub>OH (26%) was added to peptide solution and diluted to the appropriate volume before RP-HPLC analysis. The other RP-HPLC conditions were same as mentioned in Chapter 3. Ant-VY peptide was obtained with 84.67 % purity according to absorption peak at 214 nm. Mass of purified peptide was confirmed with HRMS in negative ion mode.  $[M-H]^-_{\text{cal}} : 654.2564$  and  $[M-H]^-_{\text{obs}} : 654.2545$ .

For control reaction, Fmoc-VYGGG-OH (Fmoc-VY) was also synthesized and characterized with Mass Spectroscopy and analytical RP-HPLC. Purity of peptide was calculated as 78.5% at 214nm.  $[M-H]^-_{\text{cal}} : 672.2670$  and  $[M-H]^-_{\text{obs}} : 672.2632$

#### 4.3.5 NMR analysis

<sup>1</sup>H-NMR and <sup>13</sup>C-NMR spectra were recorded on a Bruker 400 MHz spectrometer with DMSO-d<sub>6</sub> as solvent. Unless otherwise indicated, chemical shifts are reported in ppm downfield from tetramethylsilane (TMS) at room temperature using deuterated solvents as an internal standard. Abbreviations used for splitting patterns are s= singlet, br s = broad singlet, d= doublet, t= triplet and m= multiplet.

#### **4.3.6 Transmission electron microscopy (TEM)**

TEM measurements were performed on a JEM-2100F (JEOL) microscope operating at 200 kV. 0.5 mM peptide solutions were gently dripped on holey carbon coated TEM grids and grids were negatively stained with 1 wt% aqueous uranyl acetate solution in water, excess materials were removed by washing with water. The TEM samples were air-dried for 3 h prior to imaging.

#### **4.3.7 Dynamic light scattering (DLS) measurements**

Before and after irradiation hydrodynamic sizes micellar Ant-PK peptides were measured using a Zetasizer Nano-ZS equipment (Malvern Instruments Ltd.). Number average hydrodynamic sizes were obtained by cumulative analysis of autocorrelation data. Samples were placed in polystyrene cells, which were cleaned with ultrapure water. Measurements were taken 10 times at 25 °C in order to check their reproducibility.

#### **4.3.8 Photodimerization reaction**

Samples were irradiated with mercury medium pressure lamp. The lamp is contained in double-walled immersion wells made of quartz, allowing water cooling and/or filtering of excitation radiation. All irradiations were carried out for 10 minutes and repeated 3 times.

#### **4.3.9 Fluorescence Spectroscopy**

Fluorescence spectra were recorded on a Varian Cary Eclipse Fluorescence Spectrophotometer. All spectra were taken at room temperature with an integration time of 0.1 s. The slit width was set at 5 nm for excitation and emission. Emission spectra were obtained from 380 to 600nm with excitation at 365 nm. EMT Detector voltage was arranged at 480 nm.

#### 4.4 References

1. Ding, C., Tong, L., Feng, J., & Fu, J. (2016). Recent Advances in Stimuli-Responsive Release Function Drug Delivery Systems for Tumor Treatment. *Molecules*, 21(12), 1715. doi:10.3390/molecules21121715
2. Mura, S., Nicolas, J., & Couvreur, P. (2013). Stimuli-responsive nanocarriers for drug delivery. *Nature Materials*, 12(11), 991-1003. doi:10.1038/nmat3776
3. Aznar, E., Oroval, M., Pascual, L., Murguía, J. R., Martínez-Mañez, R., & Sancenón, F. (2016). Gated Materials for On-Command Release of Guest Molecules. *Chemical Reviews*, 116(2), 561-718. doi:10.1021/acs.chemrev.5b00456
4. Mal, N. K., Fujiwara, M., & Tanaka, Y. (2003). Photocontrolled reversible release of guest molecules from coumarin-modified mesoporous silica. *Nature*, 421(6921), 350-353. doi:10.1038/
5. Mal, N. K., Fujiwara, M., Tanaka, Y., Taguchi, T., & Matsukata, M. (2003). Photo-Switched Storage and Release of Guest Molecules in the Pore Void of Coumarin-Modified MCM-41. *Chemistry of Materials*, 15(17), 3385-3394. doi:10.1021/cm0343296.
6. Kihara, H., & Yoshida, M. (2013). Reversible Bulk-Phase Change of Anthroyl Compounds for Photopatterning Based on Photodimerization in the Molten State and Thermal Back Reaction. *ACS Applied Materials & Interfaces*, 5(7), 2650-2657. doi:10.1021/am400111q.
7. Wang, C., Zhang, D., Xiang, J., & Zhu, D. (2007). New Organogels Based on an Anthracene Derivative with One Urea Group and Its Photodimer: Fluorescence Enhancement after Gelation. *Langmuir*, 23(18), 9195-9200. doi:10.1021/la701142d.
8. Al-Kaysi, R., & Bardeen, C. (2007). Reversible Photoinduced Shape Changes of Crystalline Organic Nanorods. *Advanced Materials*, 19(9), 1276-1280. doi:10.1002/adma.200602741.



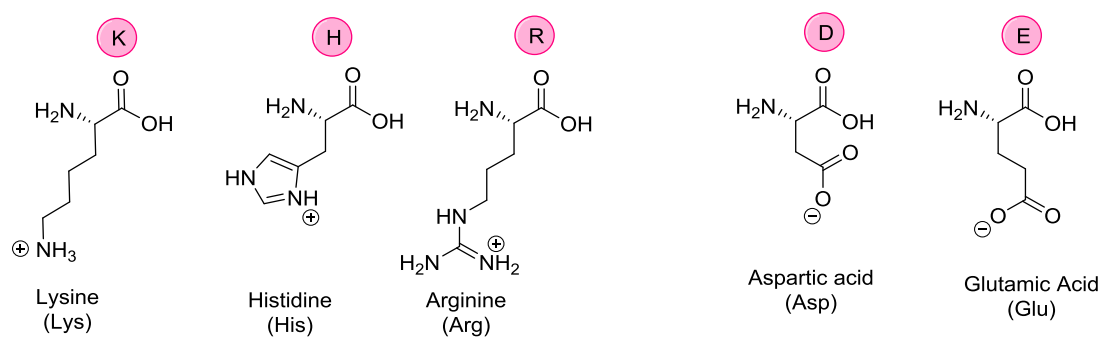
9. Ikegami, M., Ohshiro, I., & Arai, T. (2003). Hydrogen bonded molecular assembly by reversible cyclization reaction of anthracene. Electronic supplementary information (ESI) available: thermal change of  $^1\text{H}$  NMR spectrum of 2. See <http://www.rsc.org/suppdata/cc/b3/b304034h/>. *Chemical Communications*, (13), 1566. doi:10.1039/b304034h
10. Liu, Y., Chang, H., Jiang, J., Yan, X., Liu, Z., & Liu, Z. (2014). The photodimerization characteristics of anthracene pendants within amphiphilic polymer micelles in aqueous solution. *RSC Adv.*, 4(49), 25912-25915. doi:10.1039/c4ra02315c.
11. Jezowski, S. R., Zhu, L., Wang, Y., Rice, A. P., Scott, G. W., Bardeen, C. J., & Chronister, E. L. (2012). Pressure Catalyzed Bond Dissociation in an Anthracene Cyclophane Photodimer. *Journal of the American Chemical Society*, 134(17), 7459-7466. doi:10.1021/ja300424h.
12. Chen, W., Wang, J., Zhao, W., Li, L., Wei, X., Balazs, A. C., Russell, T. P. (2011). Photocontrol over the Disorder-to-Order Transition in Thin Films of Polystyrene-block-poly(methyl methacrylate) Block Copolymers Containing Photodimerizable Anthracene Functionality. *Journal of the American Chemical Society*, 133(43), 17217-17224. doi:10.1021/ja2036964.
13. Becker, H. D. (1993). Unimolecular photochemistry of anthracenes. *Chemical Reviews*, 93(1), 145-172. doi:10.1021/cr00017a008
14. Xu, J., Chen, Y., Wu, L., Tung, C., & Yang, Q. (2013). Dynamic Covalent Bond Based on Reversible Photo [4+4] Cycloaddition of Anthracene for Construction of Double-Dynamic Polymers. *Organic Letters*, 15(24), 6148-6151. doi:10.1021/ol403015s J
15. Good, J. T., Burdett, J. J., & Bardeen, C. J. (2009). Using Two-Photon Excitation to Control Bending Motions in Molecular-Crystal Nanorods. *Small*, 5(24), 2902-2909. doi:10.1002/sml.200900895
16. Islangulov, R. R., & Castellano, F. N. (2006). Photochemical Upconversion: Anthracene Dimerization Sensitized to Visible Light by a RuII Chromophore. *Angewandte Chemie International Edition*, 45(36), 5957-5959. doi:10.1002/anie.200601615

17. Dvornikov, A. S., Bouas-Laurent, H., Desvergne, J., & Rentzepis, P. M. (1999). Ultrafast kinetics of 9-decyanthracene photodimers and their application to 3D optical storage. *Journal of Materials Chemistry*, 9(5), 1081-1084. doi:10.1039/a808272c.
18. Arjunan, P., & Berlin, K. D. (1981). An Improved Synthesis Of 2-Anthraldehyde. *Organic Preparations and Procedures International*, 13(5), 368-371. doi:10.1080/00304948109356143
19. Guler, M. O., Claussen, R. C., & Stupp, S. I. (2005). Encapsulation of pyrene within self-assembled peptide amphiphile nanofibers. *Journal of Materials Chemistry*, 15(42), 4507. doi:10.1039/b509246a
20. Ma, M., Kuang, Y., Gao, Y., Zhang, Y., Gao, P., & Xu, B. (2010). Aromatic–Aromatic Interactions Induce the Self-Assembly of Pentapeptidic Derivatives in Water to Form Nanofibers and Supramolecular Hydrogels. *Journal of the American Chemical Society*, 132(8), 2719-2728. doi:10.1021/ja9088764
21. Nispen, J. W., Polderdijk, J. P., Greven, H. M. (1985). Suppression of side-reactions during the attachment of Fmoc-amino acids to hydroxymethyl polymers. *Recueil des Travaux Chimiques des Pays-Bas*, 104, 99-100. doi: 10.1002/recl.1985104030

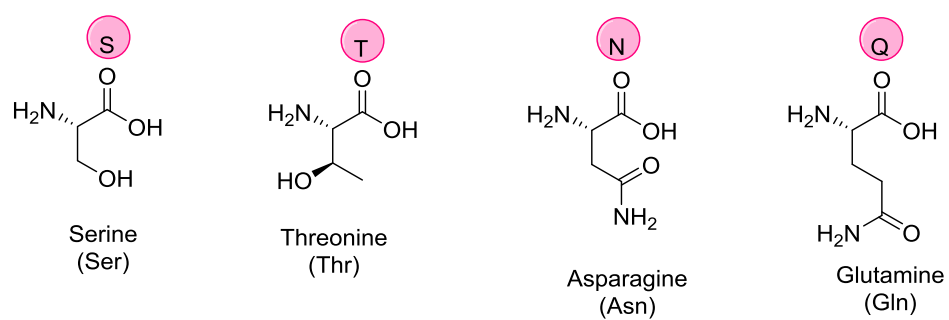
## APPENDICES

### APPENDIX A

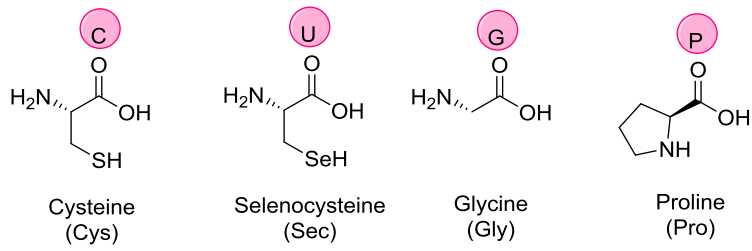
#### AMINO ACID CODE TABLE



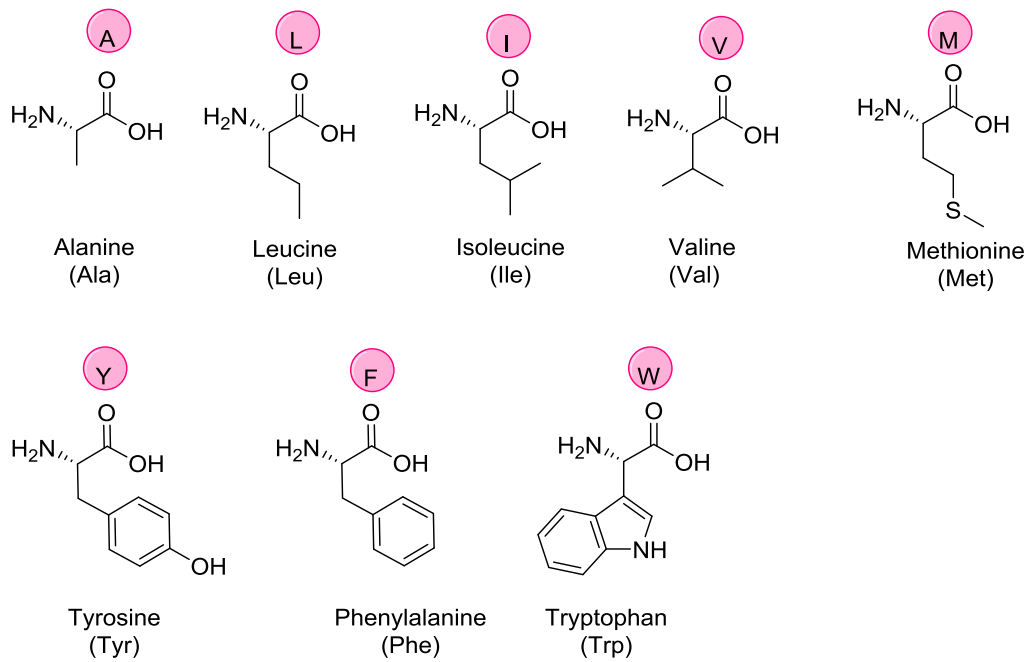
**Figure A. 1** Amino Acids with Electrically Charged Residues



**Figure A. 2** Amino Acids with Polar Uncharged Residues



**Figure A. 3** Unique Amino Acids



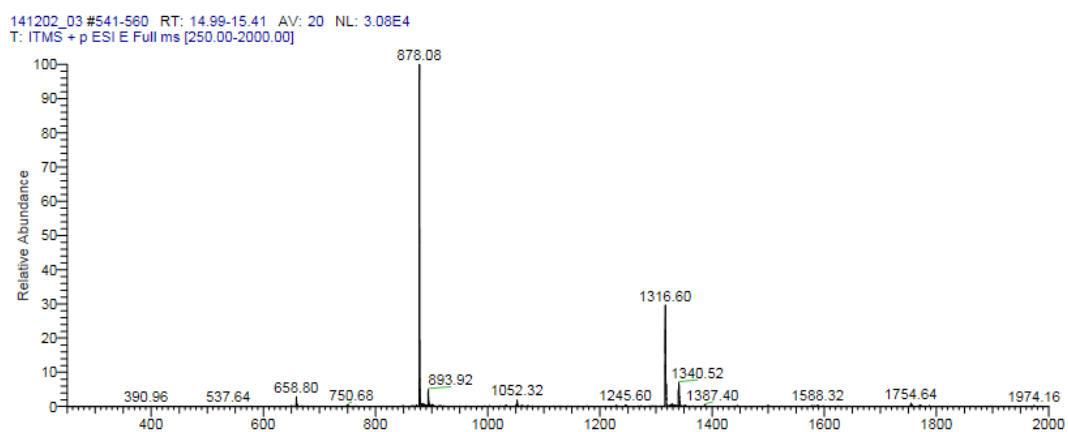
**Figure A. 4** Amino Acids with Hydrophobic residues

## APPENDIX B

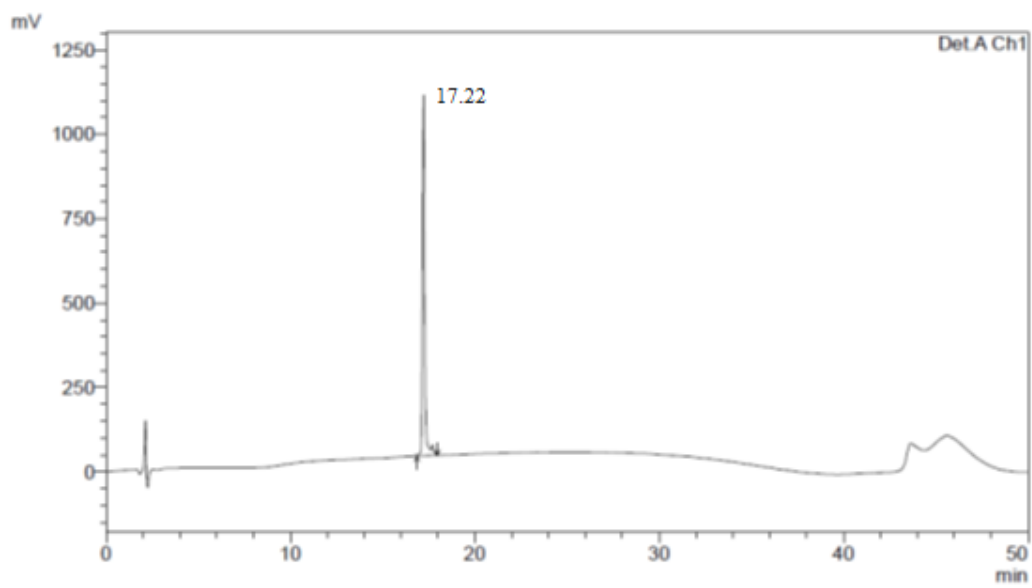
### DATA RELATED TO CHAPTER 2

**Table B. 1** Sequence, accurate mass and retention time of WT.

Entry	Sequence	[M+2] <sup>2+</sup> calculated	[M+2] <sup>2+</sup> observed	t <sub>R</sub> at 214 nm
WT	Ac-DLKNYIDKQLLPVINKQSCSISA-NH <sub>2</sub>	1316.23	1316.60	17.22



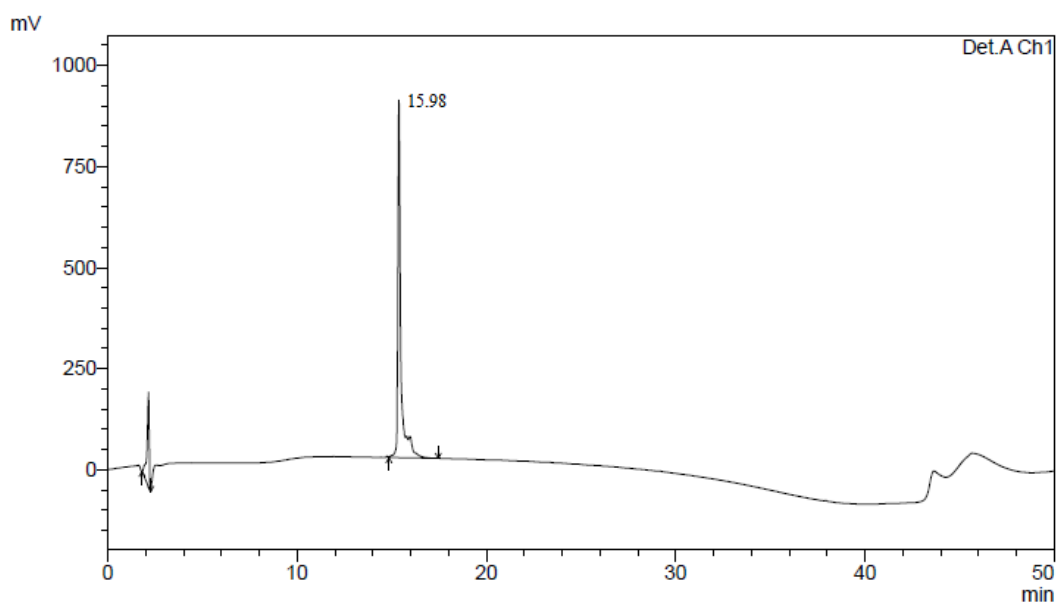
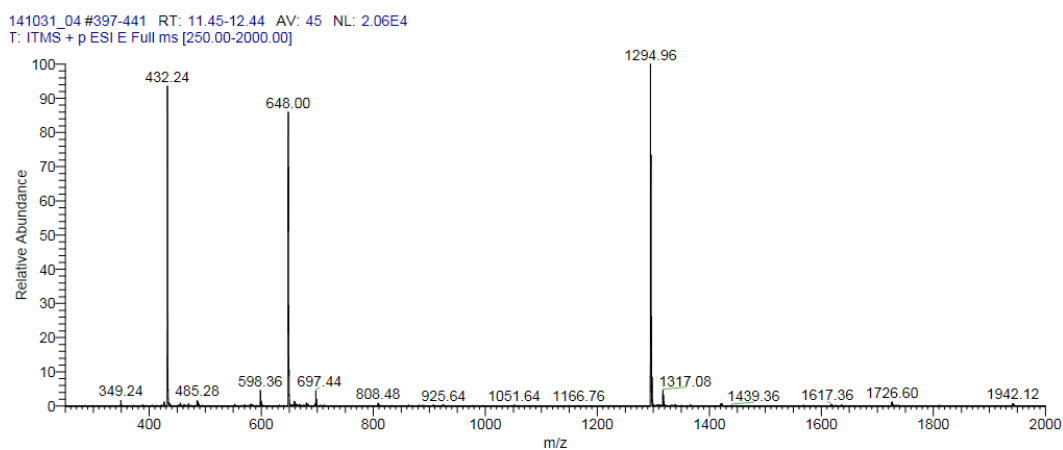
**Figure B. 1** Mass and RP-HPLC chromatogram of WT.



**Figure B.1** (Continued)

**Table B. 2** Sequence, accurate mass and retention time of  $\Delta 12$ .

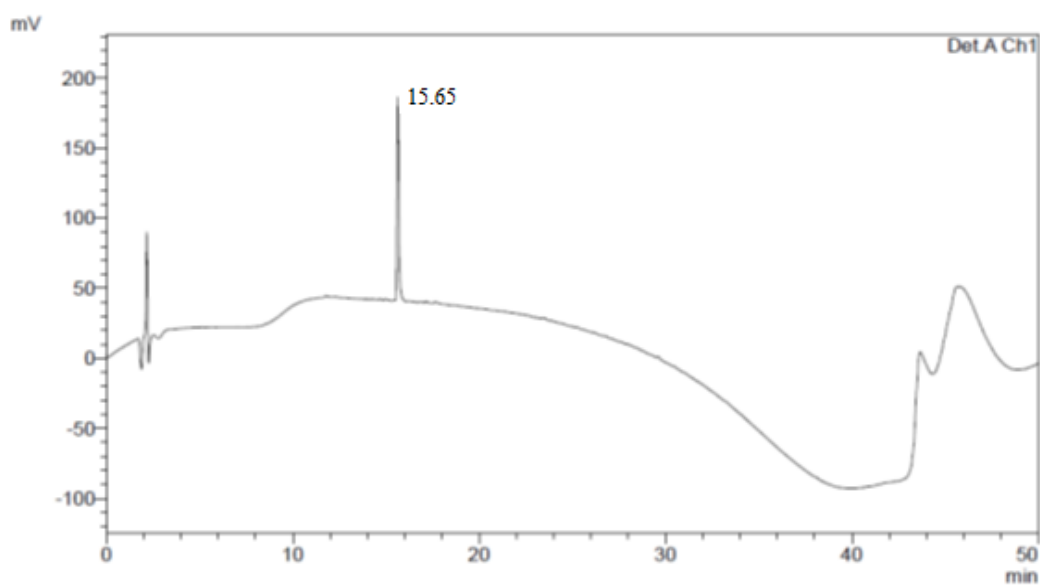
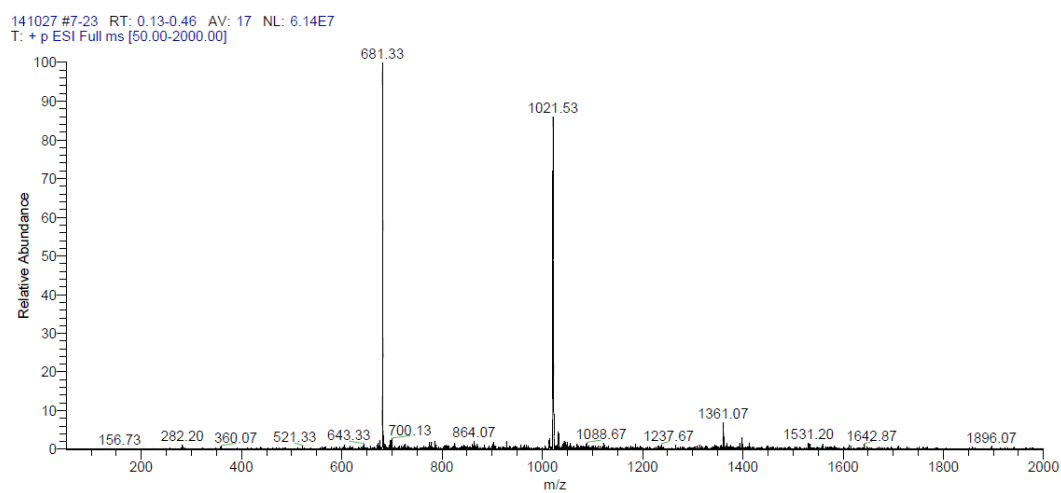
Entry	Sequence	$[M+2]^{2+}$ calculated	$[M+2]^{2+}$ observed	$t_R$ at 214 nm
$\Delta 12$	H-DKQLLPVINKQ-NH <sub>2</sub>	647.91	648.00	15.98



**Figure B. 2** Mass and RP-HPLC chromatogram of  $\Delta 12$ .

**Table B. 3** Sequence, accurate mass and retention time of  $\Delta 6$ .

Entry	Sequence	$[M+2]^{2+}$ calculated	$[M+2]^{2+}$ observed	$t_R$ at 214 nm
$\Delta 6$	H-DLKNYIDKQLLPVINKQ-NH <sub>2</sub>	1021.11	1021.53	15.65

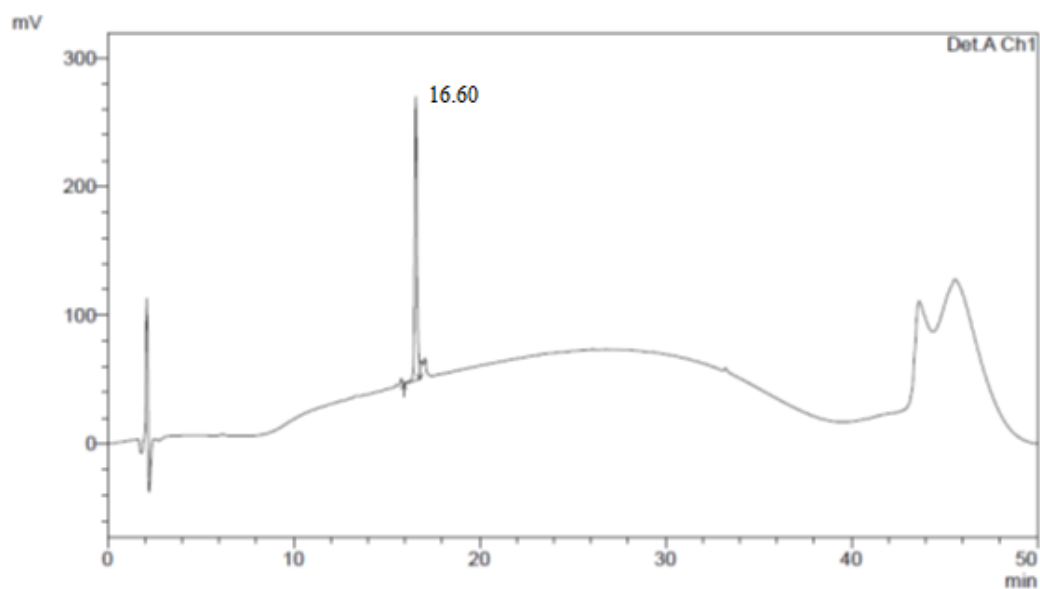
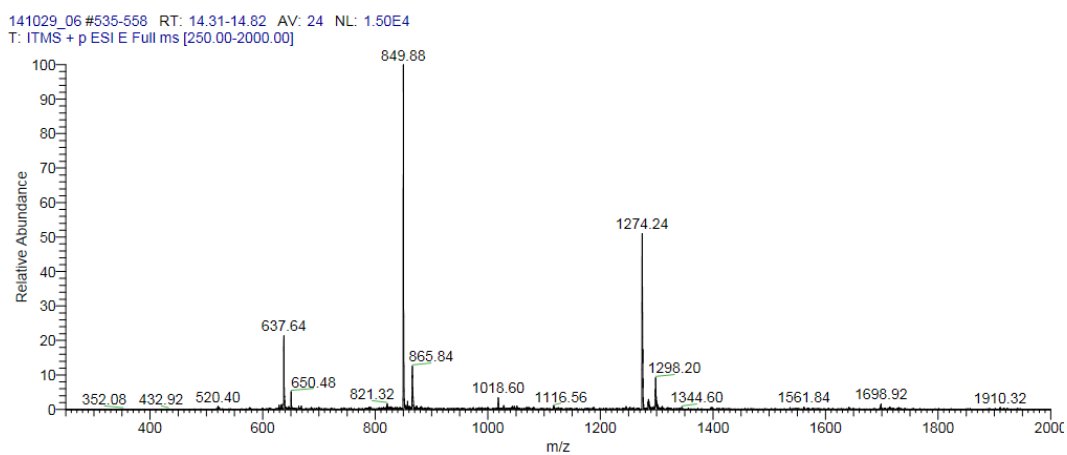


**Figure B. 3** Mass and RP-HPLC chromatogram of  $\Delta 6$ .



**Table B. 4** Sequence, accurate mass and retention time of N197A.

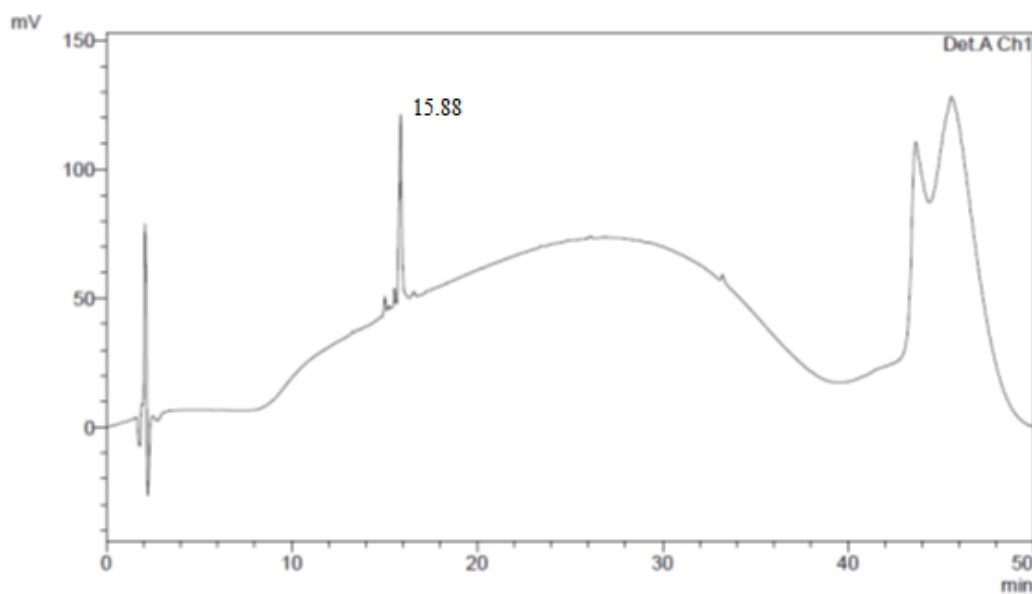
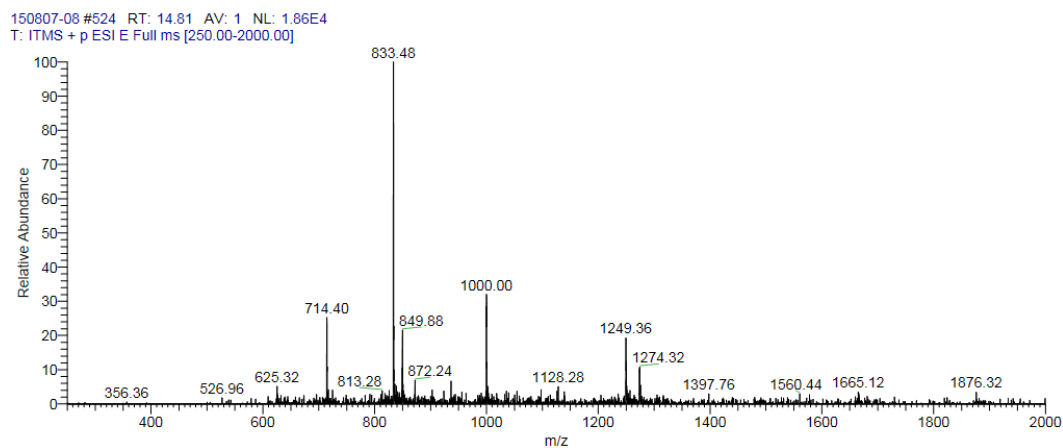
Entry	Sequence	[M+2] <sup>2+</sup> calculated	[M+2] <sup>2+</sup> observed	t <sub>R</sub> at 214 nm
N197A	H-DLKAYIDKQLLPVINKQSCSISA-NH <sub>2</sub>	1273.73	1274.20	16.60



**Figure B. 4** Mass and RP-HPLC chromatogram of N197A.

**Table B. 5** Sequence, accurate mass and retention time of Y198A.

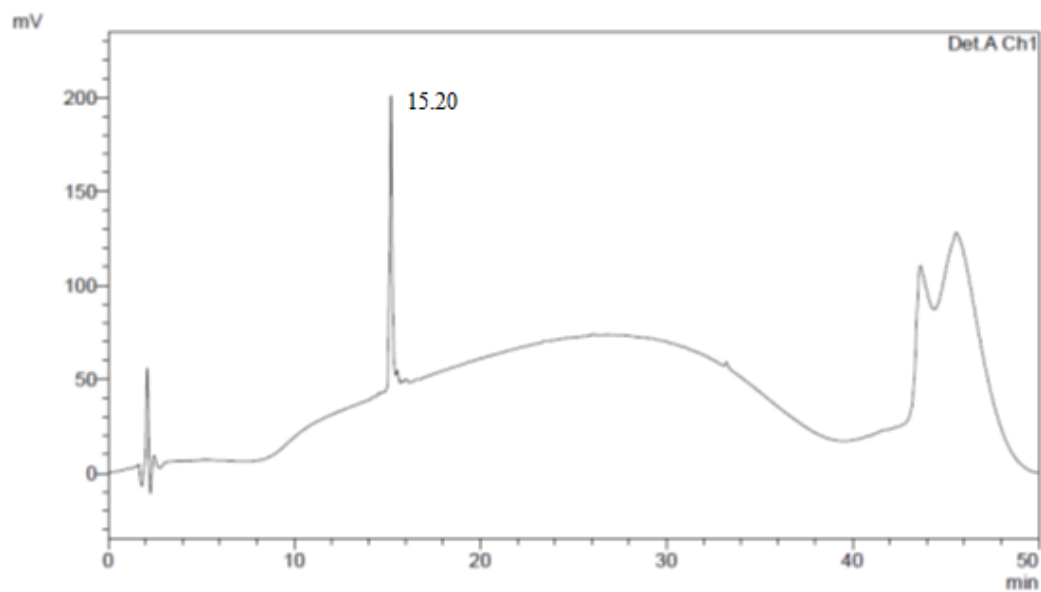
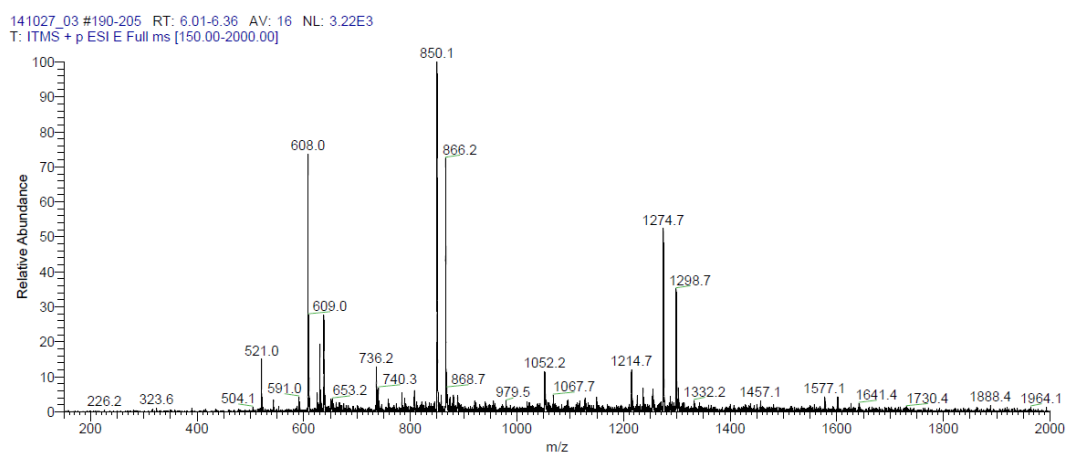
Entry	Sequence	[M+2] <sup>2+</sup> calculated	[M+2] <sup>2+</sup> observed	t <sub>R</sub> at 214 nm
Y198A	H-DLKNAIDKQLLPVINKQSCSISA-NH <sub>2</sub>	1249.22	1249.73	15.88



**Figure B. 5** Mass and RP-HPLC chromatogram of Y198A.

**Table B. 6** Sequence, accurate mass and retention time of I199A.

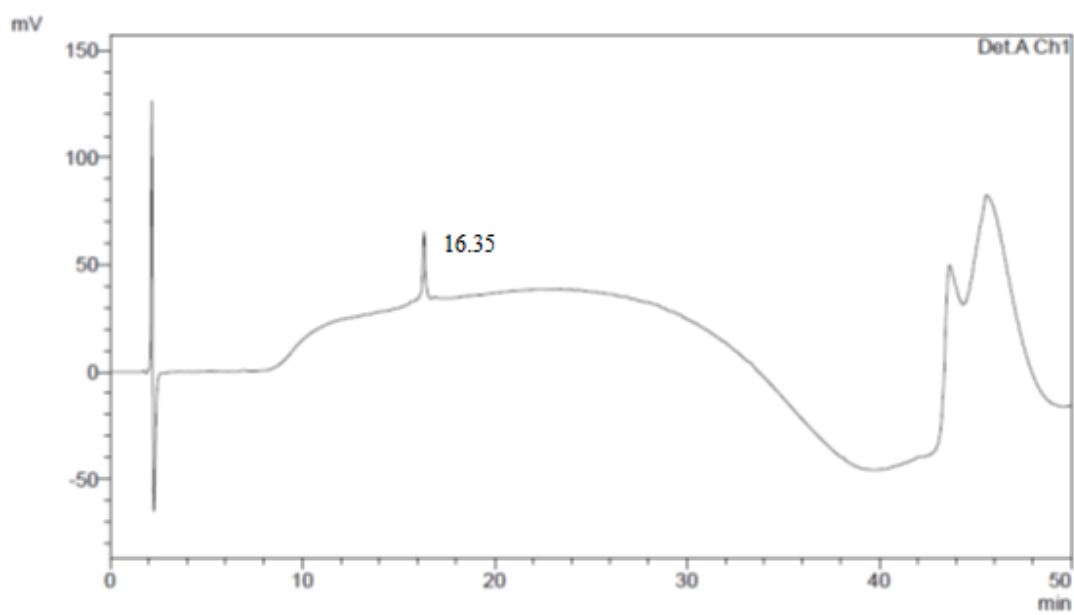
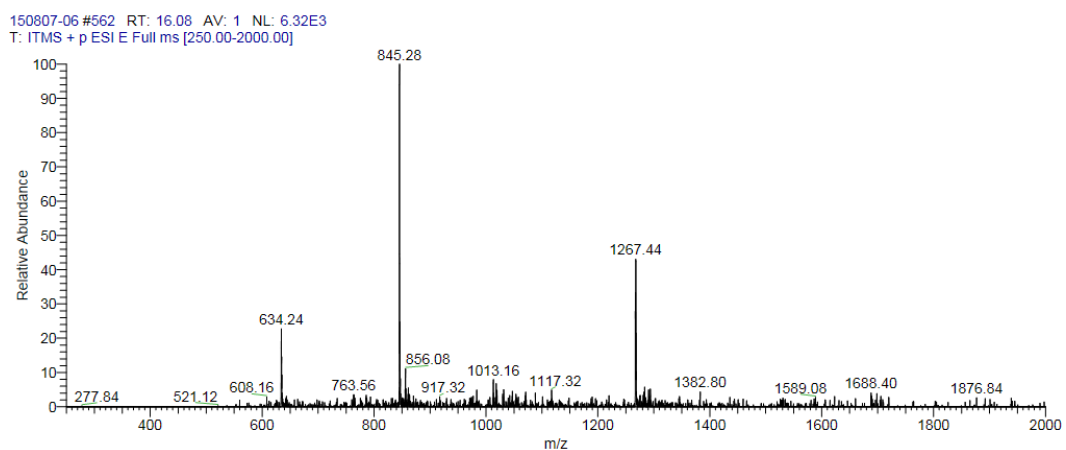
Entry	Sequence	[M+2] <sup>2+</sup> calculated	[M+2] <sup>2+</sup> observed	t <sub>R</sub> at 214 nm
I199A	H-DLKNYADKQLLPVINKQSCSISA-NH <sub>2</sub>	1274.20	1274.64	15.20



**Figure B. 6** Mass and RP-HPLC chromatogram of I199A.

**Table B. 7** Sequence, accurate mass and retention time of Q210A.

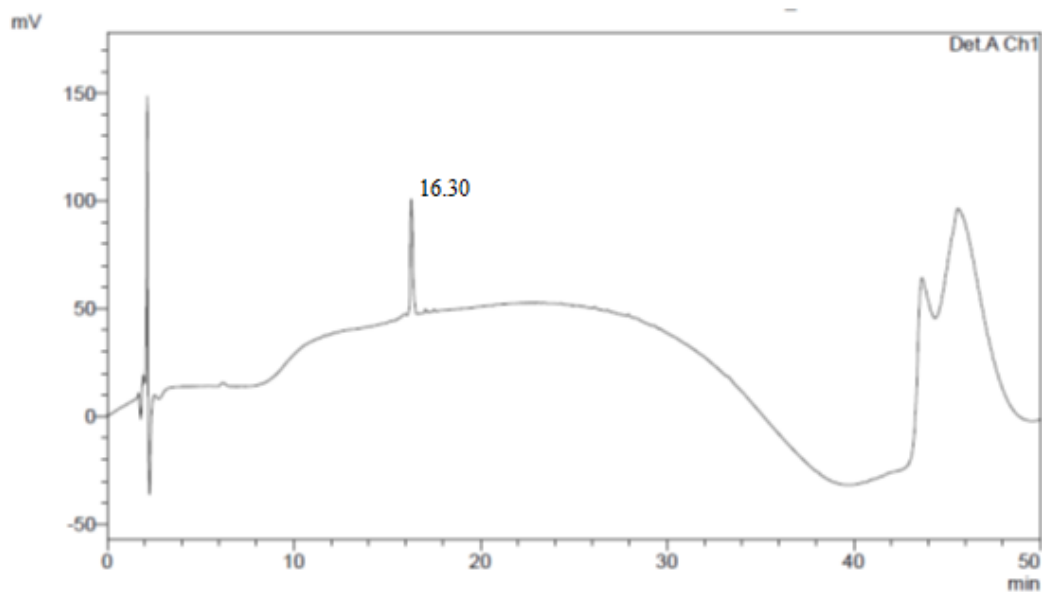
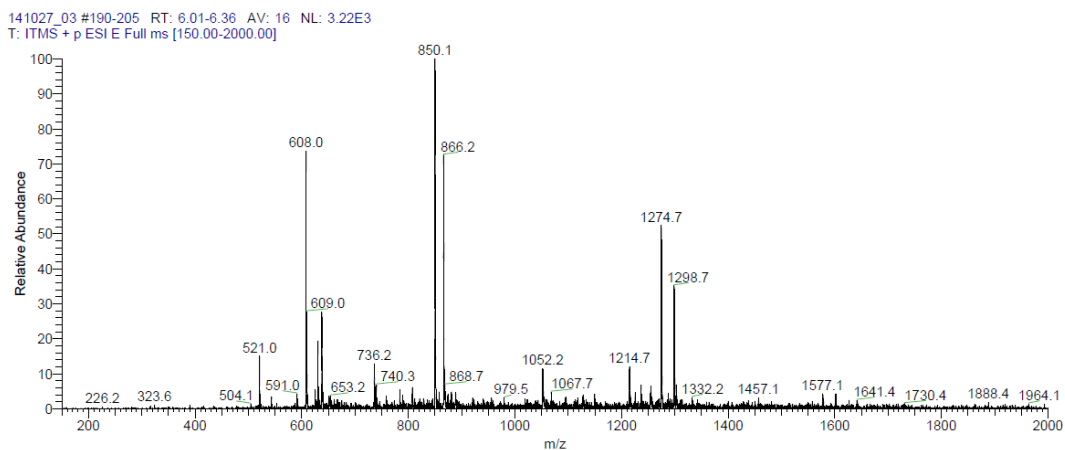
Entry	Sequence	$[M+2]^{2+}$	$[M+2]^{2+}$	$t_R$ at 214 nm
		calculated	observed	
Q210A	H-DLKNIYDKQLLPVINKASCSISA-NH <sub>2</sub>	1266.72	1267.80	16.35



**Figure B. 7** Mass and RP-HPLC chromatogram of Q210A.

**Table B. 8** Sequence, accurate mass and retention time of I214A.

Entry	Sequence	[M+2] <sup>2+</sup> calculated	[M+2] <sup>2+</sup> observed	t <sub>R</sub> at 214 nm
I214A	H-DLKNYIDKQLLPVINKQSCSASA-NH <sub>2</sub>	1274.20	1274.70	16.30

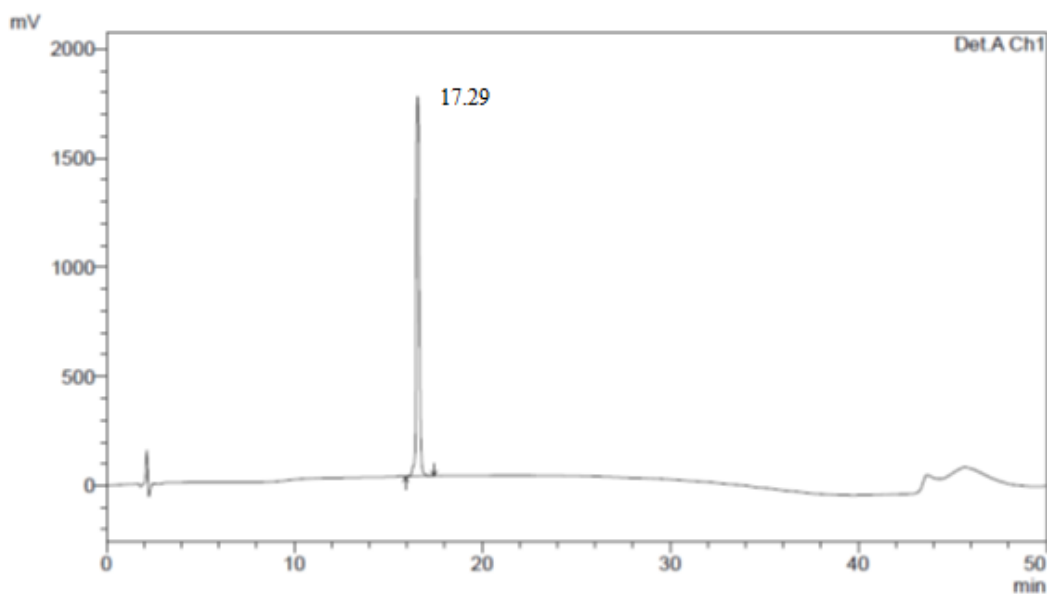
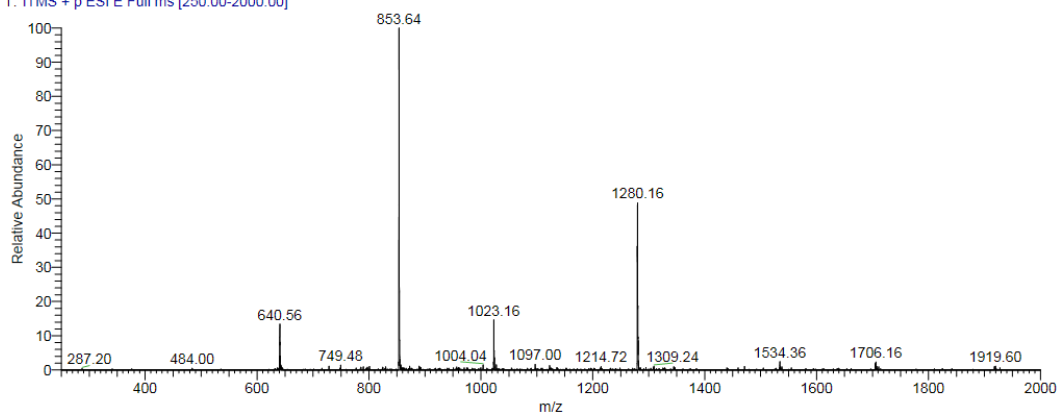


**Figure B. 8** Mass and RP-HPLC chromatogram of I214A.

**Table B. 9** Sequence, accurate mass and retention time of C212A.

Entry	Sequence	$[M+2]^{2+}$ calculated	$[M+2]^{2+}$ observed	tr at 214 nm
C212A	H-DLKNIYDKQLLPVNVKQSASISA-NH <sub>2</sub>	1279.24	1280.16	17.29

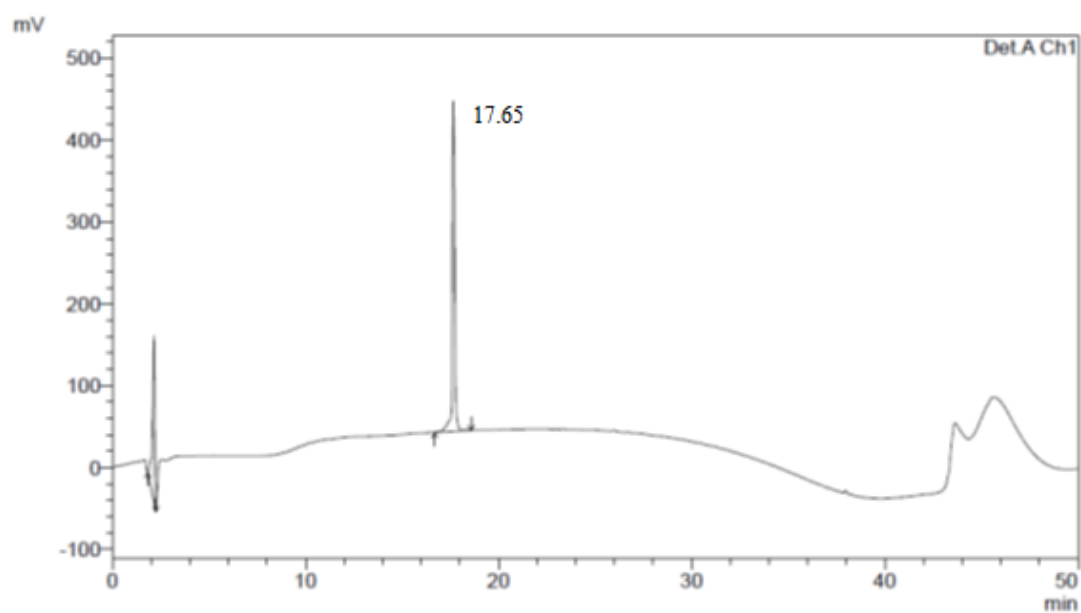
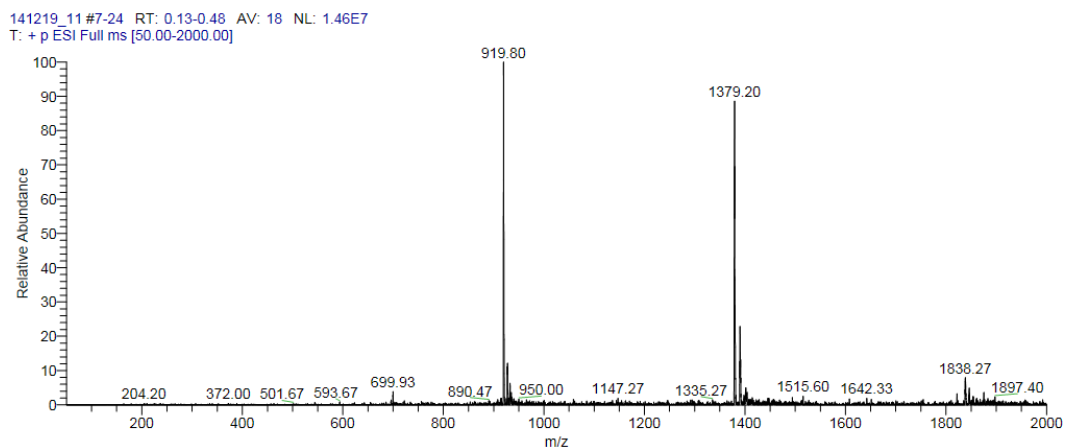
150826\_04 #535 RT: 15.33 AV: 1 NL: 1.62E5  
T: ITMS + p ESI E Full ms [250.00-2000.00]



**Figure B. 9** Mass and RP-HPLC chromatogram of C212A.

**Table B. 10** Sequence, accurate mass and retention time of K193E197.

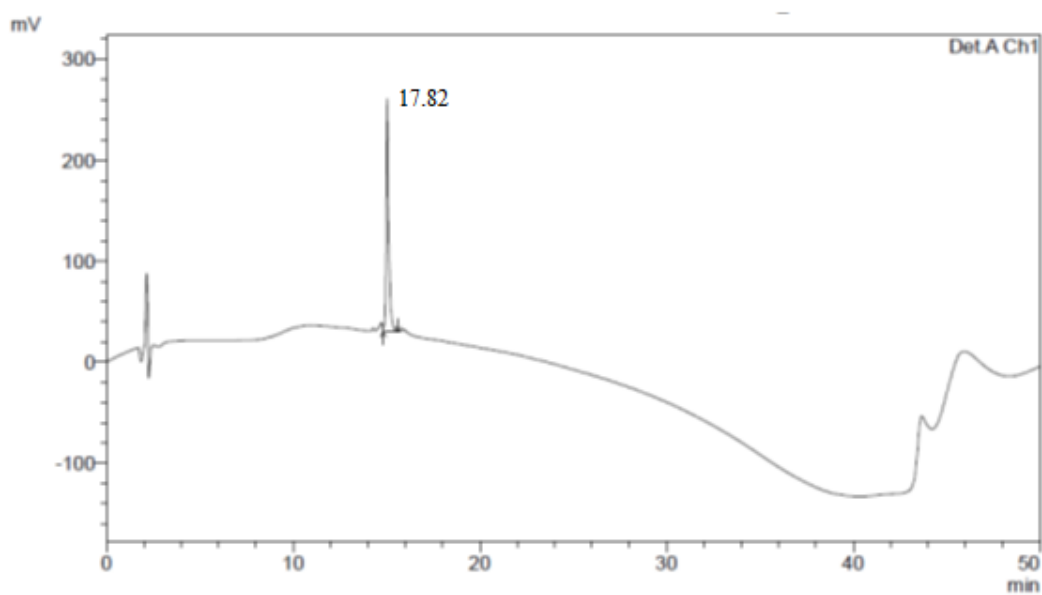
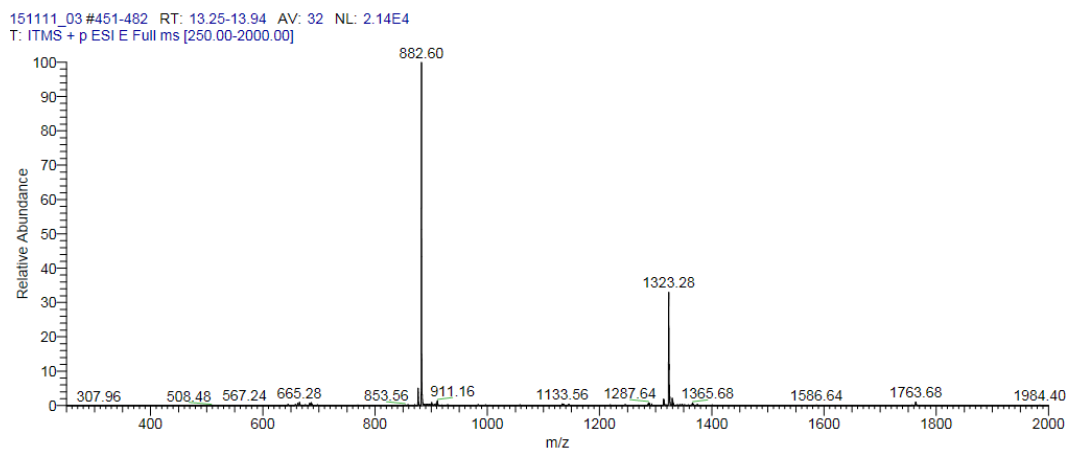
Entry	Sequence	[M+2] <sup>2+</sup> calculated	[M+2] <sup>2+</sup> observed	t <sub>R</sub> at 214 nm
K193E197	Ac-KDLKE <sup>Y</sup> IDKQLLPV <sup>NK</sup> QSCSISA-NH <sub>2</sub>	1378.78	1379.20	17.65



**Figure B. 10** Mass and RP-HPLC chromatogram of K193E197.

**Table B. 11** Sequence, accurate mass and retention time of K199E203.

Entry	Sequence	[M+2] <sup>2+</sup> calculated	[M+2] <sup>2+</sup> observed	t <sub>R</sub> at 214 nm
K199E203	Ac-DLK <del>NY</del> <u>KDKQ</u> ELPIV <del>NK</del> QSCSISA-NH <sub>2</sub>	1322.71	1323.28	17.82

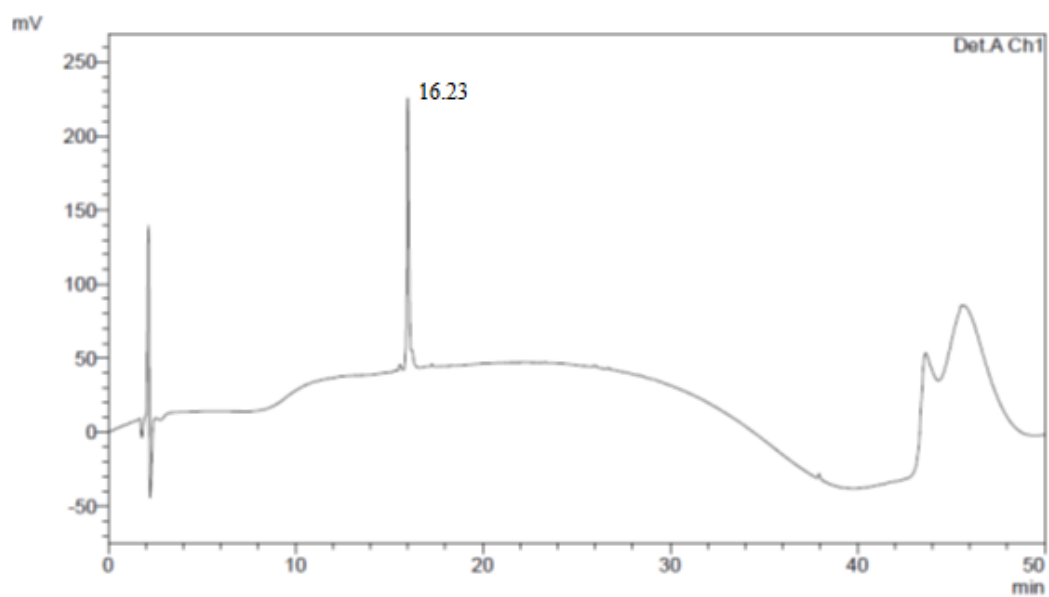
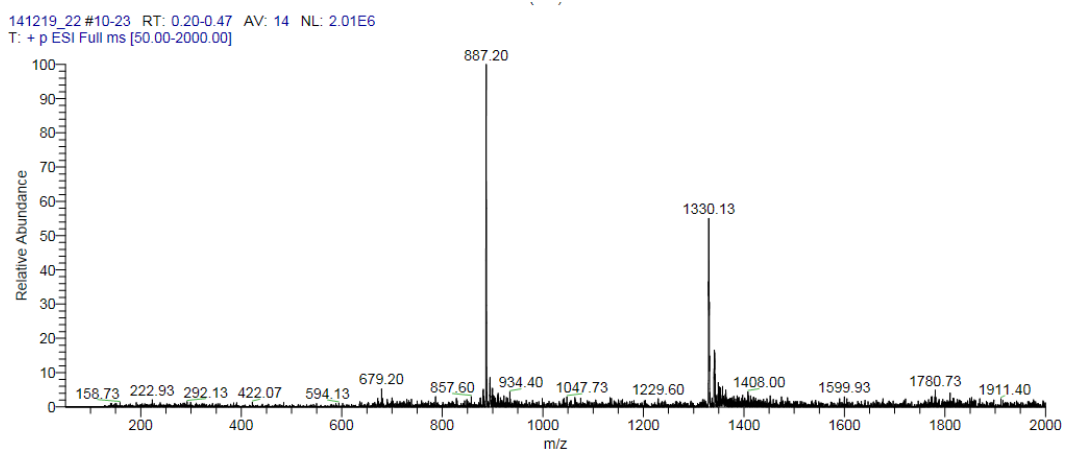


**Figure B. 11** Mass and RP-HPLC chromatogram of K199E203.



**Table B. 12** Sequence, accurate mass and retention time of K203E207.

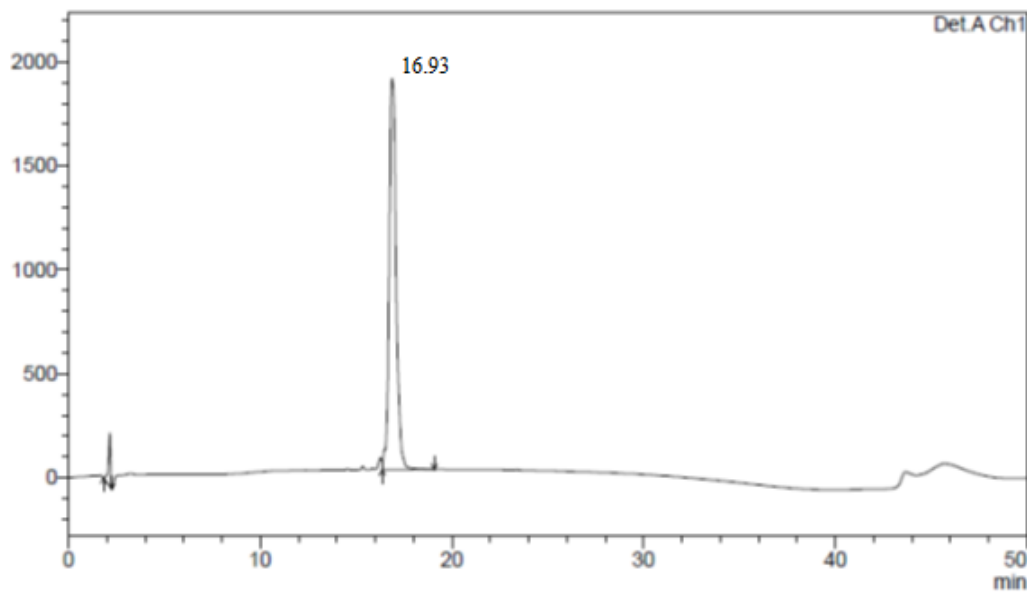
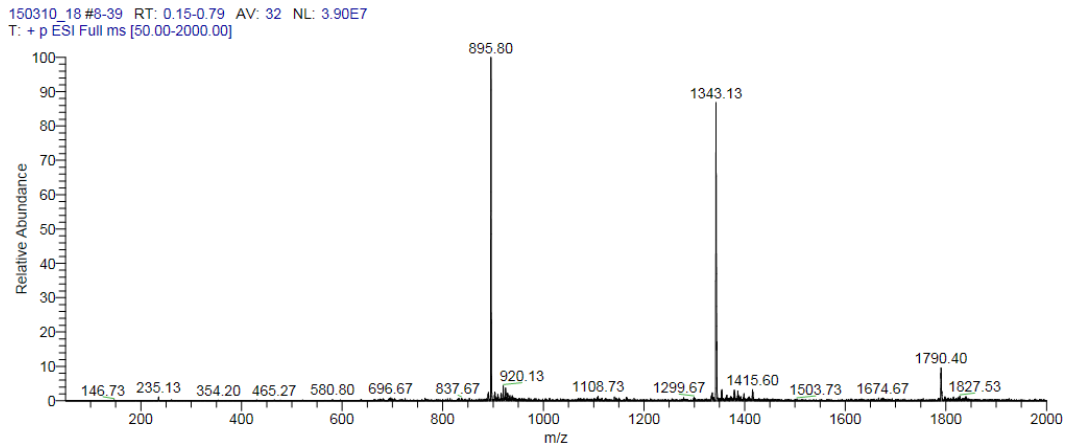
Entry	Sequence	[M+2] <sup>2+</sup> calculated	[M+2] <sup>2+</sup> observed	t <sub>R</sub> at 214 nm
K203E207	Ac-DLKNYIDKQ <u>KLPI</u> ENKQSCSISA-NH <sub>2</sub>	1329.72	1330.20	16.23



**Figure B. 12** Mass and RP-HPLC chromatogram of K203E207.

**Table B. 13** Sequence, accurate mass and retention time of K207E211.

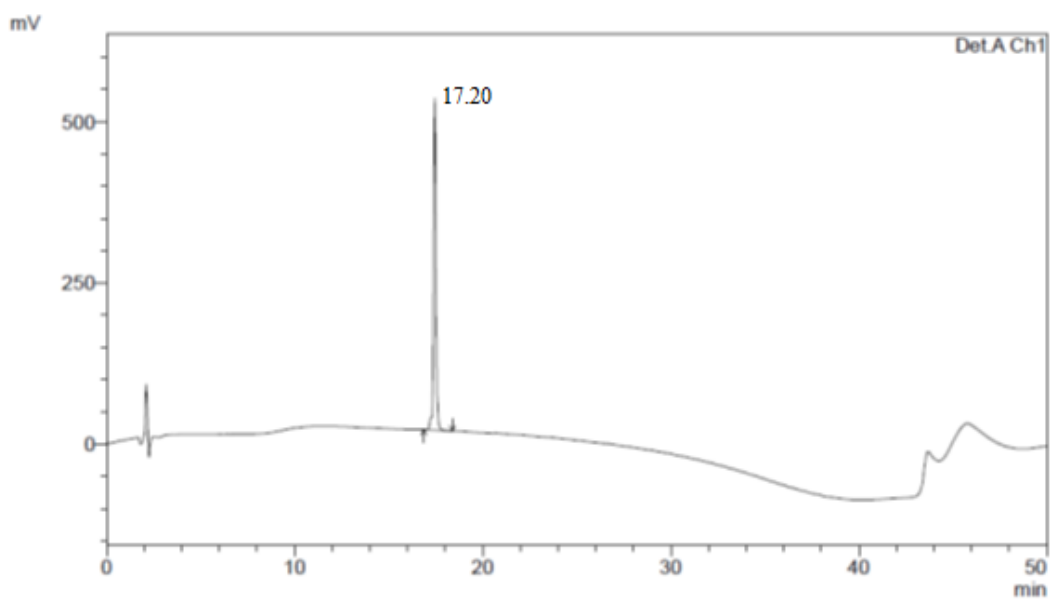
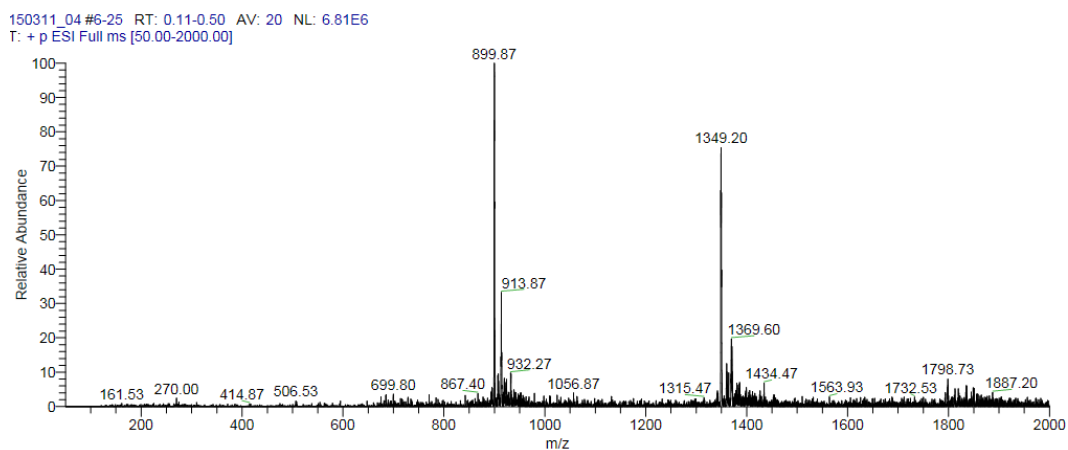
Entry	Sequence	[M+2] <sup>2+</sup> calculated	[M+2] <sup>2+</sup> observed	t <sub>R</sub> at 214 nm
K207E211	Ac-DLK <del>NYIDK</del> QLLP <b>IKNKQ</b> ECSISA-NH <sub>2</sub>	1342.75	1343.13	16.93



**Figure B. 13** Mass and RP-HPLC chromatogram of K207E211.

**Table B. 14** Sequence, accurate mass and retention time of K212E216.

Entry	Sequence	[M+2] <sup>2+</sup> calculated	[M+2] <sup>2+</sup> observed	t <sub>R</sub> at 214 nm
K212E216	Ac-DLK <del>NYIDK</del> QLLP <del>IVNK</del> QSK <del>SISE</del> -NH <sub>2</sub>	1348.77	1349.20	17.20

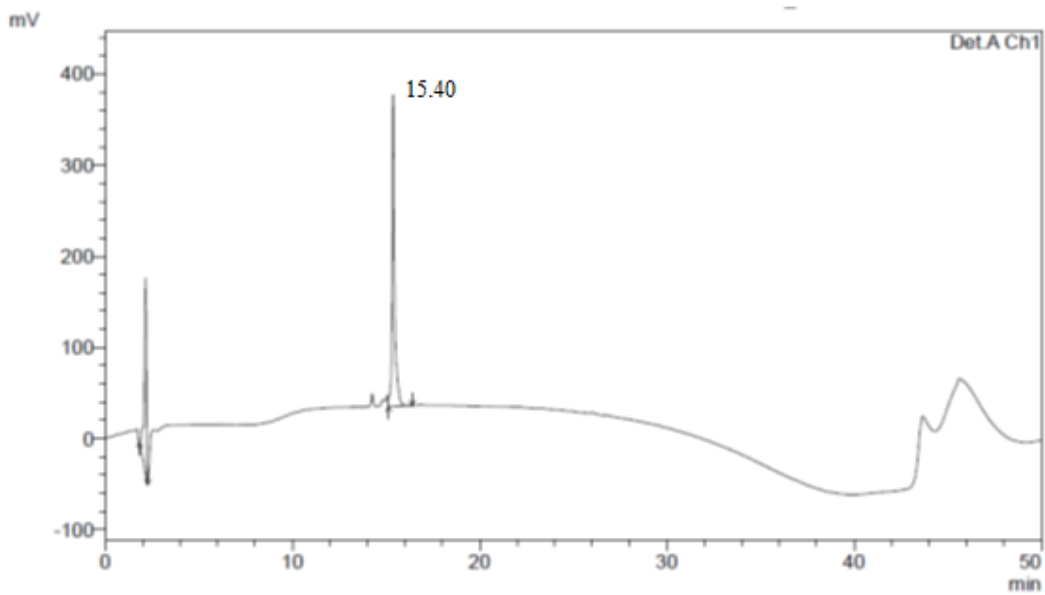
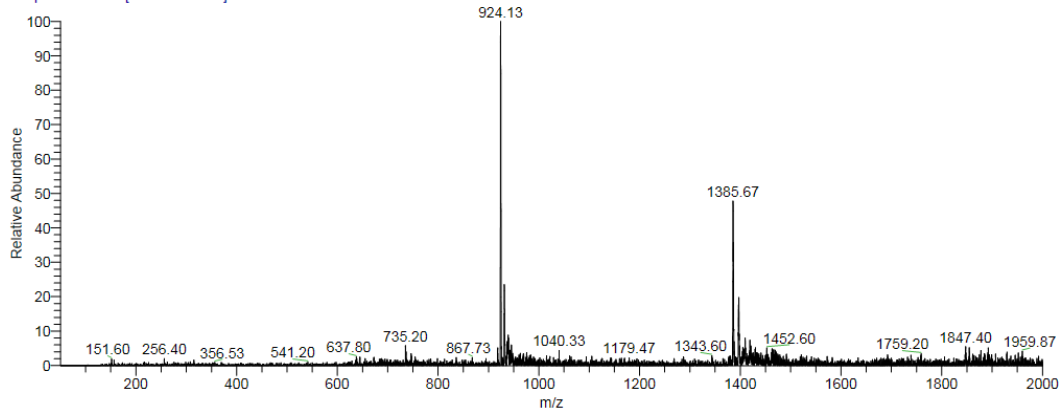


**Figure B. 14** Mass and RP-HPLC chromatogram of K212E216.

**Table B. 15** Sequence, accurate mass and retention time of K193E197-K199E203.

Entry	Sequence	[M+2] <sup>2+</sup> calculated	[M+2] <sup>2+</sup> observed	t <sub>R</sub> at 214 nm
K193E197- K199E203	Ac-KDLK <b>EY</b> KDK <b>Q</b> ELPIVNKQSCSISA-NH <sub>2</sub>	1385.26	1385.67	15.40

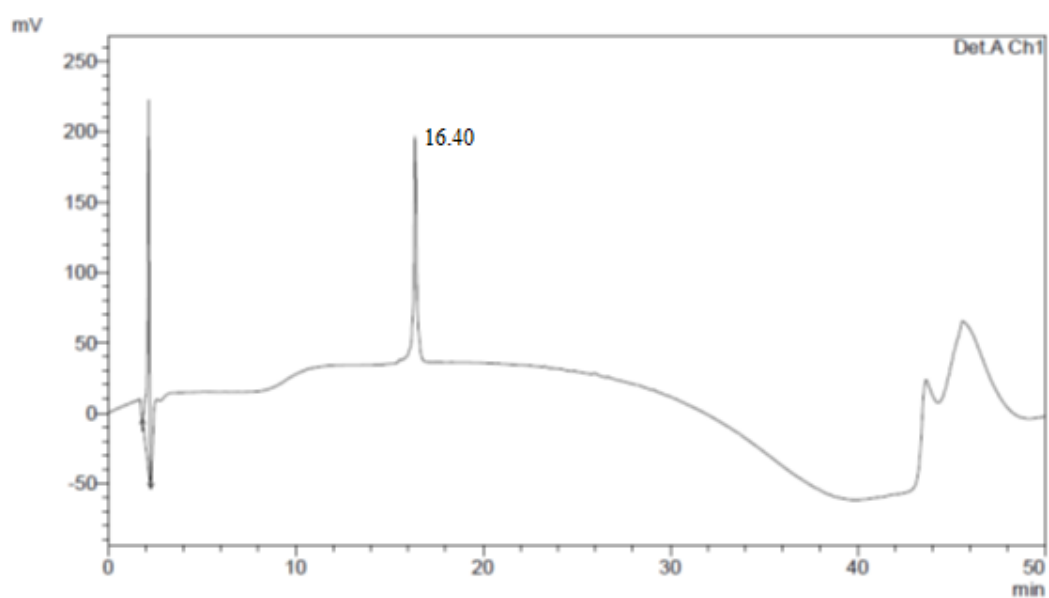
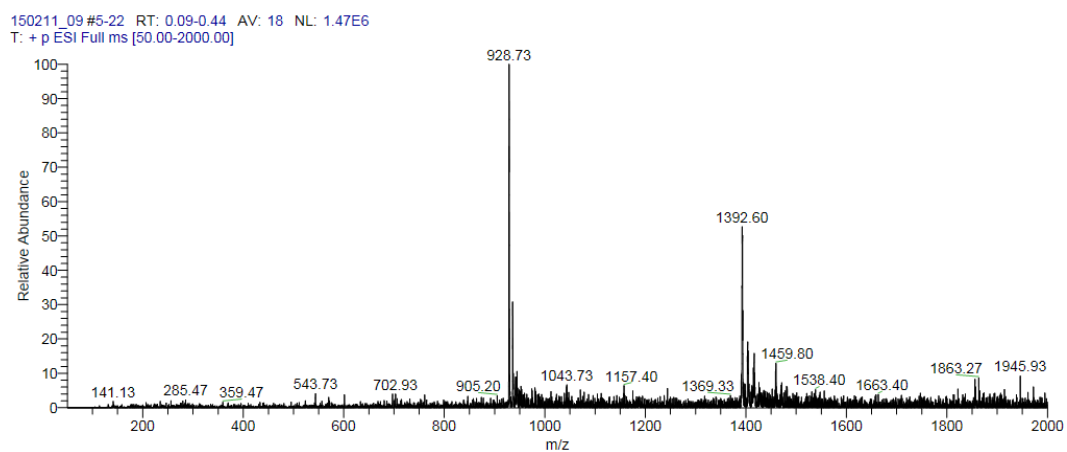
150211\_03 #6-28 RT: 0.11-0.56 AV: 23 NL: 4.72E6  
T: + p ESI Full ms [50.00-2000.00]



**Figure B. 15** Mass and RP-HPLC chromatogram of K193E197-K199E203.

**Table B. 16** Sequence, accurate mass and retention time of K193E197-K203E207.

Entry	Sequence	[M+2] <sup>2+</sup> calculated	[M+2] <sup>2+</sup> observed	t <sub>R</sub> at 214 nm
K193E197- K203E207	Ac-KDLK <b>E</b> YIDKQ <b>K</b> LPI <b>E</b> NKQSCSISA- NH <sub>2</sub>	1392.27	1392.60	16.40

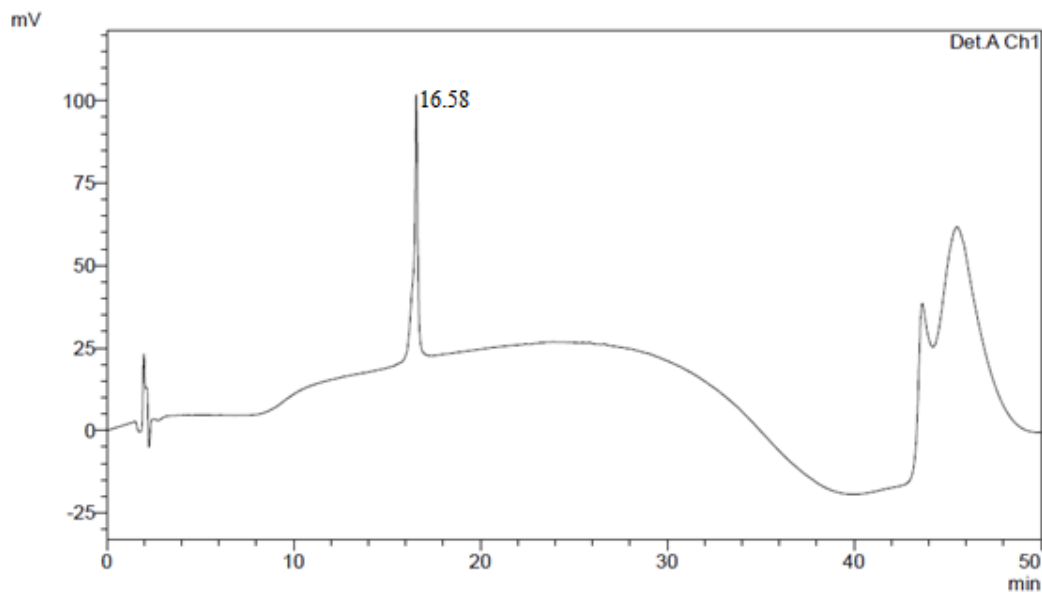
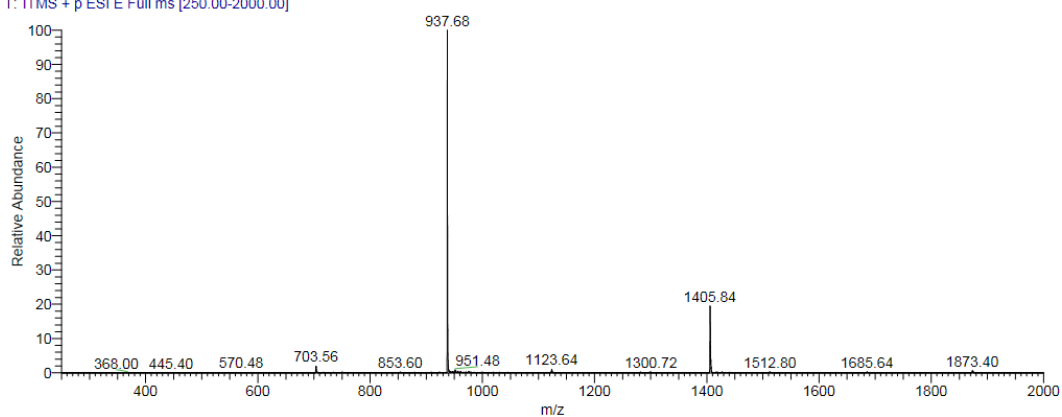


**Figure B. 16** Mass and RP-HPLC chromatogram of K193E197-K203E207.

**Table B. 17** Sequence, accurate mass and retention time of K193E197-K207E211.

Entry	Sequence	$[M+2]^{2+}$ calculated	$[M+2]^{2+}$ observed	$t_R$ at 214 nm
K193E197- K207E211	Ac-KDLK <b>E</b> YIDKQLLP <b>I</b> K <b>N</b> K <b>Q</b> ECSISA-NH <sub>2</sub>	1405.30	1405.84	16.58

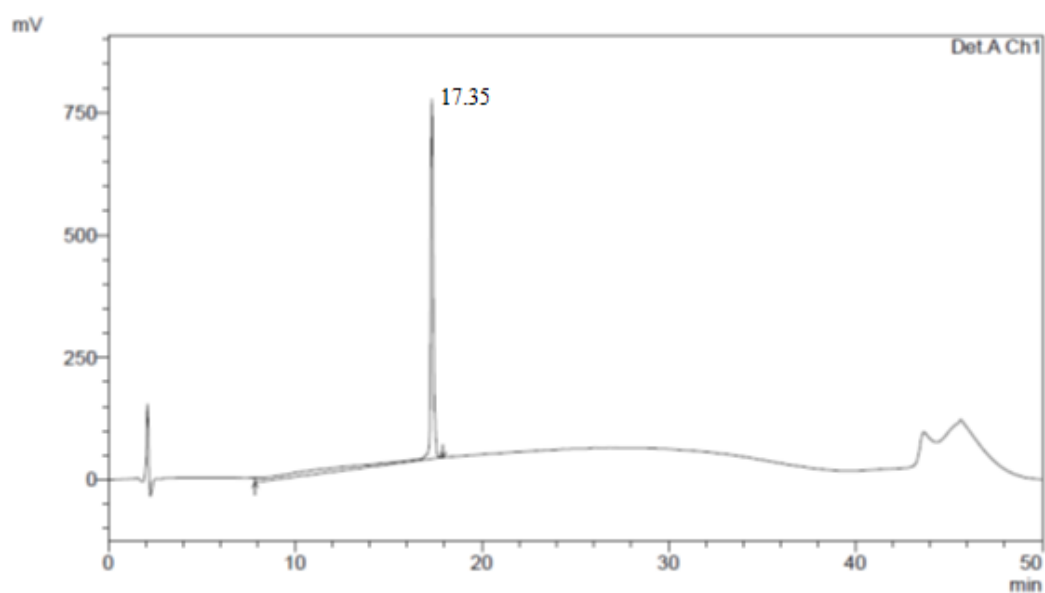
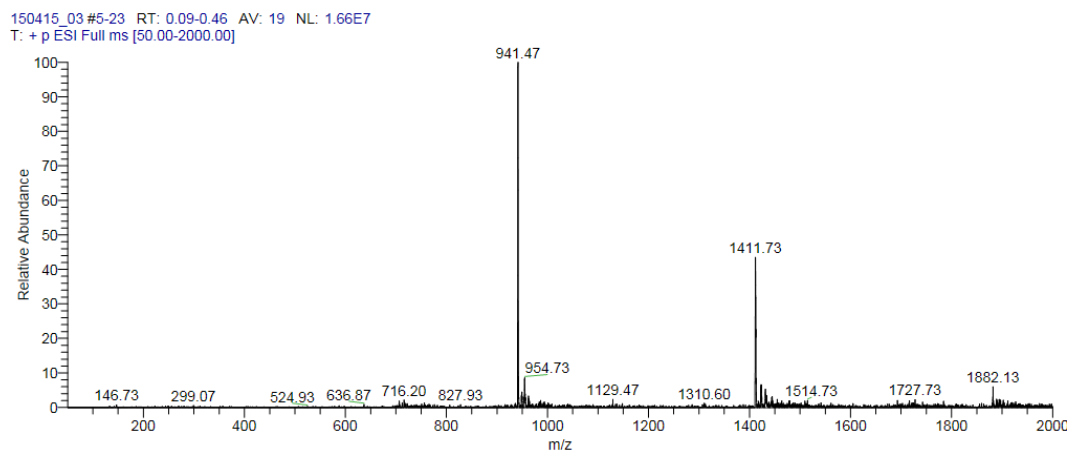
151117\_01 #550-575 RT: 15.94-16.50 AV: 26 NL: 2.34E4  
T: ITMS + p ESI E Full ms [250.00-2000.00]



**Figure B. 17** Mass and RP-HPLC chromatogram of K193E197-K207E211.

**Table B. 18** Sequence, accurate mass and retention time of K193E197-K212E216.

Entry	Sequence	$[M+2]^{2+}$	$[M+2]^{2+}$	$t_R$ at 214 nm
		calculated	observed	
K193E197-K212E216	Ac-KDLKEYIDKQLLPV NKQS KSISE-NH <sub>2</sub>	1411.32	1411.73	17.35

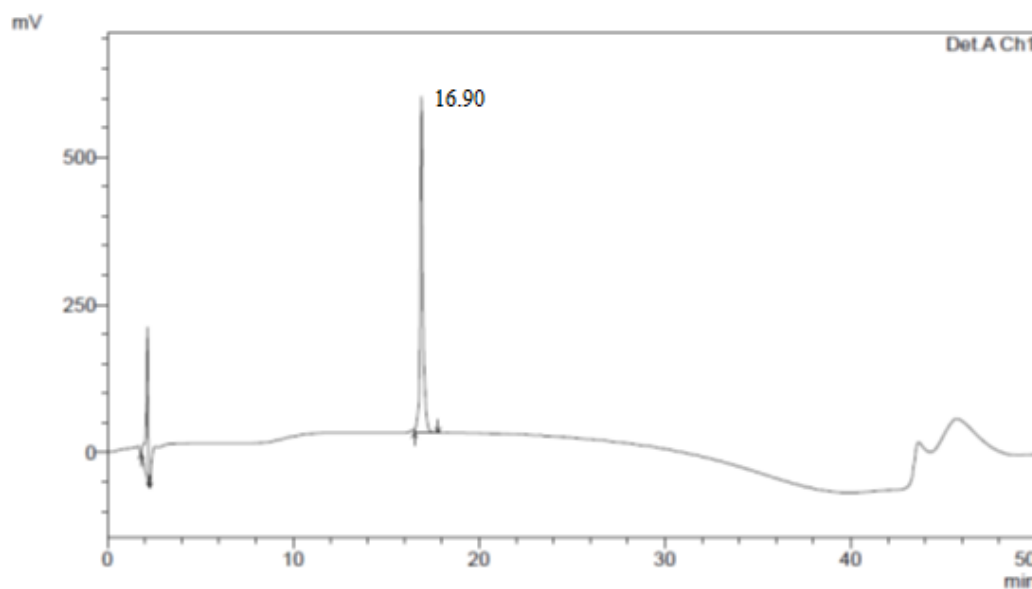
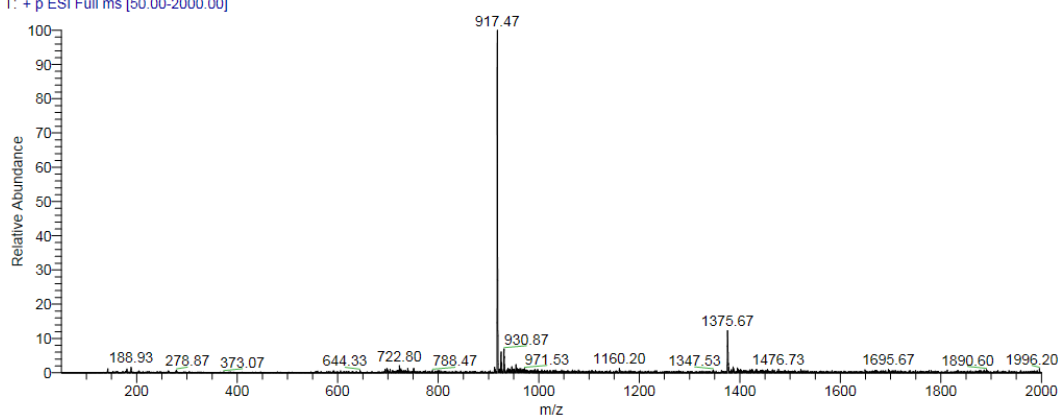


**Figure B. 18** Mass and RP-HPLC chromatogram of K193E197-K212E216.

**Table B. 19** Sequence, accurate mass and retention time of K207E211-K212E216.

Entry	Sequence	[M+2] <sup>2+</sup> calculated	[M+2] <sup>2+</sup> observed	t <sub>R</sub> at 214 nm
K207E211- K212E216	Ac-DLK <sup>N</sup> NYIDKQLLP <sup>I</sup> <u>KNKQEK</u> SISE-NH <sub>2</sub>	1375.29	1375.67	16.90

150302\_09 #5-27 RT: 0.09-0.54 AV: 23 NL: 4.37E7  
T: + p ESI Full ms [50.00-2000.00]

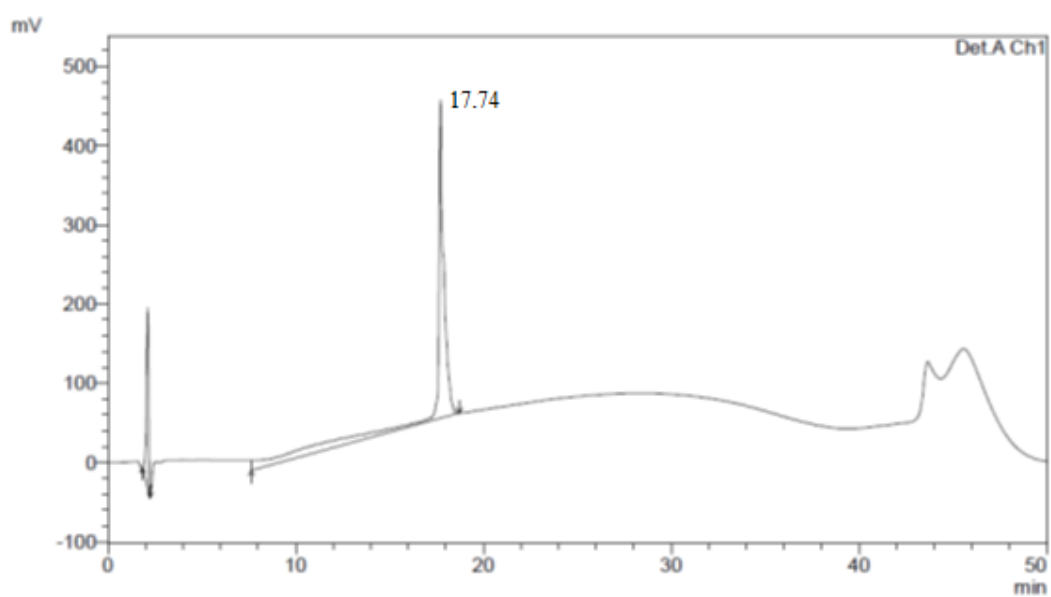
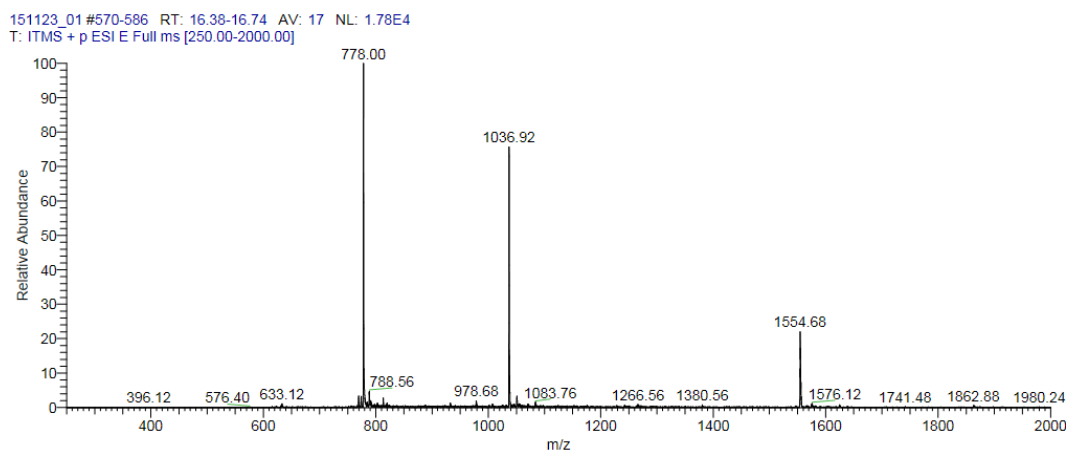


**Figure B. 19** Mass and RP-HPLC chromatogram of K207E211-K212E216.



**Table B. 20** Sequence, accurate mass and retention time of K190E194-K193E197.

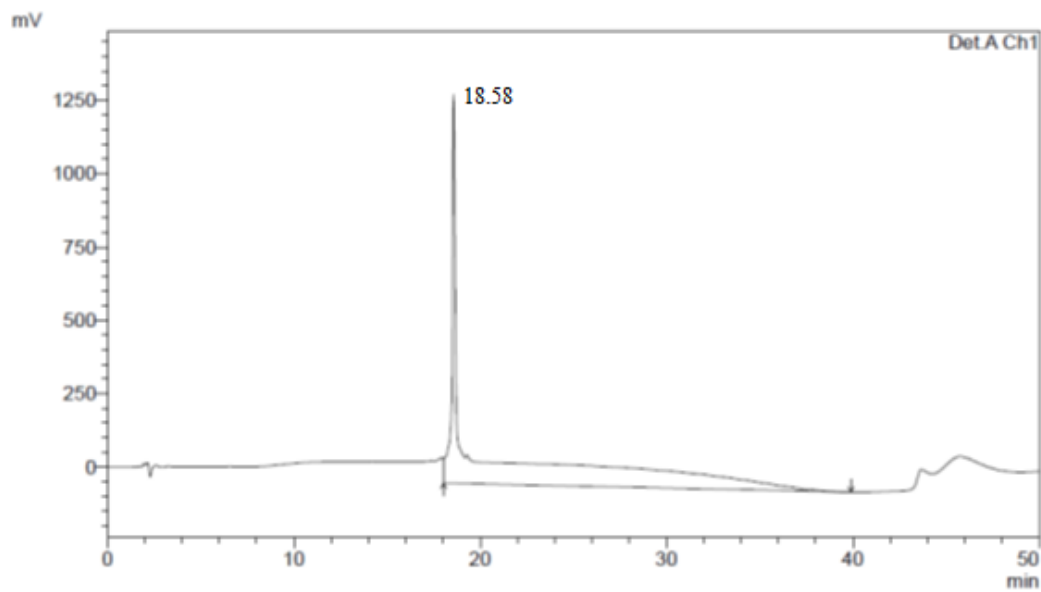
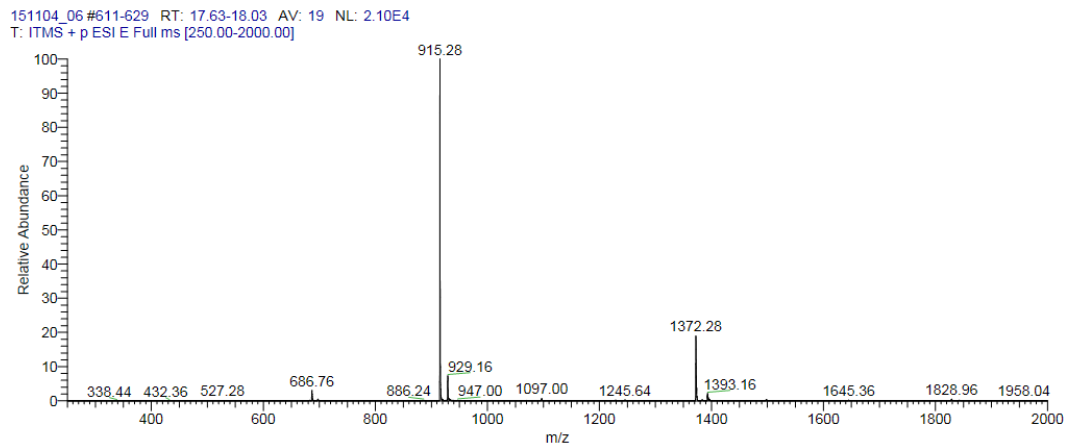
Entry	Sequence	[M+2] <sup>2+</sup> calculated	[M+2] <sup>2+</sup> + observed	t <sub>R</sub> at 214 nm
K190E194- K193E197	Ac-KKV <b>KELKE</b> YIDKQLLPVINKQSCSIS- NH <sub>2</sub>	1554.42	1554.6 8	17.74



**Figure B. 20** Mass and RP-HPLC chromatogram of K190E194-K193E197.

**Table B. 21** Sequence, accurate mass and retention time of K193D197.

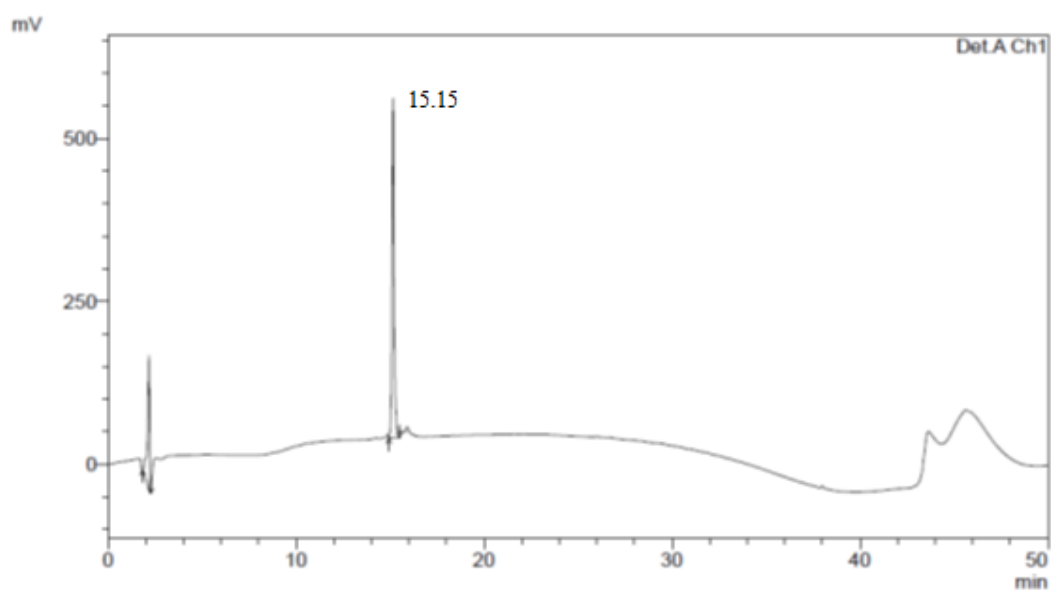
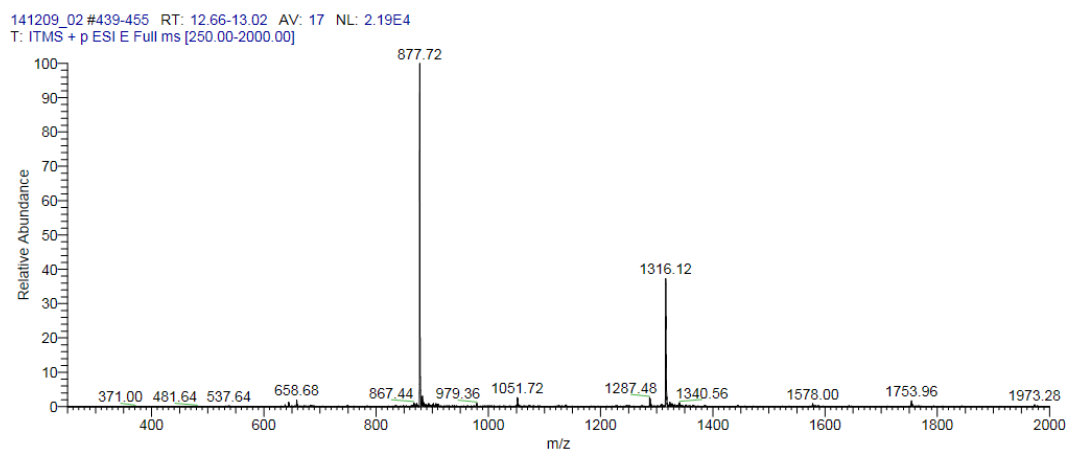
Entry	Sequence	[M+2] <sup>2+</sup> calculated	[M+2] <sup>2+</sup> observed	t <sub>R</sub> at 214 nm
K193D197	Ac-KDLKDYIDKQLLPVINKQSCSISA-NH <sub>2</sub>	1371.77	1372.28	18.58



**Figure B. 21** Mass and RP-HPLC chromatogram of K193D197.

**Table B. 22** Sequence, accurate mass and retention time of K199D203.

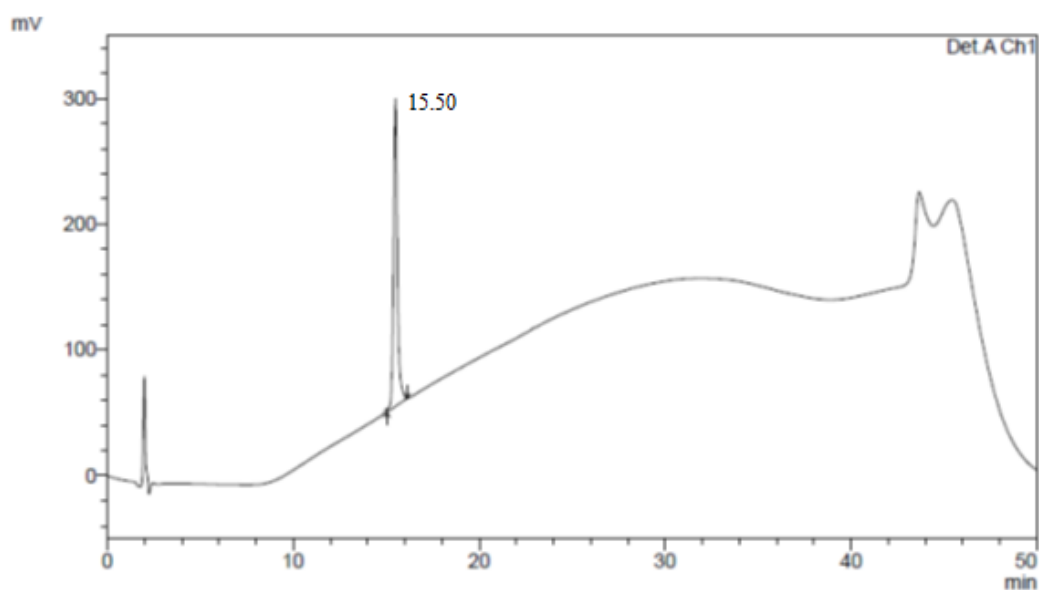
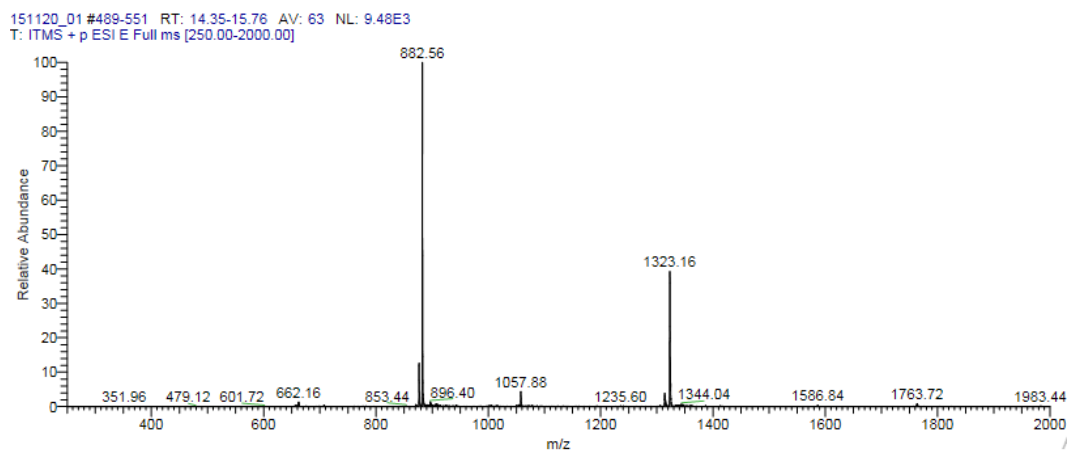
Entry	Sequence	[M+2] <sup>2+</sup> calculated	[M+2] <sup>2+</sup> observed	t <sub>R</sub> at 214 nm
K199D203	Ac-DLK <del>NY</del> <u>KDKQ</u> DLP <del>IV</del> NKQSCSISA-NH <sub>2</sub>	1315.70	1316.12	15.15



**Figure B. 22** Mass and RP-HPLC chromatogram of K199D203.

**Table B. 23** Sequence, accurate mass and retention time of K203D207.

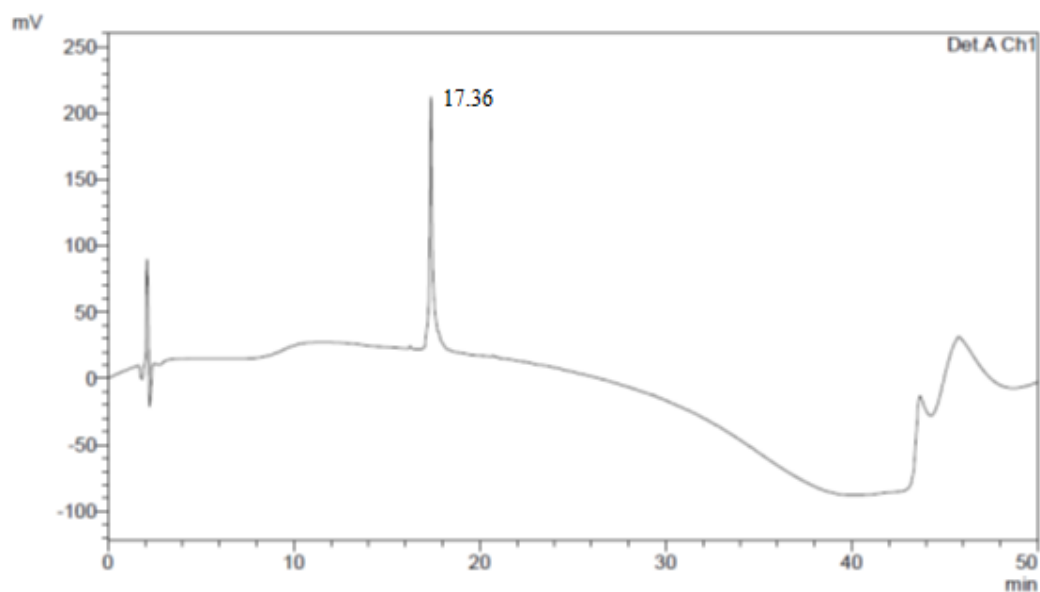
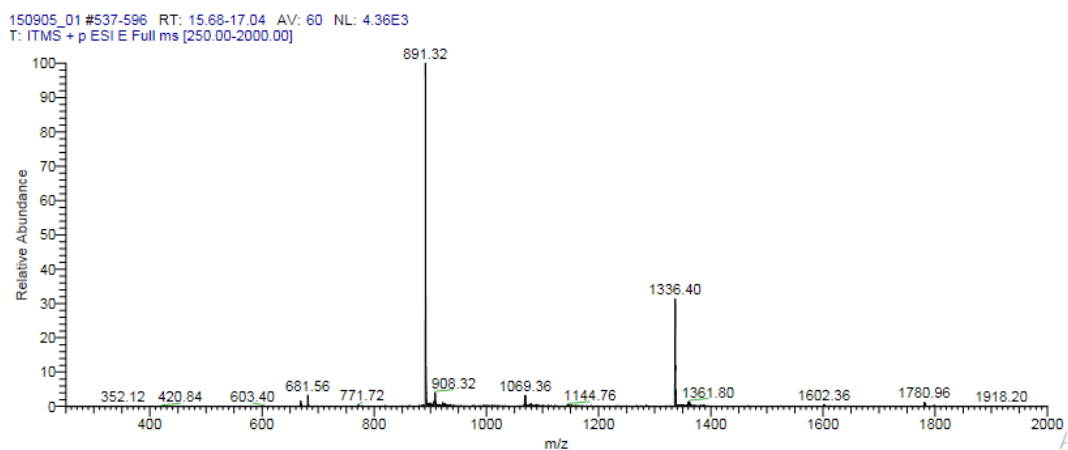
Entry	Sequence	[M+2] <sup>2+</sup> calculated	[M+2] <sup>2+</sup> observed	t <sub>R</sub> at 214 nm
K203D207	Ac-DLKNYIDKQ <b>KLPID</b> NKQSCSISA-NH <sub>2</sub>	1322.71	1323.16	15.50



**Figure B. 23** Mass and RP-HPLC chromatogram of K203D207.

**Table B. 24** Sequence, accurate mass and retention time of K207D211.

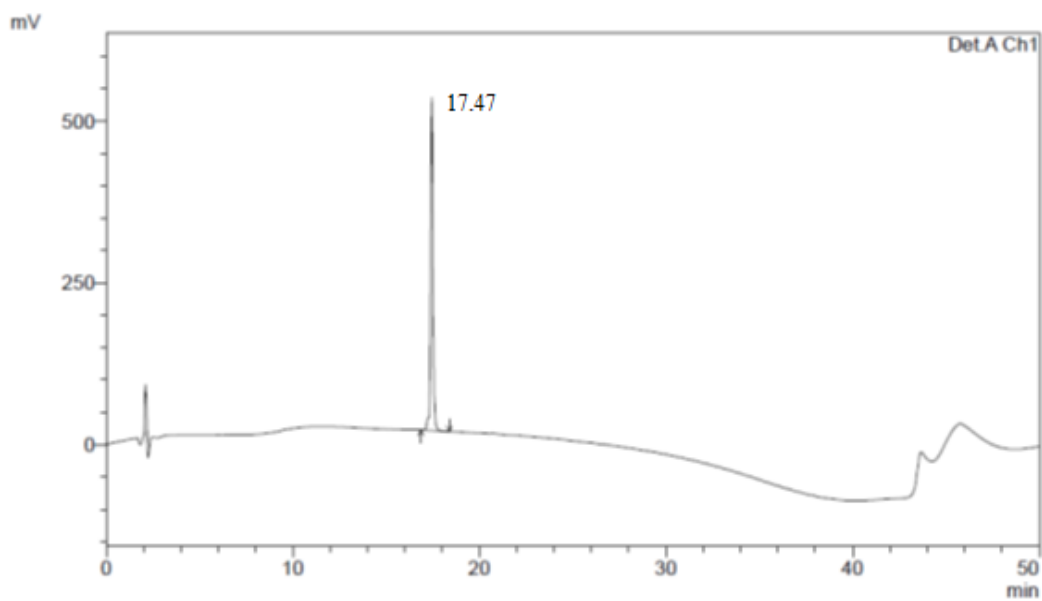
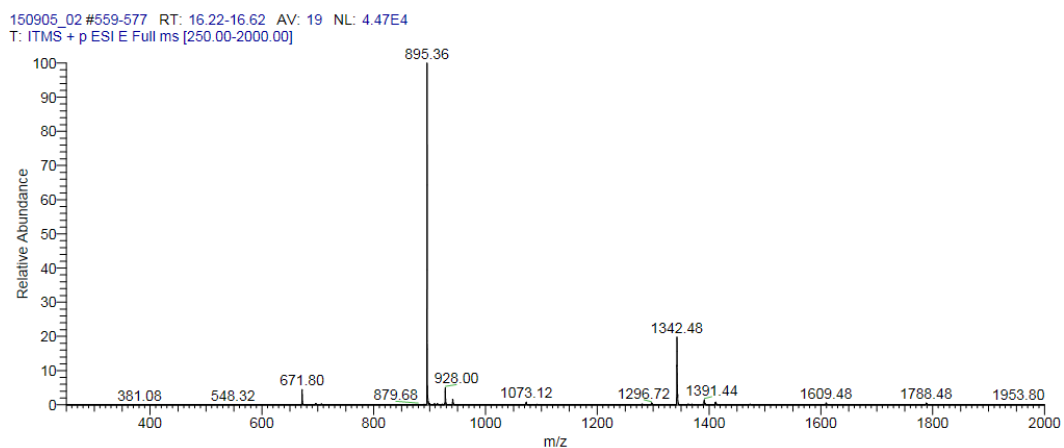
Entry	Sequence	$[M+2]^{2+}$ calculated	$[M+2]^{2+}$ observed	$t_R$ at 214 nm
K207D211	Ac-DLK <del>NYIDK</del> QLLP <del>IK</del> KNKQDCSISA-NH <sub>2</sub>	1335.74	1336.40	17.36



**Figure B. 24** Mass and RP-HPLC chromatogram of K207D211.

**Table B. 25** Sequence, accurate mass and retention time of K212D216.

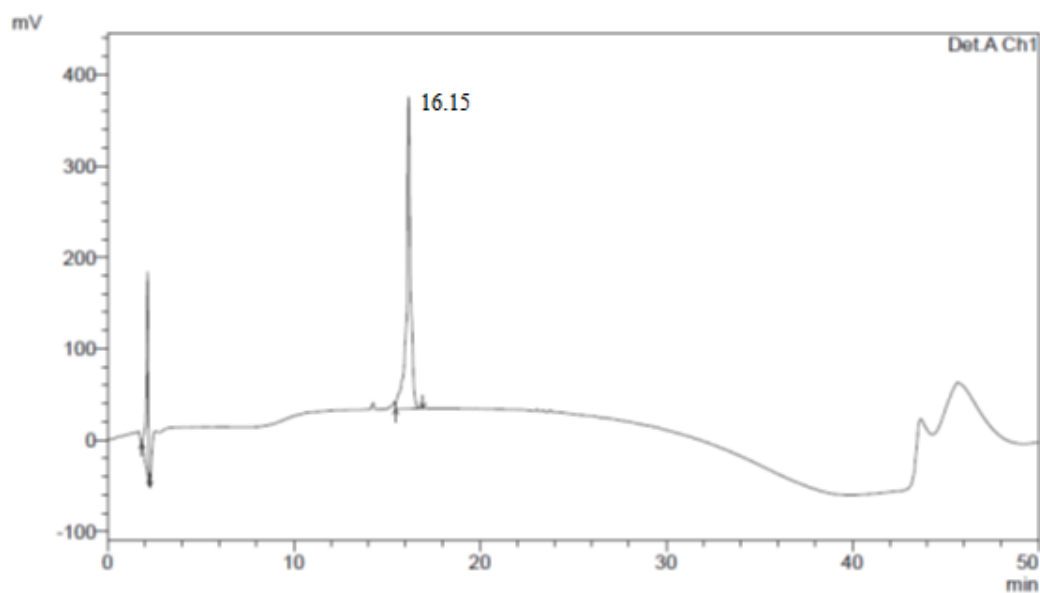
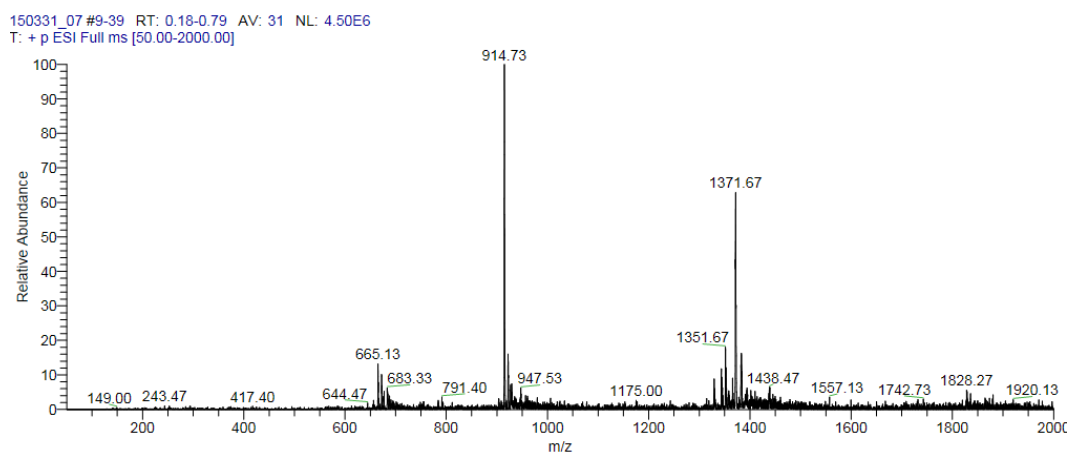
Entry	Sequence	[M+2] <sup>2+</sup> calculated	[M+2] <sup>2+</sup> observed	t <sub>R</sub> at 214 nm
K212D216	Ac-DLKNYIDKQLLPVNVKQSKSISD-NH <sub>2</sub>	1341.77	1342.48	17.47



**Figure B. 25** Mass and RP-HPLC chromatogram of K212D216.

**Table B. 26** Sequence, accurate mass and retention time of K193D197-K199D203.

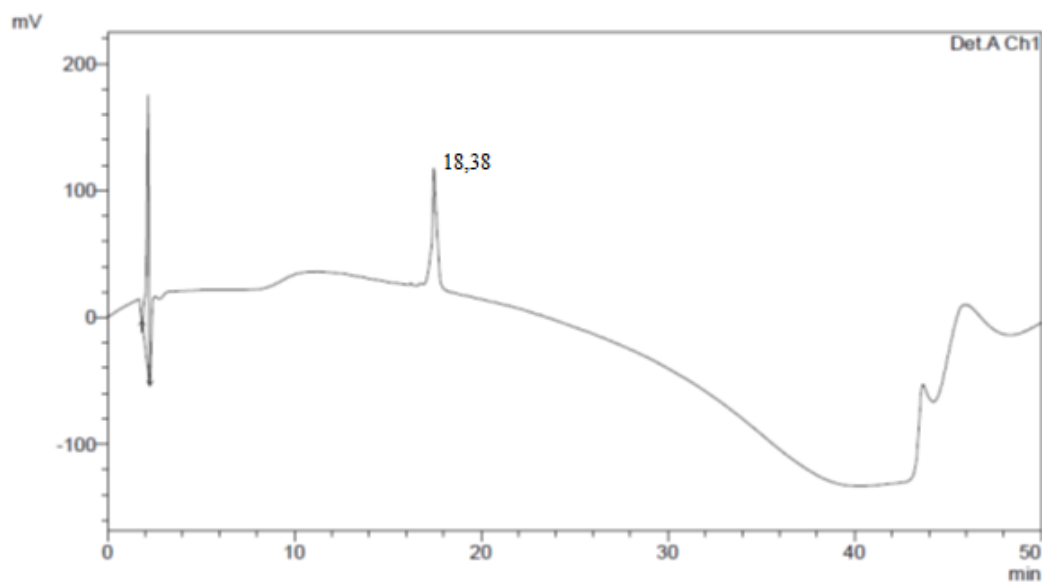
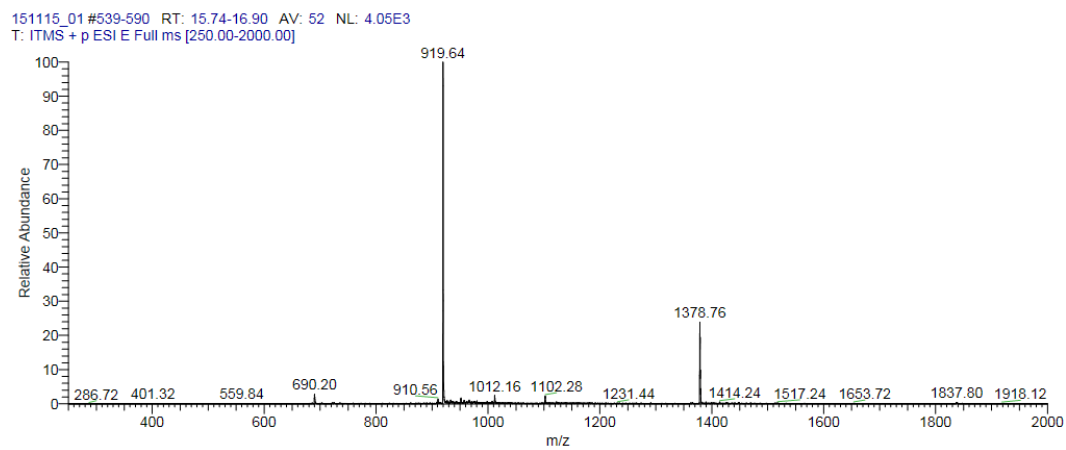
Entry	Sequence	[M+2] <sup>2+</sup> calculated	[M+2] <sup>2+</sup> observed	tr at 214 nm
K193D197- K199D203	Ac-KDLKDYKDKQDLPIV NKQSCSISA-NH <sub>2</sub>	1371.25	1371.67	16.15



**Figure B. 26** Mass and RP-HPLC chromatogram of K193D197-K199D203.

**Table B. 27** Sequence, accurate mass and retention time of K193D197-K203D207.

Entry	Sequence	[M+2] <sup>2+</sup> calculated	[M+2] <sup>2+</sup> observed	t <sub>R</sub> at 214 nm
K193D197- K203D207	Ac-KDLKD YIDKQKLPIDNKQSCSISA-NH <sub>2</sub>	1378.26	1378.76	18.38



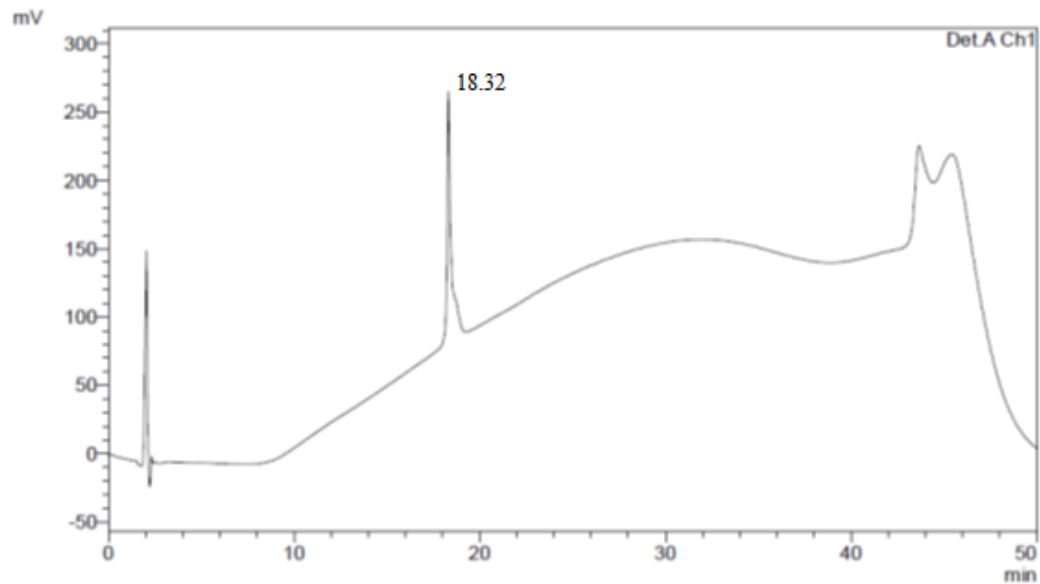
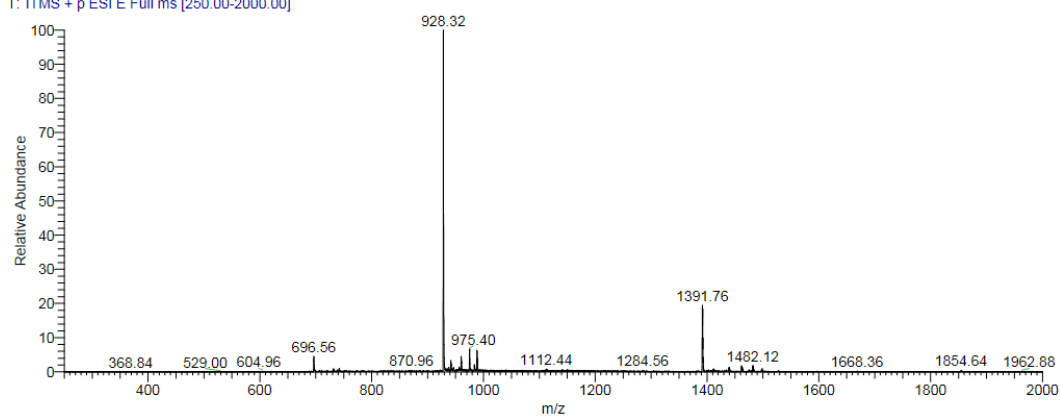
**Figure B. 27** Mass and RP-HPLC chromatogram of K193D197-K203D207.



**Table B. 28** Sequence, accurate mass and retention time of K193D197-K207D211.

Entry	Sequence	[M+2] <sup>2+</sup> calculated	[M+2] <sup>2+</sup> observed	tr at 214 nm
K193D197- K207D211	Ac-KDLKDYIDKQLLPIK <b>KNKQD</b> CSISA-NH <sub>2</sub>	1391.29	1391.76	18.32

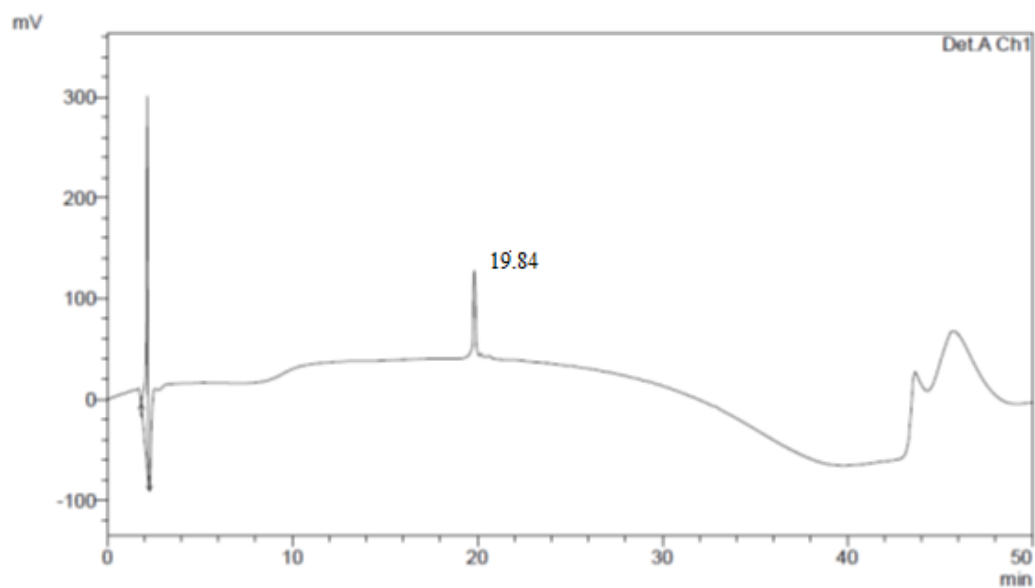
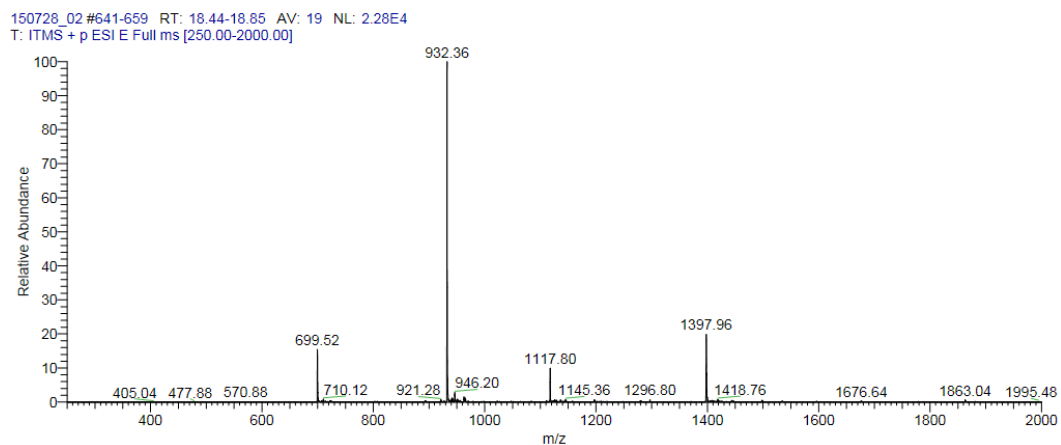
151120\_02 #605-664 RT: 17.49-18.83 AV: 60 NL: 4.61E3  
T: ITMS + p ESI E Full ms [250.00-2000.00]



**Figure B. 28** Mass and RP-HPLC chromatogram of K193D197-K207D211.

**Table B. 29** Sequence, accurate mass and retention time of K193D197-K211D215.

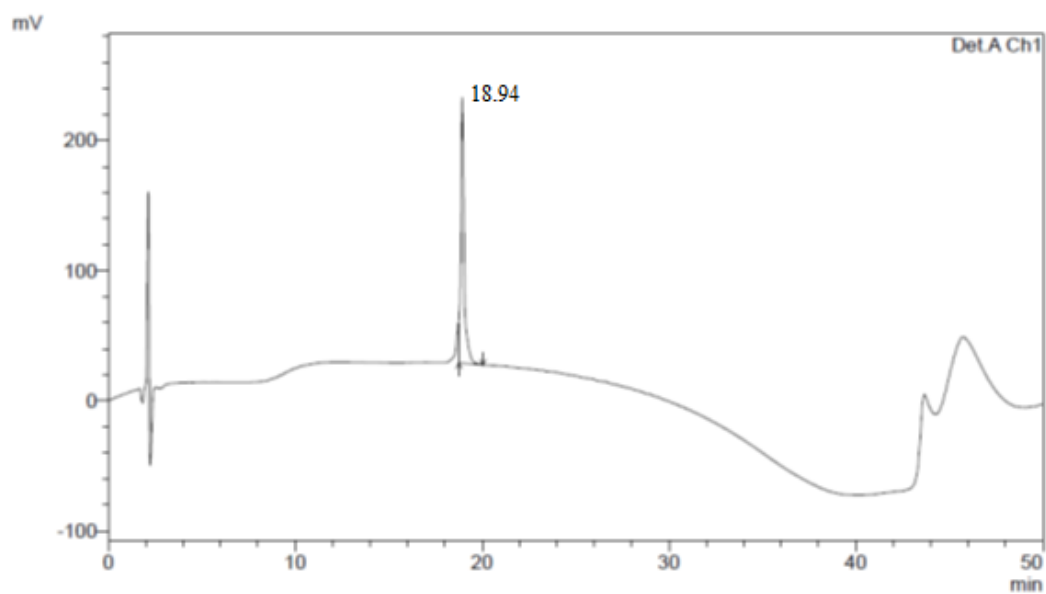
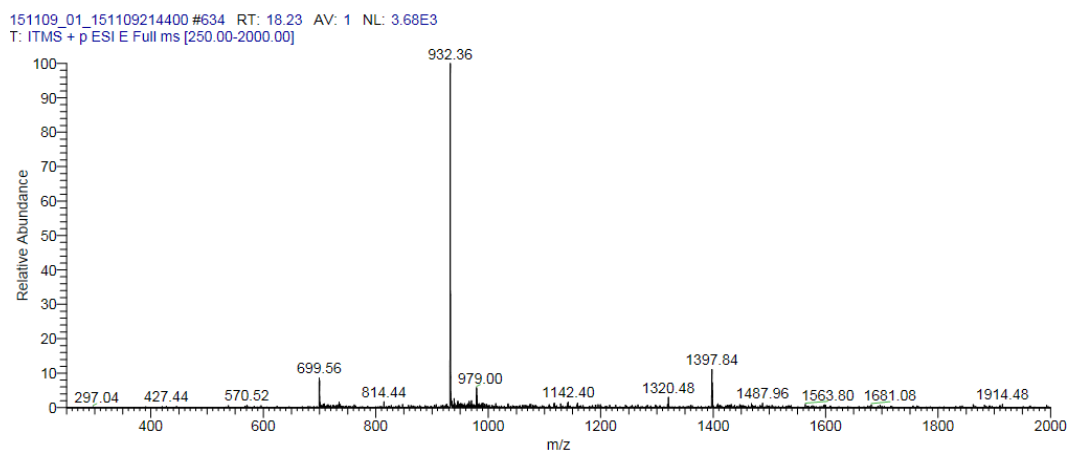
Entry	Sequence	[M+2] <sup>2+</sup> calculated	[M+2] <sup>2+</sup> observed	t <sub>R</sub> at 214 nm
K193D197- K211D215	Ac-KDLKDYIDKQLLPVFNKQKCSIDA-NH <sub>2</sub>	1397.31	1398.13	19.84



**Figure B. 29** Mass and RP-HPLC chromatogram of K193D197-K211D215.

**Table B. 30** Sequence, accurate mass and retention time of K193D197-K212D216.

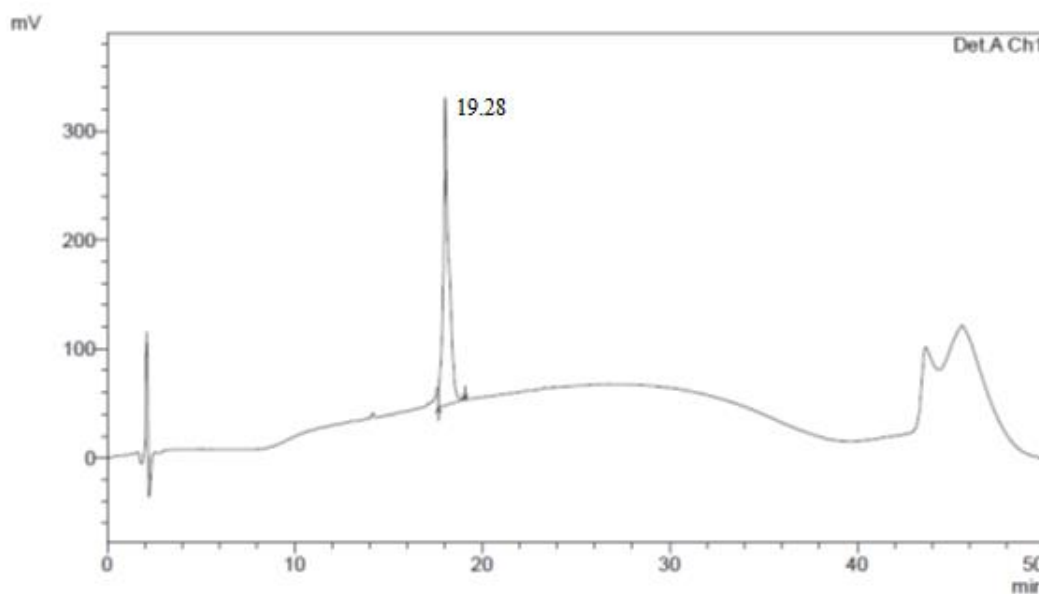
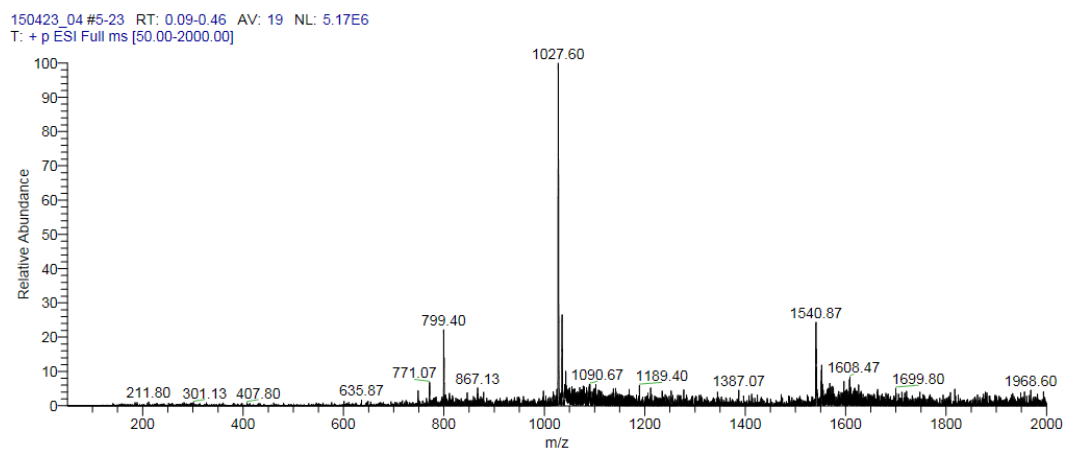
Entry	Sequence	[M+2] <sup>2+</sup> calculated	[M+2] <sup>2+</sup> observed	t <sub>R</sub> at 214 nm
K193D197- K212D216	Ac-KDLKDYIDKQLLPVINKQSKSISD-NH <sub>2</sub>	1397.31	1397.84	18.94



**Figure B. 30** Mass and RP-HPLC chromatogram of K193D197-K212D216.

**Table B. 31** Sequence, accurate mass and retention time of K190D194 K193D197.

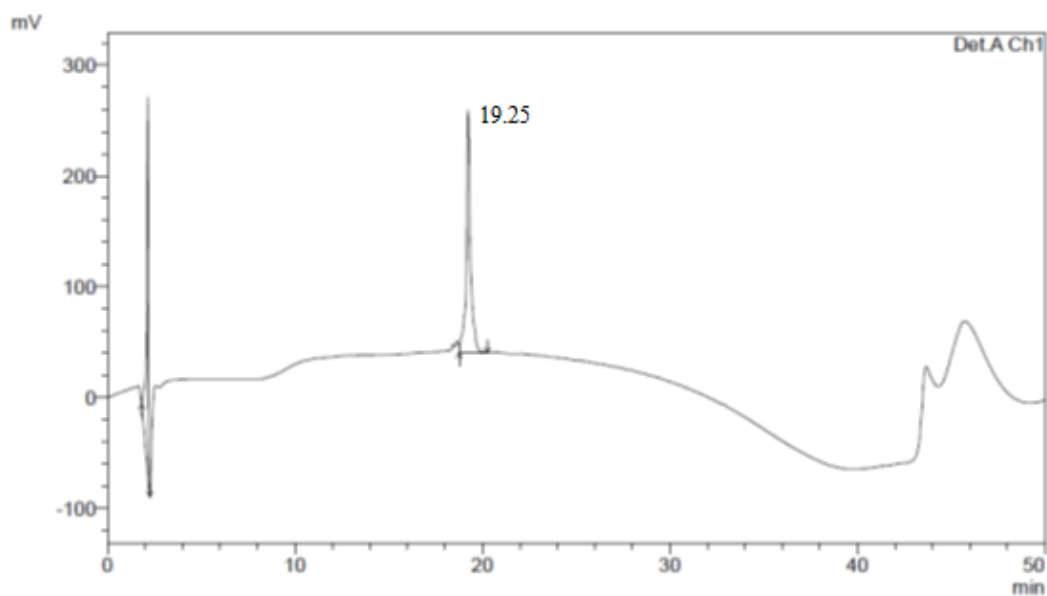
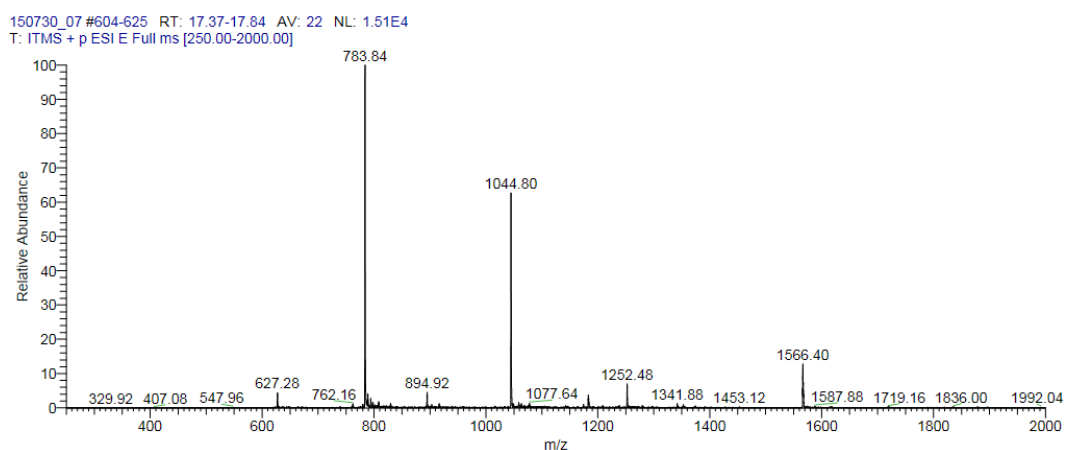
Entry	Sequence	[M+2] <sup>2+</sup> calculated	[M+2] <sup>2+</sup> observed	t <sub>R</sub> at 214 nm
K190D194- K193D197	Ac-KKV <b>KDLKD</b> YIDKQLLPV <b>NKQSCS</b> ISA NH <sub>2</sub>	1540.41	1540.87	19.28



**Figure B. 31** Mass and RP-HPLC chromatogram of K190D194-K193D197.

**Table B. 32** Sequence, accurate mass and retention time of K190D194-K193D197-K211D215.

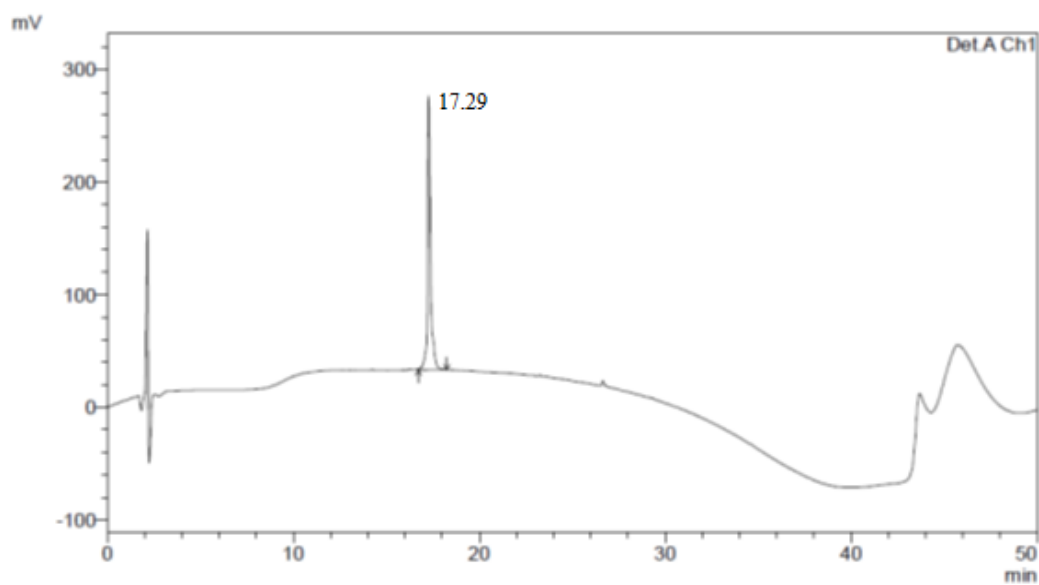
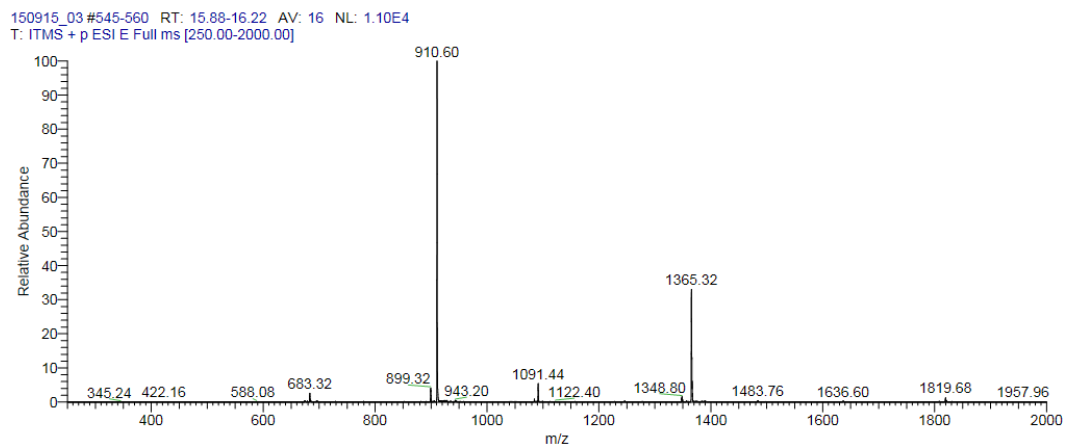
Entry	Sequence	$[M+2]^{2+}$ calculated	$[M+2]^{2+}$ + observed	$t_R$ at 214 nm
K190D194- K193D197- K211D215	Ac- <u>KKV</u> <u>KDLKD</u> YIDKQLLPVFNKQ <u>KCSIDA</u> - NH <sub>2</sub>	1565.95	1566.8 0	19.25



**Figure B. 32** Mass and RP-HPLC chromatogram of K190D194-K193D197-K211D215.

**Table B. 33** Sequence, accurate mass and retention time of O193D197.

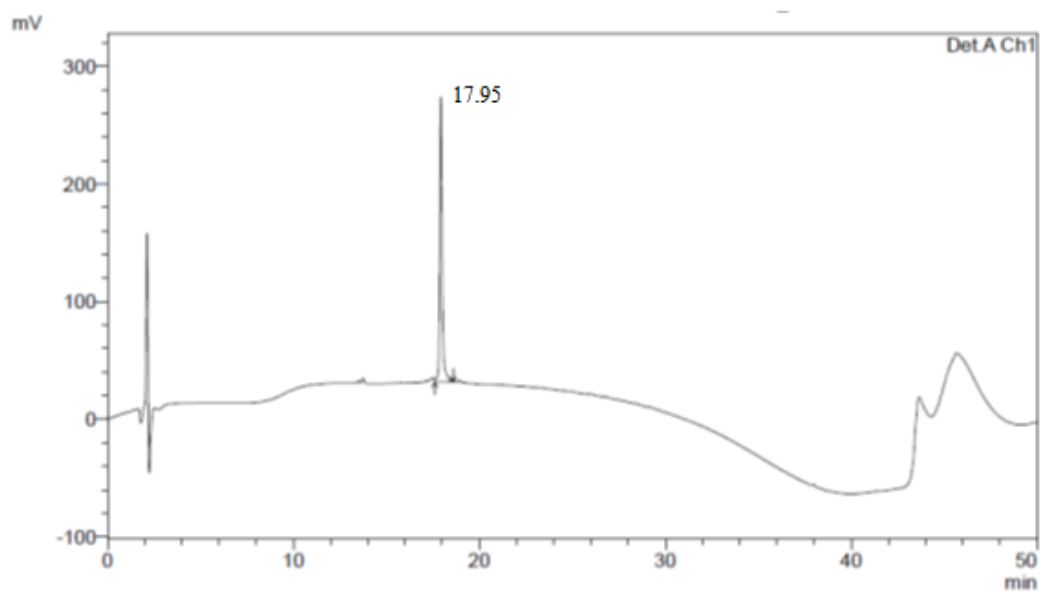
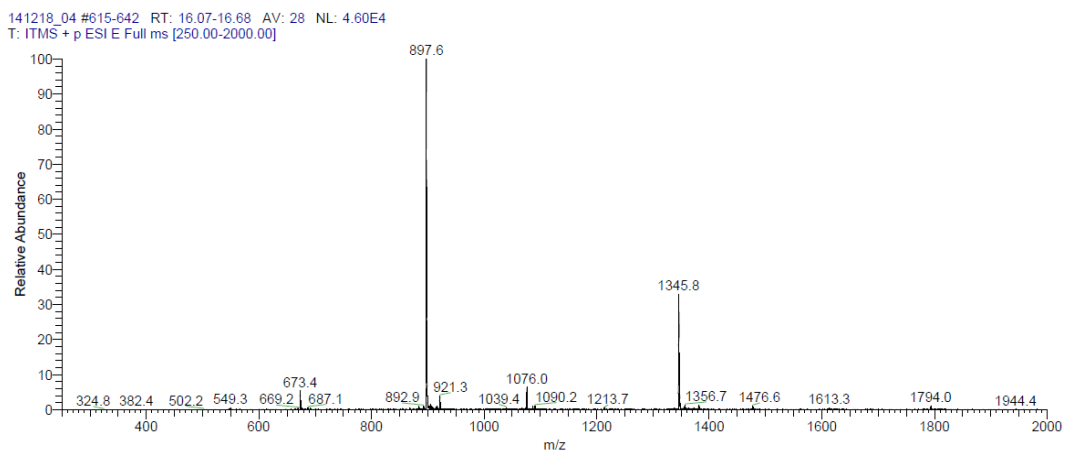
Entry	Sequence	$[M+2]^{2+}$ calculated	$[M+2]^{2+}$ observed	$t_R$ at 214 nm
O193D197	Ac- <u>ODLKD</u> YIDKQLLPVINKQSCSISA-NH <sub>2</sub>	1364.76	1365.32	17.29



**Figure B. 33** Mass and RP-HPLC chromatogram of O193D197.

**Table B. 34** Sequence, accurate mass and retention time of C193C197.

Entry	Sequence	[M+2] <sup>2+</sup> calculated	[M+2] <sup>2+</sup> observed	t <sub>R</sub> at 214 nm
C193C197	Ac- <u>CDLKC</u> YIDKQLLPVINKQSASISA-NH <sub>2</sub>	1345.23	1345.96	17.95

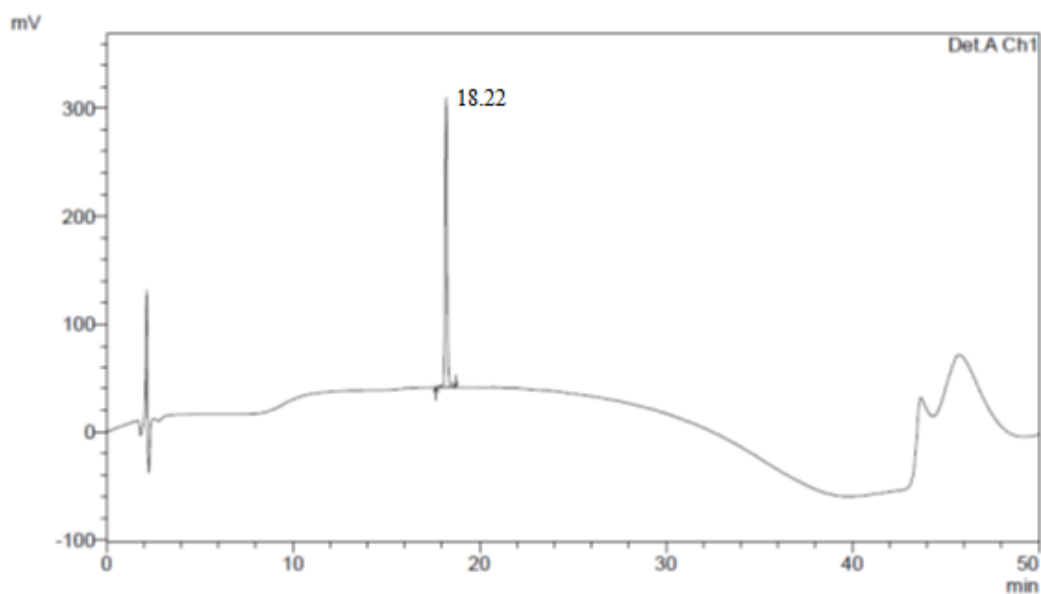
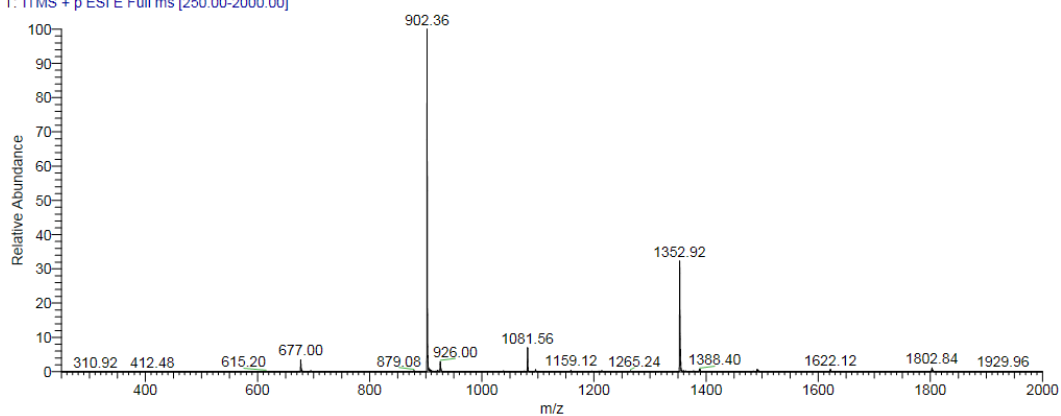


**Figure B. 34** Mass and RP-HPLC chromatogram of C193C197.

**Table B. 35** Sequence, accurate mass and retention time of C193C197.

Entry	Sequence	[M+2] <sup>2+</sup> calculated	[M+2] <sup>2+</sup> observed	t <sub>R</sub> at 214 nm
C193C197	Ac-CDLKQYIDKQLLPVINKQSASISA-NH <sub>2</sub>	1352.24	1352.92	18.22

150829\_02 #579-615 RT: 16.80-17.62 AV: 37 NL: 1.38E4  
T: ITMS + p ESI E Full ms [250.00-2000.00]

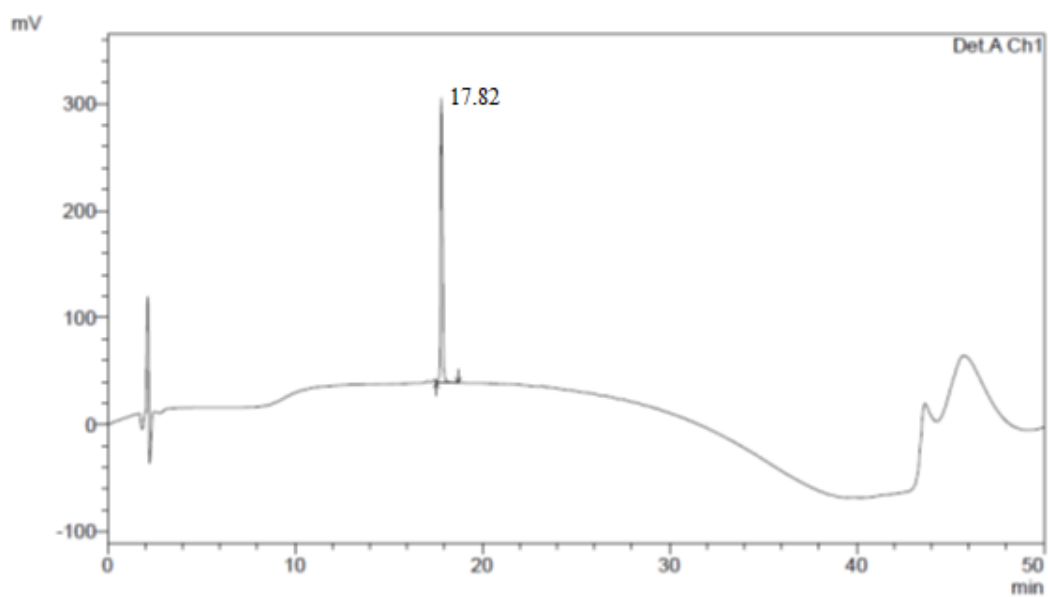
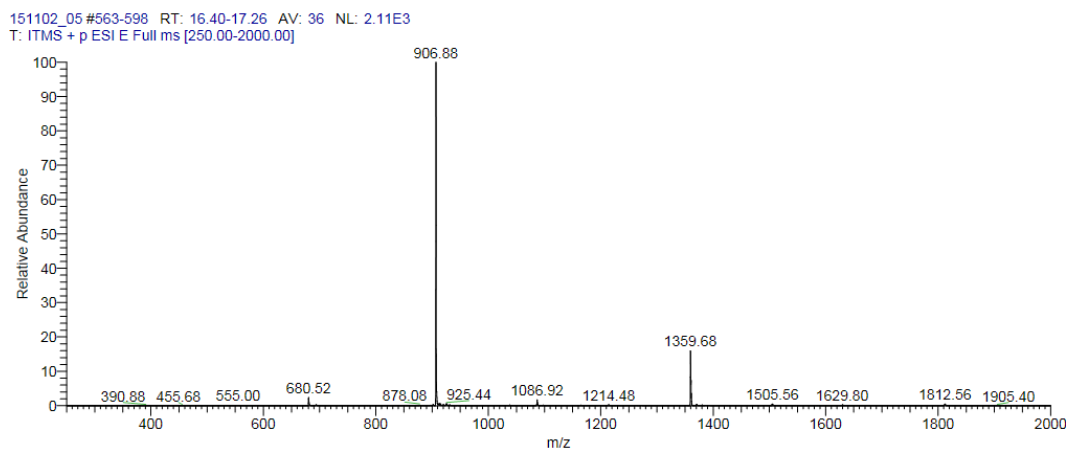


**Figure B. 35** Mass and RP-HPLC chromatogram of C193C197.



**Table B. 36** Sequence, accurate mass and retention time  $\text{C193C197}$ .

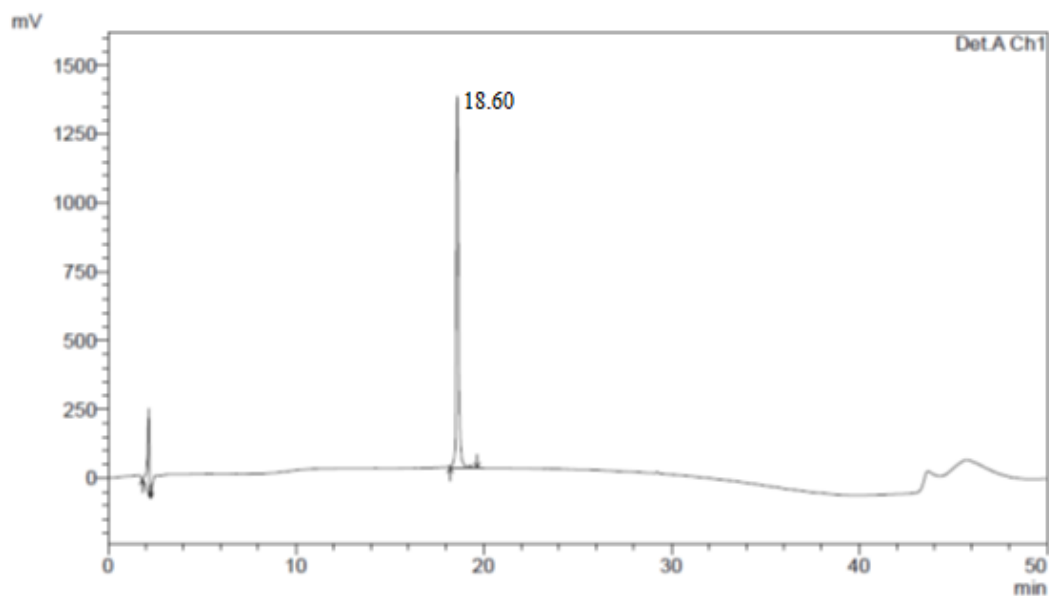
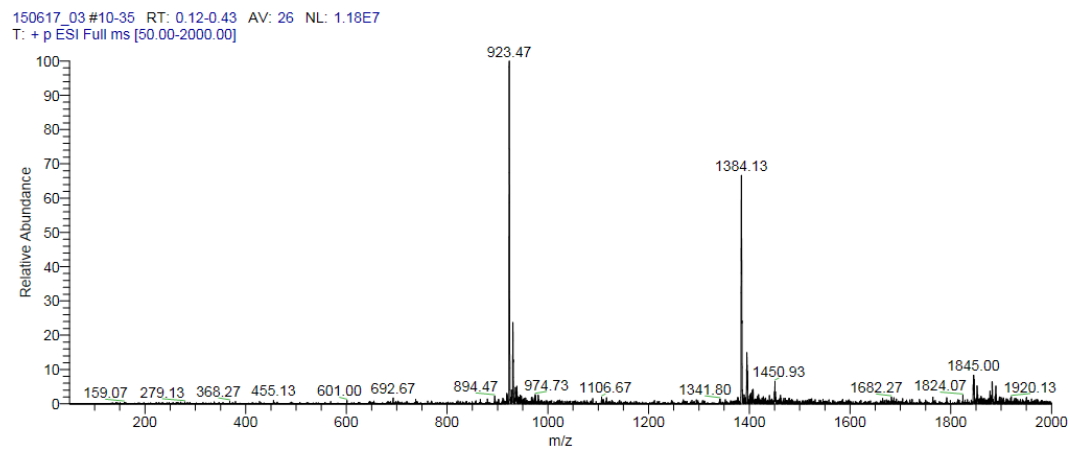
Entry	Sequence	$[\text{M}+2]^{2+}$ calculated	$[\text{M}+2]^{2+}$ observed	$t_{\text{R}}$ at 214 nm
$\text{C193C197}$	Ac- <u>DLK</u> YIDKQLLPVINKQSASISA-NH <sub>2</sub>	1359.25	1359.68	17.82



**Figure B. 36** Mass and RP-HPLC chromatogram of  $\text{C193C197}$ .

**Table B. 37** Sequence, accurate mass and retention time of X193Z197. X = azido-Lysine and Z = propargyl glycine.

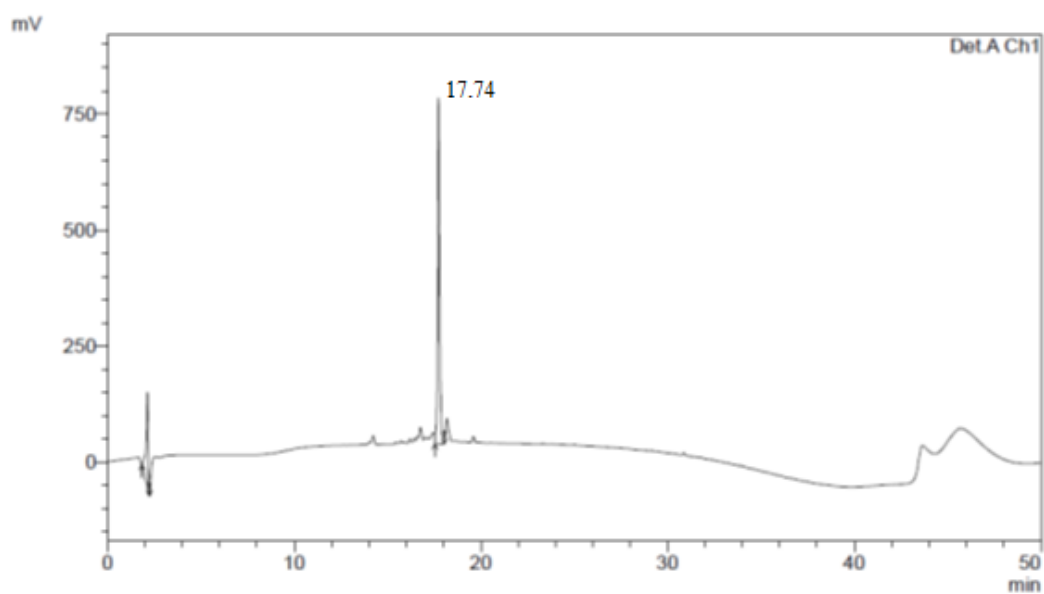
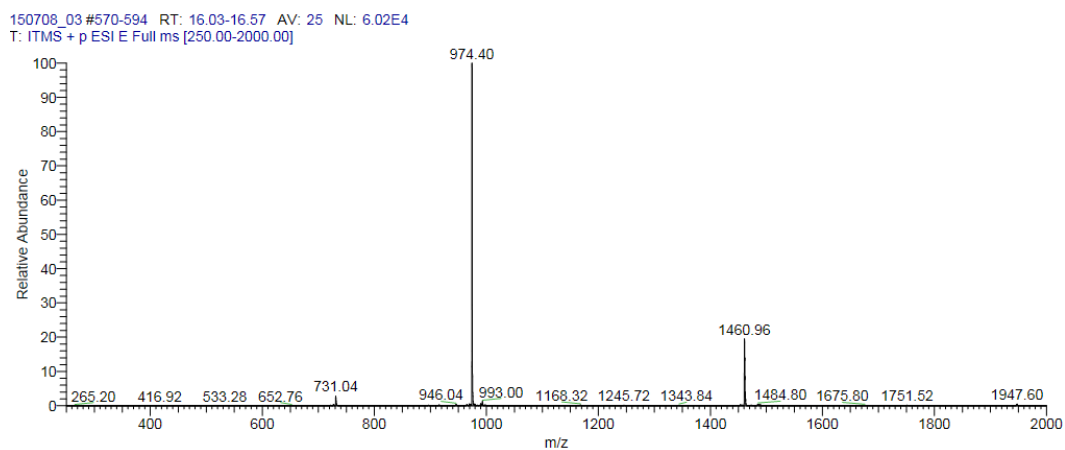
Entry	Sequence	[M+2] <sup>2+</sup> calculated	[M+2] <sup>2+</sup> observed	tr at 214 nm
X193Z197	Ac- <u>XDLKZY</u> IDKQLLPV <sup>N</sup> KNQ <sup>S</sup> ASISA-NH <sub>2</sub>	1383.77	1384.13	18.60



**Figure B. 37** Mass and RP-HPLC chromatogram of X193Z197.

**Table B. 38** Sequence, accurate mass and retention time of N<sub>3</sub>-PEG<sub>4</sub>-WT.

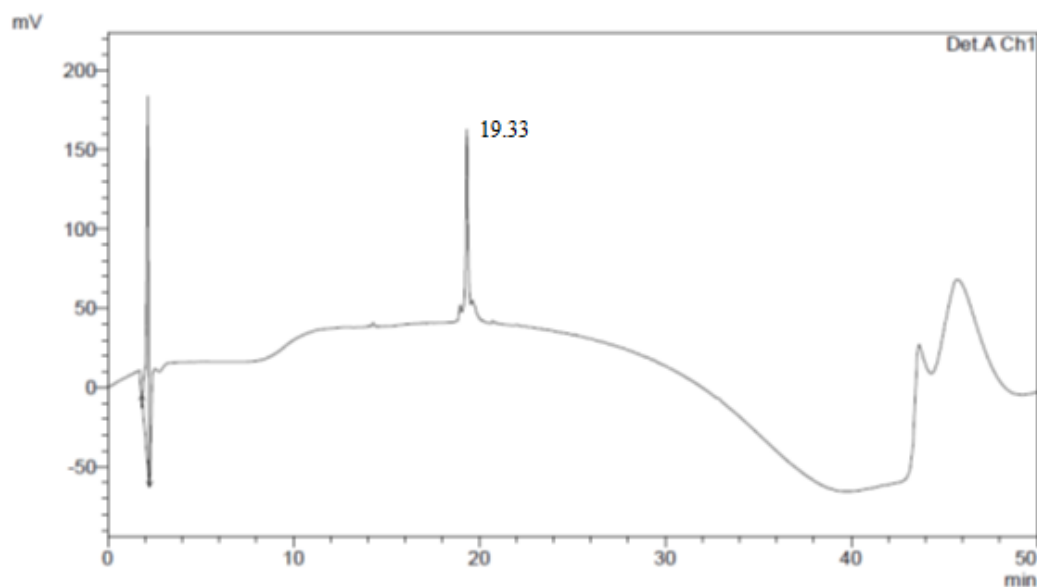
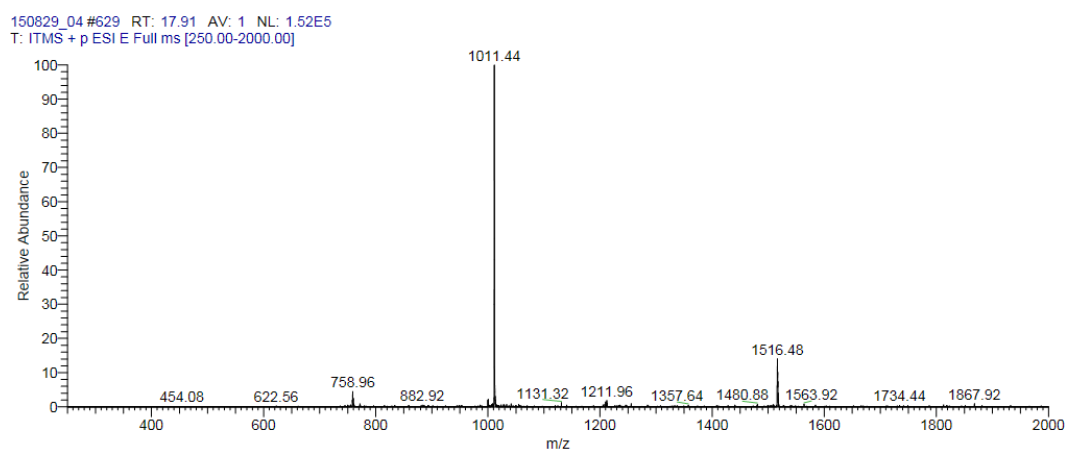
Entry	Sequence	[M+2] <sup>2+</sup> calculated	[M+2] <sup>2+</sup> observed	t <sub>R</sub> at 214 nm
N <sub>3</sub> -PEG <sub>4</sub> -WT	N <sub>3</sub> -PEG <sub>4</sub> -DLKNYIDKQLLPVINKQSCSISA-NH <sub>2</sub>	1460.31	1460.96	17.74



**Figure B. 38** Mass and RP-HPLC chromatogram of N<sub>3</sub>-PEG<sub>4</sub>-WT.

**Table B. 39** Sequence, accurate mass and retention time of N<sub>3</sub>-PEG<sub>4</sub>-K193D197.

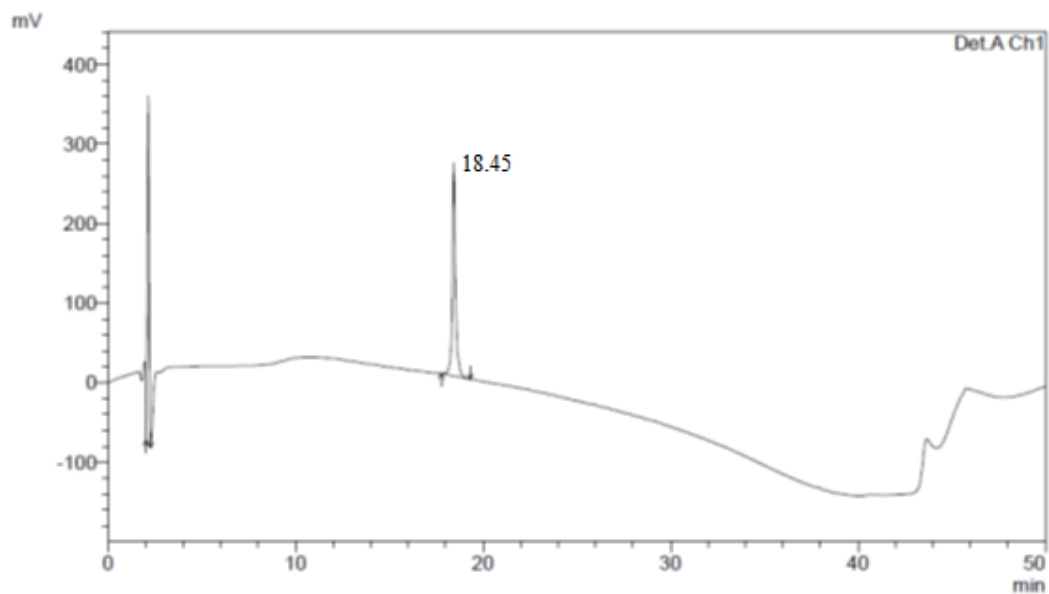
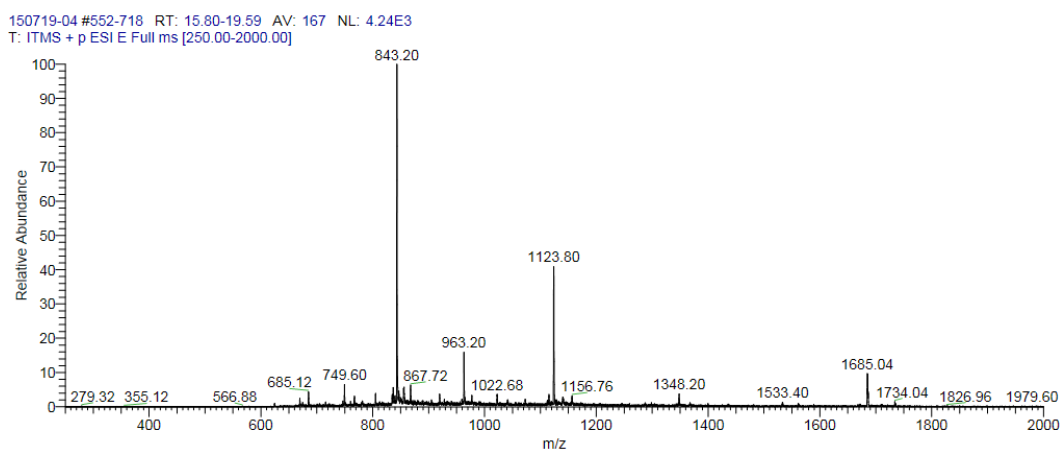
Entry	Sequence	[M+2] <sup>2+</sup> calculated	[M+2] <sup>2+</sup> observed	t <sub>R</sub> at 214 nm
N <sub>3</sub> -PEG <sub>4</sub> - K193D197	N <sub>3</sub> -PEG <sub>4</sub> - <u>KDLKD</u> YIDKQLLPVINKQSCSISA-NH <sub>2</sub>	1515.85	1516.48	19.33



**Figure B. 39** Mass and RP-HPLC chromatogram of N<sub>3</sub>-PEG<sub>4</sub>-K193D197.

**Table B. 40** Sequence, accurate mass and retention time of N<sub>3</sub>-PEG<sub>4</sub>-K190D194-K193D197.

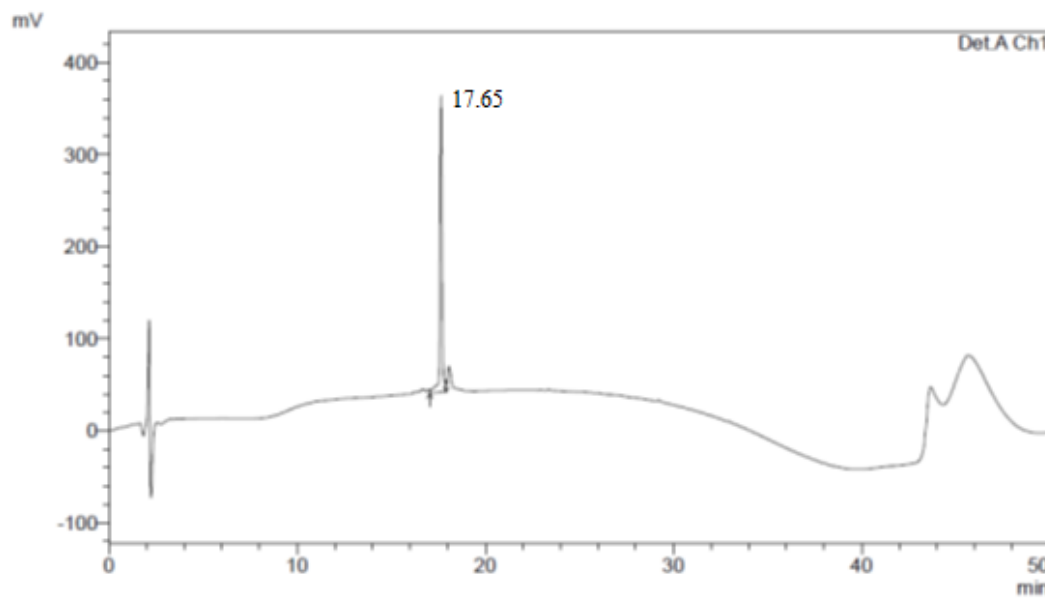
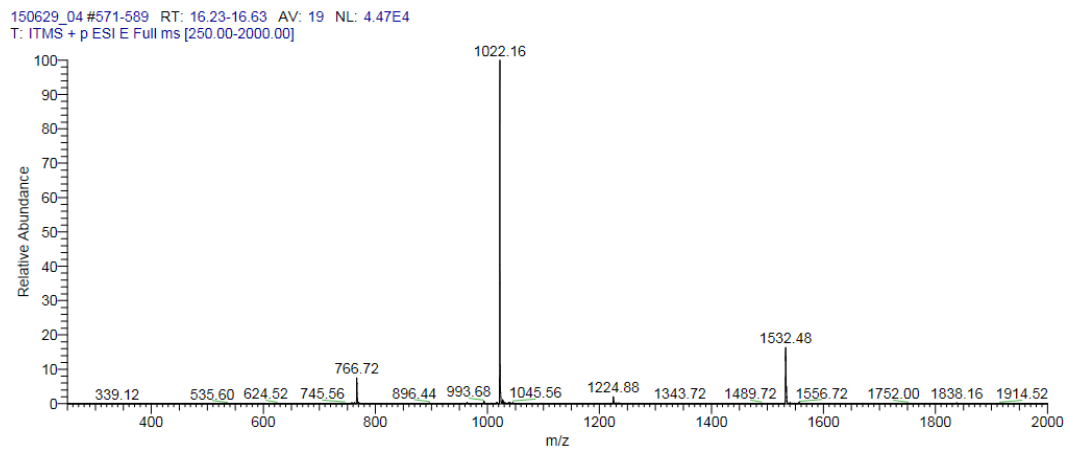
Entry	Sequence	[M+2] <sup>2+</sup> calculated	[M+2] <sup>2+</sup> observed	tr at 214 nm
N <sub>3</sub> -PEG <sub>4</sub> - K190D194- K193D197	N <sub>3</sub> -PEG <sub>4</sub> - <u>KKVKDLKD</u> YIDKQLLPVINKQSCSISA-NH <sub>2</sub>	1684.49	1685.04	18.45



**Figure B. 40** Mass and RP-HPLC chromatogram of N<sub>3</sub>-PEG<sub>4</sub>-K190D194-K193D197.

**Table B. 41** Sequence, accurate mass and retention time of Biotin-PEG<sub>4</sub>-WT. In order to proceed octet analysis, N-termini of linear peptide was biotinylated.

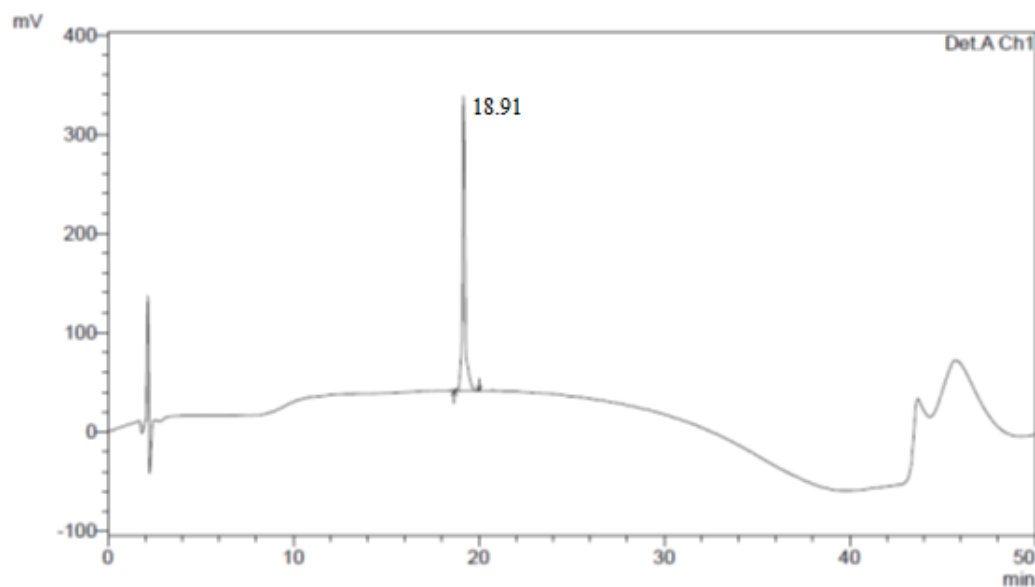
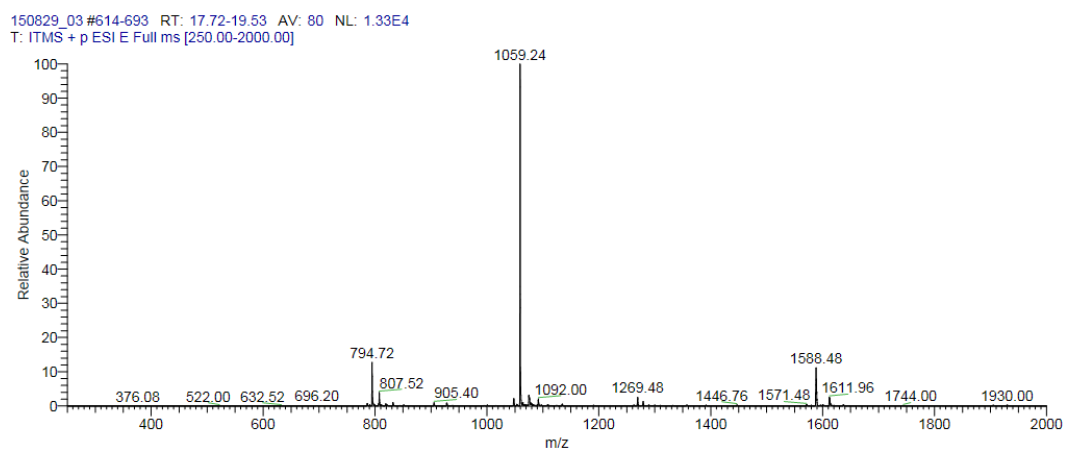
Entry	Sequence	[M+2] <sup>2+</sup> calculated	[M+2] <sup>2+</sup> observed	tr at 214 nm
Biotin-PEG <sub>4</sub> -WT	Biotin-PEG <sub>4</sub> -DLKNYIDKQLLPVINKQSCSISA-NH <sub>2</sub>	1531.84	1532.48	17.65



**Figure B. 41** Mass and RP-HPLC chromatogram of Biotin-PEG<sub>4</sub>-WT.

**Table B. 42** Sequence, accurate mass and retention time of Biotin-PEG<sub>4</sub>-K193D197. In order to proceed octet analysis, N-termini of monocyclic peptide was biotinylated.

Entry	Sequence	[M+2] <sup>2+</sup> calculated	[M+2] <sup>2+</sup> observed	tr at 214 nm
Biotin-PEG <sub>4</sub> -K193D197	Biotin-PEG <sub>4</sub> -KDLKDYIDKQLLPVINKQSCSISANH <sub>2</sub>	1587.69	1588.48	18.91

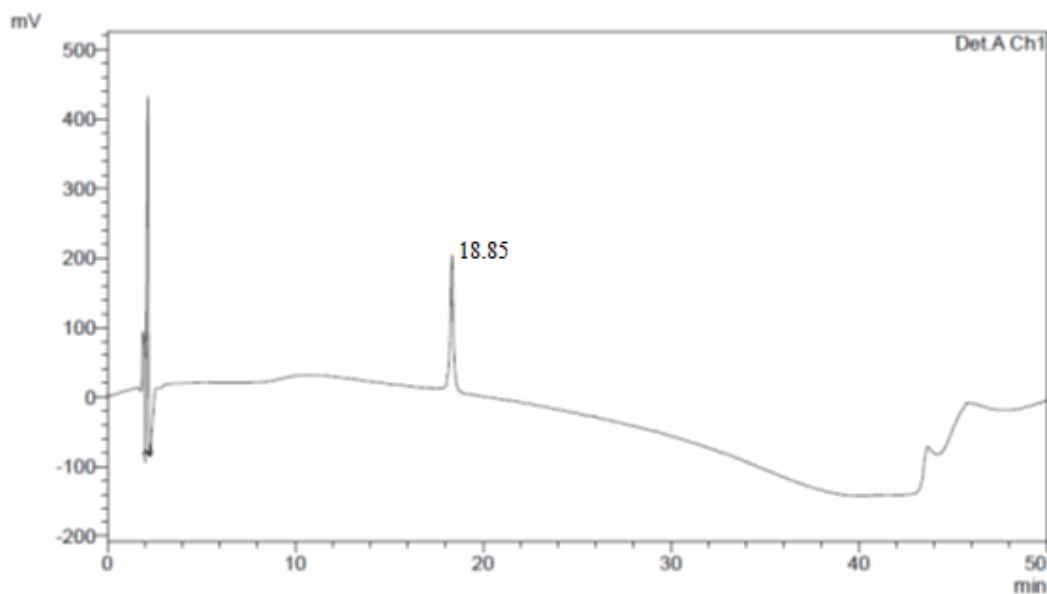
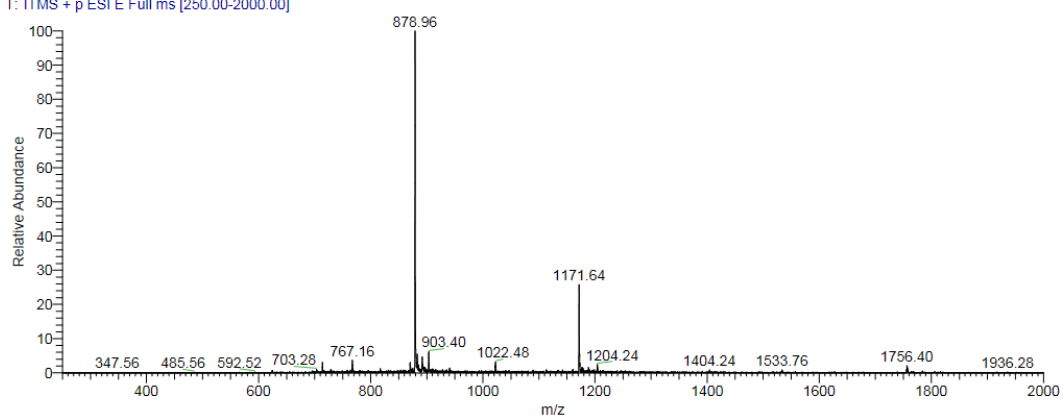


**Figure B. 42** Mass and RP-HPLC chromatogram of Biotin-PEG<sub>4</sub>-K193D197.

**Table B. 43** Sequence, accurate mass and retention time of Biotin-PEG4-K190D194-K193D197. In order to proceed octet analysis, N-termini of bicyclic peptide was biotinylated.

Entry	Sequence	[M+2] <sup>2+</sup> calculated	[M+2] <sup>2+</sup> observed	t <sub>R</sub> at 214 nm
Biotin-PEG <sub>4</sub> -K190D194-K193D197]	Biotin-PEG <sub>4</sub> - <u>KKVKDLK</u> DYIDKQLLPVINKQSCSIS-NH <sub>2</sub>	1756.33	1756.40	18.85

150711\_01 #622-640 RT: 16.87-17.27 AV: 19 NL: 4.44E3  
T: ITMS + p ESI E Full ms [250.00-2000.00]



**Figure B. 43** Mass and RP-HPLC chromatogram of Biotin-PEG4-K190D194-K193D197

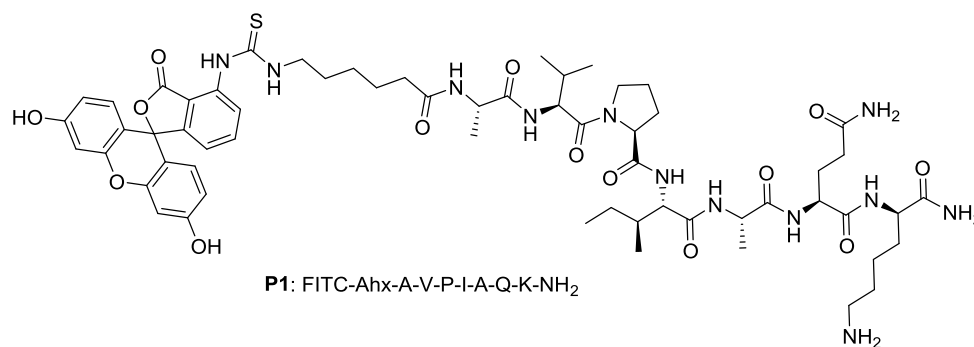


## APPENDIX C

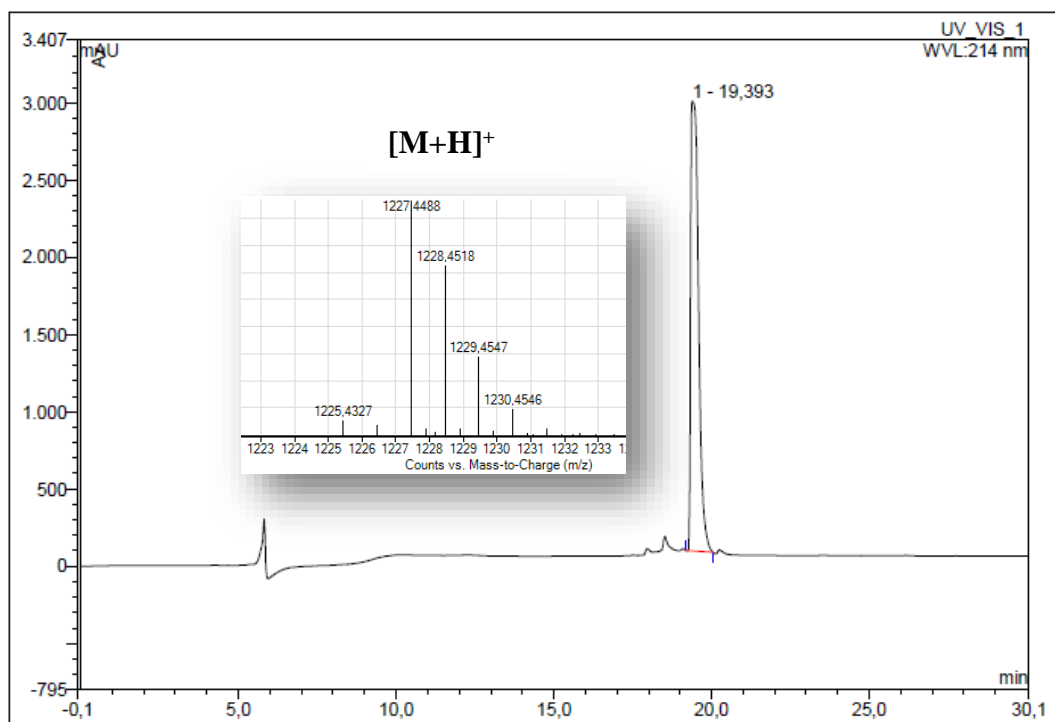
### DATA RELATED TO CHAPTER 3

**Table C. 1** Accurate mass, retention time and percentage purity of P1

P1	Formula	Calculated Mass	Calculated [M+H] <sup>+</sup>	Found [M+H] <sup>+</sup>	t <sub>R</sub> (214nm) min	% Purity at 214 nm
	C <sub>60</sub> H <sub>82</sub> N <sub>12</sub> O <sub>14</sub> S	1226.579	1227.587	1227.474	19.393	97.62



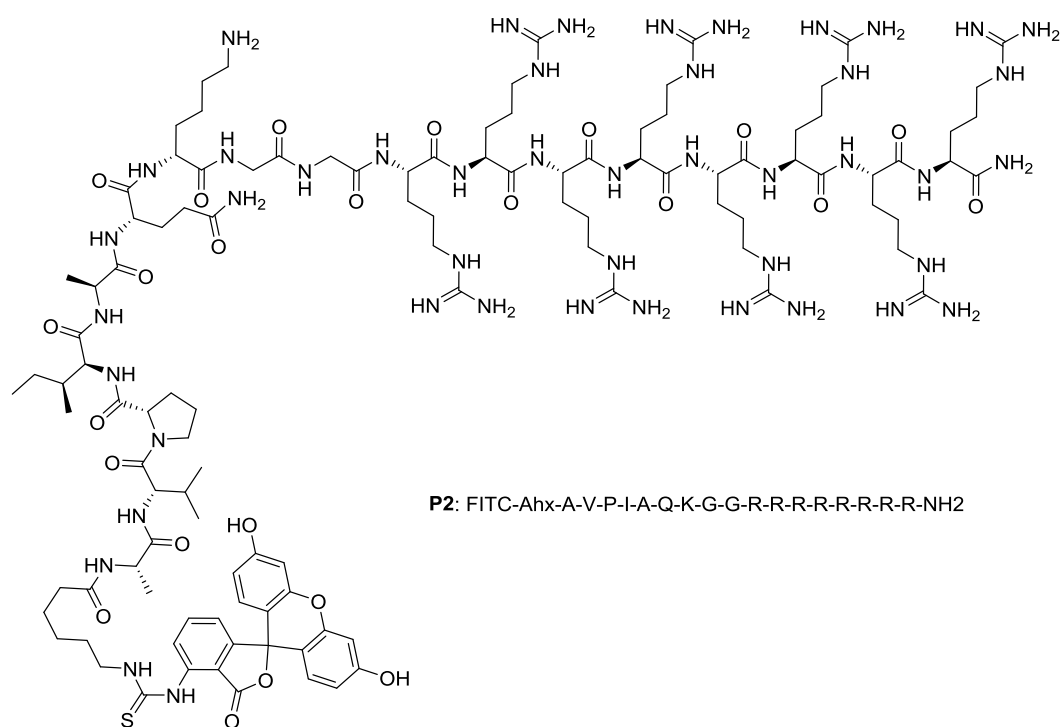
**Figure C. 1** Structure of P1



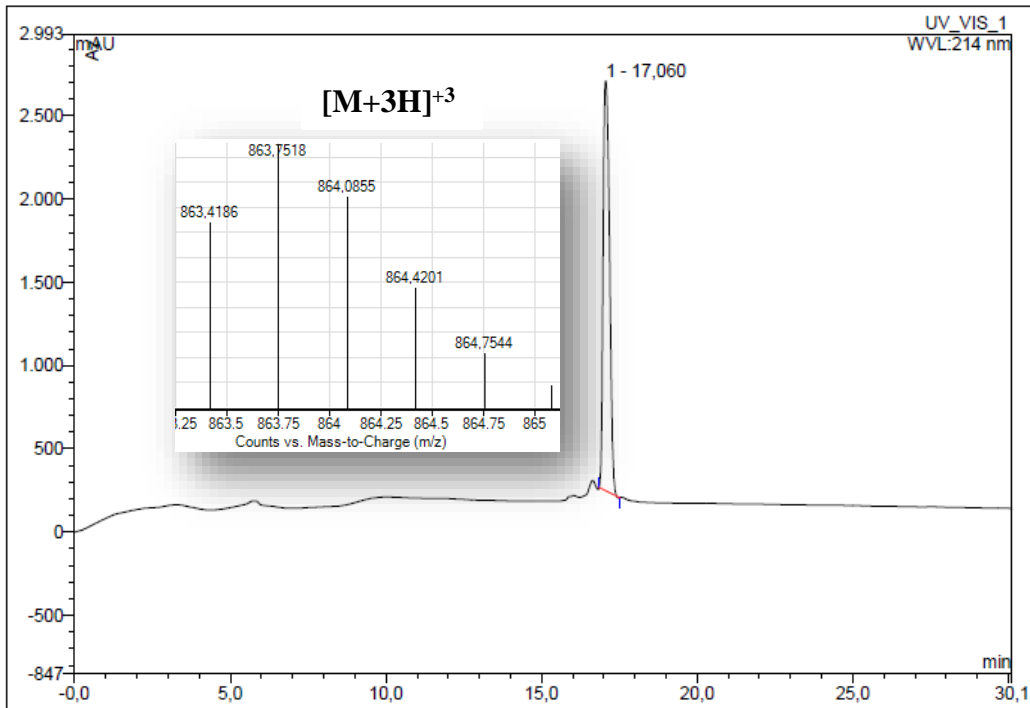
**Figure C. 2** Mass and RP-HPLC chromatogram of P1

**Table C. 2** Accurate mass, retention time and percentage purity of P2

P2	Formula	Calculated Mass	Calculated [M+3H] <sup>+3</sup>	Found [M+3H] <sup>+3</sup>	t <sub>R</sub> (214nm) min	% Purity at 214 nm
	C <sub>112</sub> H <sub>184</sub> N <sub>46</sub> O <sub>24</sub> S	2589.43123	864.1437	863.7611	17.060	97.09



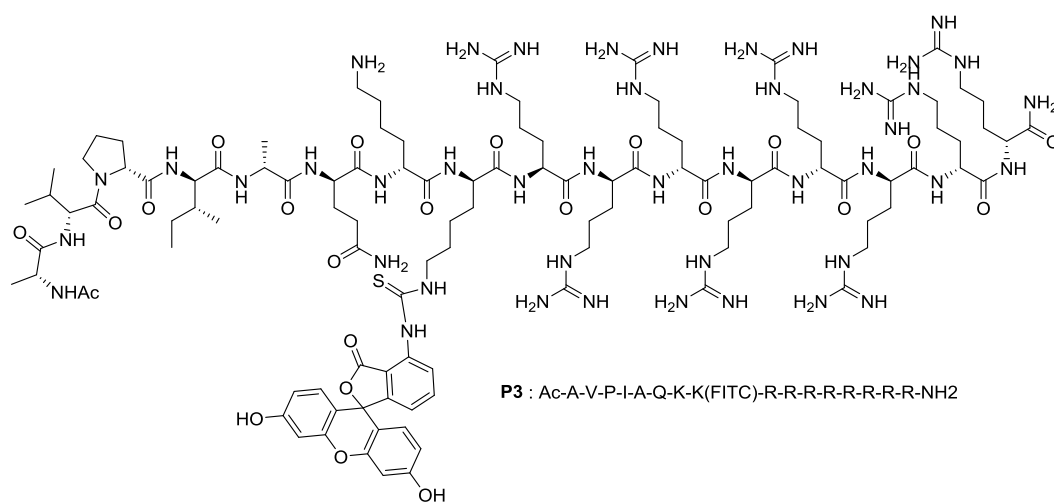
**Figure C. 3** Structure of P2



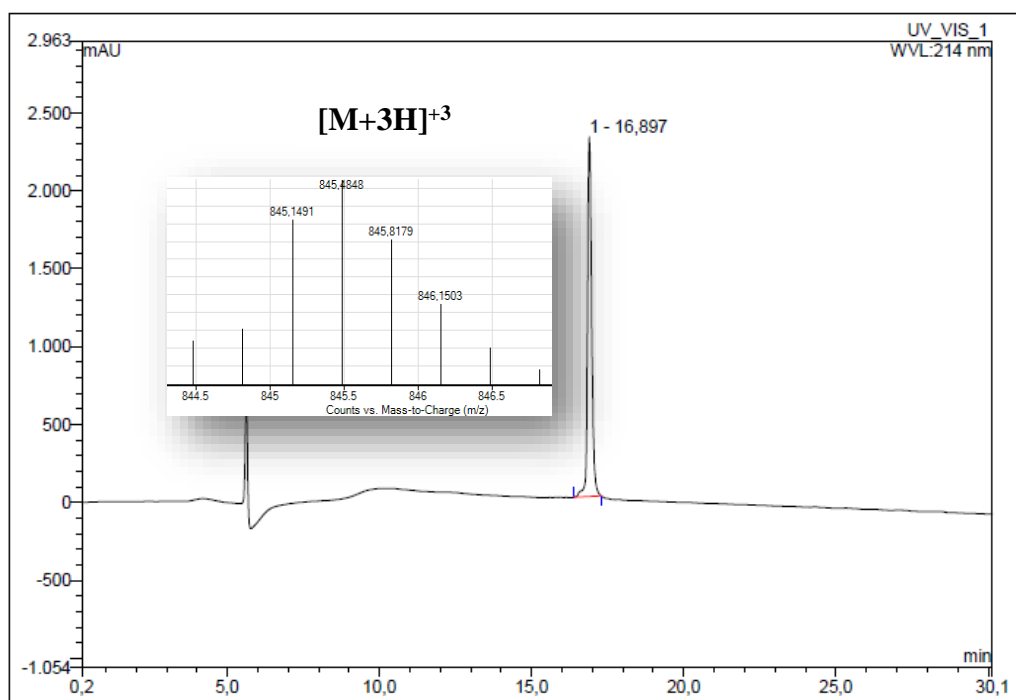
**Figure C. 4** Mass and RP-HPLC chromatogram of P2

**Table C. 3** Accurate mass, retention time and percentage purity of P3

<b>P3</b>	<b>Formula</b>	<b>Calculated Mass</b>	<b>Calculated [M+4H]<sup>+4</sup></b>	<b>Found [M+3H]<sup>+3</sup></b>	<b>t<sub>R</sub> (214nm) min</b>	<b>% Purity at 214 nm</b>
	C <sub>110</sub> H <sub>181</sub> N <sub>45</sub> O <sub>23</sub> S	2532.40977	634.1024	845.8745	16.897	100.00



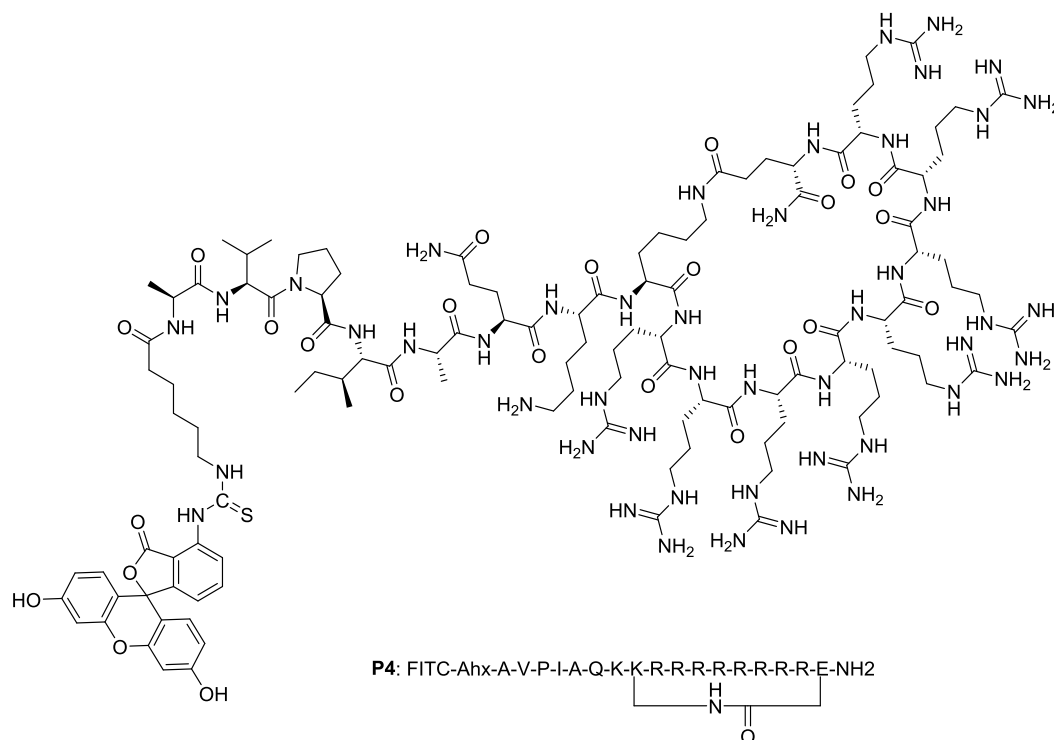
**Figure C. 5** Structure of P3



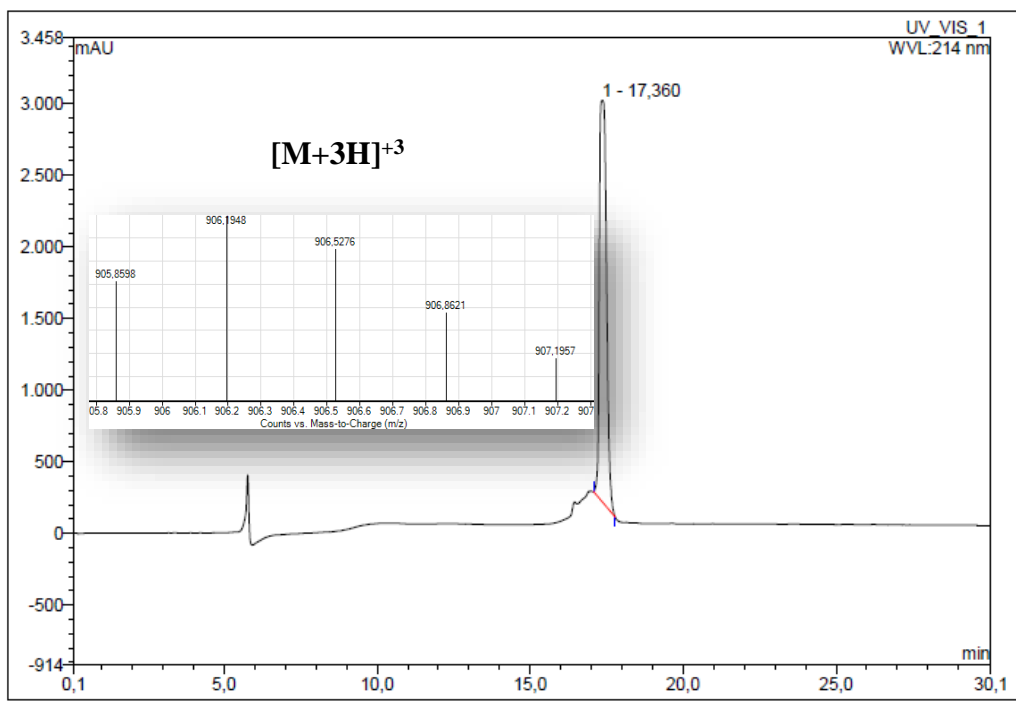
**Figure C. 6** Mass and RP-HPLC chromatogram of P3

**Table C. 4** Accurate mass, retention time and percentage purity of P4

P4	Formula	Calculated Mass	Calculated [M+3H] <sup>+3</sup>	Found [M+3H] <sup>+3</sup>	tr (214nm) min	% Purity at 214 nm
	C <sub>119</sub> H <sub>195</sub> N <sub>47</sub> O <sub>25</sub> S	2714.5153	905.8384	906.1930	17.360	97.06



**Figure C. 7** Structure of P4

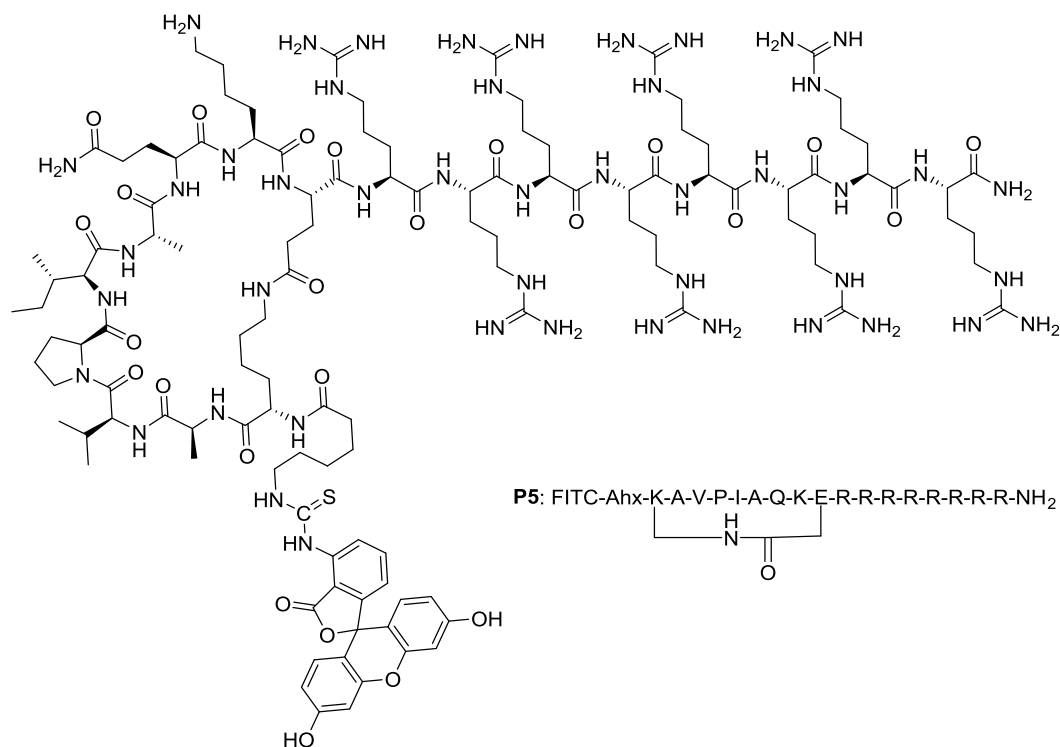


**Figure C. 8** Mass and RP-HPLC chromatogram of P4

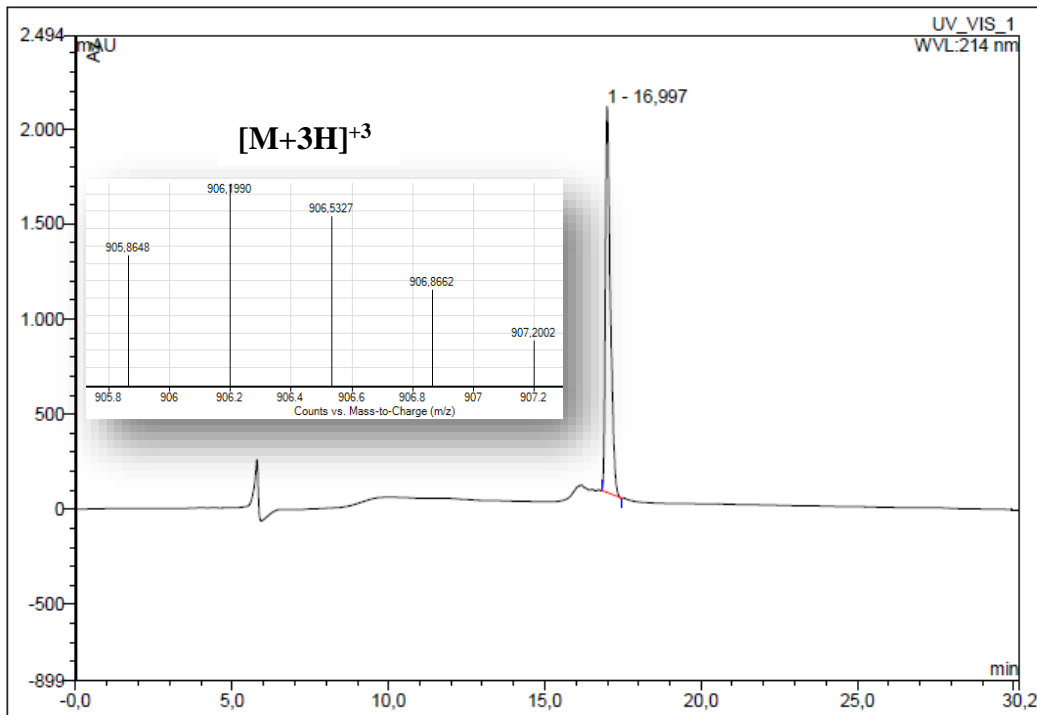


**Table C. 5** Accurate mass, retention time and percentage purity of P5

P5	Formula	Calculated Mass	Calculated $[M+3H]^{+3}$	Found $[M+3H]^{+3}$	$t_r$ (214nm) min	% Purity at 214 nm
	$C_{119}H_{195}N_{47}O_{25}S$	2714.5153	905.8384	906.1879	16.997	93.57



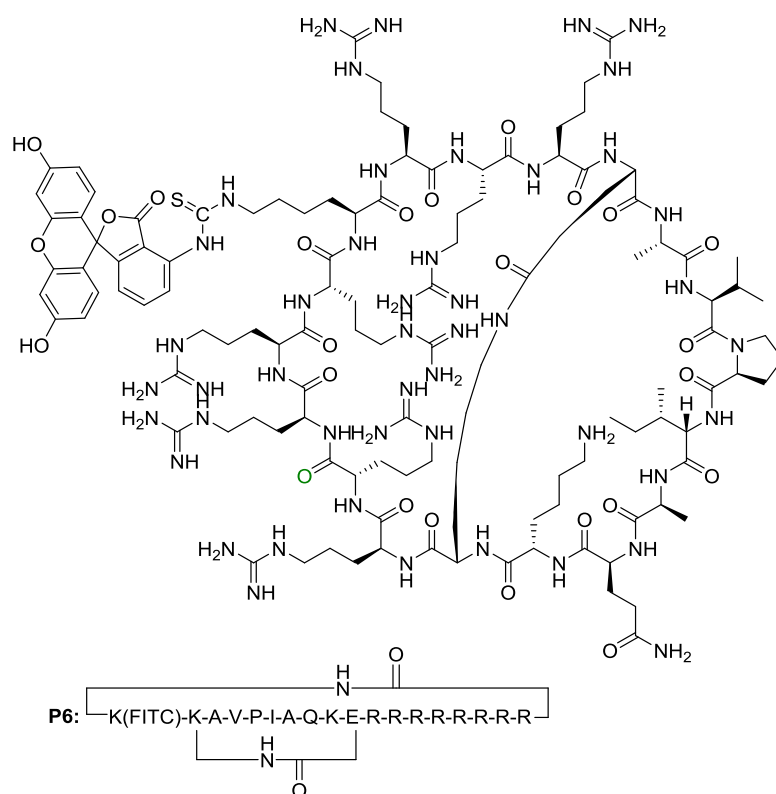
**Figure C. 9** Structure of P5



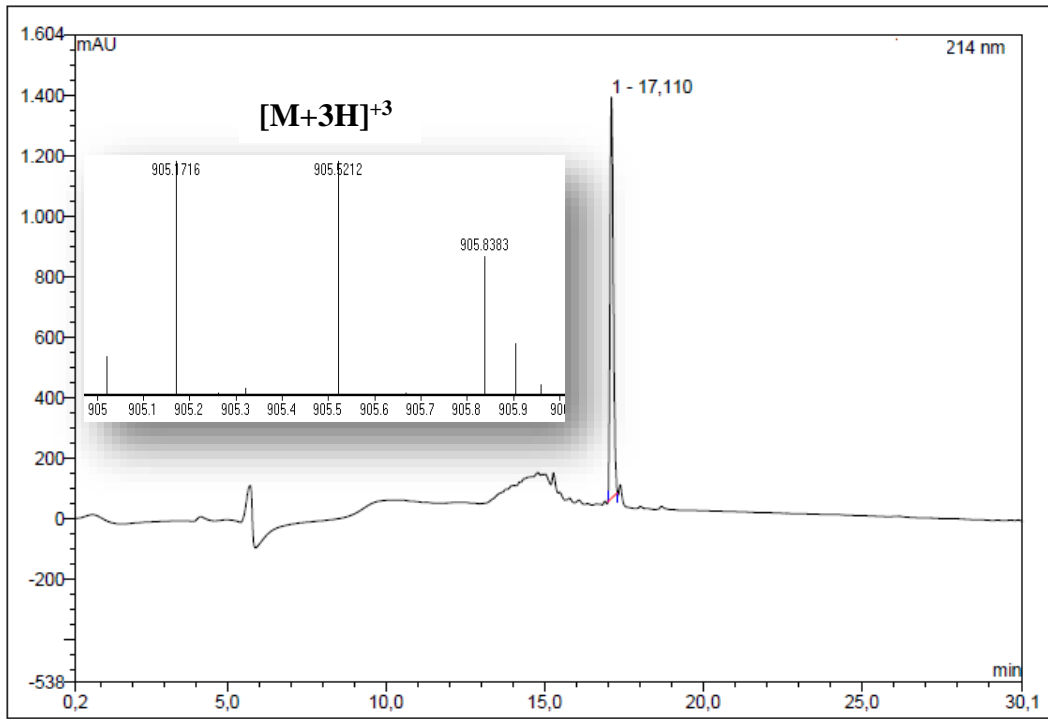
**Figure C. 10** Mass and RP-HPLC chromatogram of P5

**Table C. 6** Accurate mass, retention time and percentage purity of P6

P6	Formula	Calculated Mass	Calculated [M+3H] <sup>+3</sup>	Found [M+3H] <sup>+3</sup>	t <sub>R</sub> (214nm) min	% Purity at 214 nm
	C <sub>119</sub> H <sub>193</sub> N <sub>47</sub> O <sub>25</sub> S	2712.49965	905.16655	905.5212	17.11	81.52



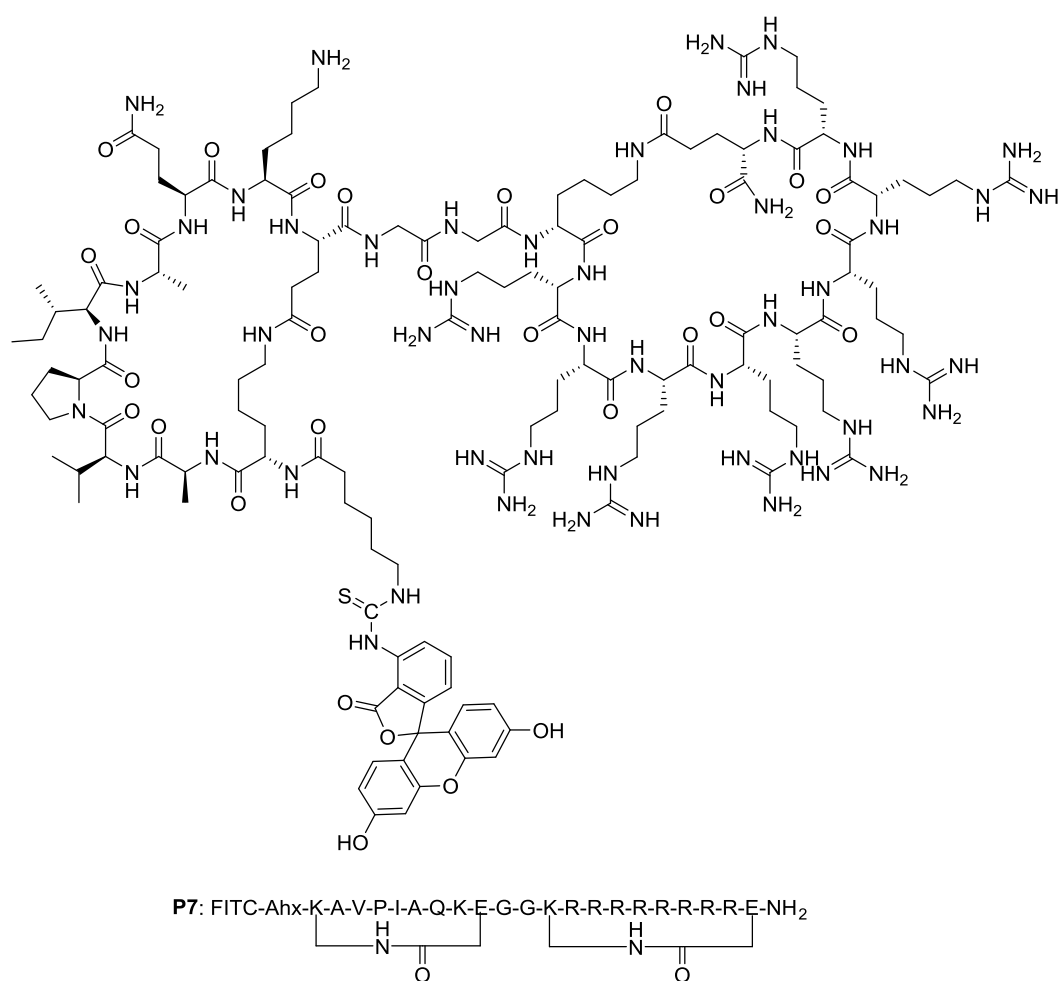
**Figure C. 11** Structure of P6



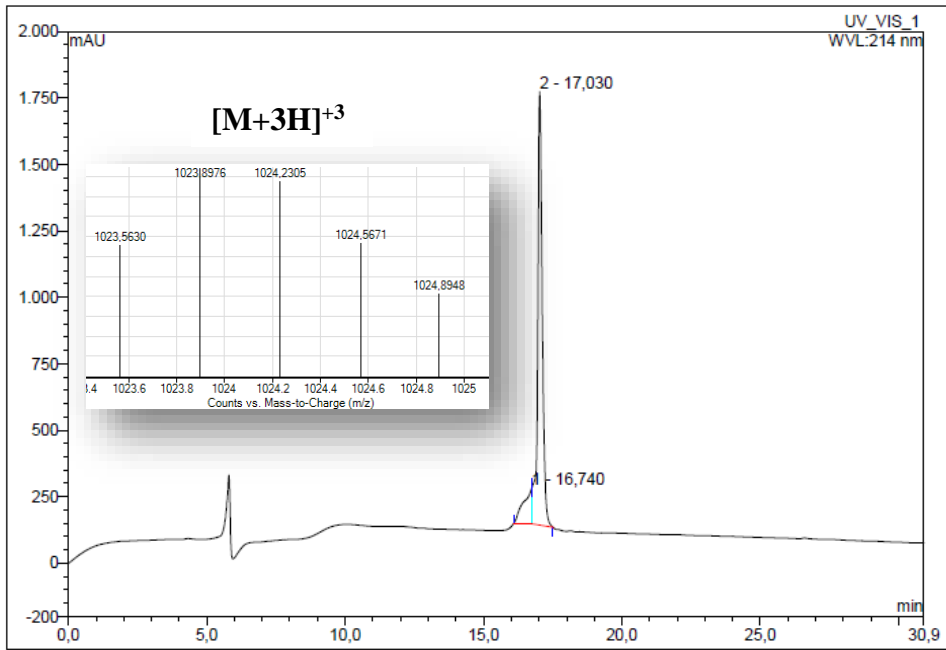
**Figure C. 12** Mass and RP-HPLC chromatogram of P6

**Table C. 7** Accurate mass, retention time and percentage purity of P7

P7	Formula	Calculated Mass	Calculated [M+3H] <sup>+3</sup>	Found [M+3H] <sup>+3</sup>	t <sub>R</sub> (214nm) min	% Purity at 214 nm
	C <sub>134</sub> H <sub>218</sub> N <sub>52</sub> O <sub>30</sub> S	3067.68521	1023.5617	1023.8948	17.030	87.33



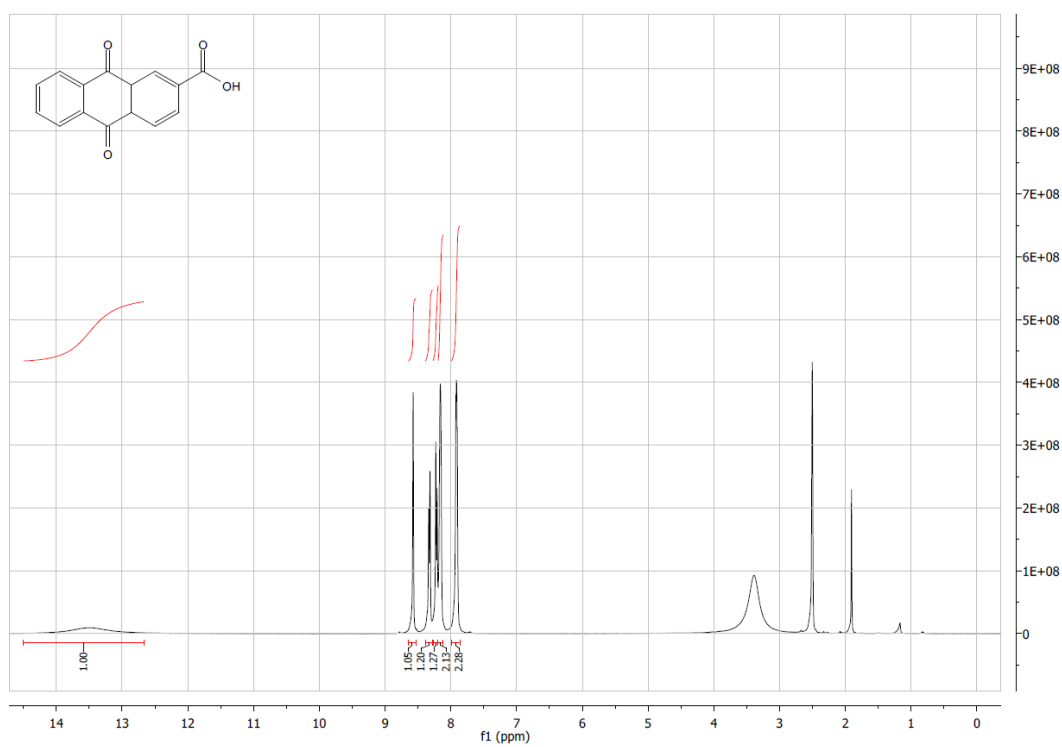
**Figure C. 13** Structure of P7



**Figure C. 14** Mass and RP-HPLC chromatogram of P7

## APPENDIX D

### DATA RELATED TO CHAPTER 4



**Figure D. 1** <sup>1</sup>H NMR spectrum of anthraquinone-2-carboxylic acid (2)

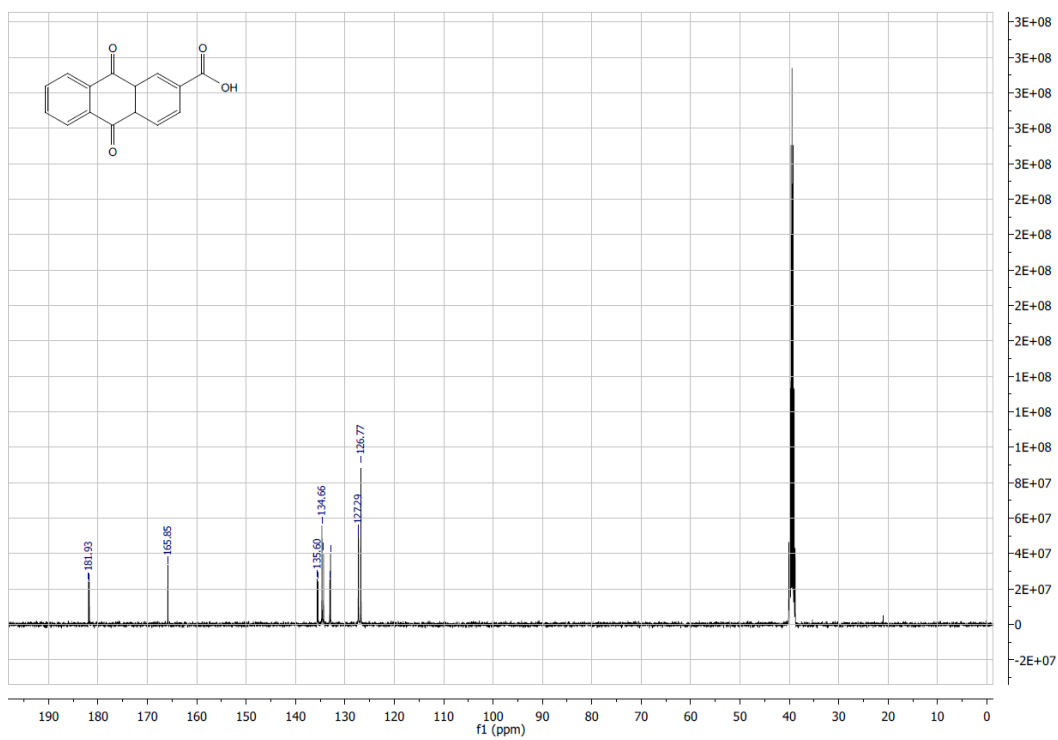


Figure D. 2  $^{13}\text{C}$  NMR spectrum of anthraquinone-2-carboxylic acid (2)

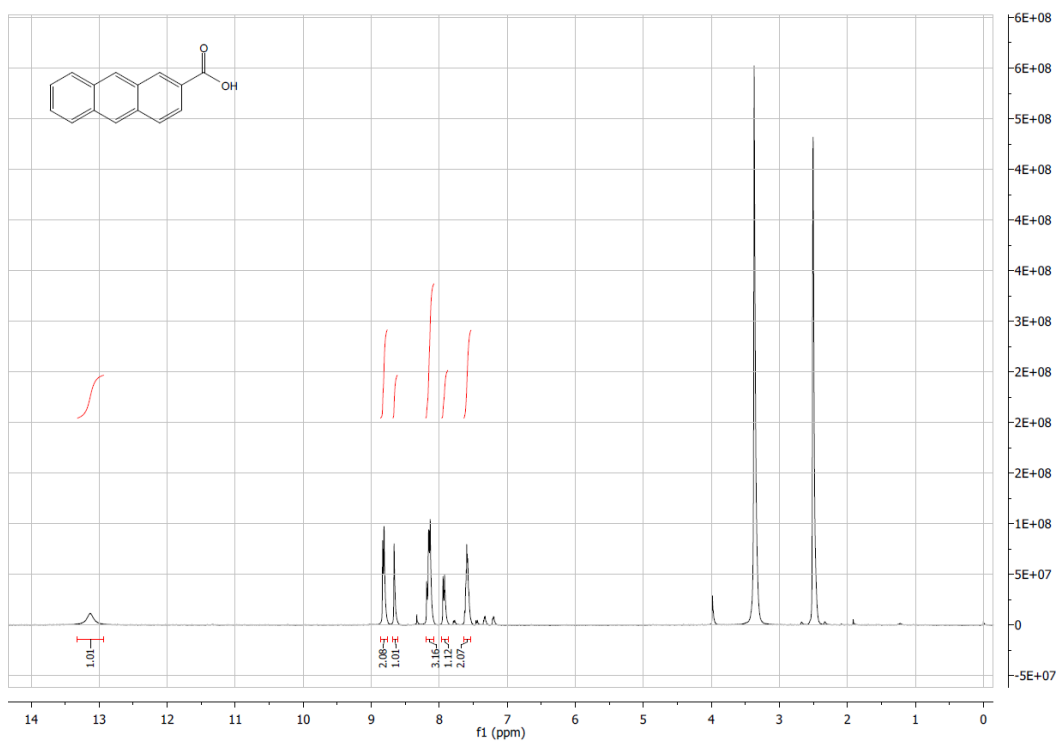
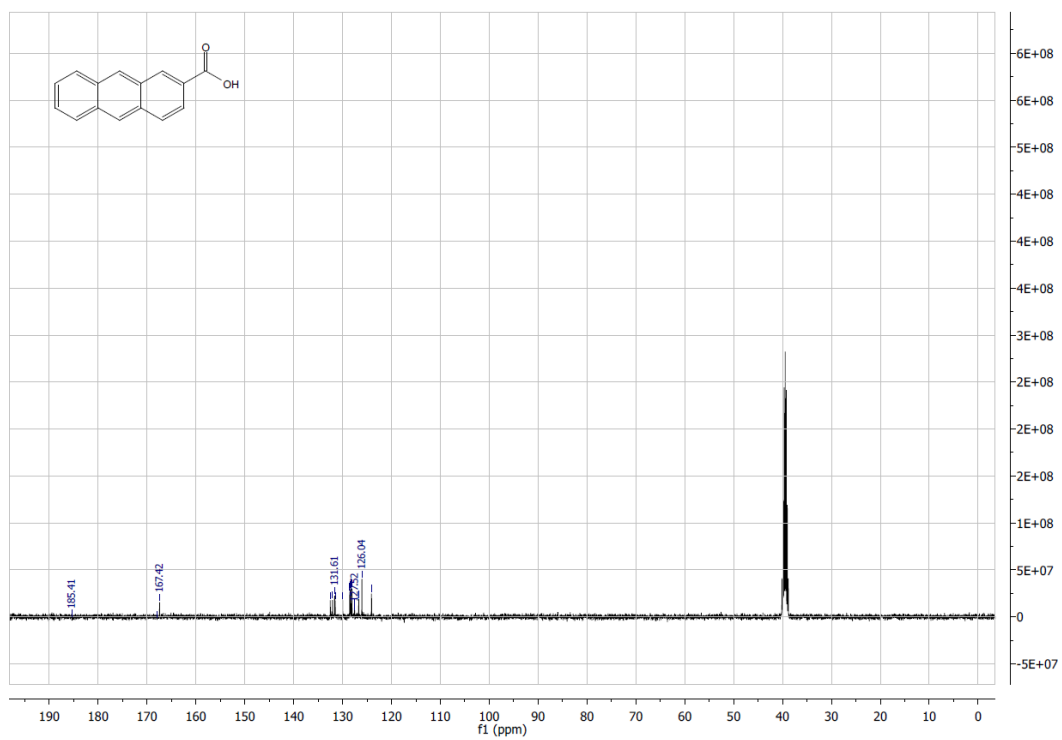
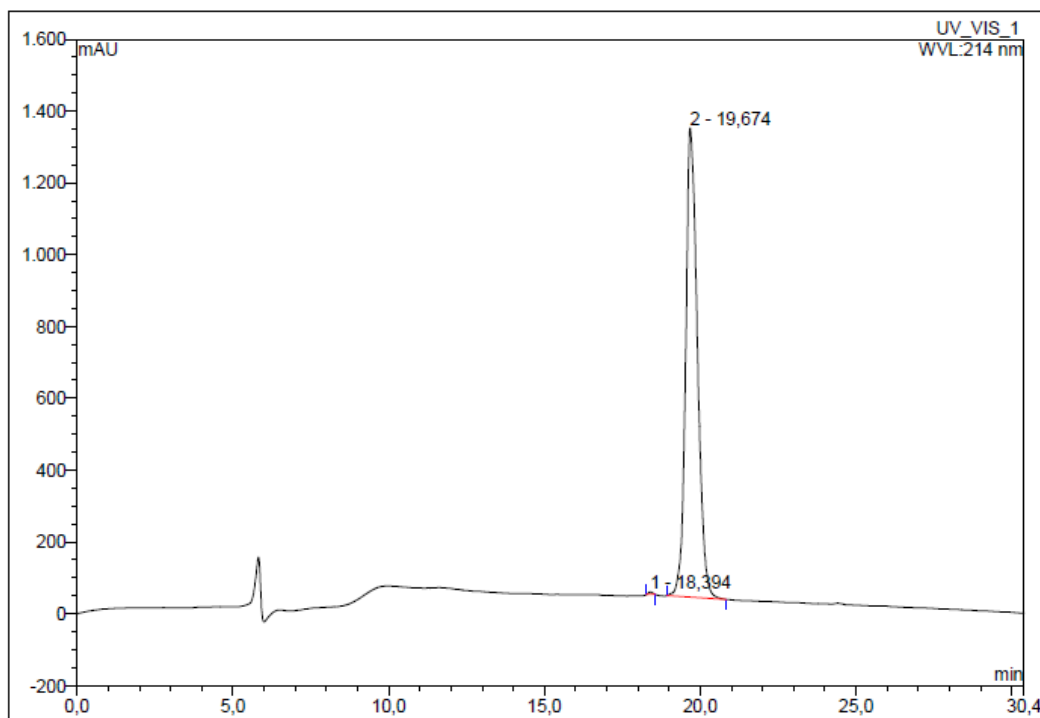
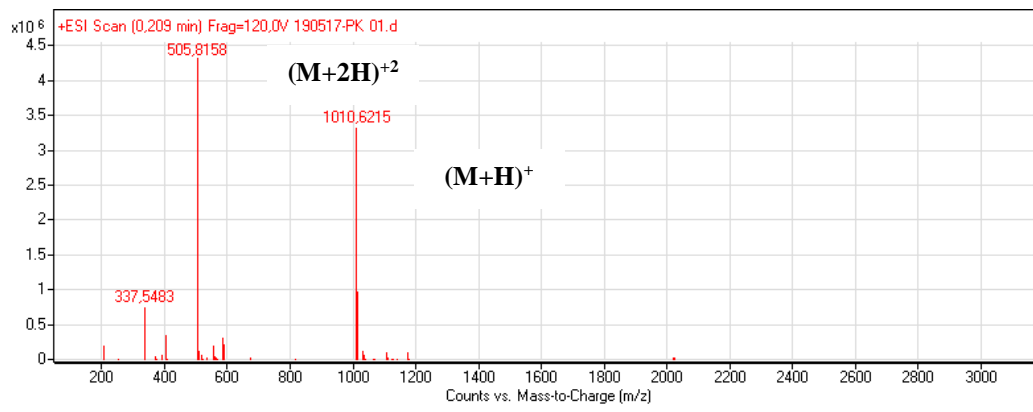


Figure D. 3  $^1\text{H}$  NMR spectrum of anthracene-2-carboxylic acid (3)

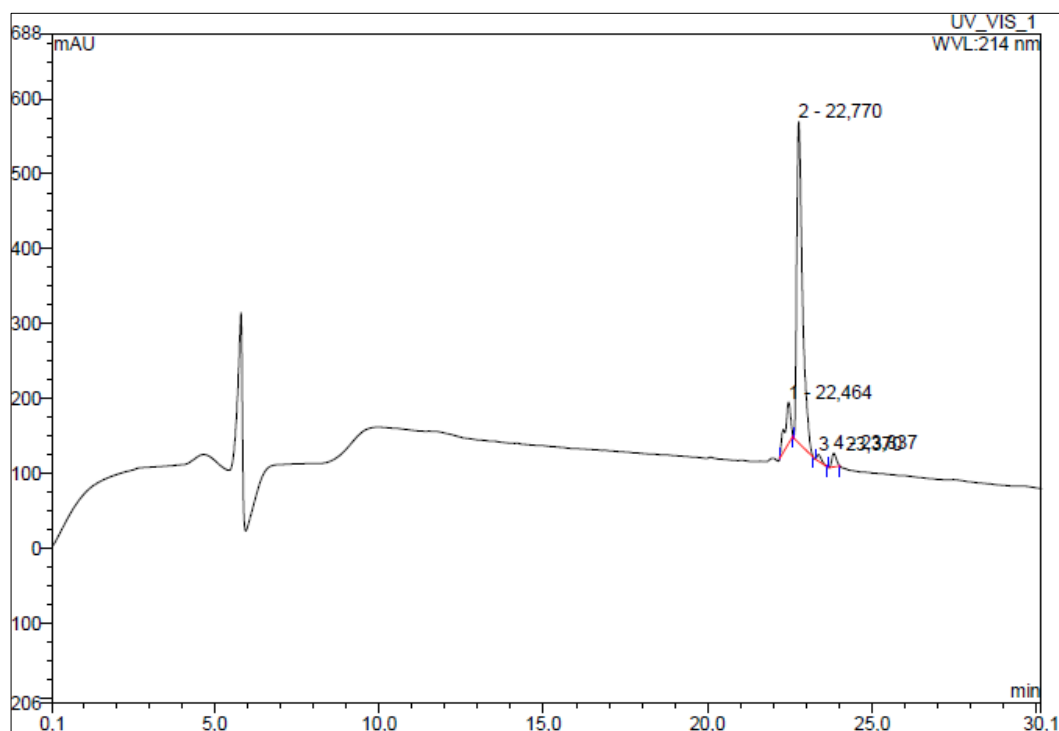
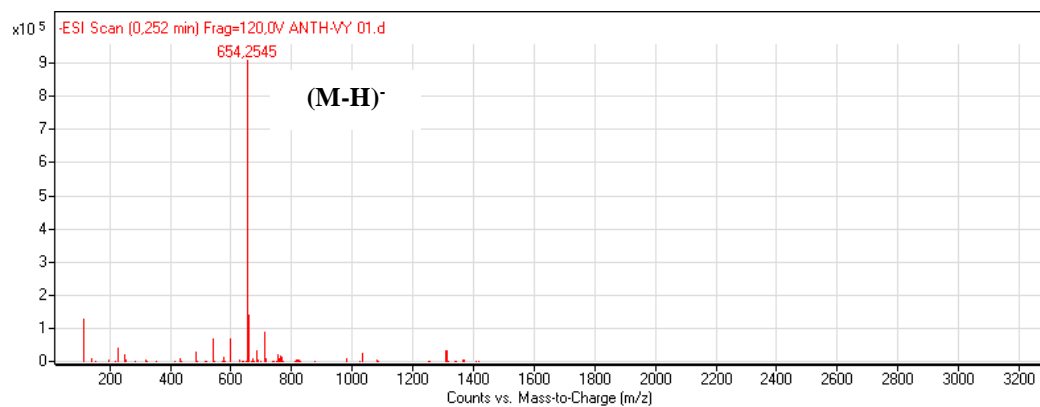




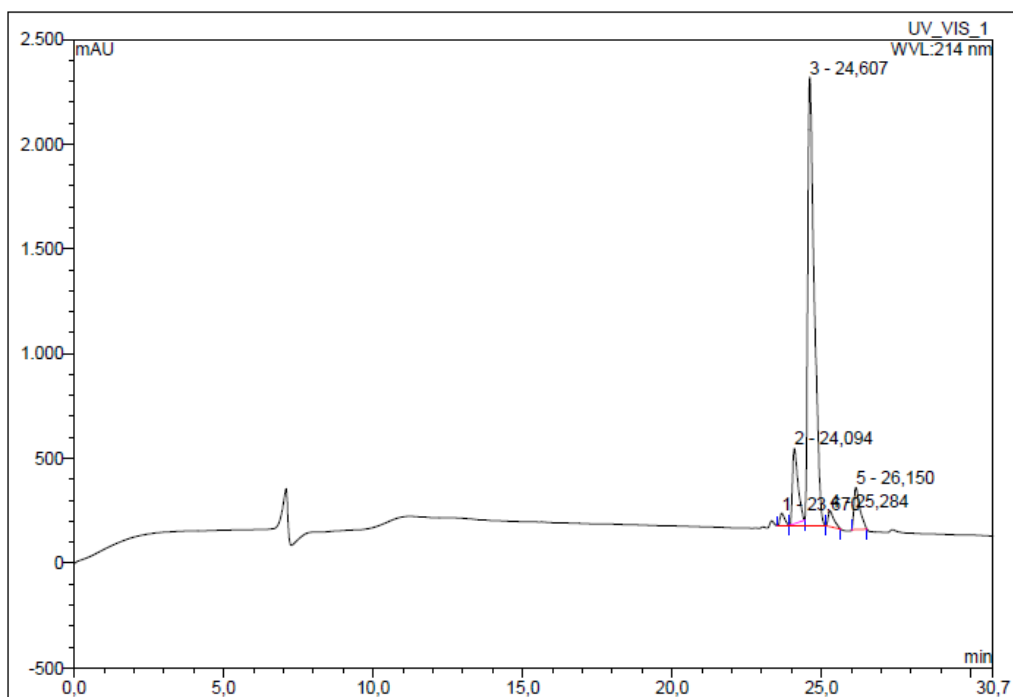
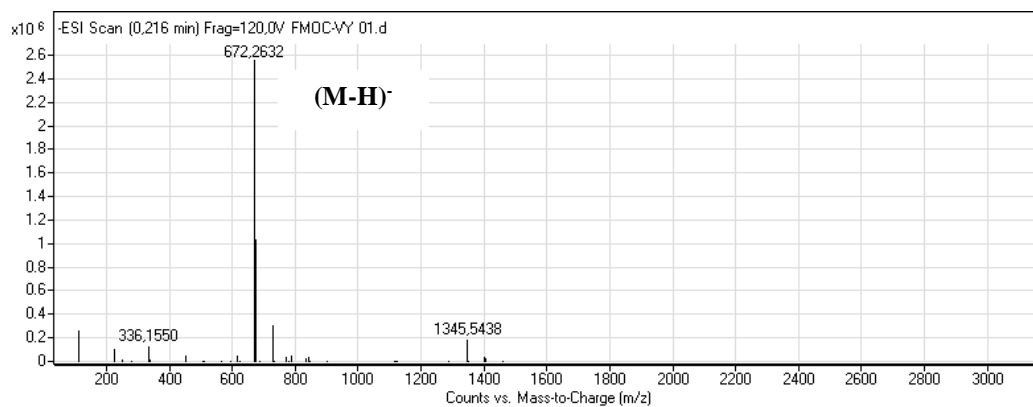
**Figure D. 4**  $^{13}\text{C}$  NMR spectrum of anthracene-2-carboxylic acid (3)



**Figure D. 5** Mass and RP-HPLC chromatogram of Ant-PK.



**Figure D. 6** Mass and RP-HPLC chromatogram of Ant-VY.



**Figure D. 7** Mass and RP-HPLC chromatogram of Fmoc-VY.

## CURRICULUM VITAE

### PERSONAL INFORMATION

Surname, Name: Parlak, Melek

Nationality: Turkish (TC)

Date and Place of Birth: 25 Haziran 1986, SORGUN

Marital Status: Married

Phone: +90 312 210 5340

Fax: +90 312 210 32 00

Email: [pmelekparlak@gmail.com](mailto:pmelekparlak@gmail.com)

### EDUCATION

- Post- Bachelor's Doctoral: (2010 – 2017)

Graduate School of Natural and Applied Science / Chemistry

Organic Chemistry

CGPA: 3.57/ 4.00

- Prep School (2009-2010 May)

- Integrated Bachelor's and Non-Thesis Master of Science: (2004 – 2009 May )

Chemistry Education, Middle East Technical University - ANKARA

CGPA: 3.86 / 4.00

Degree: Highest ranking student

- High School: (2000 – 2004)

Sokullu Mehmet Paşa Anadolu Lisesi, ÇANKAYA - ANKARA

Mathematics and Science Branch

CGPA: 5.00 / 5.00.

Degree: Highest ranking student

## **WORK EXPERIENCE**

February 2010 - September 2017: Research Assistant Middle East Technical University Faculty of Arts and Sciences Department of Chemistry

## **LABORATORY EXPERIENCE**

- September 2010 – December 2010 : Middle East Technical University-Chemistry Department

Prof. Dr. Mahinur Akkaya Research Group, Biochemistry Laboratory

- January 2010 – June 2012: Middle East Technical University-Chemistry Department

Prof. Dr. Ayhan Sıtkı Demir Research Group, Asymmetric Synthesis Laboratory

- July 2012 – September 2017: Middle East Technical University-Chemistry Department

Assist. Prof. Dr. Salih Özçubukçu Research Group, Peptide Chemistry Laboratory

- September 2014 – December 2015: Radboud University- Bio-Organic Chemistry Department

Prof. Dr. Jan Van Hest Research Group, Peptide Chemistry Laboratory

## **LANGUAGES**

English: Fluent at reading and writing and speaking

## **PRESENTATIONS AND SEMINARS**

- COST/Cascade Chemoenzymatic Processes - New Synergies Between Chemistry and Biochemistry 26 April- 1May 2011, Siena, Italy
- International Conference on Enzyme Science and Technology ICEST 2011, 31 October-4 November 2011, Kusadasi, Turkey
- 15th European Congress on Biotechnology –ECB15 23-26 September 2012, İstanbul, Turkey
- 44th World Chemistry Congress, 11-16 August 2013, İstanbul, Turkey
- PIPS 2014 Training Course, 8-10 October, 2014, Université de Cergy-Pontoise, Gennevilliers, France

- The 2015 Dutch Peptide Symposium, 27 May 2015, Radboud University, Nijmegen, The Netherlands
- Chemistry Discussion, 16 May 2017, Bilkent University, Ankara, Turkey
- American Peptide Symposium, 17-22 June 2017, Whistler, Canada